SURFACE PROFILE AND ACOUSTIC EMISSION AS DIAGNOSTICS OF TOOL WEAR IN FACE MILLING

Peter Wilkinson

SUBMITTED FOR THE DEGREE OF
DOCTOR OF PHILOSOPHY
AT HERIOT-WATT UNIVERSITY
DEPARTMENT OF PHYSICS
AUGUST 2001

Abstract

This thesis examines the relationship between progressive wear of cutting inserts during a face milling operation and the acoustic emission and surface profile generated by that process. Milling experiments were performed on a range of workpiece materials using both eight point and single point insert arrangements contained in two cutters of different geometries.

Surface profile measurements were made using a stylus profilometer at intervals during the experiments. Correlations between the wear state as measured by the length of the flank wear land (V_b) and the spatial frequency content of the surface profiles were established. Investigations into the variation of fractal dimension of a milled surface with V_b demonstrated that no correlation was observable between these quantities.

Acoustic emission (AE) measurements were made using a non-contacting fibre-optic interferometer which allowed the rms of the AE signal and its mean frequency to be determined. Correlations between these parameters and V_b were established for a range of workpiece materials and cutter geometries.

It was shown that neither AE measurements nor surface profile measurements in isolation could predict tool wear state in all situations. The advantages of fusing data from surface profile and AE sources via an artificial neural network in tool wear monitoring were demonstrated.

Acknowledgements

I wish to express my thanks to my supervisor Dr. J.S. Barton for his guidance, friendship and infinite patience throughout this work.

I also wish to acknowledge the support afforded to me by the Head of Department of the Department of Mechanical and Chemical Engineering and by the Head of Department of the Department of Physics at Heriot-Watt University. Thanks are also due to my colleagues Dr. T.A. Carolan, Dr. D.P. Hand, Mr. B. Wilson and the staff of the Advanced Manufacturing Unit.

I am especially grateful to my friend and colleague Mr. R.D. Brown for taking up my lecturing load when it was necessary.

Finally I would like to acknowledge the A.C.M.E. Directorate of the Science and Engineering Research Council who funded the majority of the work reported in this thesis.

Contents

Chapter 1

Introduction

1.1 Specification of the problem

In recent years there has been a tendency towards the use of automated manufacturing systems which increase manufacturing production rate, reduce production costs and improve quality [1.1]. A robust and accurate tool condition monitoring system is therefore desirable in order to maintain the quality of the product and adapt to the onset of process defects such as tool breakage and wear. This is of particular importance in those industries which generate either high volume products or low volume, high value products. This thesis examines the problem of measuring tool wear in milling with particular reference to acoustic emission during the cutting process and to the surface finish of the workpiece produced.

1.1.1 Aims and objectives

An aim of this work is to establish correlations between the wear state of a milling cutter and the surface finish produced by that cutter. A further aim is to examine correlations between aspects of the rms of the acoustic emission signal produced during cutting, the spectral content of the AE signal and the wear state of the milling cutter which generated the AE. The work will be confined to finish cutting in a face milling process but it will investigate the effects of axial rake angle and workpiece material on the parameters of interest.

1.2 Insert wear

In its most basic form the metal cutting process involves the separation of a metallic chip from a parent workpiece material by the passage of one or more sharp cutting edges through the workpiece material. The chip is formed by a shearing process which takes place in the workpiece material ahead of the cutting tool. The cutting edge is formed at the intersection of two surfaces of the cutting tool known as the rake face and the flank.

This arrangement is illustrated in figures 1.1a and 1.1b for two of the cutting inserts used in this work. The inserts in figures 1.1a and 1.1b are denoted *negative rake* and *positive rake* in order to differentiate between the axial rake angles of the tool holders used in this work. Each of the negative rake inserts has eight cutting edges available for use (at each corner) and each of the positive rake inserts has four cutting edges available.

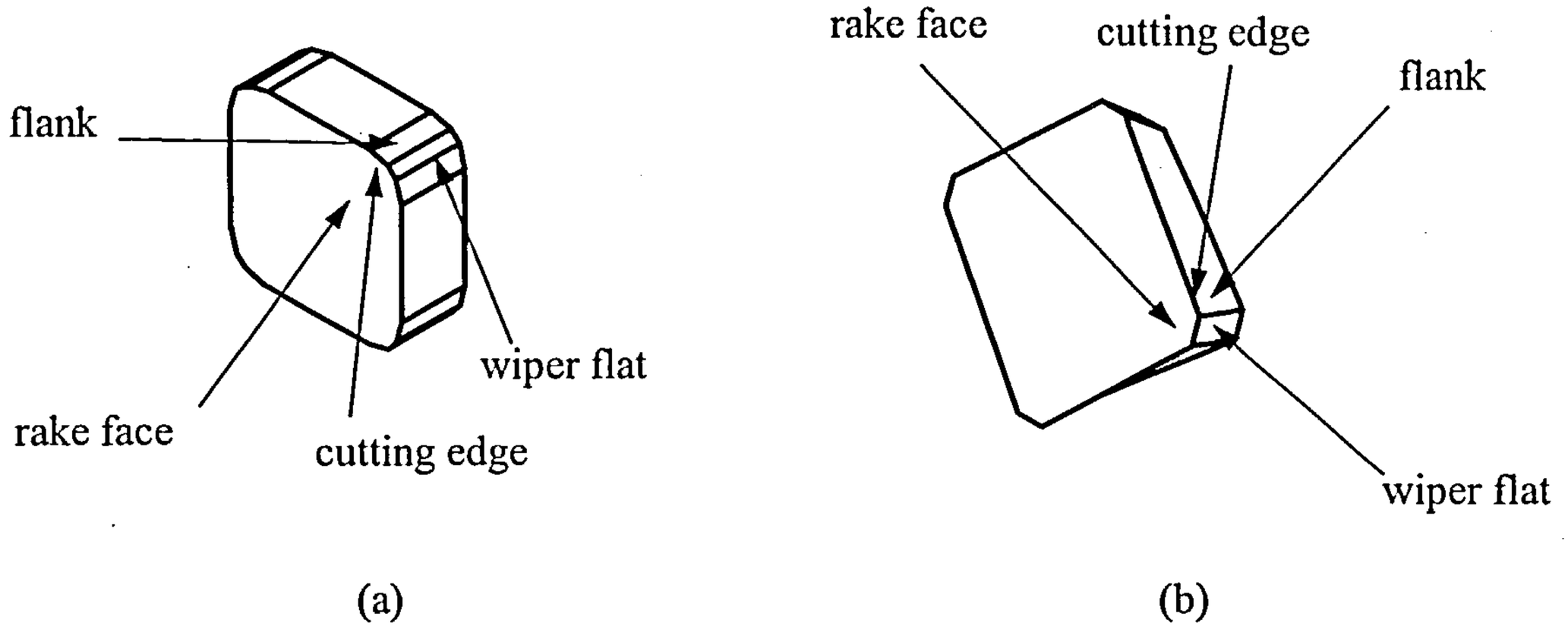

Figure 1.1 Typical cutting inserts used in this work, (a) negative rake, (b)positive rake.

The term *axial rake angle* refers to the orientation of the insert relative to a plane which is perpendicular to the workpiece as shown in figure 1.2. It may be positive or negative. The flank surface is oriented at an angle known as the *relief angle* to the workpiece surface.

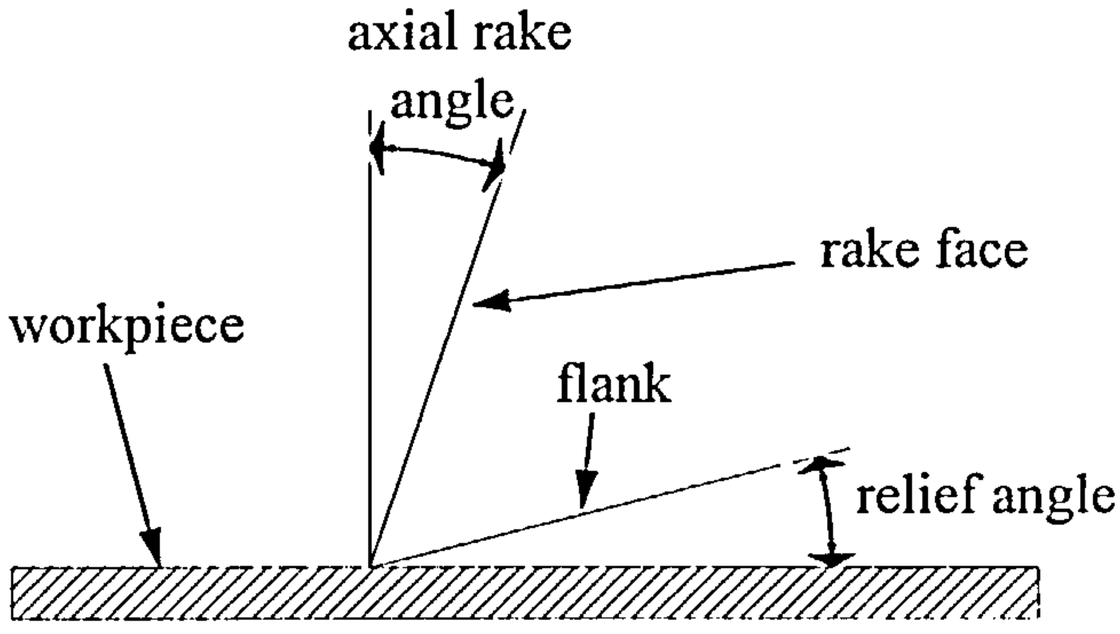

Figure 1.2 Definitions of rake angle and relief angle.

The particular geometry of a cutting tool depends on the process. In operations such as turning a single insert (cutting edge) is in contact (usually continuously) with a workpiece which rotates whereas in processes such as drilling a rotating tool with two cutting edges is in continuous contact with a stationary workpiece. This work is concerned with the face milling process in which a rotating tool with multiple cutting edges is in discontinuous contact with a workpiece which is moving in a direction perpendicular to the axis of rotation of the tool.

The material of the cutting tool must of necessity be harder than the workpiece material and ideally resistant to wear. As cutting takes place the chip moves over the rake face and the newly formed surface of the workpiece moves under the flank and it is in these regions that insert wear occurs.

The changes which take place on the insert during the cutting process are illustrated in figure 1.3. Some or all of these changes may occur during the operation depending on the cutting conditions, the insert material and the workpiece material. Typically a *wear land* develops on the *flank face*, extending from the cutting edge, which is characterised by its length V_b. Some researchers take the maximum value of V_b as being an indicator of insert wear and others take the mean value of a series of measurements as being a measure of wear. In this work the mean value of V_b is used to assess insert wear and when this parameter exceeds 0.7 mm the insert is considered to be worn out. When compared with the other possible measures of insert wear, V_b is the easiest measurement to make and this explains its overwhelming use in tool wear investigations.

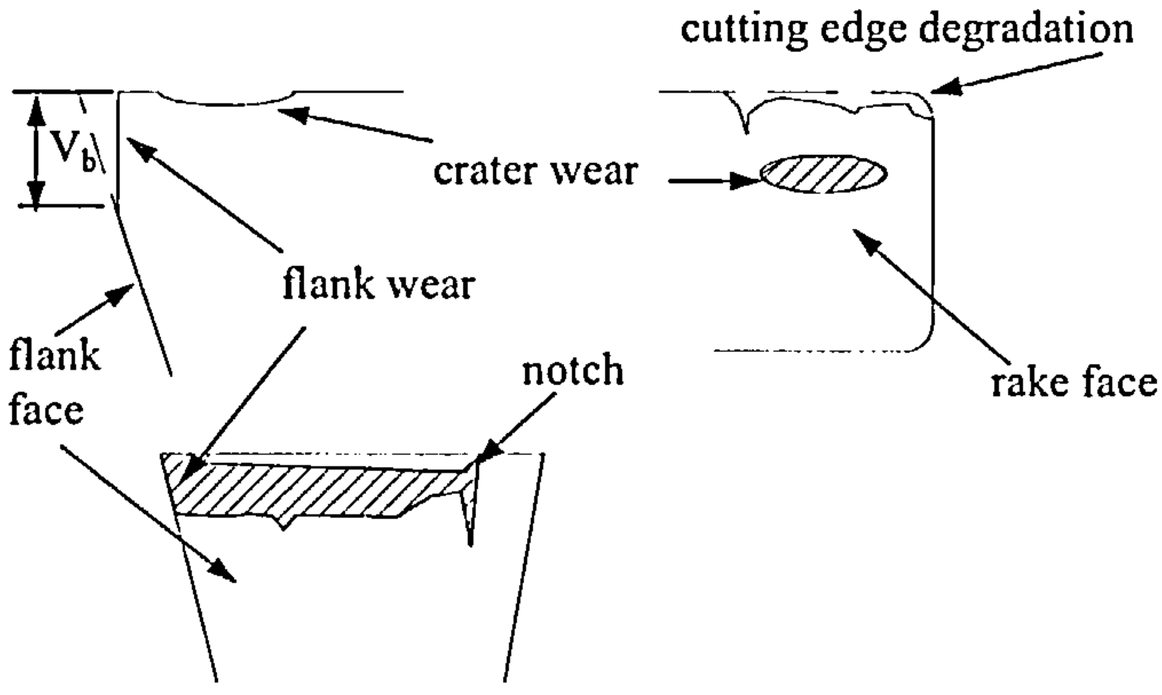

Figure 1.3 Common characteristics of insert wear

Loss of the cutting edge by *chipping* results from the high impact loading which is a distinguishing feature of the face milling operation. It is difficult to obtain a meaningful measure of this phenomenon as its effects are discontinuous and as a result it is not used as a measure of insert wear.

Crater formation may arise on the rake face of the insert displaced a small distance from the cutting edge as a result of the high temperatures associated with the frictional forces generated as the machined chip slides over the rake face. It is characterised by its maximum depth which is relatively easy to measure making it the second most common technique for assessing insert wear.

A *notch* may be produced at approximately the depth of cut on both the rake and flank faces because only part of the cutting edge is loaded during cutting. It results from a combination of factors including a complex force system at the depth of cut line and is more likely to be present when cutting materials possessing a hard outer layer. It is difficult to quantify and in consequence is not used as an insert wear indicator.

The mechanisms of tool wear will be discussed in more detail in chapter 2.

1.3 Tool wear monitoring

Broadly the monitoring of tool condition can be achieved either through direct methods which require the tool to be observed directly at intervals during the cutting process or through indirect methods in which some measurand is monitored which can be demonstrated to be sensitive to tool condition. By the nature of the process direct methods usually require an interruption to the machining process whereas indirect methods are generally continuous. Direct methods, such as those involving electrical resistance measurements or radioactive impregnation of the inserts, also suffer from the disadvantage that special inserts are required which are expensive to manufacture and which may not achieve universal acceptance because of environmental implications. Several methods of indirect determination of tool wear state in metal cutting are currently available as will be discussed in chapter 2. They include cutting and feed force measurements, vibration measurements, spindle electrical measurements and acoustic emission measurements. However none of these techniques provides a complete solution to the problems of a universal tool wear monitoring system. This is as a result of the

complex nature of the metal cutting process. For example, continuous cutting processes such as turning are likely to require different approaches to tool wear assessment than the discontinuous processes such as milling. It is also to be expected that some of the measurands used in wear monitoring will exhibit greater sensitivity to tool wear in situations such as those involving light cuts and small tools than in others. In fact it is unlikely that a single sensor will be able to be employed to monitor all metal cutting operations since a very large number of processes are involved which use a large number of cutting tools, cutting conditions and workpiece materials.

The work of this thesis concentrates on face milling which is one of the more complex metal cutting processes. The tool wear monitoring task in this process is made more difficult by the presence of multiple cutting edges and by the intermittent nature of the insert/workpiece contact which is fundamental to the process. Some of the uncertainty associated with multiple cutting edges may be removed, at least in a research environment, by the use of a single insert in a multi-insert milling cutter. However the problems of discontinuous contact still remain and in commercial practice such fly-cutting operations have found very limited application. In this work both multi-point and single point cutting are investigated.

It may be argued that the quality of a machined product is ultimately defined by the finishing process to which the product is subjected and that quality is susceptible to the wear state of the finishing tool. In order to monitor the wear state of the tool it is necessary to choose measurands which are sufficiently sensitive to long time scale degradation of the tool whilst cutting the workpiece with shallow values of depth of cut. Acoustic emission (AE) generated during the cutting process fulfils this requirement and has the further advantage that it occurs at frequencies typically above 100 kHz, significantly greater than those associated with the mechanical vibrations of the machine tool being monitored. Since the sources of AE are close to the cutting edge, AE signals may be expected to contain information on the state of wear of the insert involved in the cutting. Thus the principal requirement in using AE in a tool wear monitoring scheme is to establish a correlation between the AE signal and the wear state of the insert.

One measure of quality in a machining process is to be found in the resulting surface finish of the product. Therefore it may be considered that a measure of the surface finish

of the workpiece could be used as one aspect of a tool condition monitoring system. Until recently attempts to incorporate such a measure into a practical monitoring system have been frustrated by the requirement to remove the workpiece from the machine tool before taking profile measurements from it. However novel developments in sensor technology [1.2] have enabled surface profile measurements to be made inter-operationally with the workpiece still mounted on the machine tool. Unlike conventional profilometers this instrument does not measure absolute height variations but differential height variations from point to point on the machined surface. As a result it is difficult to extract such common surface descriptors as the centre line average, R_a, from this sensor signal but it is suited to surface analysis in the frequency domain. Thus if a relationship between some aspect of the spectral content of the machined surface and the wear state of the insert which produced the surface can be established, this may be used in a tool wear monitoring system. To ascertain this relationship it is not necessary to use this novel transducer to provide the data stream and thus for experimental purposes it is possible to employ a conventional profilometer as the data source. Part of the work of this thesis explores the relationship between the spectral content of the machined surface profile and the wear state of the cutting tool.

1.4 Workpiece and insert material properties

Since insert wear results from the intimate contact between the work piece material and the insert it is anticipated that the manner in which wear takes place will depend in part on the material properties of these contacting pairs. A wide range of cutting tool materials are available with properties which include high wear resistance, brittle fracture resistance and or high temperature stability [1.3]. In general any given tool material will not possess all of these properties. For example a material which is highly resistant to wear will not have a good resistance to brittle fracture. In this work only tungsten carbide inserts are used. This material represents a compromise between insert wear resistance, impact strength and high temperature hardness when compared with materials such as high speed steels (high impact strength, low wear resistance, reduced high temperature hardness) and ceramic materials (low impact strength, high wear resistance constant high temperature hardness). In interrupted processes such as face milling impact strength is important as is maintenance of insert hardness at the high temperatures encountered in machining. As this work is an investigation into correlations between insert wear and AE and surface

finish, a moderate amount of insert wear is desirable provided it reflects wear rates experienced in industrial applications.

As will be seen in chapter 3, workpiece mechanical and thermal properties are influential in determining AE generation and cutting forces which affect the resultant surface finish. The effects of workpiece materials on AE and surface finish were investigated by using softened En24 steel, a hardened quènched and tempered En24 steel and an austenitic stainless steel type 306 as test materials. This enabled data to be generated from materials exhibiting an industrially relevant range of machinability.

1.5 Sensor fusion

It was indicated in section 1.3 that although a range of sensors could provide data which is sensitive to tool wear in machining, there is no single sensor universally suited to a tool condition monitoring system. It is possible however to combine information extracted from several disparate sensors in a process known as sensor fusion to improve the reliability of a tool condition monitoring system. Sensor fusion may be achieved using either an expert system or an artificial neural network. An expert system uses current knowledge about the machining process and the specific machine tool being monitored to predict the wear state of the tool from sensorial data. On the other hand an artificial neural network is presented with a set of features, obtained from sensorial data, contained within which are wear sensitive patterns which the neural network learns to recognise. The learning capability of the neural network allows it to adapt to differing machining processes following presentation of the appropriate training data sets. Expert systems and artificial neural networks do not represent mutually exclusive solutions to the tool wear monitoring problem and they may be used together. In any event the acquisition of the training data is expensive for both expert systems and neural networks as will be discussed in chapter 2.

1.6 Scope of this work

This work concerns the use of acoustic emission signals and surface profile data as indicators of the wear state of inserts in a face milling process. The necessary data will be provided by *face milling experiments* performed on a CNC machine tool using En24 steel in two hardness conditions and type 306 stainless steel. The process will only involve

finish machining with a constant depth of cut for all of the experiments. Other cutting conditions will be adjusted according to the insert manufacturers instructions to ensure the use of industrially relevant wear rates.

The work will attempt to correlate the *wear state of the inserts* as characterised by the length of the flank wear land, V_b, with both the rms of the *AE signal* and the frequency content of the AE signal. The AE data will be obtained from a novel non-contacting fibre-optic transducer with a flat frequency response in the range 0 - >1 MHz thus enabling reliable frequency information to be extracted from the AE signal. It will also attempt to correlate the spatial frequency content of the milled *surface profile* with the wear state of the inserts. The spatial frequency of the surface profile will be described by the spectral content in three frequency bands: a low frequency band up to but excluding the frequency associated with spindle rotation, a kinematic band including the frequencies associated with feed per revolution and feed per tooth and a high frequency band with spatial frequencies greater than those associated with feed per tooth.

The work will further investigate the use of *fractal geometry* as a descriptor of the machined surface profile and its applicability to a tool wear monitoring system. Although fractal geometry has been used to characterise surface profiles (e.g. [1.4]) it has not been used as an indicator of tool wear state or of tool condition in general.

The application of an *artificial neural network* to the monitoring to progressive tool wear will be demonstrated. A back propagating, multi-layer perceptron will be presented with five features, two of which will be extracted from AE signals and the remaining three from surface profile signals. The AE features used will be the rms of the AE signal and the mean frequency of the signal in the range 60 kHz to 1 MHz whilst the surface profile features will be the spatial spectral content of the profile in the three frequency bands described above.

1.7 Organisation of this thesis

This thesis is organised into eight further chapters following this introduction.

Chapter 2 discusses the background literature concerning tool wear monitoring. It examines metal cutting theories discussing both analytical and mechanistic models of the

cutting process. It discusses briefly the insert wear mechanisms which occur in metal cutting and goes on to examine ways in which insert wear may be monitored. It also discusses the data processing techniques which are available for use in a tool wear monitoring system.

Chapter 3 discusses the application of the background literature to the particular problem of monitoring insert wear in face milling. It discusses surface profile generation models which are applicable to tool wear monitoring and it describes models of AE generation which show the sensitivity of insert wear to this parameter.

Chapter 4 describes the experimental arrangement used in conducting the machining tests. A description of the AE sensors and surface profilometers together with the associated data acquisition systems is presented.

Chapter 5 is concerned with the processing and analysis of the surface profile data and the establishment of correlations between insert wear as measured by the flank wear land length, V_b, and surface profile descriptors.

In chapter 6 processing and analysis of the acoustic emission data is considered and relationships between the rms of the AE signal and flank wear land length and between the mean frequency of the AE signal and flank wear land length are demonstrated.

Chapter 7 shows that the application of an artificial neural network to tool wear monitoring so that sensor fusion is achieved enhances the reliability of tool wear state recognition.

Chapter 8 will discuss the results obtained from the signal processing described in chapters 5 and 6 together with the implications for tool wear monitoring of using AE and surface profile features combined with an artificial neural network.

Chapter 9 contains the conclusions to the thesis and suggests the possibilities for further work in the field of tool wear monitoring using acoustic emission and surface finish descriptors.

1.8 Summary of new work

This work addresses the problems inherent in monitoring tool wear during face milling when finishing cuts are being made. Since these cuts are usually of shallow depth the more conventional measurands such as cutting force or spindle current are unlikely to deliver sufficient sensitivity to monitor the process.

The application of surface profile features to the problem of tool wear monitoring as discussed in chapter 5 is original. The historical difficulties encountered in measuring the profile of a machined surface profile either inter-operationally or during cutting have impeded the use of surface profile data in tool wear monitoring schemes. However with the development of the surface profile transducer described in chapter 4 it is reasonable to use surface profile data in the manner described in chapter 5.

Whilst the use of rms AE in tool wear assessment is not new its extension, in face milling, to a range of materials with differing machinability indices and the systematic investigation of differing insert geometries with natural rather than simulated wear is new. Similarly the use of AE frequency data, obtained in a manner which does not require deconvolution of the transducer response from the measured AE signal, across a range of materials and insert geometries is new. This is the content of chapter 6.

The novel application of an artificial neural network to the fusion of AE data with surface profile data to enhance the reliability of tool wear state recognition is described in chapter 7.

1.9 Published work

During the course of this work six journal papers [1.5], [1.6], [1.7,], [1.8], [1.9] and [1.10] have been published and four conference papers [1.11], [1.12], [1.13] and [1.14] have been generated. A further journal paper [1.15] is in preparation.

1.10 References

1.1) S.V. Nagalingam, G.C.I. Lin. "A methodology to select optimal system components for computer integrated manufacturing by evaluating synergy". Computer Aided Manufacturing Systems, 11(1998), 217-228.

1.2) S.R. Kidd, D.P. Hand, T.A. Carolan, J.S. Barton, J.D.C. Jones. "Measurement of aspects of surface form using an optical differential height measurement technique". Measurement Science and Technology, 7,(1996), 1579-1582.

1.3) M.C. Shaw. "Metal cutting principles". Oxford University Press, New York, 1989.

1.4) D.J. Whitehouse. "Handbook of surface metrology", I.O.P. publishing, Bristol,1994.

1.5)* T.A. Carolan, D.P. Hand, J.S. Barton, J.D.C. Jones, P. Wilkinson, R.L. Reuben. "Assessment of tool wear in milling using acoustic emission detected by a fibre optic interferometer". Transactions of the ASME, Journal of Manufacturing Science and Engineering 118,(1996) 428-433.

1.6)* T.A. Carolan, S.R. Kidd, D.P. Hand, S.J. Wilcox, P. Wilkinson, J.S. Barton, J.D.C. Jones, R.L. Reuben. "Acoustic emission monitoring of tool wear during the face milling of steels and aluminium alloys using a fibre optic sensor Part 1: energy analysis". Proceedings of the Institution of Mechanical Engineers, Part B, 211,(1997) 299-309.

1.7)* T.A. Carolan, S.R. Kidd, D.P. Hand, S.J. Wilcox, P. Wilkinson, J.S. Barton, J.D.C. Jones, R.L. Reuben. "Acoustic emission monitoring of tool wear during the face milling of steels and aluminium alloys using a fibre optic sensor Part 2: frequency analysis". Proceedings of the Institution of Mechanical Engineers, Part B, 211,(1997), 311-319.

1.8)* P. Wilkinson, R.L. Reuben, J.D.C. Jones, J.S. Barton, D.P. Hand, T.A. Carolan, S.R. Kidd. "Surface finish parameters as diagnostics of tool wear in face milling". Wear, 205,(1997), 47-54.

1.9)* P. Wilkinson, R.L. Reuben, J.D.C. Jones, J.S. Barton, D.P. Hand, T.A. Carolan, S.R. Kidd. "Surface features as indicators of tool chipping in single point face milling of Aluminium". Wear, 212,(1997), 221-228

1.10)* P. Wilkinson, R.L. Reuben, J.D.C. Jones, J.S. Barton, D.P. Hand, T.A. Carolan, S.R. Kidd. "Tool wear prediction from acoustic emission and surface characteristics via an artificial neural network". Mechanical Systems and Signal Processing 13,(1999), 955-966.

1.11)* D.P. Hand, T. Carolan, J.D.C. Jones, J.S. Barton, S. Wilcox, P. Wilkinson, R.L. Reuben. "Cutting tool condition monitoring by fibre optic interferometry". Proc. Applied Optics & Opto-Electronics 92, 53 -55, Institute of Physics.

1.12)* P. Wilkinson, R.L. Reuben, D.P. Hand, T.A. Carolan, J.S. Barton, J.D.C. Jones. "Measurement of surface profile and acoustic emission by optical fibre interferometry". Laser Metrology & Machine Performance, Lamdamap 93, D.M.S. Blackshaw, A.D. Hope, G.T. Smith (eds), Computational Mechanics Publications, Southampton 1993, 255 - 262.

1.13)* P. Wilkinson, R.L. Reuben, T.A. Carolan, D.P. Hand, J.S. Barton, J.D.C. Jones. "Tool wear monitoring in milling using non-contacting fibre optic sensors". Condition Monitoring '94,Swansea UK, March 1994.

1.14)* D.P. Hand, T.A. Carolan, J.S. Barton, J.D.C. Jones, P. Wilkinson, R.L. Reuben. "Optical fibre interferometry for cutting tool condition monitoring". Proc. Applied Optics & Opto-Electronics 1994, 159 - 160, Institute of Physics.

1.15)* M.L. Jakobsen, P. Wilkinson, D. Harvey, J.S. Barton, J.D.C. Jones and R.L. Reuben. "The effects of progressive wear on the frequency characteristic of acoustic emission acquired during face milling". In preparation.

* Publications arising from the work of this thesis.

Chapter 2

Review

This chapter describes the background in tool wear monitoring against which the work of this thesis is carried out. The currently available literature may be divided conveniently into several sub-topics; metal cutting processes and wear mechanisms, condition monitoring techniques and the use of neural computing procedures to improve the reliability of tool wear monitoring. These will be examined separately. The section on metal cutting and wear phenomena will briefly discuss metal removal processes before concentrating on the complex problems of interrupted cutting as represented by face milling. The section on monitoring techniques will consider the available range of methods by which the wear state of cutting tools may be assessed and the reasons for choosing acoustic emission and surface condition as measurands for this work will be justified. In reviewing current work on the use of artificial neural networks it will be shown that gains are to be made in the performance of a tool wear monitoring system which fuses information derived from several disparate sensors.

Some review material was considered to be more properly relevant to the chapters which deal in detail with surface generation (chapter 5), acoustic emission (chapter 6) and artificial neural networks (chapter 7) and consequently such material is presented in these chapters.

2.1 Metal cutting and wear processes

Metal removal processes are an important feature in manufacturing industry. In general these processes involve one or more cutting blades in sliding contact with a workpiece material which is caused to shear by the cutting action. The operation may involve continuous removal of material by a single cutting edge such as takes place in turning, it may involve continuous removal of material by multiple cutting edges such as in drilling or it may involve interrupted removal of material by one or more cutting edges as in grinding and milling. All of these procedures have in common the production of a chip,

which achieves intimate contact with the rake face of the cutting tool, by shearing of the parent material which passes into contact with the relief face of the insert.

In order to understand the cutting process and all the phenomena associated with it, it is useful to construct a conceptual model of the forces generated during cutting. A review of machining process modelling by Ehmann et al [2.1] identified three methodologies whereby cutting forces may be obtained. These may be categorised as analytical methods based on the work of Merchant [2.2], mechanistic and numerical methods based on the work of Martellotti [2.3],[2.4] and which in recent years have included finite element techniques and experimental methods. These divisions in methodologies are not rigid since for example both the mechanistic techniques and analytical techniques rely to a certain extent on experimentally derived workpiece material properties. Since the work of this thesis is not involved with the experimental acquisition of cutting force data but requires a mathematical model of the manner in which these forces vary with insert wear only the analytical and mechanistic techniques will be considered further.

2.1.1 Analytical Models

Among the first serious attempts to model the cutting forces Merchant [2.2] analysed the forces on the chip formed during cutting. He assumed that during orthogonal cutting the chip could be modelled as a body in equilibrium under the action of two forces; the friction force generated at the tool chip interface and the force applied to the base of the chip on the shear plane. This theory was then augmented by Merchant [2.5] with the inclusion of the plastic behaviour of the workpiece material. In this work it was shown that by considering the shear strength of the workpiece material to be a simple function of the normal stress present on the shear plane, a considerable improvement in the ability to predict shear plane angle and hence cutting forces was achieved. It was assumed that rate of shear, shearing strain and cutting temperatures were only secondary effects and were therefore neglected. However Kobayashi et al [2.6] showed that existing metal cutting theories based on the Merchant model were not completely supported by experiment. In 1968 Fenton and Oxley [2.7] included the effects of temperature and strain rate in metal cutting theory. Their model which was based on the work of Merchant incorporated the

effects of strain, strain rate and temperature together with the flow stress characteristics of the workpiece material.

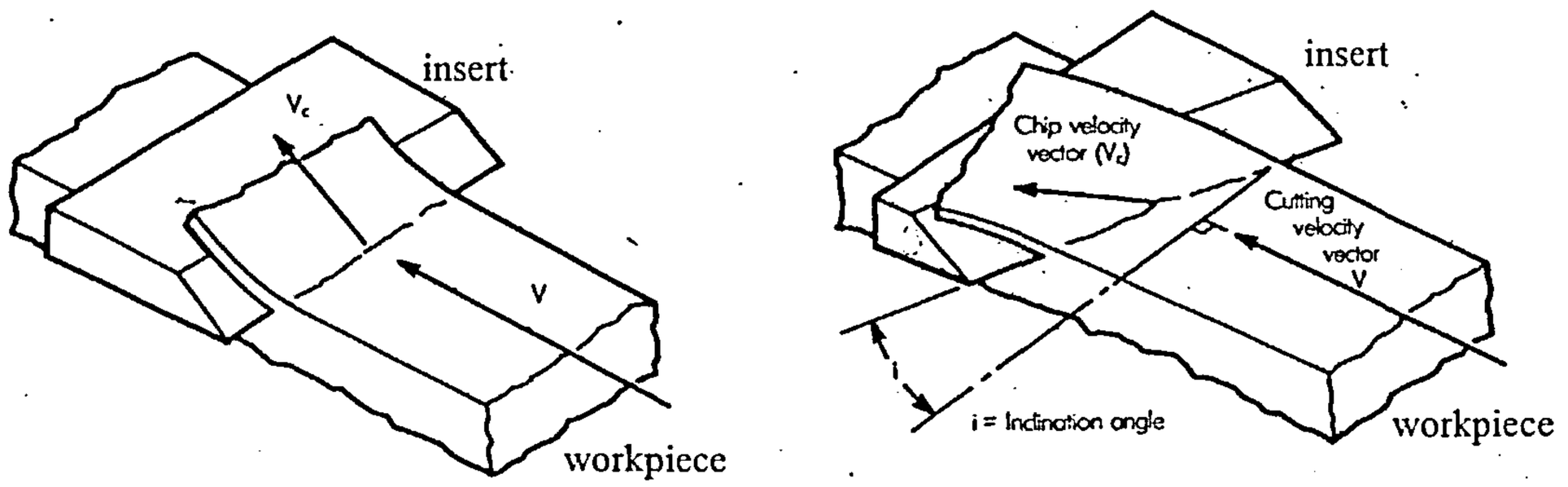

(a) (b)

Figure 2.1 Cutting modes. (a) Orthogonal cutting (b) Oblique cutting. after Drozda and Wick [2.8]

The models discussed in the previous paragraph have all concerned orthogonal cutting where the velocity of the workpiece material is orthogonal to a single cutting edge as shown in figure 2.1a. Whilst most of the published modelling work is performed with the assumption that orthogonal cutting is taking place, very few practical machining processes meet the requirements of orthogonal cutting. Truly orthogonal machining processes include parting operations and turning of a tube. Although an orthogonal cutting model represents a reasonably good approximation to the performance of a cutting tool, most machining processes are more faithfully represented by models of oblique machining in which the velocity vector of the workpiece material is inclined to the cutting edge as shown in figure 2.1b. This representation transforms the force modelling problem into a three dimensional problem which can be analysed by two dimensional theory applied on a given plane from which the radial, tangential and axial components of cutting force may be extracted by an appropriate co-ordinate transformation [2.8]. Drilling and face milling are the two most common machining processes in which oblique cutting exists. However drilling is a complex cutting operation in which cutting conditions vary along the cutting edge from the axis of the drill to its periphery. The metal removal process in drilling is illustrated by consideration of a two flute twist drill. Three regions of action may be identified: (a) at the periphery of the drill the cutting edges (lips) produce

chips by shearing, (b) on the axis of the drill, where the cutting edges are joined by a web and the cutting speed is zero, metal is extruded and (c) at other positions on the web metal is removed by cutting [2.9]. Whilst the cutting actions at the web and lips clearly affect the torque required by the drilling machine, all the metal removal process will influence the thrust force required. An analysis of the drilling process should therefore be considered as a three dimensional cutting problem which is more complex than an oblique cutting problem.

Pandey and Shan [2.10] used a shear plane model to predict the maximum forces to be expected in peripheral and face milling. These predictions were based on the maximum thickness of the undeformed chip and considered the problem as one of oblique cutting. However no account was taken of the effects of temperature variation experienced in cutting or of workpiece material property changes with strain or strain rate. Lin and Oxley [2.11] applied the Fenton and Oxley theory to oblique cutting by assuming that chip motion in a plane normal to the cutting edge is orthogonal which allows calculation of force components in directions parallel to the direction of cutting $(F_c^{'})$ and normal to the direction of cutting $(F_T^{'})$ in the normal plane. Lin and Oxley further show that from a knowledge of the inclination angle i, the chip flow angle η and the friction angle λ_n, defined in figures 2.2a and 2.2b, it is possible to calculate the forces in the direction of cutting (F_c), in the direction normal to the direction of cutting (F_T) and in a direction normal to these two forces (F_R) as shown in equations 2.1.

$$\begin{aligned} F_c &= F_c^{'}\cos i + P\sin i \\ F_T &= F_T^{'} \\ F_R &= F_c^{'}\sin i - P\cos i \end{aligned} \qquad (2.1)$$

where P is the force component normal to the normal plane given by

$$P = F^{'}\tan\eta = R\sin\lambda_n\tan\eta = \sqrt{\left[\left(F_c^{'}\right)^2 + \left(F_T^{'}\right)^2\right]}\sin\lambda_n\tan\eta \qquad (2.2)$$

where $F^{'}$ is the friction force at the tool-chip interface and R is the total reaction at the tool chip interface.

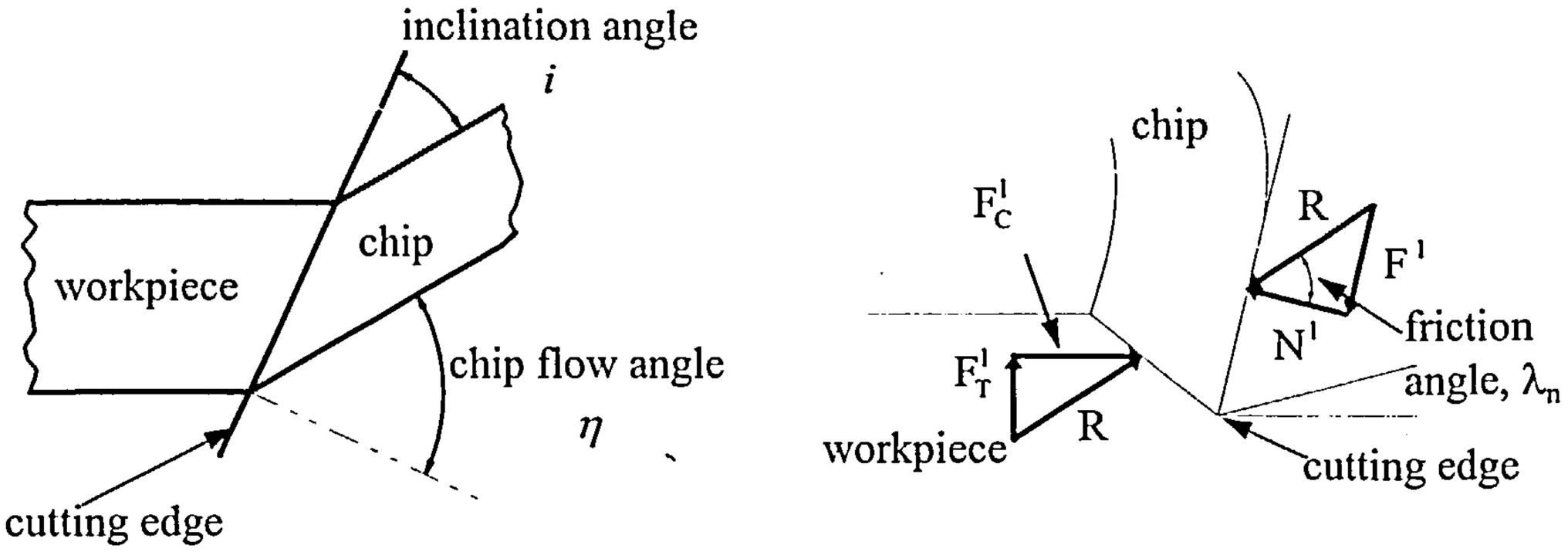

(a) (b)

Figure 2.2 (a) Plan view of cutting process showing angles i and η (b) View of forces in plane perpendicular to cutting edge and workpiece showing angle λ.

The authors in this work did not consider the effects of temperature rises at the shear plane and the tool-chip interface on the material properties of the workpiece. The flow stress σ of the workpiece material was calculated from:

$$\sigma = \sigma_1 \varepsilon^n \tag{2.3}$$

where σ_1 is a constant, ε is the strain and n is a strain hardening index. The parameters σ_1 and n were to be recognised to be functions of temperature and strain rate but for the range of experimental work examined in this paper they were considered to be strain rate dependent only. In later work Hastings et al [2.12] allowed the workpiece material properties to be influenced by temperature and replaced the shear plane concept of Merchant by a more realistic primary shear zone surrounding the shear plane and a secondary shear zone at the tool-chip interface. The shear plane near the centre of the primary shear zone and the tool-chip interface were assumed to be directions of maximum shear stress and shear strain rate. This modification makes it possible for both the average temperature rise in the chip and the maximum shear strain rate at the tool-chip interface to be calculated. Hu et al [2.13] applied this model directly to a prediction of cutting forces generated in bar turning and Young et al [2.14] used it specifically on face milling force prediction. Zheng et al [2.15] have also used the Hastings-Oxley model to estimate cutting forces in multi-insert face milling. The authors included the effects of both radial and axial insert runout. From the foregoing it may be seen that the shear plane/shear zone

model of metal cutting is a well established means of estimating cutting forces in machining processes. In the work described in this thesis the tool paths are simple linear translations and the workpiece geometry has a simple rectangular planform and therefore the model described by Hastings et al is used. This enables the determination of the change in shear plane angle with insert rake angle so that variations in the rms of the acoustic emission signals and the mean frequency of these signals may be calculated as described in chapter 3.

2.1.2 Mechanistic Models

The models discussed in the preceding paragraph involve the use of some parameters such as the thickness of the shear zones which are not readily available from published literature or from experiment. Although these models were useful in determining the variation in shear plane angle with wear as discussed in chapter 3, a second approach based on Martellotti's analysis [2.3], [2.4] of the milling process was used in this work to model cutting forces in face milling. Martellotti established that cutting forces in milling were, to a good approximation, proportional to the thickness of the undeformed chip. Koenigsberger and Sabberwal [2.16] extended this concept by proposing that the tangential component of the cutting force was proportional to the product of undeformed chip cross-sectional area and an empirically derived specific cutting pressure. The specific cutting pressure is defined as the ratio of the measured tangential cutting force to the cross-sectional area of the undeformed chip [2.8]. It is a property of the workpiece material and values of specific cutting pressure have been established from cutting experiments. DeVries [2.17] has demonstrated that specific cutting pressure values may be readily obtained from the specific cutting energy (unit power) of the workpiece material. This parameter, which is defined as the energy required to cut a unit volume of the material, is available for a wide range of materials [2.18]. Fu et al [2.19] used this approach to devise a model which predicts instantaneous cutting forces based on average chip thickness. Gu et al [2.20] extended the Fu model so that it could deal with complex workpiece geometry which could include the presence of holes. They also considered variable cutter paths and the effects of system errors such as spindle tilt. Cheng et al [2.21] demonstrated that the experimental values of specific cutting pressure were dependent not only on undeformed chip thickness but also on cutting speed, length of cut

and rate of change of chip thickness. When compared with cutting forces estimated from the Fu model the authors claim a considerable improvement in the average error between predicted and measured forces for both fly-cutting and multi-point cutting in face milling. However the Cheng model is too dependent on empirical constants to be accepted as a general model of cutting forces. Therefore the cutting force predictions in this thesis will be based on the original model proposed by Fu et al [2.19].

2.1.3 Wear Mechanisms

Several criteria have been identified as being useful in determining the useable life of a cutting insert [2.8]. These may be loosely classified as shown in table 2.1.

Life criterion	Characterisation
1) Complete failure	Insert unable to cut
2) Preliminary failure	Highly burnished areas on workpiece surface indicating rubbing
3) Flank failure	Area of wear land on flank exceeds a specified value. Usually characterised by the length of the wear land.
4) Finish failure	Sudden changes in surface finish
5) Size failure	Unscheduled changes in dimensions of machined part.
6) Cutting force failure	Increases in cutting force or consumed power.
7) Thrust failure	Increase in thrust force on the tool, indicative of end wear.
8) Feed force failure	Increase in force required to feed the workpiece, indicative of flank wear.

Table 2.1 Common tool life criteria as identified by Drozda and Wick

In a research environment any of these measures may be used to determine the end of the life of a cutting tool, but clearly in a production arena where the product is important, a life criterion which prevents damage to either the product or the machine tool is essential. This would suggest that any combination of the criteria (3), (6) and (8) is to be preferred to the other criteria which imply that the machine tool is in danger or that the product tolerances will not be met. In the work of this thesis the flank failure criterion will be used to determine insert life. This failure will be characterised by a flank wear land which has a length (V_b) in excess of 0.7 mm.

It is possible to distinguish six mechanisms of insert wear from the publications of Drozda and Wick [2.8] and Shaw [2.9]. *Adhesive wear* takes place when two surfaces, such as those of the chip and the insert, are brought together at high pressure and

temperature. Welding of the surfaces occurs and if the local strength of the insert material is less than that of the weld, tool material will pass away with the chip when fracture occurs. This type of wear is also associated with the formation and subsequent fracture of a built-up edge. Gu et al [2.22] identify this type of wear as occurring at relatively low cutting speeds. *Abrasion* occurs when hard particles on the surface of the chip or workpiece move across the tool façes and remove tool material. Some of the hard particles which cause this type of wear may also originate as a result of the collapse of a built-up edge. Gu et al [2.22] identify this type of wear as taking place at higher cutting speeds than those which cause adhesion wear although both types of wear are possible at these elevated speeds. *Diffusion wear* requires the presence of high temperatures for its activation. This type of wear results in the diffusion of atoms from an area of high concentration along a concentration gradient to an area of low concentration. For example the carbon atoms of a tungsten carbide lattice may diffuse from the lattice to the chip when machining steel at high speed [2.9]. This often results in the formation of a crater on the rake face immediately behind the cutting edge. *Chemical wear* results from the presence of suitably active chemical compounds. If this wear occurs the chemicals responsible are generally to be found in the cutting fluid or it may be caused as a consequence of galvanic action. *Mechanical fatigue* is a phenomenon which results from continuous loading and unloading of an insert. This is a feature of intermittent cutting processes such as face milling where the inserts regularly impact on the workpiece. Gu et al [2.22] observed mechanical fatigue induced cracks in the insert flank face running parallel to the cutting edge. Similarly thermal fatigue is a consequence of the rapid heating and cooling cycles which are applied to the inserts during machining. This is again a feature of face milling operations and Gu et al [2.22] detected thermally generated fatigue cracks running both perpendicular and parallel to the cutting edge.

It has been observed that when machining soft steels or other materials with a powerful inclination to strain hardening at high temperatures *groove wear* will result [2.9]. The causes of groove wear are complex and not fully understood but it is believed to be a temperature related phenomenon. In any event their presence on the cutting edge and flank face are a source of surface roughness on the machined surface.

In the course of normal machining processes, the wear processes described in the preceding paragraphs do not occur in isolation. It is to be expected that the actual wear mechanism for a machining insert will be a combination of all these basic processes.

2.2 Tool wear monitoring

A reliable tool wear monitoring system may be considered as comprising three basic elements: a *sensing element* to measure some aspect of the wear process, a *signal processing element* to extract useful information from the sensor data and a *decision making element* to assess the wear state of the cutting tool based on information from the signal processing element. Tool wear monitoring techniques may be loosely classified into direct or indirect methods, largely based on the sensing element employed. In direct techniques some property of the worn insert such as the length of the flank wear land length, V_b, or a crater dimension is measured physically. This often involves an imaging system such as a TV camera, a photograph or measurements may be taken microscopically. Figure 2.3 illustrates a typical worn insert. The assessment of the wear state of such an insert requires a physical measurement of the flank wear land.

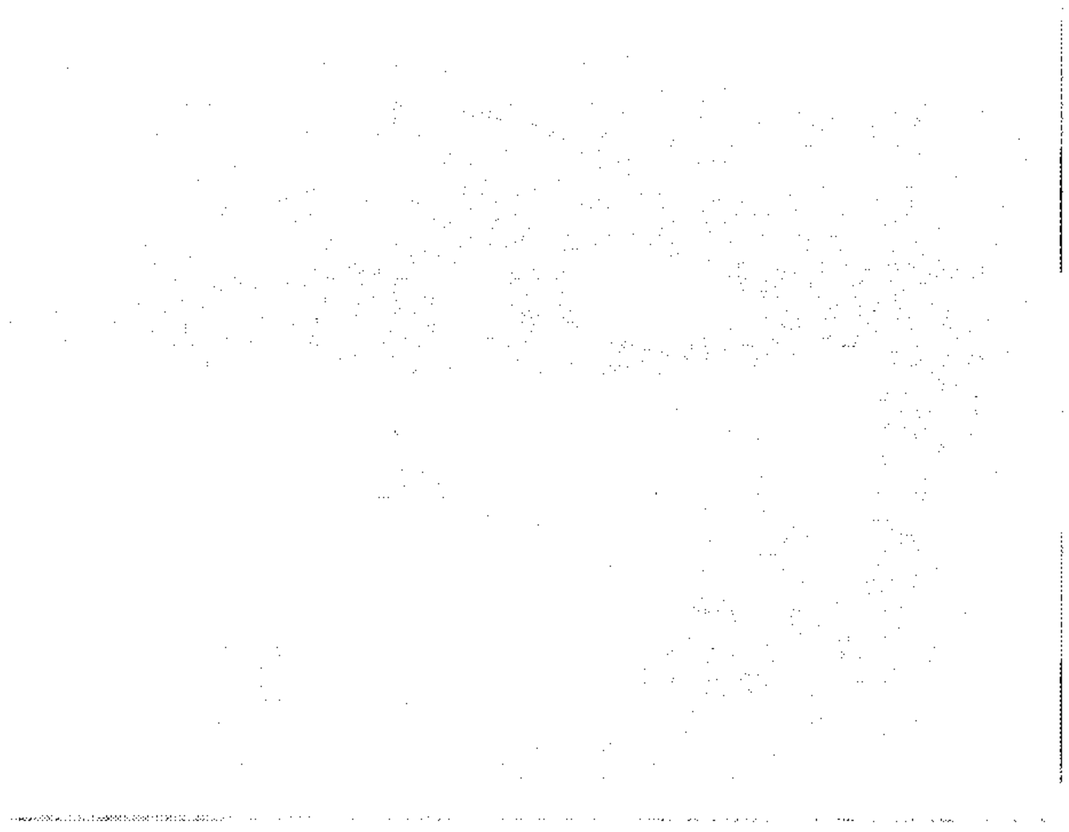

Figure 2.3 A typical worn negative rake insert.

Clearly this would be disruptive of a smooth machining operation as regular breaks in the process would be required to allow the necessary examination of the inserts resulting in extended manufacturing times. In an automated machining environment the measurements could be made automatically using image analysis techniques [2.23] but

data acquisition would be complicated by the hostile surroundings in which the acquisition hardware would be required to operate. From this it can be seen that indirect methods of tool wear monitoring are likely to be easier to implement.

Indirect methods of tool wear monitoring involve the sensing of some physical phenomenon which is known to correlate with insert wear. Cho et al [2.24], Dimla [2.25] and Prickett and Johns [2.26] have identified the most common approaches which are currently used in monitoring metal cutting processes. These are listed in table 2.1 together with an indication of the monitoring outcome achievable with each technique.

Monitoring Technique	Tool condition sensed
Cutting forces	Wear, insert breakage, chatter
Spindle power, current or torque	Wear, insert breakage
Tool temperature	Wear
Acoustic emission	Wear, insert breakage, insert chipping
Vibration (acceleration)	Wear, chatter
Surface finish parameters	Wear, chatter

Table 2.2 Monitoring techniques used in tool fault detection.

2.2.1 Sensing elements

In this section a brief examination of the published work in each of the monitoring technique areas listed in table 2.2 will be made.

Cutting force

Many researchers have investigated the relationships between cutting force measurements and insert wear in a variety of machining processes. Tarn and Tomizuka [2.27] have shown that it is possible to recognise tool breakage in end milling of AISI 1060 steel by monitoring cutting force. They showed that it was possible to differentiate between tool breakage and changes in cutting conditions by consideration of changes in the maximum force level in a tooth engagement period, the total force excursion in the same period, incremental force changes between consecutive spindle rotations and the ratio of forces between insert engagements. Altintas and Yellowley [2.28] employed cutting force measurements to detect tool breakage in milling. These authors showed that it was necessary to extract transient effects occasioned by insert entry to and exit from the workpiece from their force data. Similarly precautions had to be taken in eliminating the

effects of radial runout which could be confused with tool breakage effects from their data. After this data processing the authors established a correlation between time averaged force variations and tool breakage. In experiments on single point face milling of aluminium Lin and Yang [2.29] showed that a relationship between average cutting force coefficients and the length of the flank wear land exists. They also showed that depth of cut had a significant influence on the measured force coefficients. Lin and Lin [2.30] extended the work of Lin and Yang to include multi-insert cutting of aluminium confirming the earlier conclusions. Also in this work the authors employed a four layer back propagating neural network with features extracted from force signals to improve prediction of tool wear state. Choudhury and Rath [2.31] established a similar correlation between tangential force coefficients and flank wear when milling C45 steel with a multi-point cutter. Again it was shown that depth of cut had an influence on the force coefficients. Drozda and Wick [2.8] give an empirical expression which relates cutting forces F, feed per revolution s, and depth of cut d.

$$F = C_F s^{0.8} d \tag{2.4}$$

where C_F is a constant depending on the workpiece material and the true rake angle of the tool.

From this it can be seen that in finish cutting where the depth of cut is small, the cutting forces are likely to be small. The subtle changes in these cutting forces resulting from flank wear are small and therefore it can be argued that although cutting force measurements are useful in monitoring tool wear they are of limited application in finish machining. This will be particularly true in interrupted cutting operations such as face milling where the small changes in cutting force due to flank wear will be contaminated by large forces associated with multiple insert impacts occurring at insert entry and exit from the workpiece. Work by Taraman et al [2.32] appears to confirm this in finish turning where it was observed that increases in feed force due to flank wear were so small that difficulties were encountered in identifying them. In this work the authors recommend that feed force measurements should not be used to indicate flank wear levels in finish turning.

Spindle power

Electric power consumed by the spindle motor, torque developed by the motor and motor current are all inter-related These quantities are in turn dependent on the cutting forces and thus only one of them need to be measured by a tool condition monitoring system [2.25]. Shuaib et al [2.33] used a specially designed dynamometer mounted between the spindle and tool to measure torque vàriations experienced in cutting. This data was used to identify the cutting process dynamics. Stein and Wang [2.34] analysed the power consumed by an AC induction motor which formed the part of the drive train of a CNC milling machine. They concluded that under steady state conditions the input power is linearly related to the motor torque. They also concluded that, since for a given machining operation the spindle speed is sensibly constant, the relationship between input power and motor torque could be used to monitor dynamic cutting performance. Jones and Wu [2.35] have also used a system which continually monitors the power consumed by an electric motor during machining processes. This device operates in two modes: a learning mode and a monitoring mode. In the learning mode data is gathered on the power consumed in a series of test cuts. This data, after processing, is used to set thresholds on the power consumed, the crossing of which is deemed to indicate a worn tool in the monitoring mode. This monitoring system suffers from the disadvantage that a series of learning cycles will be required for each set of cutting conditions which are likely to be encountered since the power consumed and hence the thresholds vary with cutting conditions. Measurements of the feed drive electrical parameters have also been used to monitor tool wear. Altintas [2.36] has used the feed drive current to indicate tool breakage in milling operations. Altintas identified light cutting processes such as finish milling as being difficult to monitor by this system since the drive friction forces were of the same order as the cutting forces. A concern expressed in both the papers by Altintas and by Stein and Wang [2.34] was that the bandwidth of the servo drives imposed a limitation on the use of electrical measurements in tool wear monitoring. Li et al [2.37] have used measurements of feed motor current to represent the feed component of cutting force in turning. They then established the functional dependence of cutting force on tool wear and obtained a difference equation to establish the relationship between the two. Comparison of successive force estimates could then be used to identify the onset of

unacceptable wear. The authors concluded that this system was industrially viable for all but light cutting operations.

From the previous paragraph it can be seen that electrical measurements taken from the machine tool can be used to monitor tool wear state in a wide range of machining processes. Most investigators have used the electrical measurements to establish a relationship between cutting force and the electrical parameter measured and therefore these electrical measurements may be assumed to suffer from the same disadvantages as force measurements. The most serious of these drawbacks, from the point of view of this thesis, is the unreliability of making the relevant measurements when light cutting operations such as finish milling are being performed.

Tool temperature

Kapoor and Nemat-Nasser [2.38] have shown that almost all the energy consumed in metal cutting is converted to heat. Therefore it would appear that temperature measurements could be used to monitor tool wear. A large amount of research effort has been expended in producing analytical models of temperature variations in metal cutting (for example [2.39], [2.40]) though little experimental evidence has been obtained to verify these models. However Stephenson and Ali [2.41] have attempted to predict tool temperatures in interrupted cutting and to substantiate their model with experimental data. These authors measured temperatures by using a tool-chip thermocouple when it was possible to gain access to the tool-chip interface and a non-contacting infrared video system when it was not. Although their model was qualitatively validated by these measurements it was not possible to predict the measured temperatures from it. This may be accounted for partially by the difficulties encountered in obtaining the temperatures at the cutting edge. The infrared probe was affected by the stream of chips leaving the workpiece and only the average temperature of this stream was measured by the probe. Da Silva and Wallbank [2.42] claim that the tool-chip thermocouple technique is useful in showing the effects of cutting conditions but that the absolute values of temperature recorded are inaccurate. Young [2.43] has used an infrared thermographic technique to investigate the relationship between the chip back (the chip-air interface) temperature and flank wear in turning. He showed a strong correlation between the temporal variation of maximum temperature measured and the temporal variation of flank wear. It was not possible to measure the temperatures at the cutting edge with this technique and it is

unlikely that it could be employed in processes where the cutting edge is in motion, such as in milling, instead of the workpiece. Temperatures have also been measured on the rake face by means of a thermocouple inserted into the tool close to the cutting edge [2.9]. It is unlikely that such a system could be used to monitor temperatures in milling because of the difficulties in retrieving the measurements from the rotating tool.

Temperature measurements have been used with varying degrees of success to monitor tool wear in a research setting. The techniques employed have resulted in the measurements of average temperatures contaminated by extraneous chip temperatures (IR techniques), the requirement to gain access to the tool-chip interface (tool-chip thermocouples) which restricts the machining process to which the technique may be applied or the production of special inserts (embedded thermocouples) which would add cost to the process. As a result it is unlikely that temperature measurements will be used routinely in industrial tool wear monitoring.

Acoustic emission

Wadley and Mehrabian [2.44] define acoustic emission (AE) as the elastic waves emitted by sudden localised changes in stress from the formation of cracks, plasticity and phase transformations. Measurements of AE have been used in a wide range of non-destructive testing environments to locate flaws in structures subjected to stress. They have been used with some success to detect defects in fabrication processes and to inspect engineering structures [2.45]. In fields outside manufacturing processes there is interest in using AE measurements to detect seismic activity along geological fault lines [2.46]. AE has many features which make it an attractive candidate for inclusion in a tool wear monitoring system. The AE signals are emitted by the mechanisms which govern the cutting process and they are emitted close to the cutting edge which is to be monitored. The emissions are high frequency phenomena typically containing components in the range 60 kHz to 1 MHz and they are present in an environment where the background noise created by other aspects of the machining process contains frequencies of less than 50 kHz. This makes the contamination of the recorded AE signals by machining noise unlikely. However the signals suffer from attenuation and reflection at material interfaces such as those between the workpiece and any clamping devices and therefore care has to be exercised in locating AE transducers. Conventionally AE has been measured using contacting piezo-electric transducers located as close to the source of AE generation as possible. In milling this

introduces the additional complication of changing transmission path lengths if the transducer is not mounted on the headstock of the machine and of complex transmission paths if it is. Jakobsen et al [2.47] have reported some success in obtaining AE signals from the rotating tool holder using a fibre-optic probe thus reducing transmission path complications.

Because of the separation between ambient noise and the AE signals, monitoring of AE signals would appear to be better suited to tool wear monitoring in finish machining than the other approaches described in this section which involve poorer signal to ambient noise ratios when light cuts are being taken. Dolinsek and Kopac [2.48], recognising the problems associated with finish turning, have used an AE transducer in monitoring tool wear in such a process. In an industrial setting Jemielniak [2.49] has identified AE sensors as being ideally suited to detecting wear related phenomena in applications which generate small cutting forces.

In the work of this thesis acoustic emission measurements are used as one of the sensing mechanisms to assess tool wear state. As a result it is considered more appropriate to discuss the theoretical aspects of AE and tool wear monitoring in detail in chapter 3 and to discuss the results of application of AE to tool wear monitoring in chapter 6.

Vibration and acceleration

Acceleration measurements are relatively easy to make in tool wear monitoring using small piezo-electric accelerometers. As in the case of AE measurements it is desirable to place the transducer close to the source of the vibrations which are generated by inserts which are wearing. However they are sensitive to noise arising from the drive train of the machine tool and from other sources unrelated to tool wear and this will lead to poor signal to noise ratios in a machining environment. Braun and Lenz [2.50] report that there is distinct separation between the frequency content of the background noise signals (usually less than 2 kHz) and the frequency content of the wear related signal (up to 50 kHz) and thus appropriate signal processing may result in significant noise rejection. The authors measured accelerations generated in single insert milling of 1060 AIAI steel plate. They high pass filtered acceleration signals above 25 kHz and extracted a range of acceleration features using the resulting signal in the range 25 kHz to 50 kHz (the limit imposed by their accelerometer). They also suggested that the technique could be

extended to multi-point milling. However in multi-point interrupted cutting it is to be expected that the acceleration signals would be dominated by multiple entry and exit components making the signal to noise problems acute. This will be exacerbated in the case of finish milling where the signal to background noise ratio is even more unfavourable.

As a result of the nature of the milling process acceleration measurements are more likely to be used in monitoring tool wear in continuous processes such as drilling and turning. For example, El - Wardany et al [2.51] used a time domain analysis of an acceleration signal in the form of the kurtosis of the time series and a spectral analysis of the signal to identify both tool wear and tool breakage in drilling. As a further example, Lim [2.52] showed a correlation between the amplitude of the acceleration signal and the length of the insert wear land V_b in turning.

Surface finish

Measurement of a machined surface finish has been thought of as possessing attributes of both direct and indirect modes of measuring tool wear. In order to make measurements of the surface characteristics it has been necessary to stop the machining process and remove the workpiece from the machine tool to place it in a profilometer; these are the characteristics of a direct method of measuring tool wear. From the profile measurement it is then possible to infer the state of the cutting tool which produced the surface, thus exhibiting the characteristics of an indirect method of assessing tool wear. Clearly this is not a practical augmentation to a tool condition monitoring system and as a result little published work is available on characterising machined surfaces with a view to using the information in a tool wear monitoring system. However Kidd et al [2.53] have described a fibre-optic interferometer which may be used to make non-contacting differential height measurements of machined aluminium surfaces without the necessity of removing the workpiece from the machine tool. Although this instrument is used inter-operationally, it enables surface finish measurements to be incorporated into a tool wear monitoring scheme. The nature of operation of the instrument does not allow easy extraction of conventional surface finish features such as R_a or R_t but information on the spatial spectral composition of the machined surface may be readily determined from the interferometer measurements. Wilkinson et al [2.54], [2.55] have shown that spatial spectral information obtained from profiles measured using both a conventional

contacting profilometer and a scanning white light interferometer will yield information regarding the wear state of inserts in face milling. Coker and Shin [2.56] have made in-process measurements of surface finish using an ultrasonic profilometer. They calculated R_a values for surfaces produced by single point milling of free machining type 6061 type aluminium and achieved some correlation with tool wear. However, as discussed in chapter 3, single number measures of surface finish such as R_a depend on the location on the machined surface at which the measurement is made and are therefore unreliable as tool wear indicators. As a result of this the work of this thesis will examine the use of surface profile data in tool wear monitoring applying the techniques of Wilkinson et al.

2.2.2 Data processing

It can be seen from table 2.2 that three of the phenomena of interest in a machine tool monitoring system are insert wear, insert breakage and chatter. Chatter and insert breakage are sudden events which must be recognised by the monitoring system quickly whereas insert wear results in a prolonged, subtle degradation of the cutter performance which does not require swift identification. The signal processing strategy must be chosen accordingly. Methods which impose a heavy computational burden on the monitoring system are unsuitable for monitoring chatter and insert breakage as are inter-operational measurements such as those currently used to assess surface finish. However these techniques will detect tool breakage and chatter although with insufficient alacrity to prevent damage to the tool and/or workpiece. Detection of insert wear may be achieved by monitoring trends in the measured data which evolve over a relatively long period and therefore the computational burden and speed of detection are of lesser importance.

There are four basic approaches to extracting information on tool condition from sensor signals obtained during cutting. These are listed in table 2.3.

Technique	Characteristic	Suitability
Time series modelling	Comparison of measured data with predictive model	Wear Breakage
Time series analysis	Fault signatures Amplitude analysis Statistical analysis	Breakage Wear Chatter
Spectral analysis	Fast Fourier transform Walsh functions	Wear
Dual feature analysis	Wavelet transforms Wigner transforms	Wear Chatter

Table 2.3 Signal processing techniques commonly used in tool condition monitoring.

The use of time series modelling techniques requires the generation of a predictive model which either relates the measurand directly to the length of the flank wear land [2.29],[2.30],[2.31] or predicts a value of the measurand which may be compared with the actual value of the measurand [2.36]. The former approach is more usually applied to tool wear monitoring since it will predict wear land length directly and the latter is more applicable to insert breakage detection since abrupt changes in the differences between actual and model parameter values are readily observable. In milling there is usually a time delay of the order of one revolution of the cutter between the occurrence of insert breakage and its recognition by the monitoring system [2.26].

Time series analysis techniques are concerned with the calculation of some attribute of the measurand such as its rms value, its amplitude variation or other statistical properties. Comparison of this property with a predetermined threshold enables the establishment of the occurrence of a short time scale event such as insert breakage [2.28] whereas examination of the trend of the property with time [2.52] allows an estimation of insert wear to be made. It is necessary to establish the thresholds which indicate an unusual occurrence by experimentation before implementation of the tool wear monitoring system and, as these may vary between processes and even within processes as cutting conditions are varied, the generality of application of these techniques may be limited.

The nature of FFT calculations means that spectral analysis techniques are used almost solely for tool wear assessment because of the relatively long time period over which tool wear develops [2.26]. El-Wardany et al [2.51] used the spectral content of acceleration signals to detect wear in drilling and Carolan et al [2.57] successfully used the spectral

content of AE signals to monitor insert wear in face milling. Wilkinson et al [2.54] showed a correlation between the spectral content of surface profiles and the length of the insert flank wear land in face milling. In all of these references the length of time required to calculate the fast Fourier transforms on which the methods were based restricted their use to detecting insert wear. Further, as the procedure used by Wilkinson et al requires inter-operational measurement of the surface profile practical detection of insert breakage is precluded.

As an alternative to Fourier analysis, Rao et al [2.58] have applied Walsh functions to force measurements in attempt to monitor insert wear in milling. Walsh functions are a set of orthogonal rectangular waveforms which take amplitude values of +1 and -1. The continuous Walsh function is defined by [2.59]:

$$WAL(n,t) = \prod_{r=0}^{p-1} (-1)^{n_{p-1-r}(t_r + t_{r+1})} \qquad (2.5)$$

where n is the number of zero crossings of the function occurring in time interval t and N is the number of terms in the Walsh function defined by $N = 2^p$. Using the orthogonality property of this function it is possible to express a time series $x(t)$ as the sum of a series of Walsh functions in exactly the same manner as is performed with sine-cosine series in Fourier transforms. i.e.

$$x(t) = a_0 WAL(0,t) + \sum_{1}^{N-1} a_n WAL(n,t) \qquad (2.6)$$

where the a_i are the coefficients of the Walsh transform. This transform is more suited to extracting spectral information from time series containing sharp or pulse components than is the Fourier transform. Rao et al argue that force signals generated in milling possess some of these characteristics and that therefore Walsh functions are more applicable to analysing force signals than are Fourier transforms. Their results showed a greater variation in the harmonics of the spindle speed obtained from Walsh processing than in those obtained from Fourier processing. However it was not obvious that this would give more information about the wear state of the inserts as characterised by the length of the flank wear land when applied to surface profiles

Zheng and Whitehouse [2.60] have investigated the use of the Wigner distribution as applied to surface profile measurements to determine the condition of a lathe. They concluded that the frequency information contained in the Wigner distribution was useful in monitoring the lathe and the spatial information was useful in determining the functional performance of the workpiece. In applying this technique to the work of this thesis it was judged that the computational burden involved in calculating the Wigner distribution was too great to be used if only the wear state of the insert were required.

The application of wavelet decomposition to tool condition monitoring is a relatively new approach. It is essentially a filtering exercise which may be used to isolate the process dependent part of the signal from process noise. Wu and Du [2.61] used wavelet transforms to identify chatter in turning and to recognise tool wear in drilling. The authors employed a six level decomposition of acceleration signals and identified wavelet packages in the fifth level which were sensitive to the onset of chatter in turning. They used a similar technique to identify wavelet packages also in the fifth level of decomposition which were sensitive to tool wear in drilling. The wavelet packages were able to differentiate between a new tool, a partially worn tool and a fully worn tool. In order to achieve this a series of experiments had to be performed to establish thresholds corresponding to the three wear states. Kamarthi and Pittner [2.62] compared Fourier transform methods with wavelet transform methods in conjunction with an artificial neural network in an attempt to improve recognition of tool wear state in turning. They concluded that Fourier transforms were better suited to processing vibration signals whereas wavelet transforms were better matched to force signals. However they suggested that both processing methods would lead to better estimations of flank wear during cutting. It is of course to be expected that the use of multiple sensors will lead to improved estimation of tool wear state in any event.

Since part of the work of this thesis concerns the extraction of features from surface profiles which may correlate with tool wear, a new technique for characterisation of surface finish will be investigated. There is considerable evidence that machined surfaces may be described by means of fractal geometry [2.63],[2.64],[2.65] and it is reasonable to assume that changes in the cutting tool which produced the machined surface would be reflected in changes in the fractal geometry of the surface. Although some work has been carried out into the use of fractal geometry to monitor surface finish [2.66] there is no

evidence that this work has been extended into the field of tool wear monitoring. In consequence part of this thesis will examine the changes in the fractal dimension of a machined surface profile with flank wear to establish if this quantity may be used as a component in a tool wear monitoring system.

2.2.3 The decision making process

It is clear from the preceding sections that although any single sensor/processing technique can provide information on the wear process in some situations such information is by no means universally available from all machining processes. It is possible to envisage a process in which signal to noise ratios differ greatly between types of sensors. Under such circumstances the use of a single sensor is likely to generate misleading information regarding the wear state of the cutting tool. Therefore reliance on a single source of information for a tool wear monitoring system is inadvisable. It is possible to gain substantially improved information about the wear state of a cutter from the integration of sensorial information from a number of sources. It is possible to extract multiple features from a single signal but Dimla [2.25] is of the opinion that this does not constitute multi-sensing. However it may be argued that extraction of multiple independent features may be used to provide valuable wear sensitive information which would not be available in a single feature from the same sensor.

Sensor fusion as described above is most readily achieved through the application of some form of artificial intelligence. The deployment of artificial intelligence requires the process of tool wear monitoring to be considered as being made up of two activities: a learning activity and a classification activity. Prickett and Johns [2.26] have distinguished three aspects of artificial intelligence which are most commonly used in tool wear monitoring systems: expert systems, fuzzy classification and neural networks.

An *expert system* generally consists of an inference engine, a human/machine interface and a knowledge base. The majority of effort in developing such a system is absorbed in the production of the knowledge base [2.67] which may be regarded as the learning activity in this case. The base is made up of a set of rules which are established from empirical results, computer simulations and interviews with domain experts.

Fuzzy systems are intended to classify tool wear state by taking into account the uncertainty contained in the sensorial data as to the exact relationship between wear state and sensorial information. This is achieved by calculating the degree of membership of the data in a set of wear states which are established by experimentation. The rules which govern the degree of membership resemble conventional boolean logic statements but which also consider the probability that the sensorial information refers to a particular state. The generation of the rules may be considered to constitute the learning activity associated with this decision making process. The work of both Du et al [2.67] and Prickett and Johns [2.26] indicates that fuzzy systems have not achieved commercial acceptance to any great extent and therefore they will not be considered further in this work.

If tool condition monitoring is considered as a problem in pattern recognition within the data provided by diverse sensors, it is ideally suited to solution by *artificial neural networks*. These networks may be divided roughly into two groups depending on the learning mode required to train them to recognise the patterns initially. In a supervised learning mode the neural network is exposed to a set of training vectors created from a set of experiments together with a set of target vectors which represent the known results of the experiments. The network parameters are then adjusted iteratively until the network can reproduce the target vectors when presented with the training vectors. This is supervised learning in the sense that the target vectors are known a priori and the network is taught to reproduce them. In unsupervised or self organising training the neural network is presented with a set of training data but no target vectors. The network then finds patterns within that data and assigns a specific output node to specific pattern clusters. Then the presentation of like patterns within the classification activity will activate like output nodes. It is of course necessary to provide some feature patterns with known wear states in the training period so that interpretation of the resulting output patterns can be made. This does not constitute supervised learning since the known output patterns are not used to adjust the network parameters during training. In a recent survey Dimla et al [2.68] concluded that over 60% of researchers used neural networks based on an architecture known as a multi-layer perceptron and employed supervised learning to train the network. A typical multi-layer perceptron architecture is illustrated in Figure 2.4.

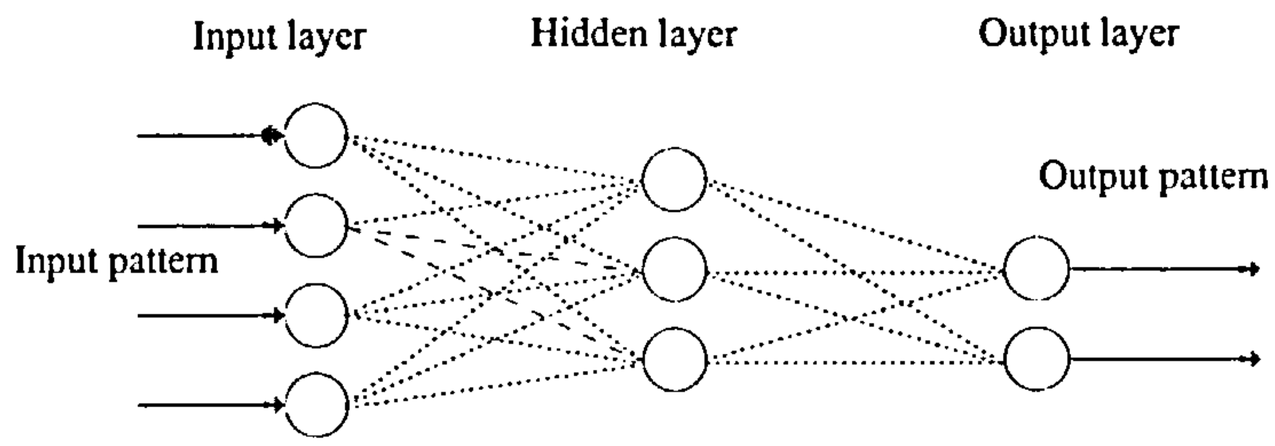

Figure 2.4 Typical multi-layer perceptron architecture for an artificial neural network.

The number of nodes in the input layer is dictated by the complexity of the input feature pattern and the number of output nodes is determined by the required number of classification sets. There are no set rules which dictate the number of hidden layers nor of the number of nodes on them but there is a loss of computing efficiency if the number of hidden layers exceeds three and the number of nodes associated with them is large. The use of multi-layer perceptrons in tool condition monitoring is discussed in greater detail in chapter 7.

Despite the availability of neural network solutions to the problems of tool condition monitoring in research establishments these have not been adopted by industry to any great extent. Leem and Dornfeld [2.69] have identified four reasons for this lack of enthusiasm for neural network deployment in commercial systems:

1) The information in the form of training data for the neural network is expensive to obtain.

2) The selection of wear sensitive features to present to the network varies with the machining process and this militates against a universal solution.

3) If the network can recognise only new or worn inserts the possibilities of mis-classification are greater and this could result in either uneconomic insert replacement or failure of the machine tool

4) The use of sensor signals measured at a single point in time may distort the true wear state of the inserts since both the stationary and time varying aspects of the signal will be analysed together.

It is agreed that the acquisition of training data is expensive and this especially so if items 1 and 2 are considered together. Leem and Dornfeld suggest that this could be mitigated by resorting to unsupervised training of the network which may require fewer training samples to be presented. The authors verify that small numbers of training samples are required for their network but they do not draw a comparison with the number of samples required for a supervised network.

In order to reduce the number of features presented to their neural network the authors use an additional supervised procedure to identify those features of a sensor signal which are most important to wear classification. This avoids the problems of off-line selection of the most important features in the sensor signals. However if the number of features is relatively small as in the present work the problem of feature selection is not as acute as when large numbers of features are available.

The problems noted in item 3 may be overcome by a finer division of the recognisable wear states. Instead of classification of wear state into new or worn inserts the introduction of intermediate wear state classes between these two extremes will reduce the difficulties associated with mis-classification by introducing a smoother progression to the approach of the end of tool life. This is considered in the work of this thesis as indicated in chapter 7.

The authors used a series of wear states predicted at times t, $t-1,....,t-k$ to arrive at a majority verdict as to the actual wear state at time t to reduce the mis-classification associated with item 4. This technique has some of the attributes of integral action as employed in feedback control systems and care must be taken to avoid the difficulties of instability. This will not be investigated further in this work.

2.3 Summary

From the foregoing it can be seen that there are a number of sensors which can provide data which is sensitive to tool wear and tool breakage. However none of the sensors is

universally applicable to all machining processes and the choices of which sensors to use must be matched to the process to be monitored. The work of this thesis concerns the identification of tool wear state as characterised by the length of the insert flank wear land length V_b during face milling. The cutting conditions are those associated with finish machining and the measurands required to achieve this were chosen accordingly. It has been seen that acoustic emission sensors are sensitive to wear in finish machining where other sensors may not be operating in an optimum signal/noise environment. The availability of a fibre optic AE transducer, as described in chapter 4, which can be used to provide both spectral and statistical data about the AE signal has resulted in an examination of the correlation between AE and insert wear as described in chapter 6.

It has been seen that the wear state of the inserts is intimately connected to the surface finish of the machined workpiece The possibility of using a novel inter-operational surface profilometer as described in chapter 4 make surface finish parameters available as possible candidates in tool wear monitoring systems. The requirement for this instrument to provide information about the surface profile in the frequency domain has led to an investigation into the relationship between the frequency content of a machined surface profile and the wear state of the inserts which produced the surface as described in chapter 5. Fractal geometry has been used to characterise machined surfaces, but has not been extended to tool wear assessment. Hence this thesis will examine the use of fractal geometry to characterise machined surfaces and hence to identify the wear state of the tool which generated the surface.

Fusion of the data provided by AE measurements and surface profile measurements has been achieved by means of an artificial neural network employing supervised learning as described in chapter 7. This neural network exhibited an improved reliability in recognising tool wear state over that which could be achieved when using a single sensor.

2.4 References

2.1) K.F. Ehmann, S.G. Kapoor, R.E. DeVor, I. Lazoglu. "Machining process modelling: a review". Transactions of the ASME, Journal of Manufacturing Science and Engineering, 119,(1997), 655-663.

2.2) M.E. Merchant. "Mechanics of the metal cutting process. I. Orthogonal cutting and a type 2 chip". Journal of Applied Physics, 16,(1945), 267-275.

2.3) M.E. Martellotti. "An analysis of the milling process". Transactions of the ASME, 63,(1941) 677-700.

2.4) M.E. Martellotti. "An analysis of the milling process, Part II - Down milling". Transactions of the ASME, 67,(1945), 233-251.

2.5) M.E. Merchant. "Mechanics of the metal cutting process. II. Plasticity conditions in orthogonal cutting". Journal of Applied Physics, 16,(1945), 318-324.

2.6) S. Kobayashi, R.P. Herzog, D.M. Eggleston, E.G. Thomsen. "A critical comparison of metal-cutting theories with new experimental data". Transactions of the ASME, Journal of Engineering for Industry, (1960), 333-347.

2.7) R.G. Fenton, P.L.B. Oxley. "Mechanics of orthogonal machining: Allowing for the effects of strain rate and temperature on tool-chip friction". Proceedings of the Institution of Mechanical Engineers, Part 1, 183,(1968), 417-438.

2.8) T.J. Drozda, C. Wick. Tool and Manufacturing Engineers Handbook. Volume 1 Machining. Society of Manufacturing Engineers, 1983.

2.9) M.C. Shaw. "Metal cutting principles". Oxford University Press, New York, 1989.

2.10) P.C. Pandey, H.S. Shan. "Analysis of cutting forces in peripheral and face milling operations". International Journal of production Research, 10,(1972), 379-391.

2.11) G.C.I. Lin, P.L.B. Oxley. "Mechanics of oblique machining: predicting chip geometry and cutting forces from work material properties and cutting conditions". Proceedings of the Institution of Mechanical Engineers, 186,(1972), 813-820.

2.12) W.F. Hastings, P. Mathew, P.L.B. Oxley. "A machining theory for predicting chip geometry, cutting forces etc. from work material properties and cutting conditions". Proceedings of the Royal Society of London A, 371,(1980), 569-587.

2.13) R.S. Hu, P. Mathew, P.L.B. Oxley and H.T. Young. "Allowing for end cutting edge effects in predicting forces in bar turning with oblique machining conditions". Proceedings of the Institution of Mechanical Engineers, Part C, 200(1986) 89-99.

2.14) Hong-Tsu Young, P. Mathew, P.L.B. Oxley. "Predicting cutting forces in face milling". International Journal of Machine Tools and Manufacture, 34,(1994), 771-783.

2.15) H.Q. Zheng, X.P. Li, Y.S. Wong, A.Y.C. Nee. "Theoretical modelling and simulation of cutting forces in face milling with cutter runout". International Journal of Machine Tools and Manufacture, 39,(1999), 2003-2018.

2.16) F. Koenigsberger, A.J.P. Sabberwal. "An investigation into the cutting force pulsations during milling operations". International Journal of Machine Tool Design Research, 1,(1961), 15-33.

2.17) W.R. DeVries. "Analysis of Material Removal Processes". Springer-Verlag, New York, 1992.

2.18) H.E. Boyer, T.L Gall Editors. "Metals Handbook. Desk Edition". American Society for Metals, Metals Park, Ohio, 1997.

2.19) H.J. Fu, R.E. DeVor, S.G. Kapoor. "A mechanistic model for the prediction of the force system in face milling operations". Transactions of the ASME, Journal of Engineering for Industry, 106,(1984), 81-88.

2.20) F. Gu, S.G. Kapoor, R.E. DeVor, P. Bandyopadhyay. "An enhanced cutting force model for face milling with variable cutter feed motion and complex workpiece geometry". Transactions of the ASME, Journal of Manufacturing Science and Engineering, 119,(1997), 467-475.

2.21) P.J. Cheng, J.T. Tsay, S.C. Lin. "A study of instantaneous cutting force coefficients in face milling". International Journal of Machine Tools and Manufacture, 37,(1997), 1393-1408.

2.22) J. Gu, G. Barber, S. Tung, R-J. Gu. "Tool life and wear mechanism of uncoated and coated milling inserts". Wear, 225(1999), 273-284.

2.23) T. Pfeifer, L. Wiegers. "Reliable tool wear monitoring by optimized image and illumination control in machine vision". Measurement, 28,(2000), 209-218.

2.24) D-W. Cho, S.J. Lee, C.N. Chu. "The state of machining process monitoring research in Korea". International Journal of Machine Tools and Manufacture, 39,(1999), 1697-1715.

2.25) D.E. Dimla Snr. "Sensor signals for tool-wear monitoring in metal cutting operations - a review of methods". International Journal of Machine Tools and Manufacture, 40,(2000), 1073-1098.

2.26) P.W. Prickett, C. Johns. "An overview of approaches to end milling tool monitoring". International Journal of Machine Tools and Manufacture, 39,(1999), 105-122.

2.27) J.H. Tarn, M. Tomizuka. "On-line monitoring of tool and cutting conditions in milling". Transactions of the ASME, Journal of Engineering for Industry, 111,(1989) 206-212.

2.28) Y. Altintas, I. Yellowley. "In-process detection of tool failure in milling using cutting force models". Transactions of the ASME, Journal of Engineering for Industry, 111,(1989) 149-157.

2.29) S.C. Lin, R.J. Yang. "Force based model for tool wear monitoring in face milling". International Journal of Machine Tools and Manufacture, 35,(1995), 1201-1211.

2.30) S.C. Lin, R.J. Lin, "Tool wear monitoring in face milling using force signals". Wear, 198,(1996), 136-142.

2.31) S.K. Choudhury, S. Rath. "In-process tool wear estimation in milling using cutting force model" Journal of materials Processing Technology, 99,(2000), 113-119.

2.32) K. Taraman, R. Swando, W. Yamauchi. "Relationships between tool forces and flank wear". SME Technical paper, MR74-704, March 11-15, 1974.

2.33) A.R.N. Shuaib, E. Garcia-Gardea, S.M. Wu. "Dynamic analysis of milling machine by torque signals". Transactions of the ASME, Journal of Engineering for Industry, 103,(1981), 235-240.

2.34) J.L. Stein, Churn-Hway Wang. "Analysis of power monitoring on AC induction drive systems". Transactions of the ASME, Journal of Dynamic Systems, Measurement, and Control, 112,(1990), 239-248.

2.35) J.W. Jones, Y. Wu. "Tool condition monitoring system". U.S. Patent number 5,587,931. December 1996.

2.36) Y. Altintas. "Prediction of cutting forces and tool breakage in milling from feed drive current measurements". Transactions of the ASME, Journal of Engineering for Industry, 114,(1992), 386-392.

2.37) X. Li, A. Djordjevich, P.K. Venuvinod. "Current-sensor-based feed cutting force intelligent estimation and tool wear condition monitoring". IEEE Transactions on Industrial Electronics, 47,(2000), 697-702.

2.38) Rajeev Kapoor, Sia Nemat-Nasser. "Determination of temperature rise during high strain rate deformation". Mechanics of Materials, 27(1998), 1 - 12.

2.39) R. Radulescu, S.G. Kapoor. "An analytical model for prediction of tool temperature fields during continuous and interrupted cutting". Transactions of the ASME, Journal of Engineering for Industry, 116,(1994), 135-143.

2.40) A.A.O Tay. "A review of methods of calculating machining temperature". Journal of Materials Processing Technology, 36,(1993), 225-257.

2.41) D.A. Stephenson, A. Ali. "Tool temperatures in interrupted metal cutting", Transactions of the ASME, Journal of Engineering for Industry, 114,(1992), 127-136.

2.42) M.B. da Silva, J. Wallbank. "Cutting temperature: prediction and measurement methods - a review". Journal of Materials Processing Technology, 88,(1999), 195-202.

2.43) Hong-Tsu Young. "Cutting temperature responses to flank wear". Wear, 201(1996), 117-120.

2.44) H.N.G. Wadley, R. Mehrabian. "Acoustic emission for materials processing: a review". Materials Science and Engineering, 65,(1984), 245-263.

2.45) R.W. Nichols Editor. "Acoustic emission". Applied Science Publishers Ltd., 1976, London.

2.46) S.A. Paipetis, N.G. Malakis. "Investigation of seismic activity by real-time acoustic emission signal processing". Engineering Aspects of Earthquake Phenomena, Edited by A. Koridze, Omega Scientific, Oxford, 1987.

2.47) M.L. Jakobsen, T.A. Carolan, J.S. Barton, J.D.C. Jones, R.L. Reuben. "Optical probing of acoustic emission from a rotating tool". 8th Sensors and their application conference, Institute of Physics, 1997, 109-114.

2.48) S. Dolinsek, J. Kopac. "Acoustic emission signals for tool wear identification". Wear, 225(1999), 295-303.

2.49) K. Jemielniak. "Commercial tool condition monitoring systems". The International Journal of Advanced Manufacturing Technology, 15,(1999), 711-721.

2.50) S. Braun, E. Lenz. "Machine - tool wear monitoring" Mechanical Signature Analysis, Edited by S. Braun, Academic Press, London, 1986, 321-342.

2.51) T.I. El - Wardany, D. Gao, M.A. Elbestawi. "Tool condition monitoring in drilling using vibration signature analysis". International Journal of Machine Tools and Manufacture, 36,(1996), 687-711.

2.52) G.H. Lim. "Tool-wear monitoring in machine turning". Journal of Materials Processing Technology, 51,(1995), 25-36.

2.53) S.R. Kidd, D.P. Hand, T.A. Carolan, J.S. Barton, J.D.C. Jones. "Measurement of aspects of surface form using an optical differential height measurement technique". Measurement Science and Technology, 7,(1996), 1579-1582.

2.54) P. Wilkinson, R.L. Reuben, J.D.C. Jones, J.S. Barton, D.P. Hand, T.A. Carolan, S.R. Kidd. "Surface finish parameters as diagnostics of tool wear in face milling". Wear, 205,(1997), 47-54.

2.55) P. Wilkinson, R.L. Reuben, J.D.C. Jones, J.S. Barton, D.P. Hand, T.A. Carolan, S.R. Kidd. "Surface features as indicators of tool chipping in single point face milling of aluminium". Wear, 212,(1997), 221-228.

2.56) S.A. Coker, Y.C. Shin. "In-process control of surface roughness due to tool wear using a new ultrasonic system". International Journal of Machine Tools and Manufacture, 36,(1996), 411-422.

2.57) T.A. Carolan, S.R. Kidd, D.P. Hand, S.J. Wilcox, P. Wilkinson, J.S. Barton, J.D.C. Jones and R.L. Reuben. "Acoustic emission monitoring of tool wear during the face milling of steels and aluminium alloys using a fibre optic sensor Part 2: frequency analysis". Proceedings of the Institution of Mechanical Engineers, Part B, 211(1997), 311-319.

2.58) B.K.N. Rao, A.D. Hope, Z. Wang. "Application of Walsh spectral analysis to milling tool wear monitoring". Measurement and Control, 31,(1998), 268-273.

2.59) K.G. Beauchamp. "Applications of Walsh and Related Functions". Academic Press, London, 1984.

2.60) K. Zheng, D.J. Whitehouse. "The application of the Wigner distribution function to machine tool monitoring". Proceedings of the Institution of Mechanical Engineers, Part C: Journal of Mechanical Engineering Science, 206(1992), 249-264.

2.61) Y. Wu, R. Du. "Feature extraction and assessment using wavelet packets for monitoring of machining processes". Mechanical Systems and Signal Processing, 10,(1996), 29-53.

2.62) S.V. Kamarthi, S. Pittner. "Fourier and wavelet transform for flank wear estimation - a comparison". Mechanical Systems and Signal Processing, 11,(1997), 791-809.

2.63) G. Galante, A. Lombardo, M. Piacentini. "Fractal dimension: a useful tool to describe the microgeometry of machined surfaces". International Journal of Machine Tools and Manufacture, 33,(1993), 525-530.

2.64) S. Ganti, B. Bhushan. "Generalized fractal analysis and its applications to engineering surfaces". Wear, 180,(1995), 17-34.

2.65) M. Hasegawa, J. Liu, K. Okuda, M. Nunobiki. "Calculation of the fractal dimension of machined surface profiles". Wear, 192,(1996), 40-45.

2.66) G. Zhang, S. Gopalakrishnan. "Fractal geometry applied to on-line monitoring of surface finish". International Journal of Machine Tools and Manufacture, 36,(1996), 1137-1150.

2.67) R. Du, M.A. Elbestawi, S.M. Wu. "Automated monitoring of manufacturing processes, part 1: monitoring methods". Transactions of the ASME, Journal of Engineering for Industry, 117,(1995), 121-132.

2.68) D.E. Dimla JR, P.M. Lister, N.J. Leighton. "Neural network solutions to the tool condition monitoring problem in metal cutting - a critical review of methods". International Journal of Machine Tools and Manufacture, 37,(1997), 1219-1241.

2.69) C.S. Leem, D.A. Dornfeld. "Design and implementation of sensor-based tool-wear monitoring systems". Mechanical Systems and Signal Processing, 10,(1996), 439-458

Chapter 3

Modelling of Surface Finish and Acoustic Emission

3.1 Introduction

It is well known that, in face milling operations, an increase in the length of insert wear lands will be accompanied by an increase in the cutting forces experienced by a machine tool [3.1],[3.2]. In consequence cutting force measurements are widely used to give an indirect measure of insert wear state. However the absolute values of cutting force vary with depth of cut [3.3] and it is to be expected that in the case of finish milling cutting forces will be small. This implies that changes in cutting force resulting from changes in flank wear lands will be correspondingly small and difficult to measure with conventional instruments. Therefore it is necessary to examine other phenomena associated with the cutting process in order to establish their sensitivities, if any, to the wear state of the inserts to allow indirect monitoring of the wear process in finish milling.

An important output of the finish milling process is the surface texture generated by the process. Since the surface texture is produced by a complex interaction between the cutting tool and the workpiece it is to be expected that some measure of the surface finish will contain information regarding the wear state of the cutting tool. The most commonly used parameter in assessing surface finish is the centre line average R_a defined by [3.4]

$$R_a = \frac{1}{L}\int_0^L |z| dx \qquad (3.1)$$

where L is the length along the x axis of the profile under consideration and z is the profile measured from its mean reference line. As with all single-number measures of surface finish, it is possible for several surfaces to have entirely different characteristics yet have the same value of R_a. This suggests that such traditional measures of surface finish are insufficiently sensitive to the subtle changes in surface profile caused by tool wear to be used in a tool wear monitoring environment. A system of measure based on the spectral content of milled surfaces is expected to provide a more faithful representation of

the surfaces since such a measure could only be derived from detailed consideration of the shape of the profile. This will be discussed later in this chapter.

Acoustic emission measurements made during the cutting process have been used successfully to monitor events occurring at the cutting edge of the inserts [3.5]. Conventionally, acoustic emission signals which are of small amplitude (of the order of nano-meters) and high frequency (60 kHz to 1 MHz), are measured by resonant piezo-electric devices. Most of the work using acoustic emission measurements exploits the correlation between the energy of the AE signal and the wear state of the inserts [3.6]. This may be attributed in part to the suitability of conventional sensors to make such measurements. However there have been some attempts to establish correlations between the frequency content of the AE signal and the wear state of the cutter [3.7]. The extraction of frequency information from a piezo-electric transducer is complicated by the frequency response of the sensor which must be deconvolved from the sensor output signal. This leads to the conclusion that the subtle changes in the AE spectrum resulting from tool wear may be concealed by the frequency response of the transducer. In this work a novel fibre-optic transducer [3.8] with a flat frequency response measures an AE signal from which frequency information may be extracted with some confidence. The modelling of the AE generation process is discussed later in this chapter and the fibre-optic transducer is described briefly in chapter 4.

Both the texture of the machined surface and the acoustic emission signals are generated by complex interactions between the cutter and the workpiece. Figure 3.1 shows that these interactions may be considered to occur in distinct zones of the cutting cycle.

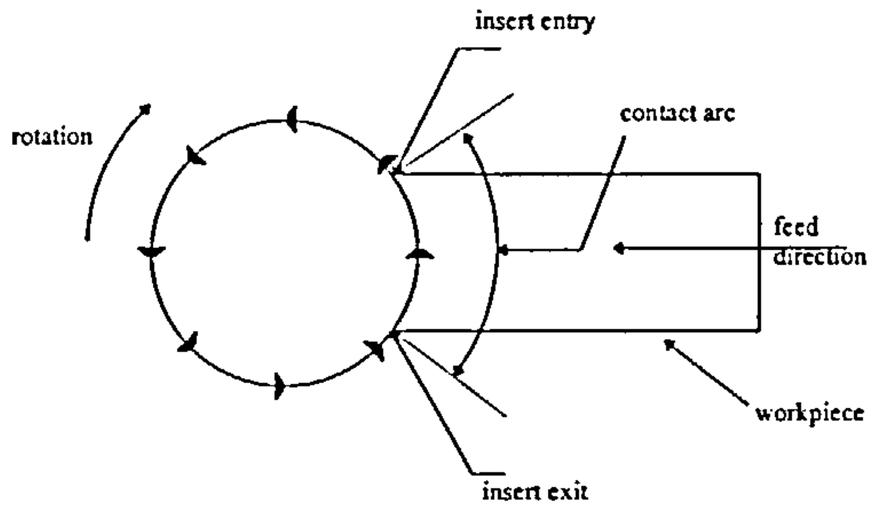

Figure 3.1 Regions of interaction between cutter and workpiece.

Initial contact between the insert and workpiece occurs at the point marked 'insert entry'. This contact is always characterised by an impact [3.9] which will produce a burst of AE activity. The severity of this impact can be ameliorated by off-setting the cutter with respect to the workpiece centre line in such a manner as to reduce the entry angle of the insert. This impact is then followed by a region designated as the 'contact arc'. In this region cutting takes place and chips of workpiece material are produced by a shearing mechanism. During chip formation the workpiece material undergoes high strain rate deformation and in such a process it has been shown by Kapoor and Nemat-Nasser [3.10] that almost all of the work done on the deforming material is converted to heat. The generation of heat in the shear zone results in temperature rises in the workpiece, the tool and the chip, with a subsequent change in the properties of the deformed material. In particular the flow stress of the material will change resulting in modifications to the shear plane angle [3.3] which will ultimately affect the generation of acoustic emission [3.11], [3.12]as will be discussed in section 3.3.

3.2 Surface finish and tool wear

The surface profile generated in a face milling operation is as a result of complex interactions between the geometry of the inserts, the dynamics of the cutter head and the dynamics of the table [3.13], [3.14]. Figure 3.2 shows a typical surface generated by face milling aluminium alloy type 6082 with a single insert.

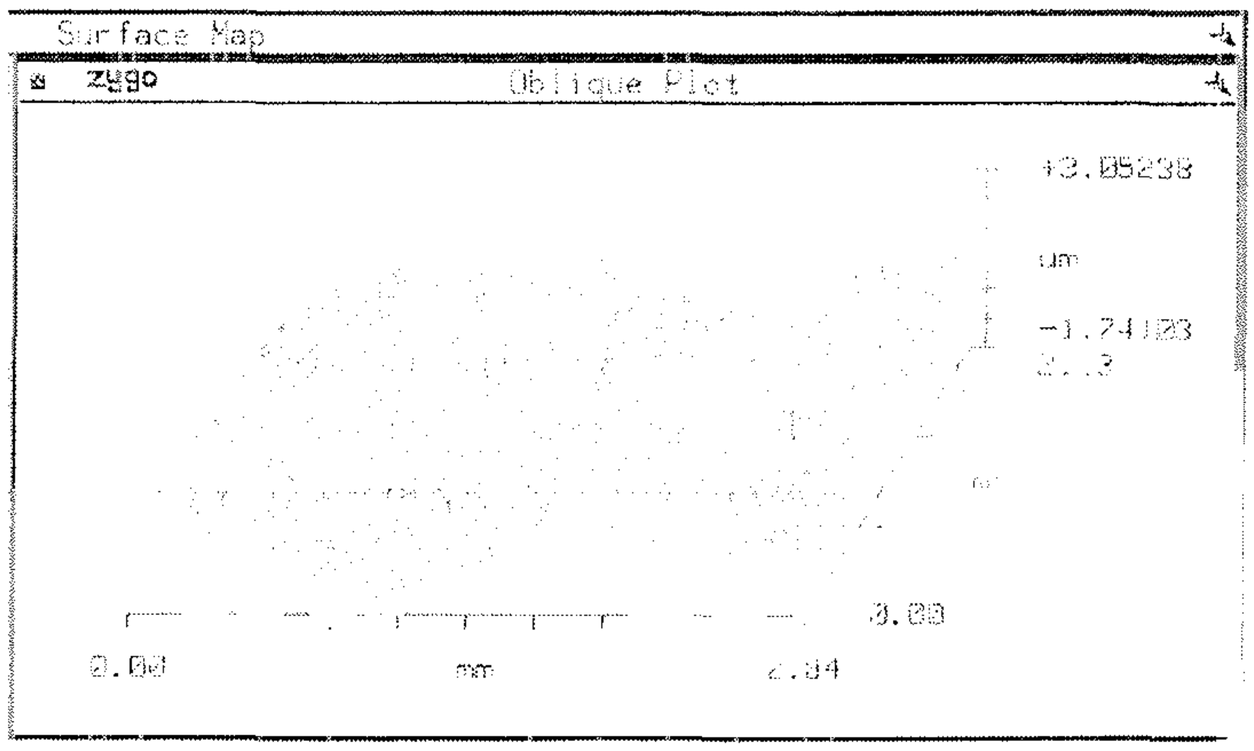

Figure 3.2 A typical machined surface generated by face milling aluminium alloy type 6082 with a single insert.

This figure was obtained from a ZYGO corporation New View 100 3D Surface Structure Analyser using a ×2.5 objective. The three dimensional characteristics of the surface are readily apparent. Each point in the surface may be considered to have been formed by the intersection of the cutter arc of contact (arcs aa'----ii') with imaginary lines (lines 11'----αα') drawn on the surface as shown in figure 3.3. A measurement of the surface made with a stylus profilometer, as in this work, would be made along one of the lines 11' to αα' and would record only a sample of the surface characteristics.

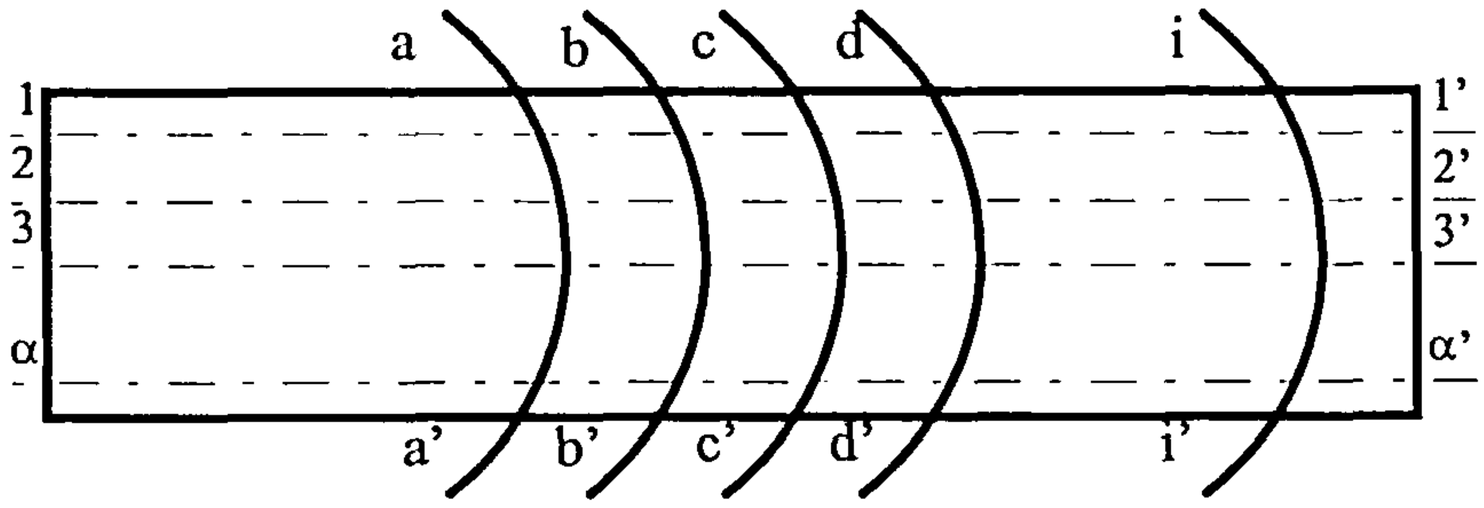

Figure 3.3 Suggested mechanism for the formation of the machined surface in face milling.

3.2.1 Modelling of forces in milling

It is possible to model the surface profile produced in a milling process from consideration of the static and dynamic forces acting on the cutter and the geometry of the individual inserts. Baek et al. [3.13] show that modelling the cutter as a single degree of freedom system in the vertical direction and the tool table as second single degree of freedom system produces reasonable agreement between simulated and measured surface profiles. In their work Baek et al excited their model by experimentally measured forces. It is of course possible to excite the Baek model by means of simulated forces calculated from the works of Fu et al [3.15] with further modifications by DeVries [3.2].

The Fu model is based on the widely held assumption that the normal force acting on a chip is equal to the product of the chip cross-sectional area and the specific cutting pressure K_T. The specific cutting pressure is an empirically determined characteristic of the material being cut and depends on the undeformed chip thickness. Fu and co-workers demonstrated that K_T followed a power law with the undeformed chip thickness. However further work by DeVries [3.2] showed that good results in simulating cutting forces could

be obtained from using an average chip thickness during a milling cut provided that correction factors for chip thickness were included in the calculations. This removes the necessity of calculating a continually varying value of K_T as the instantaneous chip thickness changes through the cut. It is further assumed in the Fu model that the radial force acting along the cutting edge is related to the tangential force by an empirically determined dimensionless constant, K_R. Thus it is possible to obtain the following for expressions for the tangential and radial forces at the cutting edge.

$$\begin{aligned} F_T(i,\phi) &= K_T h\big(\theta_i(\phi)\big) d \\ F_R(i,\phi) &= K_R F_T(i,\phi) \end{aligned} \tag{3.2}$$

where

ϕ is the angle of cutter rotation

$\theta_i(\phi)$ is the angular position of insert i at cutter rotation angle ϕ

$F_T(i,\phi)$ and $F_R(i,\phi)$ are the tangential and radial forces on the cutting edge at cutter rotation angle ϕ.

$h(\theta_i(\phi))$ is the chip thickness for insert i at cutter angular position $\theta_i(\phi)$

d is the axial depth of cut.

The angles ϕ and $\theta_i(\phi)$ are defined in figure 3.4

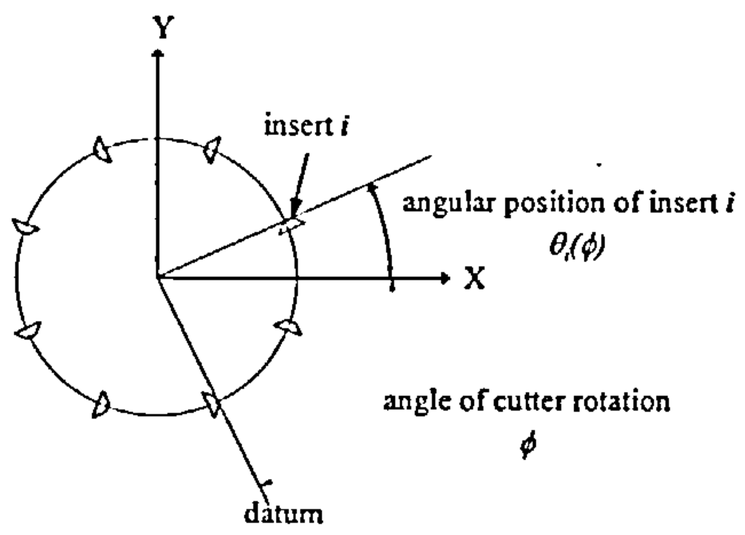

Figure 3.4 Definition of cutter angle of rotation and insert angular position

Equations 3.2 make no allowance for the geometry of the tool and assume that the insert lead angle is zero. If the geometry of the tool is considered, the forces acting on the cutting edge may be resolved into tangential, radial and axial directions defined by cylindrical polar co-ordinates (r-θ-z) attached to the cutter so that the axial (z) co-ordinate is directed along the cutter axis. Hence the forces may be expressed by [3.15]:

$$\begin{bmatrix} F_T(i,\phi) \\ F_R(i,\phi) \\ F_A(i,\phi) \end{bmatrix} = K_T h\left(\theta_i(\phi)\right) d \begin{bmatrix} 1 + K_R \dfrac{\cos\gamma_L \tan\gamma_R}{\cos\gamma_A} \\ -\tan\gamma_R + K_R \dfrac{\cos\gamma_L}{\cos\gamma_A} \\ -\dfrac{\tan\gamma_A}{\cos\gamma_R} + K_R \dfrac{\sin\gamma_L}{\cos\gamma_A \cos\gamma_R} \end{bmatrix} \tag{3.3}$$

where

$F_A(i,\phi)$ is the axial component of force on insert i at cutter rotation angle ϕ which is parallel to the Z-axis.

γ_A is the axial rake angle

γ_R is the radial rake angle

γ_L is the lead angle

From the geometry of the chip it may be seen that the chip thickness $h(\theta_i(\phi))$ is related to the maximum chip thickness h_{max} by the expression

$$h\left(\theta_i(\phi)\right) = h_{\max} \cos\left(\theta_i(\phi)\right) \tag{3.4}$$

and h_{max} is related to the feed per tooth f_t and the lead angle γ_L by the expression

$$h_{\max} = f_t \cos\left(\gamma_L\right) \tag{3.5}$$

In practice, the value of $\theta_i(\phi)$ in equation 3.4 will lie between the entry angle to the workpiece and exit from it, as described below, as it is only in this range that any particular insert is engaged in cutting.

If a rectangular cartesian co-ordinate system is attached to the cutter centre in such a way that the X-axis coincides with the *cutter* feed direction and the Z-axis is directed upwards perpendicular to the machined surface, the Y-axis will be determined by the right hand rule. It is possible to resolve the radial, tangential and axial forces into components of force parallel to these axes directions.

$$\begin{bmatrix} F_X(i,\phi) \\ F_Y(i,\phi) \\ F_Z(i,\phi) \end{bmatrix} = \begin{bmatrix} \cos(\theta_i(\phi)) & -\sin(\theta_i(\phi)) & 0 \\ \sin(\theta_i(\phi)) & \cos(\theta_i(\phi)) & 0 \\ 0 & 0 & 1 \end{bmatrix} \begin{bmatrix} F_T(i,\phi) \\ F_R(i,\phi) \\ F_A(i,\phi) \end{bmatrix} \tag{3.6}$$

Where

$F_X(i,\phi)$, $F_Y(i,\phi)$ and $F_z(i,\phi)$ are the X-direction, Y-direction and Z-direction forces on insert i at cutter rotation angle ϕ.

For multi-point cutting the total force components in the X-, Y- and Z- directions may be calculated by summing the forces on each insert over the cutter. In this summation it is of course only necessary to consider the inserts which are actively engaged in cutting for any given rotational position of the cutter. Therefore the total force on the cutter is given by

$$\begin{bmatrix} F_X(\phi) \\ F_Y(\phi) \\ F_Z(\phi) \end{bmatrix} = \sum_{i=1}^{N_t} \delta(\theta_i(\phi)) \begin{bmatrix} F_X(i,\phi) \\ F_Y(i,\phi) \\ F_Z(i,\phi) \end{bmatrix} \tag{3.7}$$

where N_t is the total number of inserts and $\delta(\theta_i(\varphi))$ is an indicator which takes the value 1 if the angular position of insert i lies between the entry angle to the workpiece and the exit from it (i.e. it lies within the arc of contact of figure 3.1), and is zero elsewhere. The extent of the arc of contact may be determined from the relative positions of the centre of the cutter and the workpiece as shown in figure 3.5.

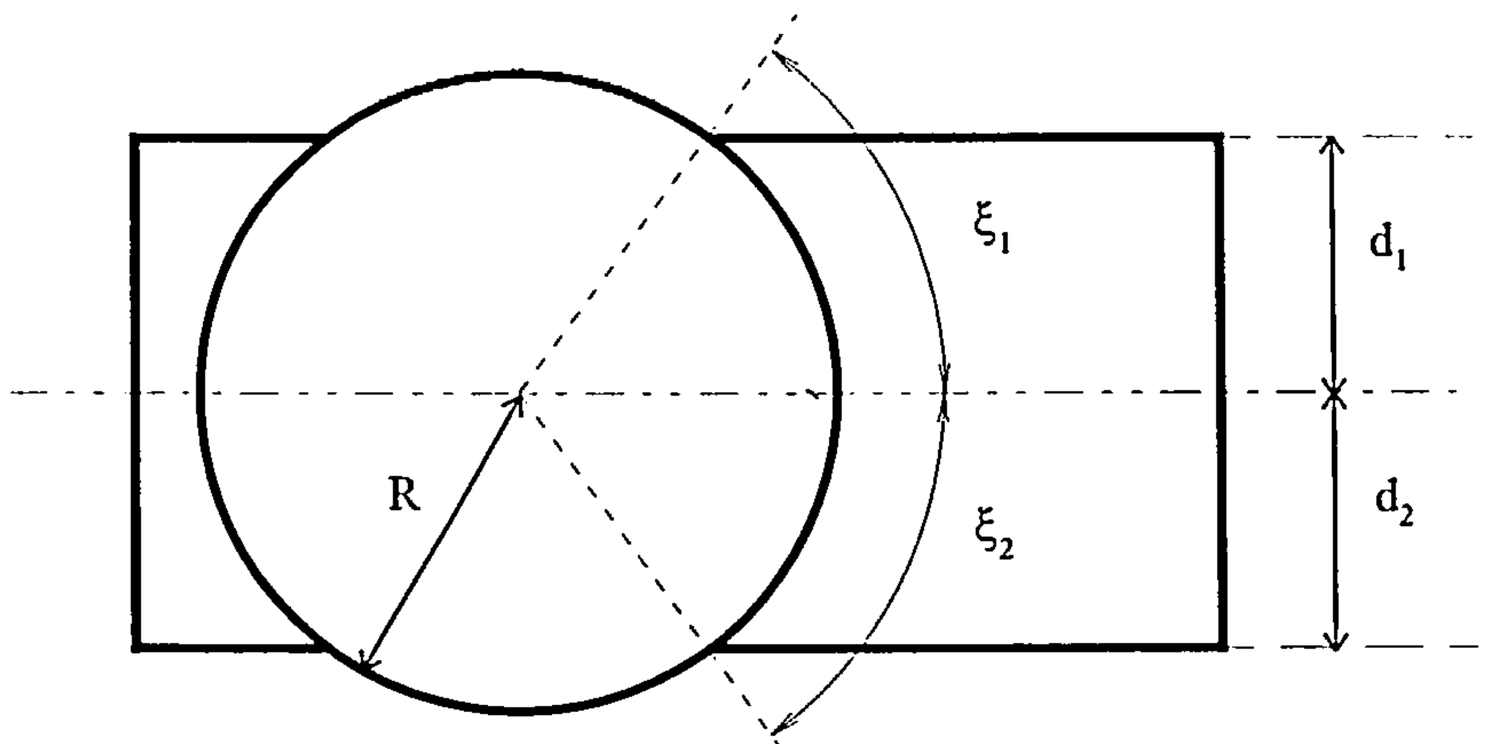

Figure 3.5 Calculation of insert entry and exit angles

From this figure it may be seen that

$$\xi_1 = \sin^{-1}\left(\frac{d_1}{R}\right)$$

$$\xi_2 = \sin^{-1}\left(\frac{d_2}{R}\right) \qquad (3.8)$$

$$\xi = \xi_1 + \xi_2$$

where ξ is the angle of contact.

ξ_1 is the entry angle

ξ_2 is the exit angle.

For symmetrical cutting where the cutter moves along the centre line of the workpiece $d_1 = d_2$ and hence $\xi_1 = \xi_2$. In this work cutting was arranged so that

$$d_1 = d_2 = 30 \text{ mm}$$

and since the diameter of the cutter was 100 mm this resulted in an entry angle of 36.9°, an exit angle of -36.9° and a total angle of contact of 73.8°.

In order to use equations 3.2 to 3.8 to calculate the cutting forces generated in milling the two coefficients K_T and K_R of equations 3.2 and 3.3 were calculated according to the methods of DeVries [3.2]. Specific cutting energy E_s is defined as the energy required to

cut a unit volume of material and may be treated as a material property. Values of E_s have been determined experimentally and are readily available in tabulated form [3.2],[3.16] as the results of standardised test conditions. This data was extracted from turning tests using a new tool with a rake angle of 0^0 and an uncut chip thickness of 0.25 mm. Cutting fluid was not used. From the definition of specific cutting energy it may be seen that

$$E_s = \frac{P}{Z} \tag{3.9}$$

where P is the power consumed in making the cut and Z is the volumetric removal rate of material.

The power consumed in cutting is related to the cutting speed v and to the tangential force F_T on the insert, hence

$$P = F_T v = E_s Z \tag{3.10}$$

If corrections are made for deviations from the standardised test conditions used to obtain the tabulated values of specific cutting energy [3.2], an estimate of the cutting force tangential to the insert may be deduced

$$F_T = \frac{P}{v} K_c\left(h_{avg}\right) K_r\left(\gamma_R\right) K_w\left(V_b\right) \tag{3.11}$$

where

$K_c(h_{avg})$ is a correction factor resulting from the use of the average chip thickness in calculating cutting forces.

$K_r(\gamma_R)$ is a correction resulting from deviations in the radial rake angle from the test conditions

$K_w(V_b)$ is a correction factor for wear of the insert as milling progresses.

These correction factors have been determined experimentally and are available in graphical form in DeVries [3.2]. An estimate of the specific cutting pressure K_T may then be generated from

$$K_T = \frac{F_T}{A_c} = \frac{F_T}{dh_{avg}} \tag{3.12}$$

where A_c is the cross sectional area of the uncut chip.

It should be noted that K_T is not a true pressure but is titled 'specific cutting pressure' because it possesses the appropriate dimensions. It is acknowledged that this technique only gives an estimate of the cutting forces in the feed, transverse and axial directions but in this work precise values of these forces are not required. However this approach demonstrates the manner in which the cutting forces vary with tool wear V_b through the factor $K_w(V_b)$. If precise values of the instantaneous forces were required it would be necessary to calculate instantaneous values of K_T which varies with uncut chip thickness, a process which would be impractical [3.15] because of the large associated computational penalty.

Several investigators have estimated expressions for K_R. Fu et al derive an expression from experimental work which relates K_R to the average undeformed chip thickness C_{avg} in the form

$$K_R = 0.0974 C_{avg}^{-0.2977} \text{ with units of pounds/square inch}$$

This expression is specific to the work of Fu and associates and is not readily applicable to the present work owing to the lack of available experimental material constants for other work piece materials. However Shaw [3.17] states that as a first approximation, the relationship between the radial and tangential forces of equation 3.2 may be taken as

$$F_R(i,\phi) = \frac{F_T(i,\phi)}{2}$$

hence fixing the value of K_R as 0.5. In further work DeVries introduced compensation factors into the expression for F_R to allow for deviations in cutting conditions from the standard conditions discussed earlier. The DeVries expression may be written

$$F_R(i,\phi) = F_T(i,\phi) C_c(h_{avg}) C_r(\gamma_R) C_w(V_b) \tag{3.13}$$

where

$C_c(h_{avg})$ is a correction factor resulting from the use of the average chip thickness in calculating cutting forces.

$C_r(\gamma_R)$ is a correction resulting from deviations in the radial rake angle from the test conditions

$C_w(V_b)$ is a correction factor for wear of the insert as milling progresses.

$F_T(i,\phi)$ is the tangential component of cutting edge force calculated for insert i from equation 3.11 using the experimental values of specific cutting energy.

It can be seen that if the radial force $F_R(i,\phi)$ were to be estimated from this equation at the standardised cutting conditions with all the compensation terms equal to unity, the relationship between the tangential and radial forces would be

$$F_R(i,\phi) = F_T(i,\phi) \tag{3.14}$$

In the light of Shaw's initial estimation equation 3.14 represents an overestimation of the magnitude of the radial force. It is proposed that if Shaw's first approximation is combined with DeVries' experimental expression a more realistic relationship between radial force and tool wear state results

$$F_R(i,\phi) = \frac{F_T(i,\phi)C_c(h_{avg})C_r(\gamma_R)C_w(V_b)}{2} \tag{3.15}$$

If equations 3.2 and 3.15 are compared it may be seen that

$$K_R = \frac{C_c(h_{avg})C_r(\gamma_R)C_w(V_b)}{2} \tag{3.16}$$

3.2.2 Simulations of cutting force

Simulations of the cutting forces were carried out using equations 3.2 to 3.16 for several combinations of cutter and workpiece material as shown in table 3.1. The values for the compensation terms in equations 3.11 and 3.16 were obtained from DeVries [3.2].

Insert geometry	No. of inserts	Workpiece material
Negative rake	single	annealed En24
Negative rake	eight	annealed En24
Positive rake	single	annealed En24
Positive rake	eight	annealed En24
Negative rake	eight	quenched & tempered En24
Positive rake	eight	quenched & tempered En24
Positive rake	single	type 304 stainless steel

Table 3.1 Cutter/workpiece combinations used in simulations

Simulated forces: new inserts

Figures 3.6a and 3.6b show the results of the simulation carried out for single point negative rake cutting of annealed En24 steel with an unworn insert. Both of these figures illustrate the forces experienced by the cutter during two revolutions of the spindle in the feed direction (figure 3.6a) and the depth of cut direction (figure 3.6b).

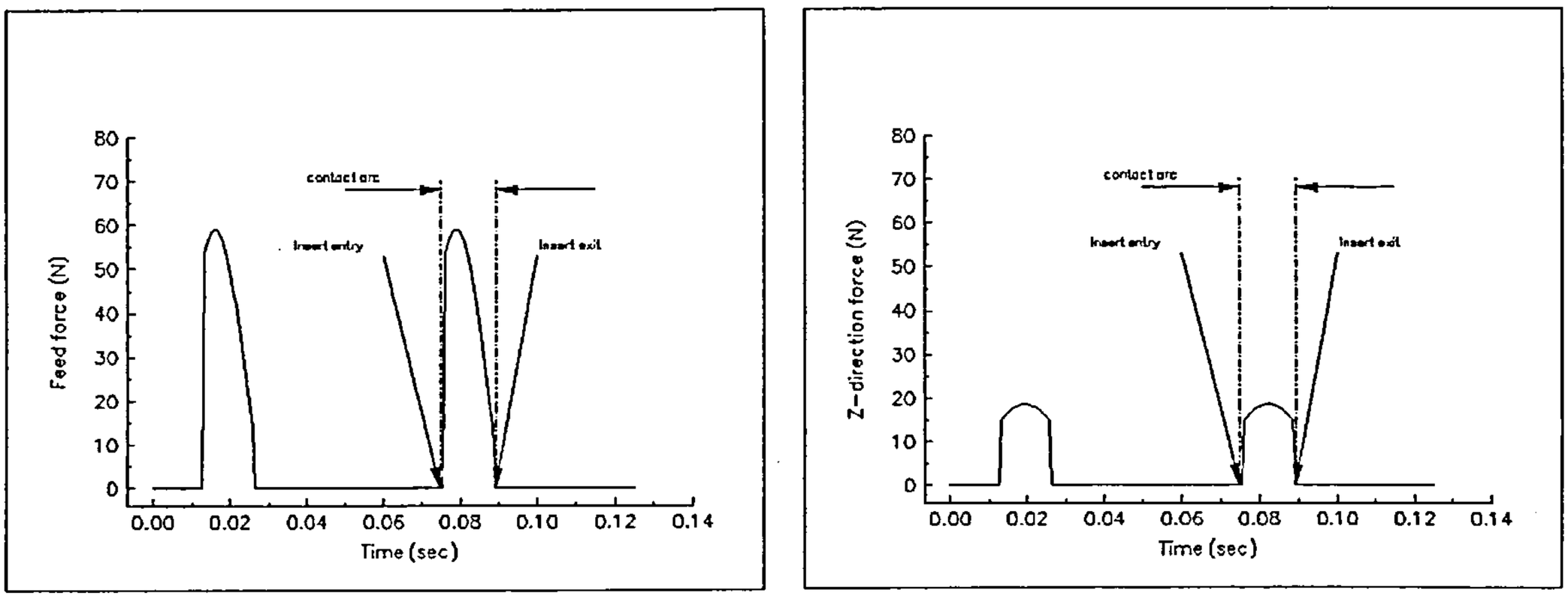

(a) (b)

Figure 3.6 Cutting forces generated by the Fu model in the (a) feed direction (b) depth of cut direction for single point negative rake cutting of annealed En24.

The entry impact is clearly visible in these figures as are the forces generated by the insert as it moves round the arc of contact. It should be noted that the maximum in the feed force does not occur when the insert is in the centre of the cut but rather before this position since this force is the vector sum of the tangential and radial forces acting on the cutter.

The simulation results over one revolution of the cutter for eight point negative rake cutting of annealed En24 with unworn inserts are shown in figure 3.7.

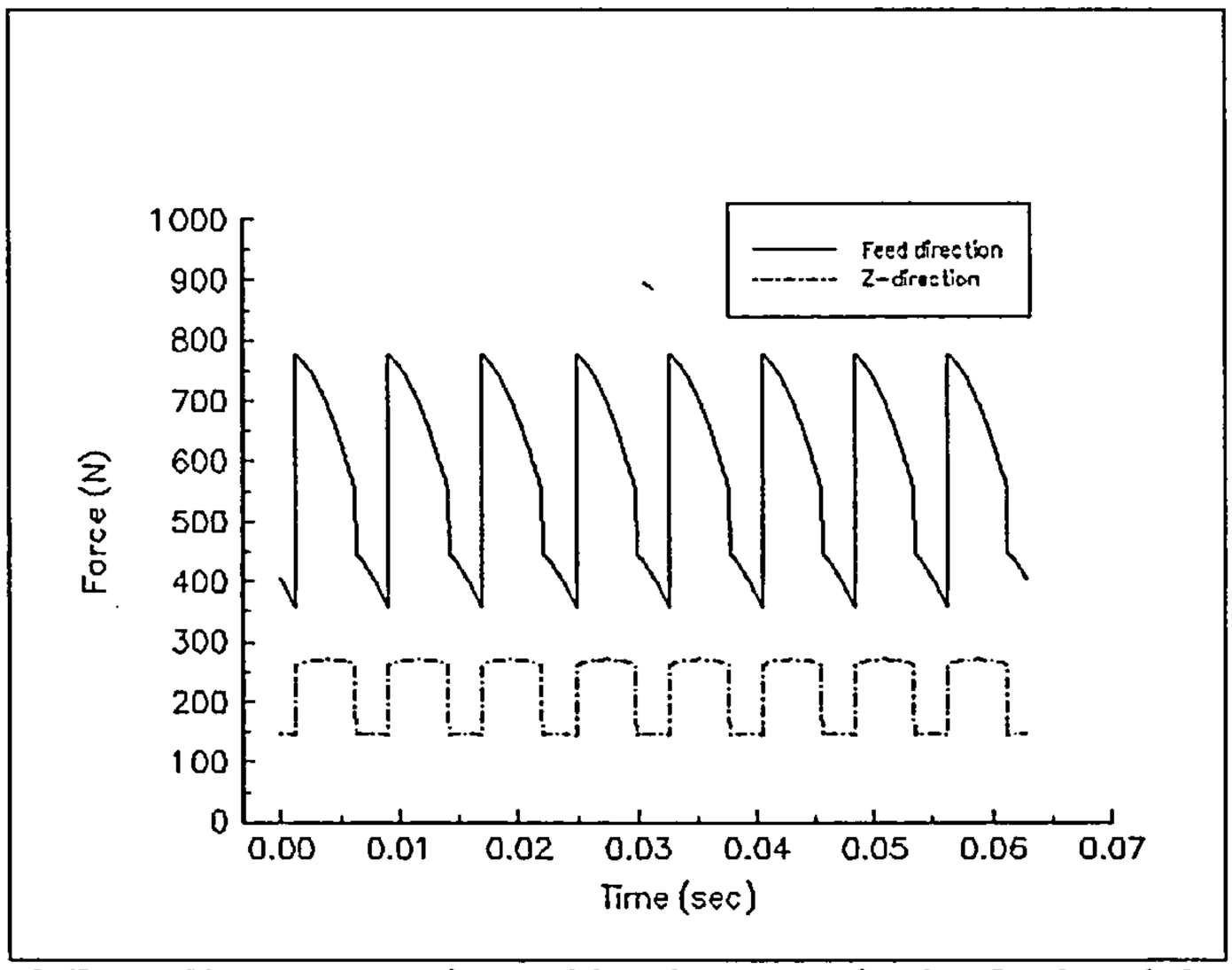

Figure 3.7 Forces experienced by the cutter in the feed and depth of cut directions during 8-point negative rake cutting of annealed En24.

In this case the forces experienced by the cutter are more complicated than in the case of single point cutting. The feed force depicted in figure 3.7 is generated by a combination of forces associated with several inserts cutting simultaneously. In this example, following the initial entry impact of an insert, the discontinuities in the feed force arise from the varying numbers of inserts cutting as the cutter rotates.

Figure 3.8a shows the results of the simulation over two revolutions of the cutter for single point positive rake cutting of annealed En24 with a new insert. As can be seen the feed force briefly takes on a negative value immediately prior to the exit of the insert from the workpiece.

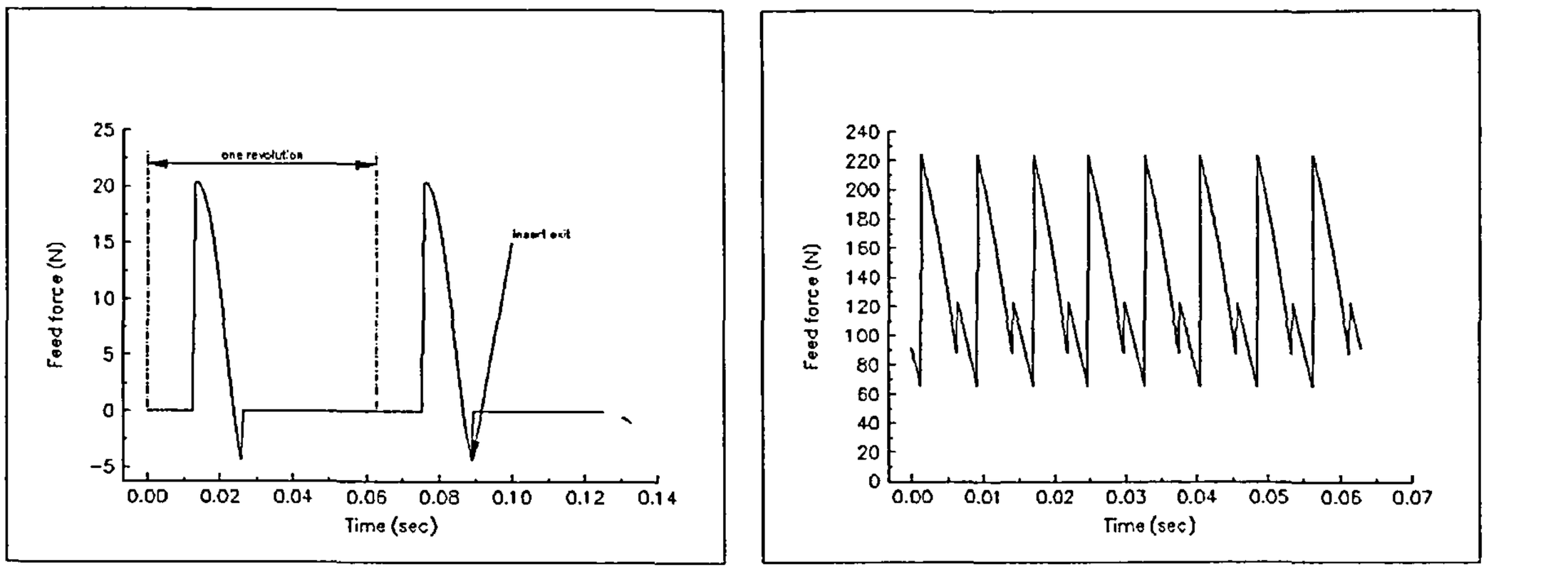

(a) (b)

Figure 3.8 Cutting forces generated by the Fu model in the feed direction for (a) single point, (b) 8-point positive rake cutting of annealed En24

Figure 3.8b shows the feed force experienced by the cutter when cutting annealed En 24 with a positive rake eight point cutter using new inserts. This figure displays one revolution of the cutter. As in the case of multi-point negative rake cutting, the discontinuities in the feed force arise from the sudden exit from the workpiece of an insert which is generating a negative force at the end of its cut.

In simulating the cutting forces for a different workpiece material it is only necessary to alter the value of specific cutting pressure through use of the appropriate specific cutting energy, E_s, and the cutting conditions. Figure 3.9a shows the results of the simulation carried out for cutting a quenched and tempered specimen of En24 steel with an eight point positive rake cutter using new inserts. Similarly figure 3.9b shows the results when cutting the same material with new inserts in an eight point negative rake cutter. In both of these examples two revolutions of the cutter are displayed.

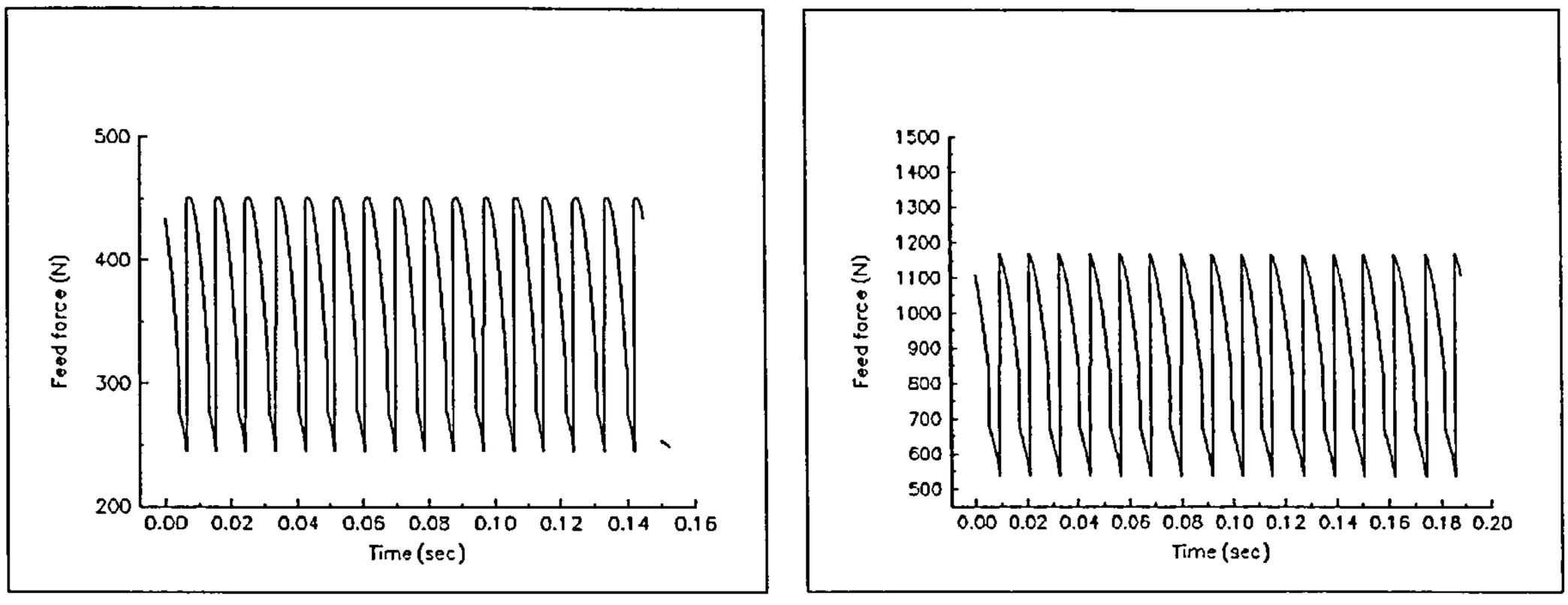

(a) (b)

Figure 3.9 Cutting forces generated by the Fu model in the feed direction for eight point cutting of quenched and tempered En24 using new inserts in (a) a positive rake cutter, (b) a negative rake cutter.

Figure 3.10 shows the simulated feed force variation when cutting type 304 stainless steel with a single new insert in a positive rake cutter. Again two revolutions of the cutter are demonstrated in this figure.

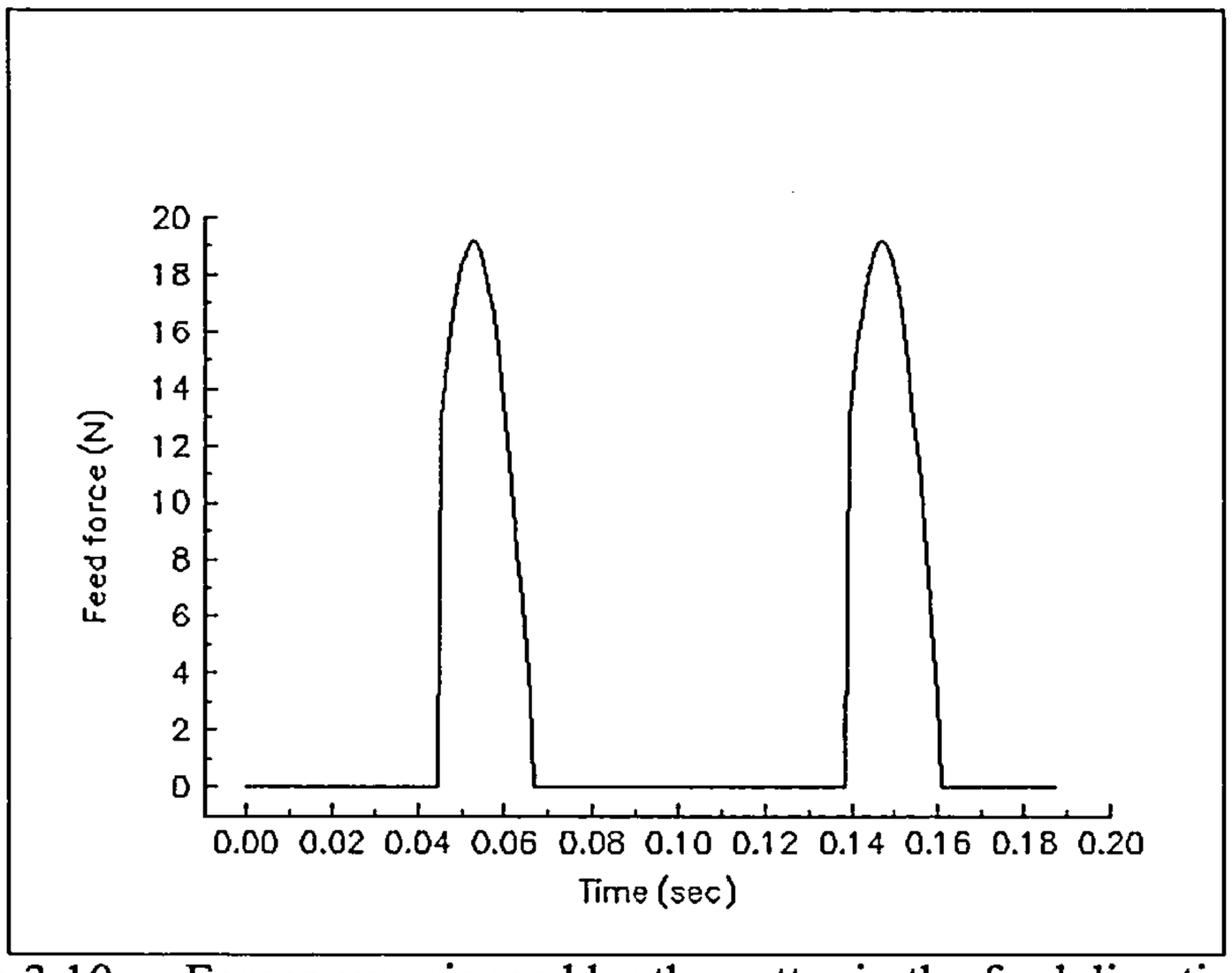

Figure 3.10 Forces experienced by the cutter in the feed direction during single point positive rake cutting of type 304 stainless steel.

Simulated forces: worn inserts

Figures 3.6a to 3.10 were generated by assuming that the inserts were new in all cases. The effects of flank wear may be demonstrated using equations 3.11 and 3.15. For the new inserts the value of the correction terms K_w in equation 3.11 and C_w in 3.15 were both taken to be unity [3.2]. In the case of a worn insert the correction terms were increased in accordance with the technique proposed by DeVries [3.2]. It can be seen that the effect of wear is to increase both the tangential and radial forces experienced by the insert cutting edge. Since the feed force and transverse force are vector sums of the radial and tangential forces it is expected that the effects of wear will be to increase the magnitude of the feed and transverse forces and to alter their phasing with respect to the insert rotational position. These effects are demonstrated in figures 3.11 to 3.17. In each case the simulation for the worn insert was performed assuming a flank wear land length (V_b) of 0.7 mm.

From figure 3.11 it can be seen that wear raises the peak feed forces substantially in single point cutting of annealed En24. The impact which this large increase in force has on the generation of the surface finish of the workpiece will be discussed below. Figure 3.12 confirms that the expected increase in both peak feed force and average feed force does occur when using an eight point negative rake cutter with annealed En24. Figure 3.13 shows the effects of insert wear on feed force when cutting annealed En24 with a single point positive rake cutter. It can be seen that one of the effects of wear in this case is to alter the balance of tangential and radial components of force in such a way as to prevent the feed force from becoming negative prior to insert exit from the workpiece.

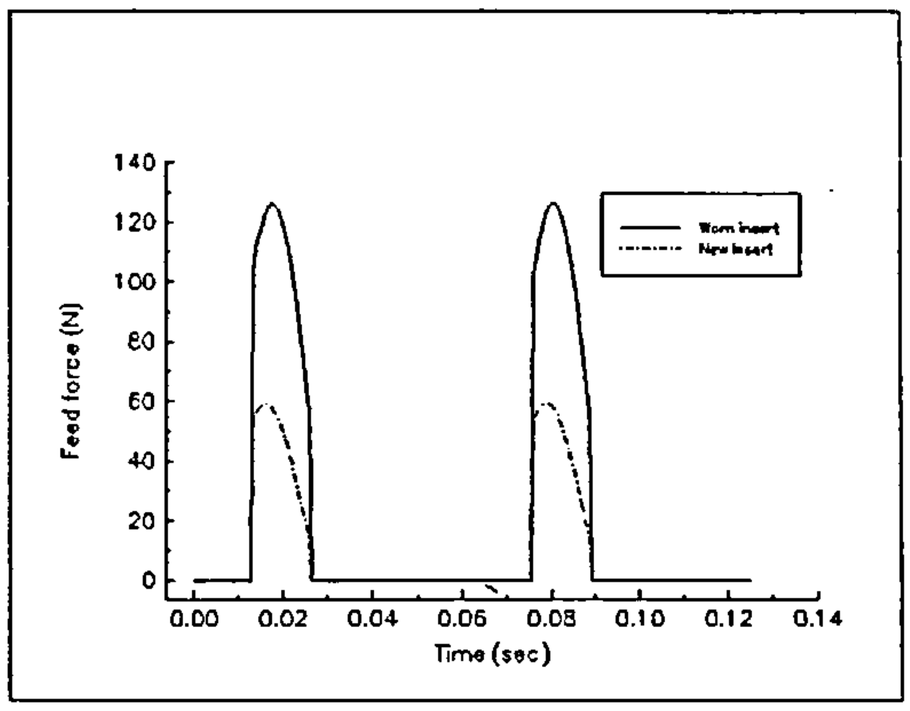

Figure 3.11 Feed force experienced by the cutter when cutting annealed En24 with a single negative rake insert showing the effects of wear

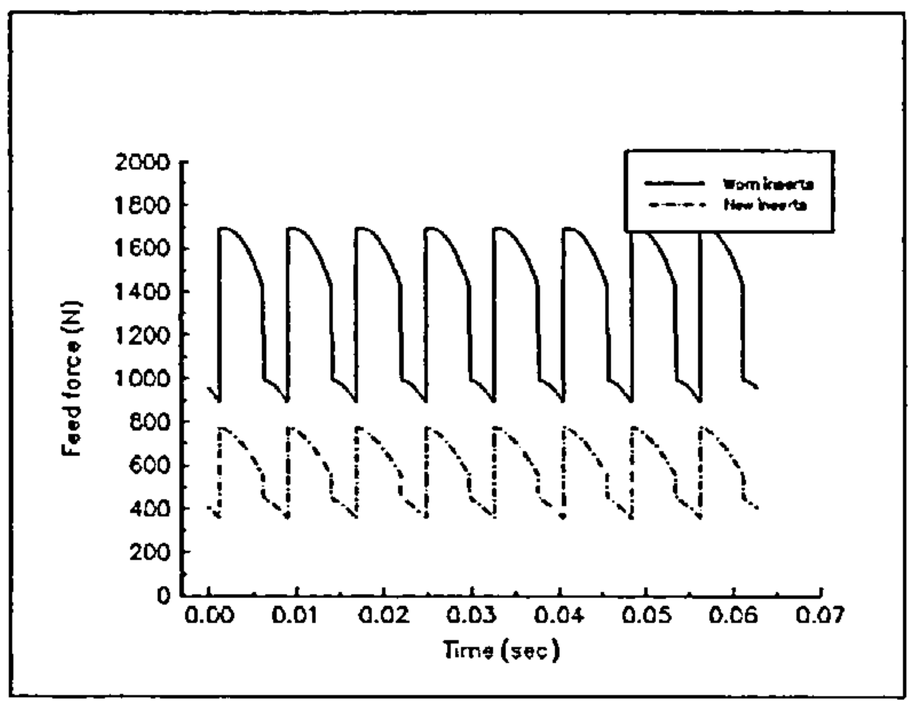

Figure 3.12 Feed force experienced by the cutter when cutting annealed En24 with eight negative rake inserts showing the effects of wear

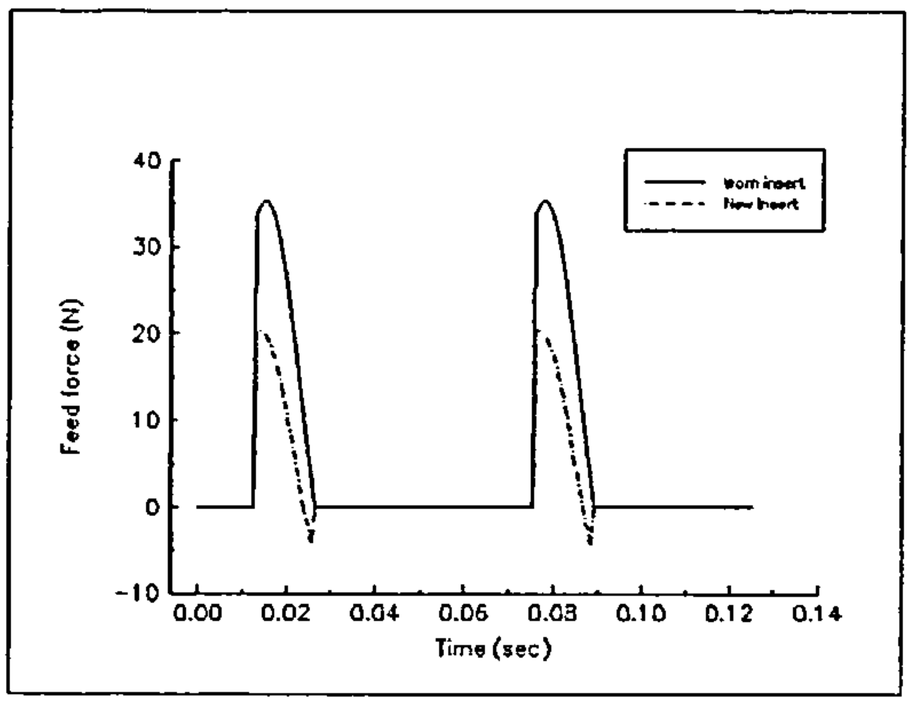

Figure 3.13 Feed force experienced by the cutter when cutting annealed En24 with a single positive rake insert showing the effects of wear

Figure 3.14 confirms the effect observed in figure 3.13 of wear on feed force when cutting annealed En24 steel. It can be seen that the discontinuity generated by a new tool is no longer present in the force generated by the worn tool. However the primary effect of tool wear as measured by the length of the flank wear land length is to raise both the mean level of feed force and the peak values of feed force. This is confirmed by figure 3.15 which illustrates the effects of flank wear on feed force generated in cutting the harder quenched and tempered En24 with an eight point positive rake cutter and by figure 3.16 which depicts the feed force experienced by the cutter when cutting the same material with an eight point negative rake cutter.

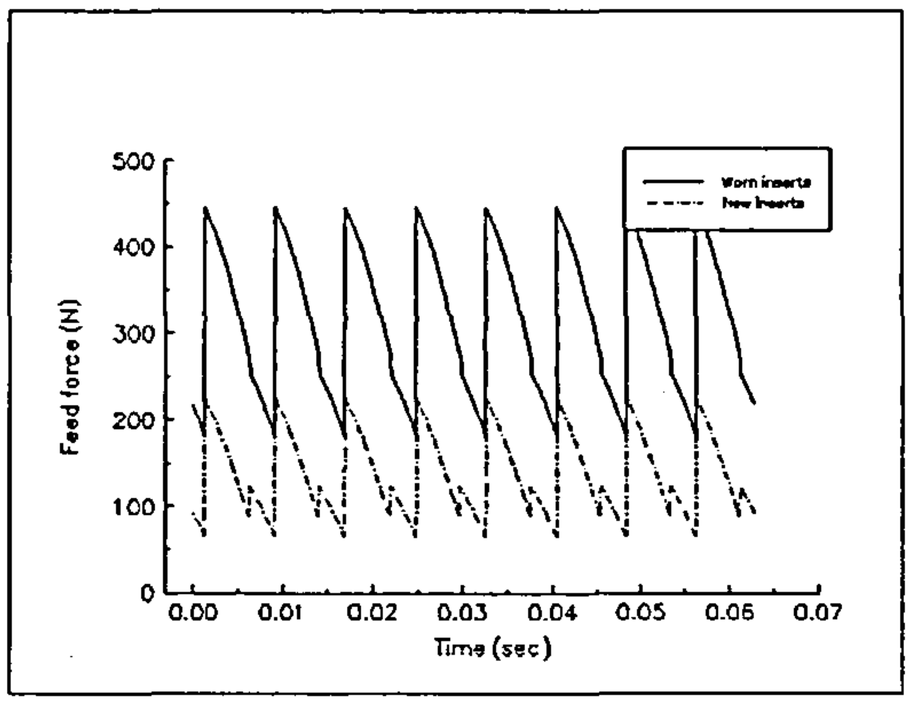

Figure 3.14 Feed force experienced by the cutter when cutting annealed En24 with an 8-point positive rake cutter showing the effects of wear

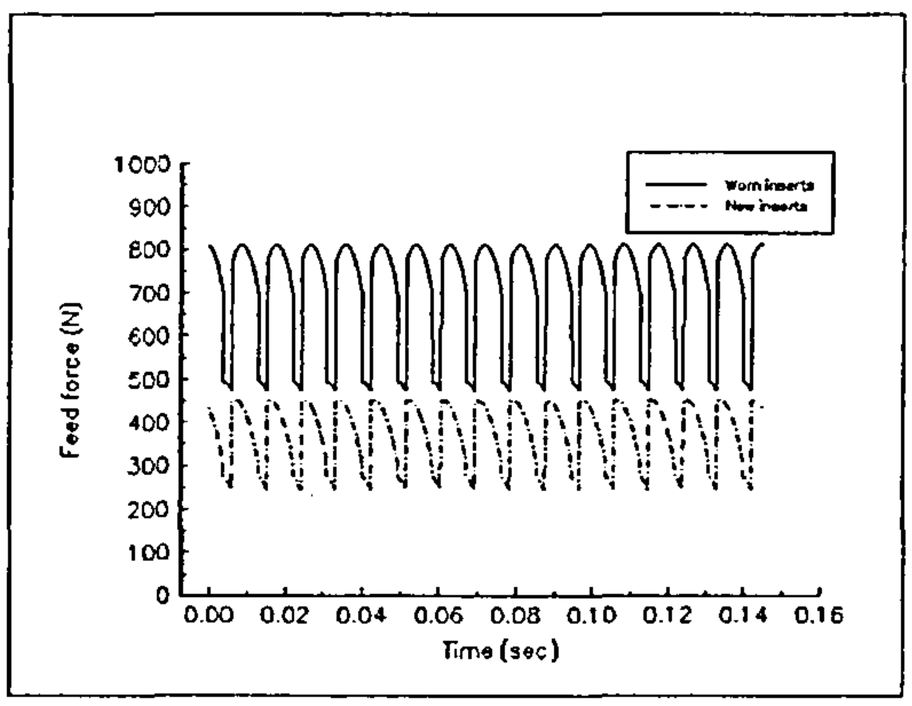

Figure 3.15 Feed force experienced by the cutter when cutting quenched and tempered En24 with an 8-point positive rake cutter showing the effects of wear

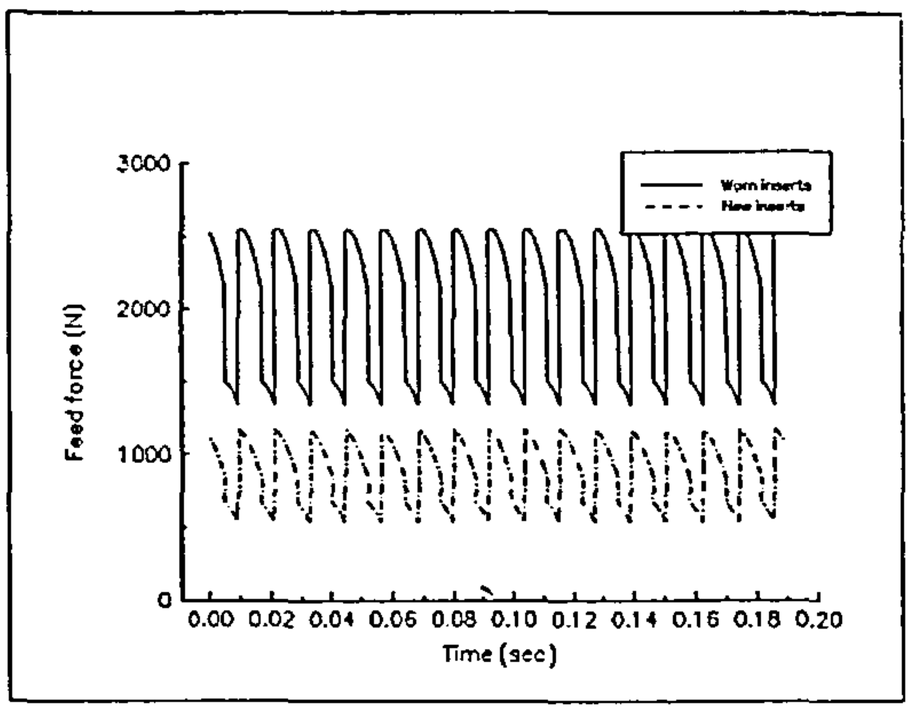

Figure 3.16 Feed force experienced by the cutter when cutting quenched and tempered En24 with an 8-point negative rake cutter showing the effects of wear

Figure 3.17 demonstrates the feed force generated in cutting type 304 stainless steel using a single point cutter employing both a new insert and a worn insert. As in previous simulations the primary effect of wear is to raise the peak forces experienced.

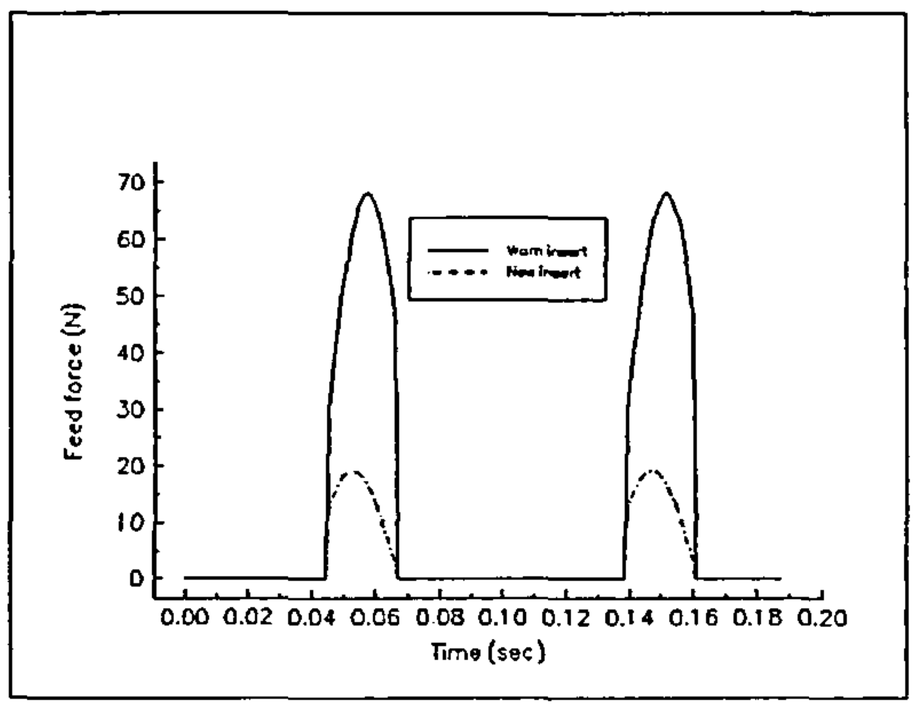

Figure 3.17 Feed force experienced by the cutter when cutting type 304 stainless steel with a single positive rake insert showing the effects of wear

3.2.3 Frequency spectra of simulated feed forces

By comparing the forces generated by the new inserts with those generated by the worn inserts in figures 3.11 to 3.17 it is clear that another effect of flank wear is to change the shape of the graphs. This is particularly obvious in figure 3.14 where a secondary peak in the feed force generated by new inserts is not present in the force generated by worn

inserts. A measure of this change of shape could be obtained from the frequency content of the graphs as demonstrated in figures 3.18a and 3.18b.

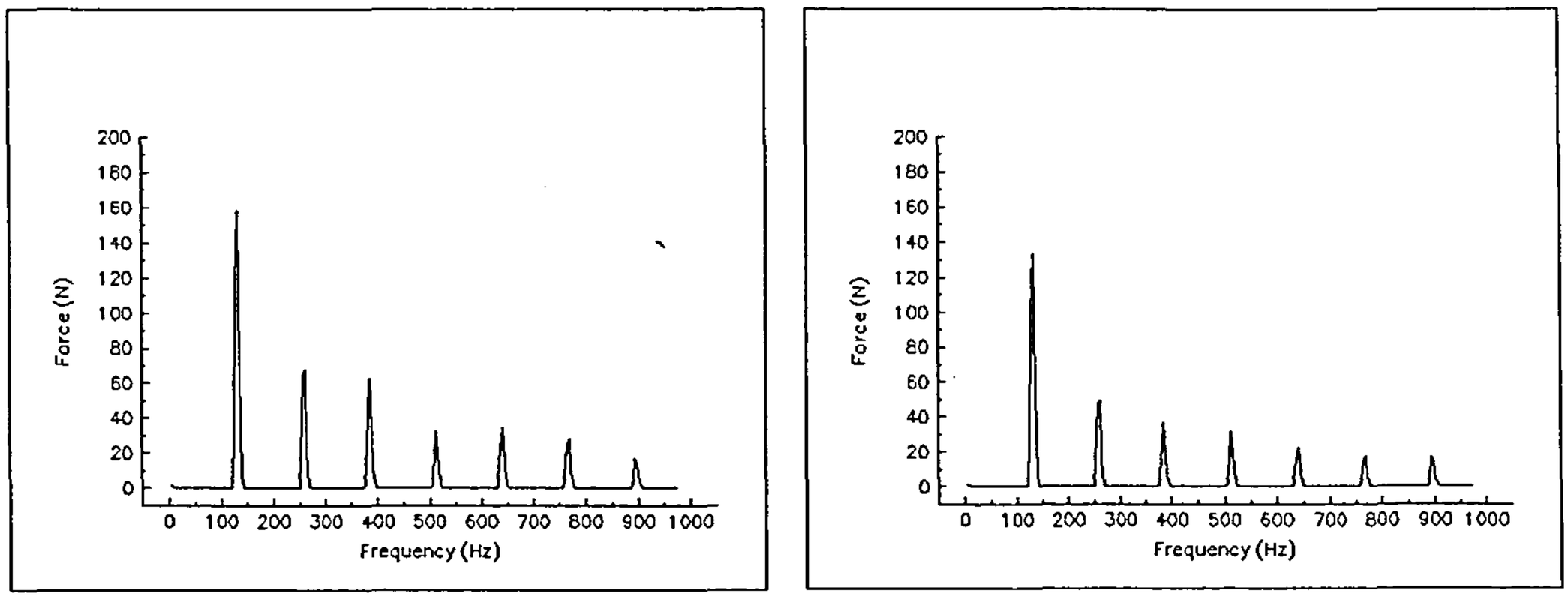

(a) (b)

Figure 3.18 Spectrum of the simulated feed force (fig. 3.14), normalised to the mean feed force, experienced by an eight point positive rake cutter when cutting annealed En24 (a) new insert, (b) worn insert.

These figures show the frequency content of the simulated feed force experienced by an eight point positive rake cutter when cutting annealed En24 for both new inserts and worn inserts. The forces were normalised to their respective mean values to emphasise the balance between the tooth passing frequency (127 Hz) and its harmonics. It is clear that a reduction in the relative contributions of the first two harmonics (255 Hz and 382 Hz) accompanies the increase in flank wear land length. This is also observable, although to a lesser extent, in the higher harmonics of the force. In a tool wear monitoring system which included force measuring instruments this change in the balance of the frequency content of the feed force would be a useful measurand. However this work concerns a measure of surface finish and as will be explained below the frequency content of the feed force is not reflected in the surface trace obtained from a profilometer which measures only a sample of the total profile.

3.2.4 Modelling of the cutter displacement

It has been seen that the forces in the feed, transverse and depth of cut directions constitute a train of pulses and it is to be expected that these pulses will excite a

vibrational response in the machine tool structure. The dominant modes of vibration response will resemble a forced response of a cantilever in the feed and transverse directions and of a simple mass/spring combination in the depth of cut direction. Forces and vibrations in the direction normal to the plane containing the feed and depth directions (y-axis) do not contribute to the generation of surface roughness [3.13] as measured by a profilometer (figure 3.3). As a result the cutter may be modelled in its simplest form by two single degree of freedom equations, one describing the cantilever deflection, η of the cutter in the feed direction and the other describing its motion in the depth of cut direction.

$$I\ddot{\eta} + C_\eta \dot{\eta} + K_\eta \eta = \tau(t) \tag{3.17}$$

where I is the moment of inertia of the cutter/spindle about an axis through one end in the transverse (y) direction

C_η is the damping of the cutter/spindle

K_η is the cantilever stiffness of the spindle/cutter

and in the depth of cut (z) direction

$$m\ddot{z} + c\dot{z} + kz = F(t) \tag{3.18}$$

where m is the mass of the cutter

c is the damping coefficient in the z-direction

k is the stiffness of the spindle in the z-direction

Estimates of the headstock natural frequencies and stiffnesses in the feed direction (x-axis) and depth of cut direction (z-axis) were obtained from impulse tests as described in chapter 5. From these measurements and the geometry of the spindle/cutter very simple estimates of the coefficients required in equations 3.17 and 3.18 were made. Using these coefficients the cantilever displacement of the cutter was calculated by using a fourth order Runge-Kutta integration technique applied to the differential equation 3.17. A similar estimate of the translational displacement of the cutter in the z-direction was made

using the same technique with equation 3.18. Table 3.2 shows the values of coefficients of equations 3.17 and 3.18 used in these simulations.

Coefficient	Value
I	0.28 kgm^2
C_η	32.2 Nm sec/rad
K_η	70780 Nm/rad
m	4.52 kg
c	454 N sec/m
k	$453.9x10^6$ N/m

Table 3.2 Values of coefficients used in numerical solutions of equations 3.17 and 3.18

Figure 3.19a shows the simulated cantilever displacement response of the cutter when cutting annealed En24 with a single new insert in a negative rake cutter. The feed force which produced this response is also shown in the figure. It can be seen that whilst the cutter is engaged in the work piece the cantilever deflection of the cutter does not exhibit vibrational characteristics. Vibrational motion only occurs when the insert is not in contact with the workpiece. When the insert is in contact with the workpiece the cantilever deflection of the cutter behaves as if it were a forced deflection response to a steadily varying applied force.

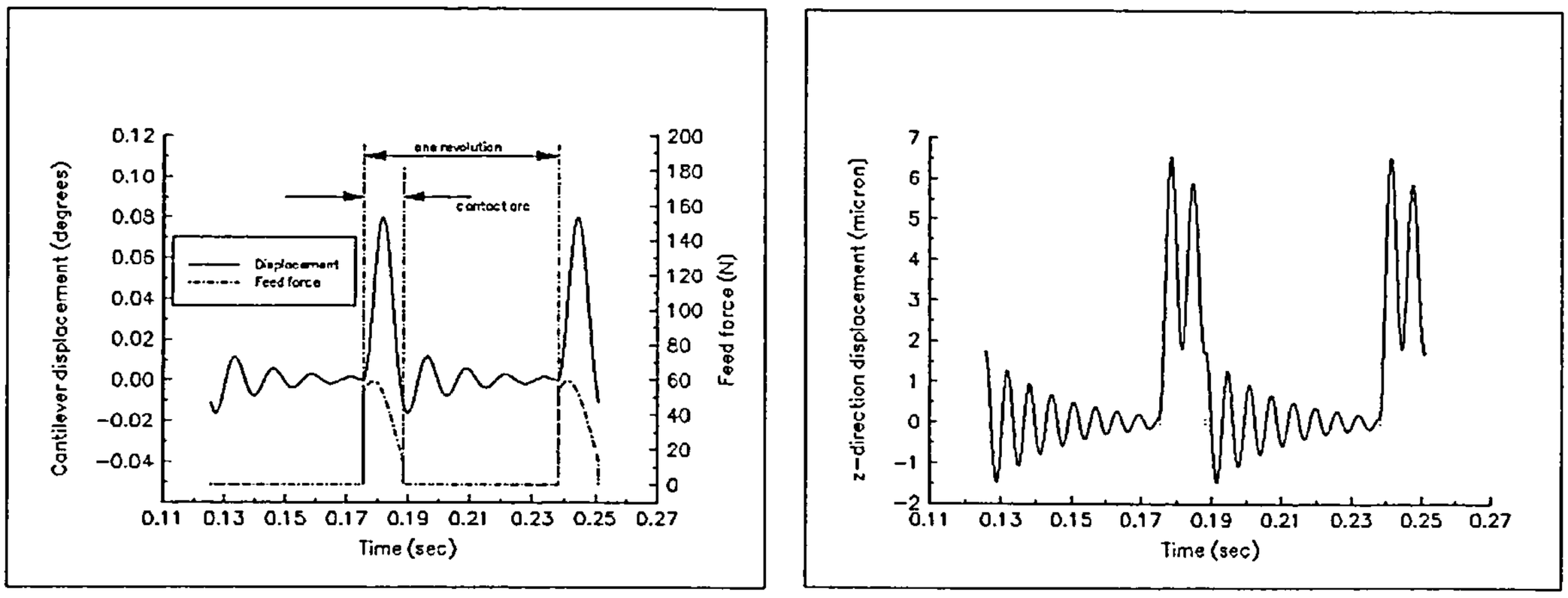

(a) (b)

Figure 3.19 Displacements of the cutter when cutting annealed En24 with a new single point negative rake cutter (a) cantilever displacement with feed force superimposed, (b) z-direction displacement.

Figure 3.19b shows the response of the cutter in the depth of cut direction when cutting annealed En24 with a single point negative rake cutter. In this direction the cutter does exhibit vibrational motion whilst the insert is in contact with the workpiece. The differences in response illustrated in figures 3.19a and 3.19b may be explained by the two different natural frequencies used to model the system response for cantilever deflection in the x-z plane and translational motion in the z-direction and hence by the differences in impact response.

Figure 3.20a shows the cantilever displacement response and the translational response of the cutter when cutting annealed En24 with new inserts in an eight point negative rake cutter. In contrast with the results for single point cutting (figure 3.19a) the free response of the cutter is suppressed by the force generated by each succeeding insert. This represents a forced response of the cutter with a frequency equal to that of the tooth passing frequency.

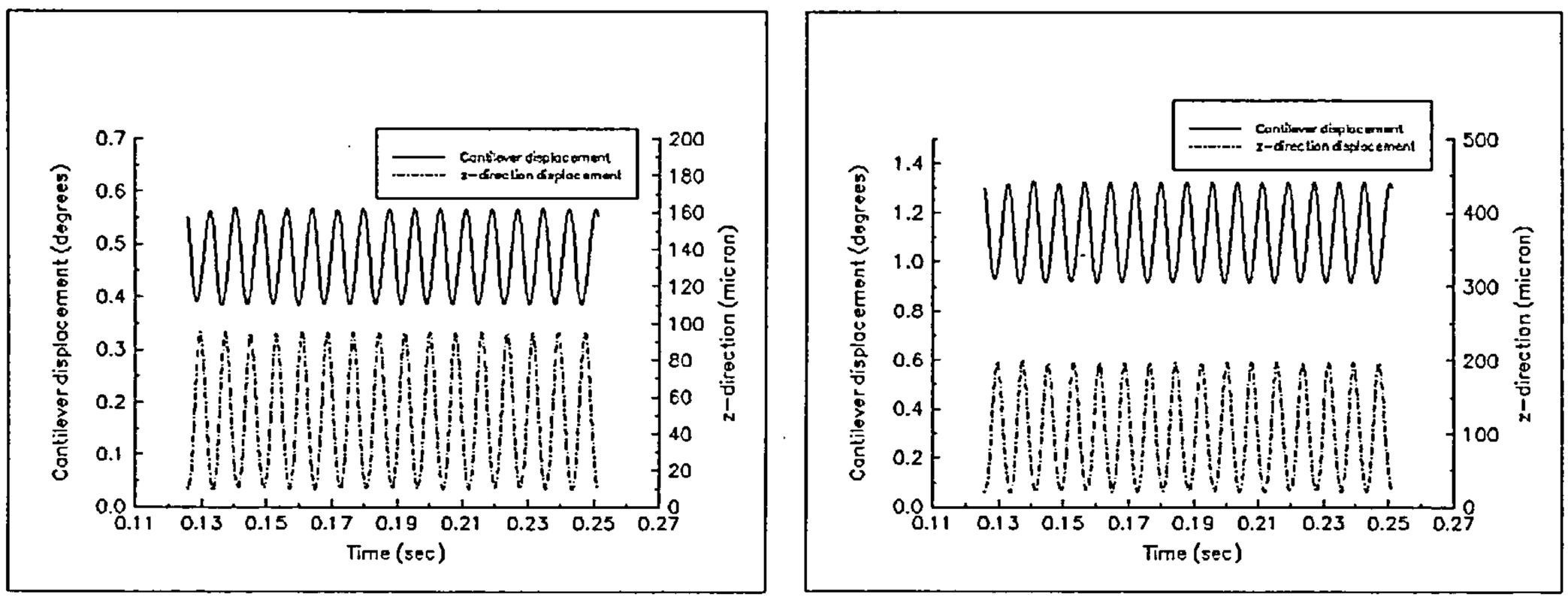

(a) (b)

Figure 3.20 Displacements of the cutter when cutting annealed En24 with an 8-point negative rake cutter (a) new inserts, (b) worn inserts.

Figure 3.20b shows that similar response characteristics occur when cutting the same material with the same cutter but with worn (V_b = 0.7 mm) inserts. As expected the mean displacements and peak displacements achieved with the worn inserts are greater than those reached with the new inserts resulting from the larger forces being generated by the worn inserts.

Figures 3.21a to 3.24b show similar vibration responses for all the force simulations discussed above.

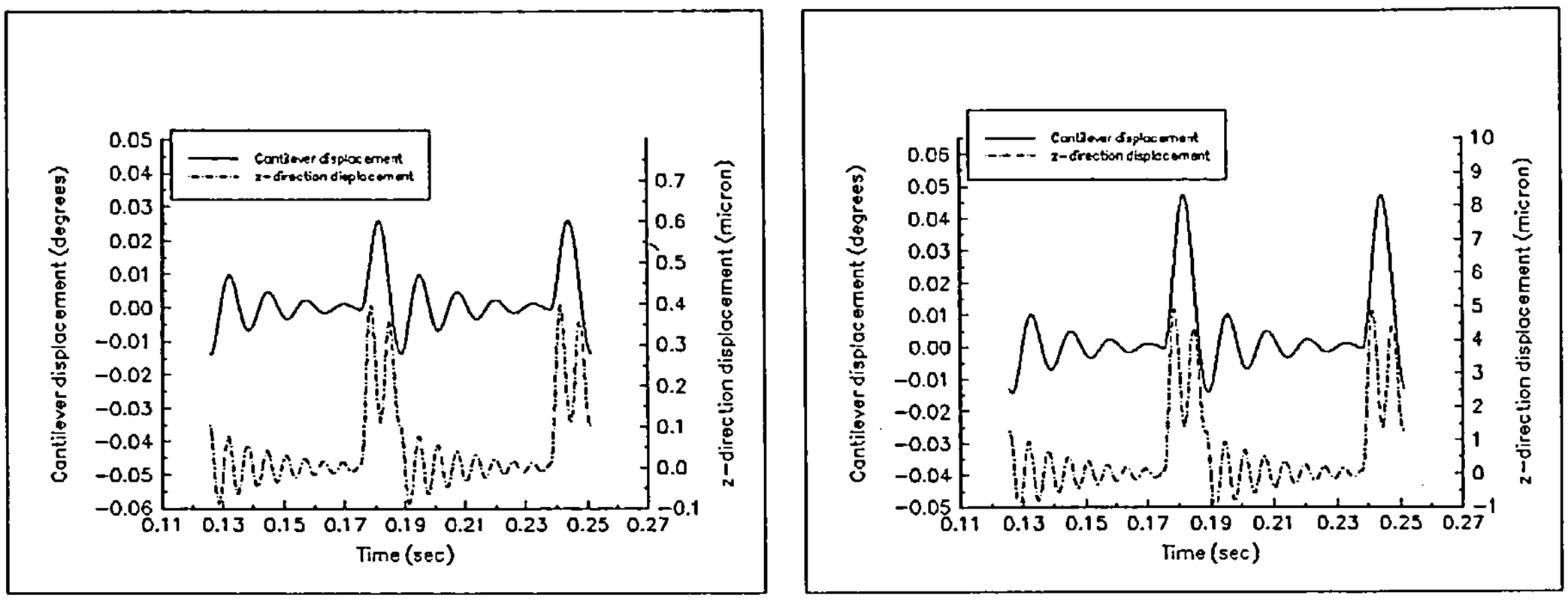

(a) (b)

Figure 3.21 Displacements of the cutter when cutting annealed En24 with a single point positive rake cutter (a) new inserts, (b) worn inserts.

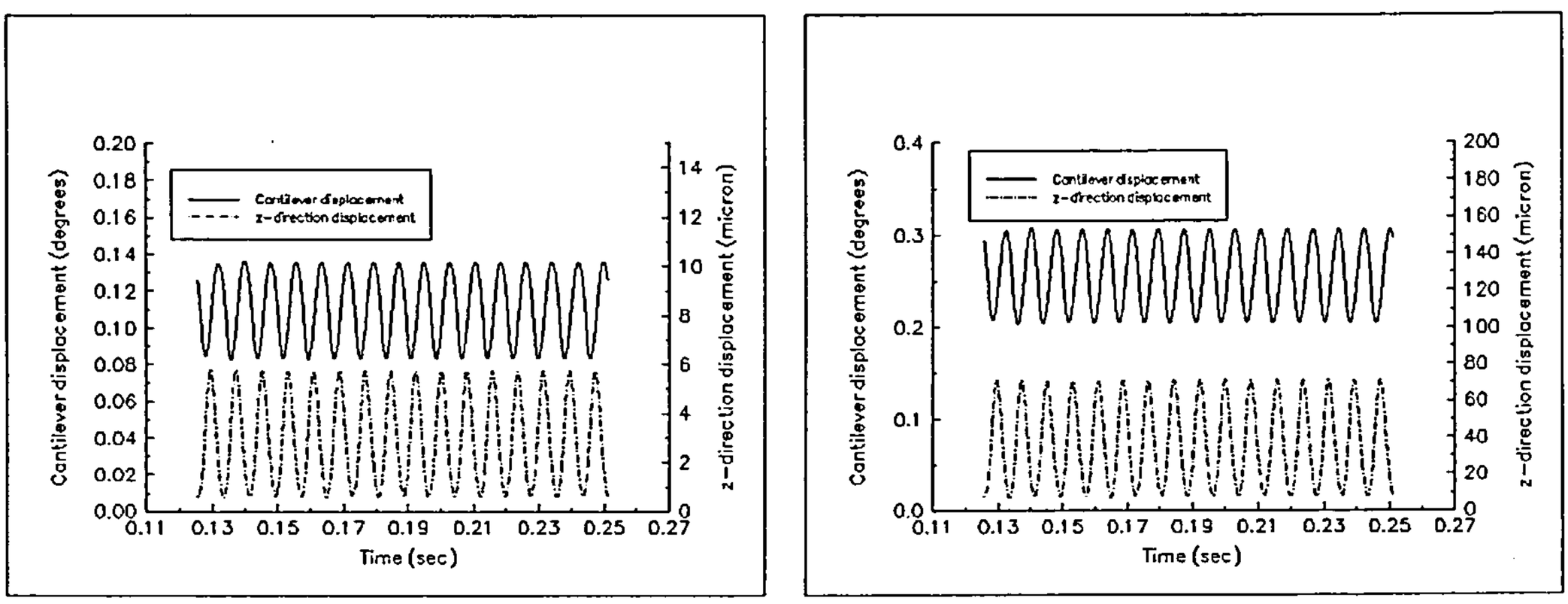

(a) (b)

Figure 3.22 Displacements of the cutter when cutting annealed En24 with an 8-point positive rake cutter (a) new inserts, (b) worn inserts.

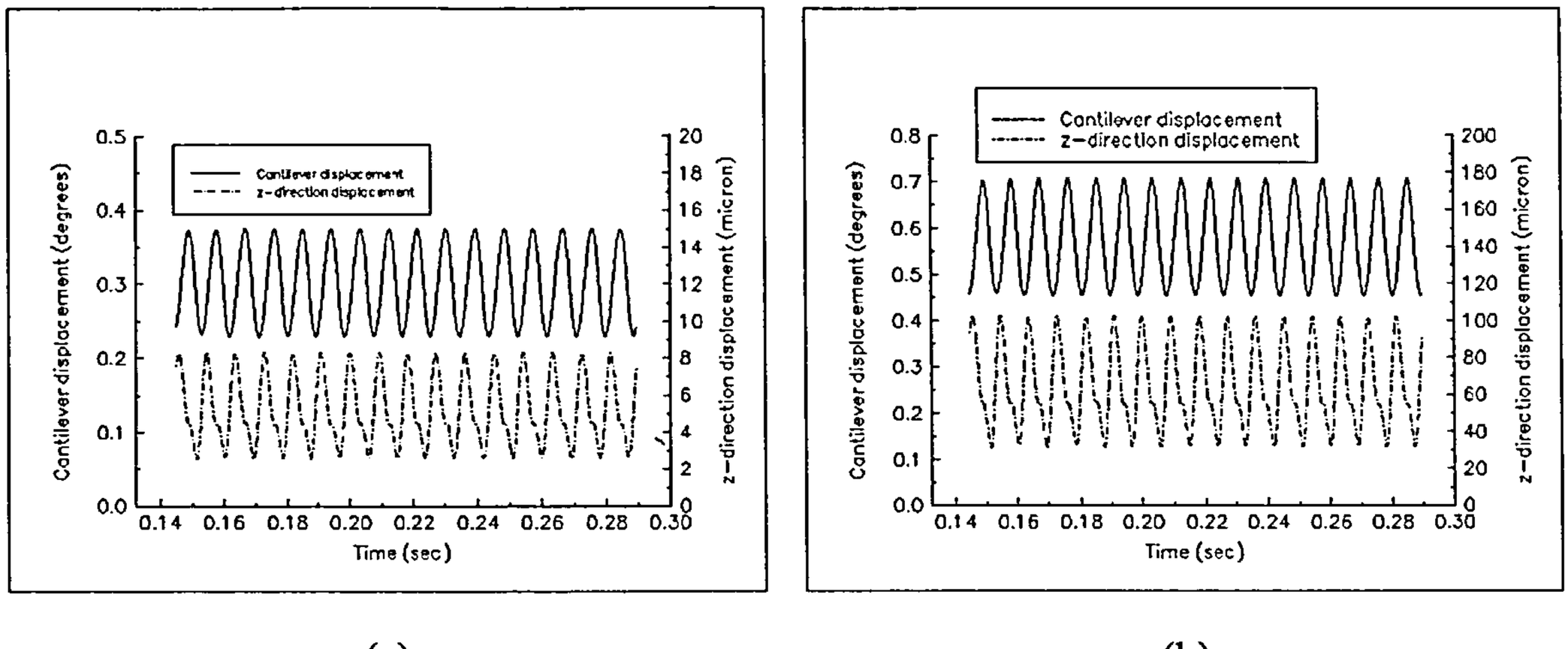

(a) (b)

Figure 3.23 Displacements of the cutter when cutting quenched & tempered En24 with an 8-point positive rake cutter (a) new inserts, (b) worn inserts.

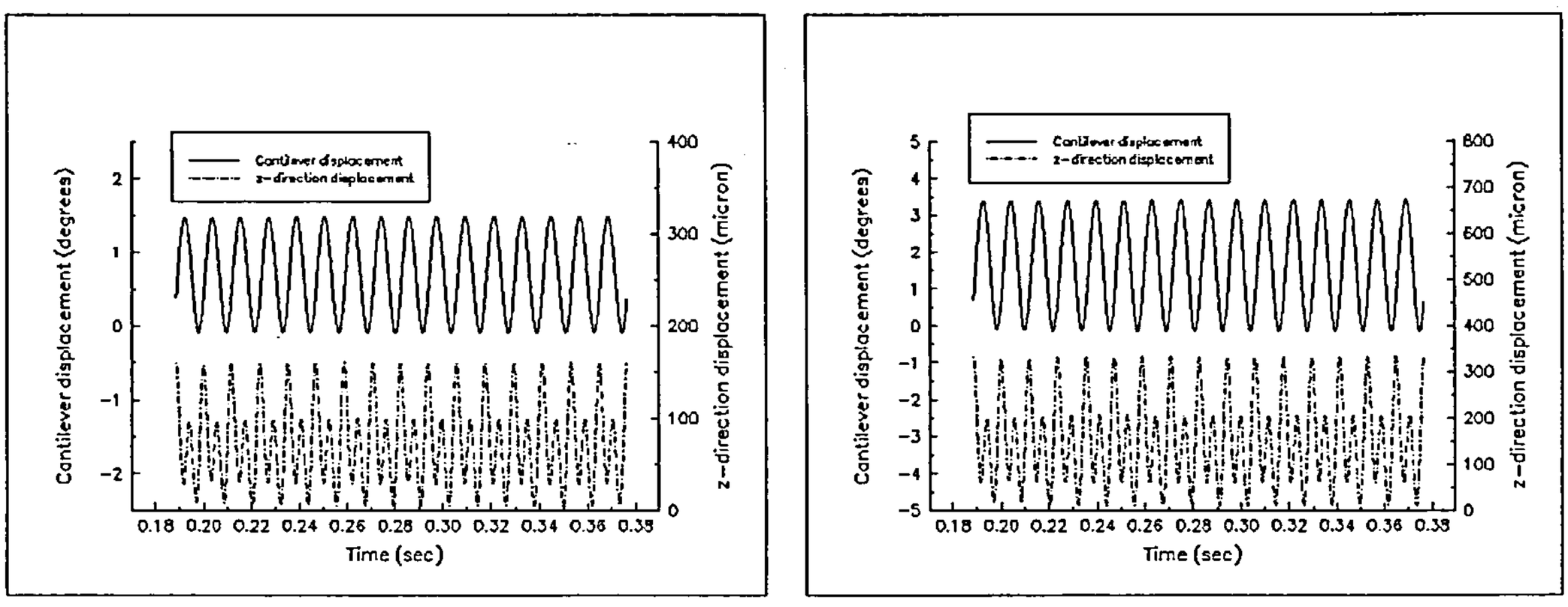

(a) (b)

Figure 3.24 Displacements of the cutter when cutting quenched & tempered En24 with an 8-point negative rake cutter (a) new inserts, (b) worn inserts.

The higher frequency component observed in the z-direction displacement shown in figures 3.24a and 3.24b arises from the natural frequency of the model in this direction. The spindle speed used in the simulation in this case (510 rev/min) was less than that used in the simulation for eight point cutting of quenched and tempered En24 (828 rev/min) and this allowed time for the impact response of the cutter to develop before being suppressed by succeeding inserts.

Figures 3.25a and 3.25b show the vibration response of the cutter when it is cutting type 304 stainless steel with a single insert in a positive rake cutter. Again the residence time of the insert in the workpiece material was sufficiently long to allow development of the cutter impact response whilst the insert was still cutting.

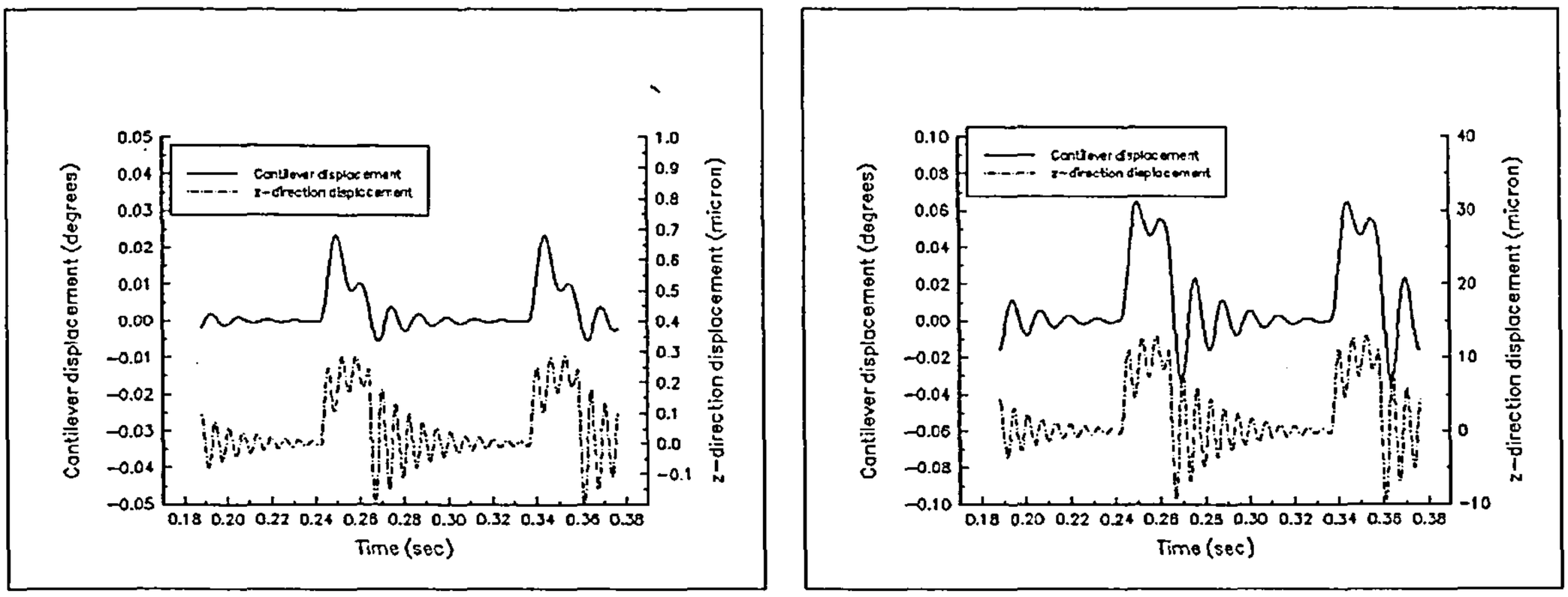

Figure 3.25 Displacements of the cutter when cutting type 304 stainless steel with a single point positive rake cutter (a) new inserts, (b) worn inserts.

The foregoing simulations of cutter forces and cutter deflections are not intended to be exact predictions of actual forces and deflections but are presented to demonstrate trends in these quantities to be expected resulting from flank wear. Indeed the model of the cutter response is recognised to be a gross simplification and could not be expected to produce exact cutter deflections without further knowledge of the dynamics of the machine tool used in this work. For example, in this work the cutter was considered only as a two degree of freedom lumped parameter system with no cross coupling between the modes of vibration. In fact the machine tool is a multi-degree of freedom system and incorporation of the associated (currently unknown) modes of vibration into the model would improve its performance. In developing the lumped parameter model estimates of the system *static* stiffnesses and damping were used. Under load it is likely that these values would change and it would be more appropriate to use *dynamic* values.

3.2.5 Modelling the cut surface

It must be noted that these figures show the displacements of the *cutter* and not the resultant surface profile. In order to establish the form of the cut surface the interactions between the deflected cutter and the work piece must be considered. In single point cutting, for example, the shape of the insert is imprinted upon the machined surface for each pass of the of the insert through the workpiece. In single point cutting this occurs once per revolution and therefore the image of the insert appears on the surface at a rate equal to the feed per revolution of the cutter. This would be shown by a profile measurement taken parallel to the feed direction. If the profile were measured along a line close to the centre of the workpiece it could be assumed that the insert which produced the profile was close to the centre of the workpiece and that the cutting force experienced by it was close to the maximum. This would produce the maximum cantilever deflection of the cutter parallel to the feed direction. Any subsequent vibrational motion of the cutter would occur with the insert no longer on the line of the profilometer trace and would not be observed in the measured profile until the insert returned to the line of the trace one revolution later. As the cutter would be experiencing forcing at tooth passing frequency, the deflection of the cutter would be identical to that of the previous insert pass through the workpiece. Therefore the profile registered on a profilometer trace would appear to have been generated by a cutter with a fixed static deflection. The profile measured from a different line on the workpiece would have similar characteristics albeit generated by a cutter with a different static deflection. For example the cantilever deflection variation shown in figure 3.19a was produced by simulating cutting of annealed En24 at a spindle speed of 955 rev/min which results in a period of 0.063 seconds per revolution. Examination of figure 3.19a shows that the cantilever deflection of the cutter every 0.063 seconds (every revolution) is again close to the maximum value assumed for the first pass of the insert. This would be expected if the cutter is being forced to vibrate at the tooth passing frequency. This implies that the surface profile appears to have been generated with the cantilever deflection of the cutter produced by a static force the magnitude of which corresponds to the once per revolution peak force. A similar argument may be deployed for the effects of the forced response in the depth of cut direction. This suggests that the effect of vibration in this direction as observed on a *line profile* parallel to the

feed direction is to reduce the effective depth of cut by a constant amount. Similar effects are expected in multi-point cutting.

The inserts used in this work for both positive rake and negative rake cutting possessed wiper flats of length 1.6 mm and provided the feed per tooth were to be less than this a featureless surface would result in theory. The feed per tooth in this work was never greater than 0.15 mm per tooth. The plan geometry of the positive rake insert is illustrated in figure 3.26a and that of the negative rake insert is shown in figure 3.26b.

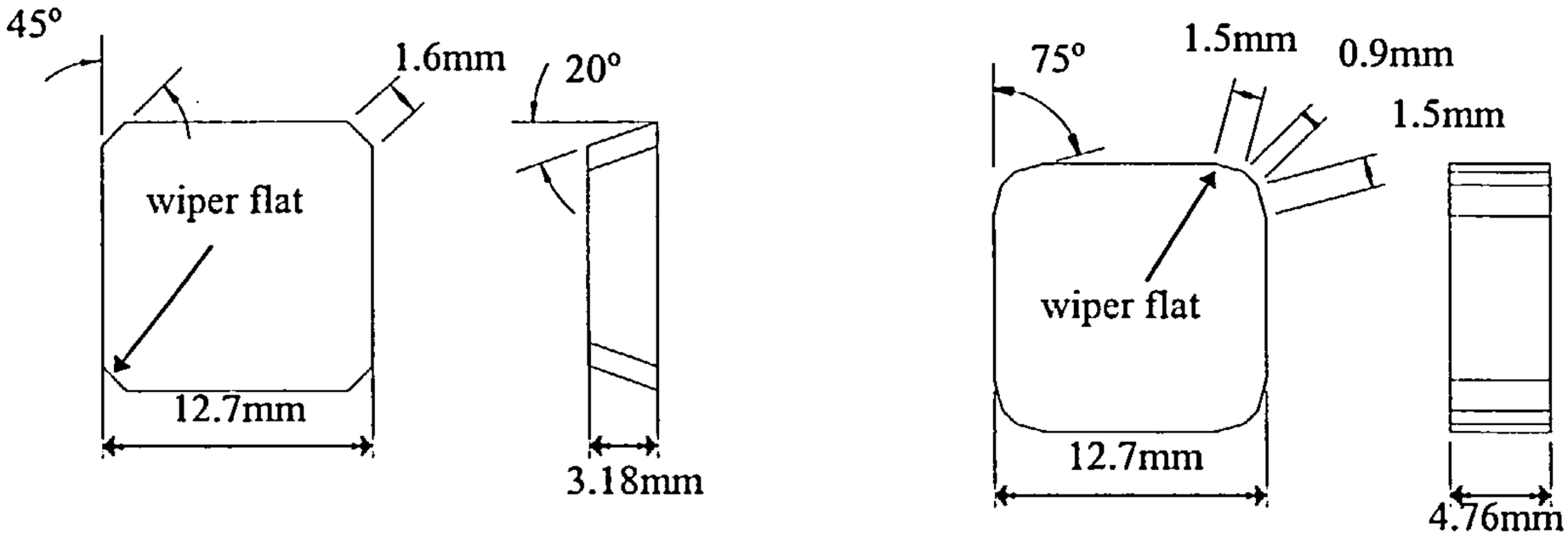

Figure 3.26 Plan geometry of (a) positive rake insert, (b) negative rake insert.

However as was explained above, the cutter takes on the appearance of a static deflection in response to the cutting forces when generating the cut surface as seen by a profilometer. This causes the insert and hence the wiper flat to be inclined to the direction of feed and the cut surface will take on the appearance of a saw-tooth as shown in figure 3.27.

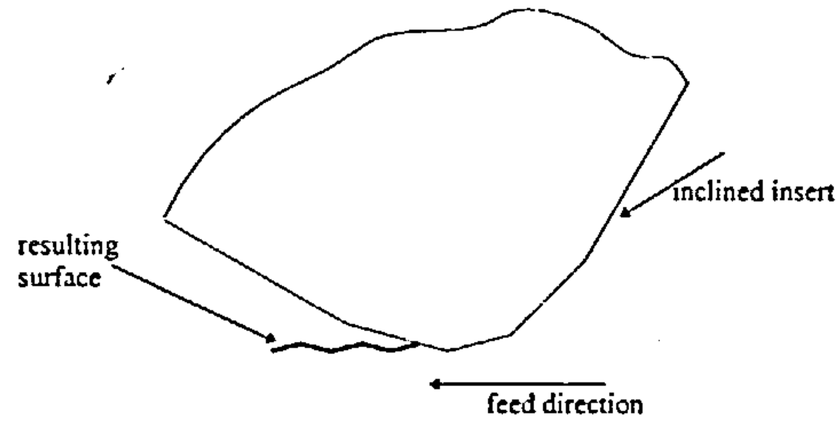

Figure 3.27 Generation of "saw-tooth" simulated surface by an inclined insert

Larger forces have been shown to produce larger cutter deflections which in turn will produce deeper saw-tooth patterns on the surface. This is illustrated in figure 3.28.

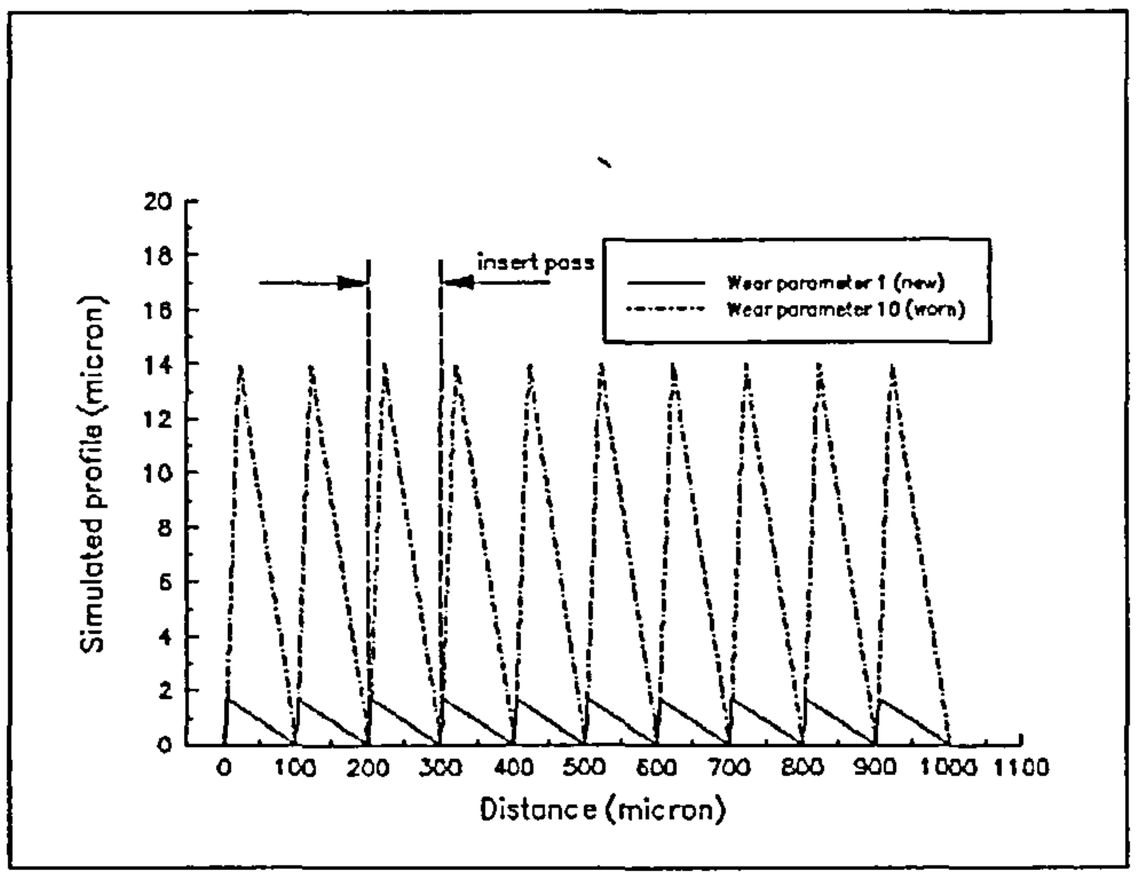

Figure 3.28 Variation in simulated surface profile as flank wear increases

<u>Expected evolution of surface spectra with insert wear</u>

As was discussed above, the model used to explore the progression of cutter response to increased cutting forces resulting from increased flank wear was not exactly representative of the true forces and deflections. Therefore a term "wear parameter" was used in this figure to characterise a measure of flank wear. The larger this parameter, the larger the length of the flank wear land and hence the larger the forces producing the cutter deflection.

It is to be expected that the spatial frequency spectra of surfaces such as those depicted in figure 3.28 would be different for the two surfaces. This is illustrated in figures 3.29a and 3.29b.

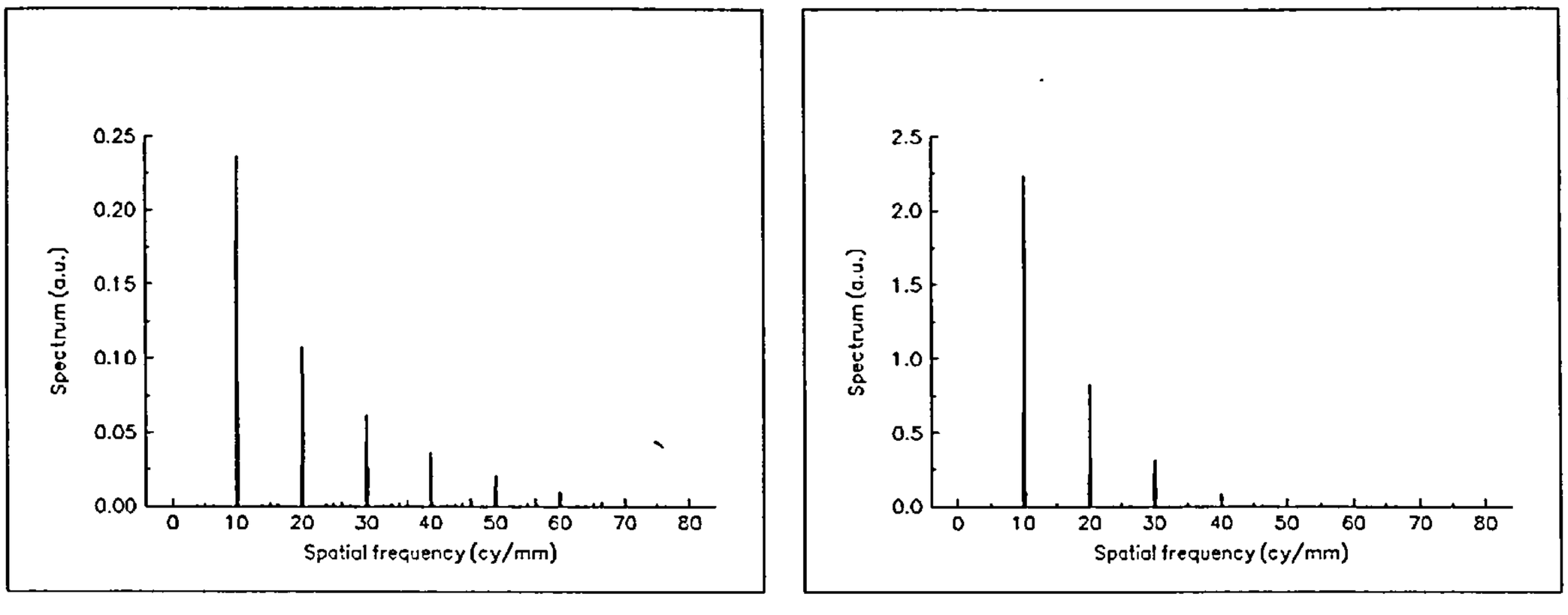

(a) (b)

Figure 3.29 Spatial frequency spectra of simulated surfaces (a) wear parameter 1, (b) wear parameter 10.

It can be seen that not only are the scales of these figures substantially different but the relative contributions of the higher spatial frequencies are less in the simulated surface generated by the worn inserts. In fact these changes are progressive with the wear parameter used to generate the surfaces. One way in which the variations may be measured is from a consideration of the energy content (integrated spectral content) of the surfaces in a set of frequency bands. Wilkinson et al recommended the use of a *low frequency band* up to but excluding the frequency associated with spindle rotation (the feed per revolution), a *kinematic band* including the frequencies associated with feed per revolution and feed per tooth and a *high frequency band* with spatial frequencies greater than those associated with feed per tooth [3.18] to examine real surfaces. In examining simulated surfaces only the kinematic band and the high frequency band will be examined since the low frequency band has its origin in vibrations of the machine tool table and these were not modelled in the force simulation. Figure 3.30 shows the variation of integrated spectral content in the kinematic and high frequency bands of the simulated surface with wear parameter.

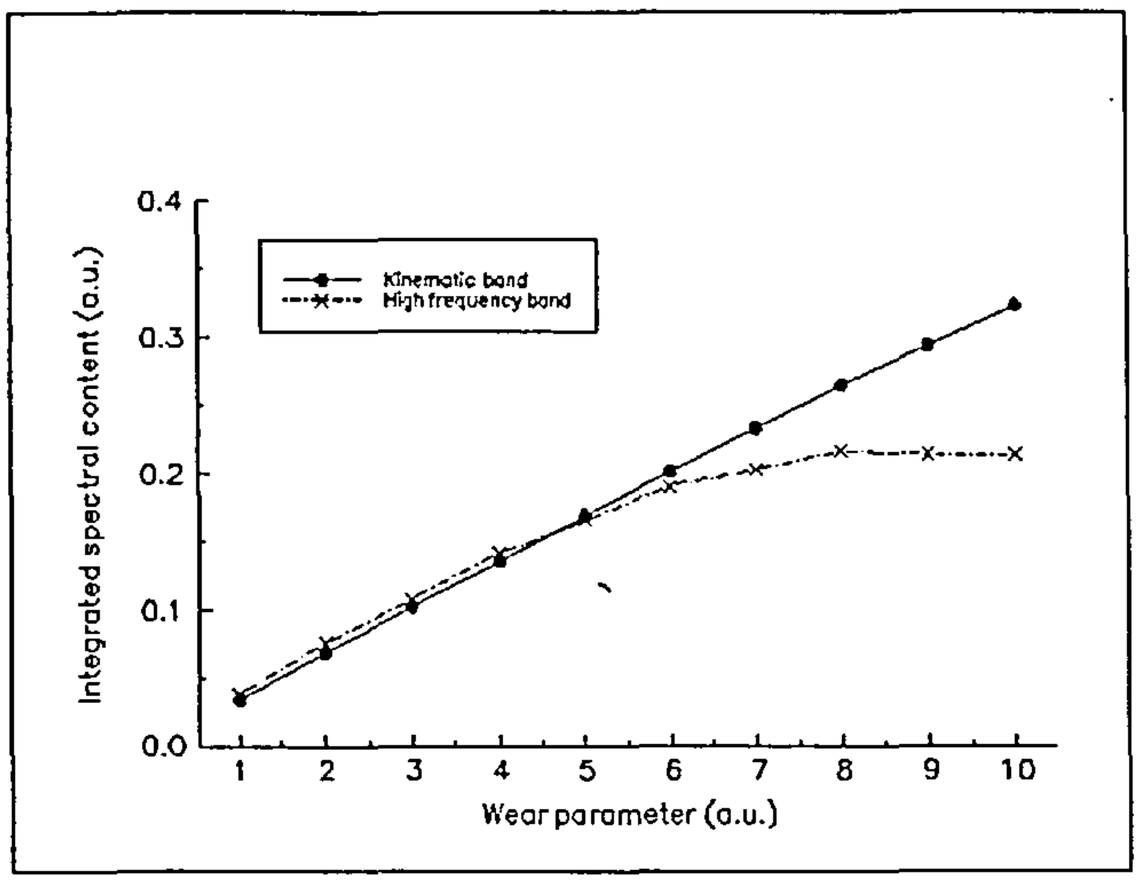

Figure 3.30 Variation in integrated spectral content of the simulated surface profile as flank wear increases

Effect of insert chipping

It can be seen that there is a linear increase in the energy contained in the kinematic frequency band as wear increases but that the energy content of the high frequency band ultimately attains a constant value. These figures assume that as the flank wear progresses no degradation of the cutting edge occurs. It is possible to model the geometric effects of edge deterioration by means of an edge "chip" as shown in figure 3.31. The effects of the chip are two-fold: an increase in the cutting force would occur which may be assumed to be included in the forcing associated with the wear parameter and an imprinting of the deformed shape of the insert would appear on the surface profile.

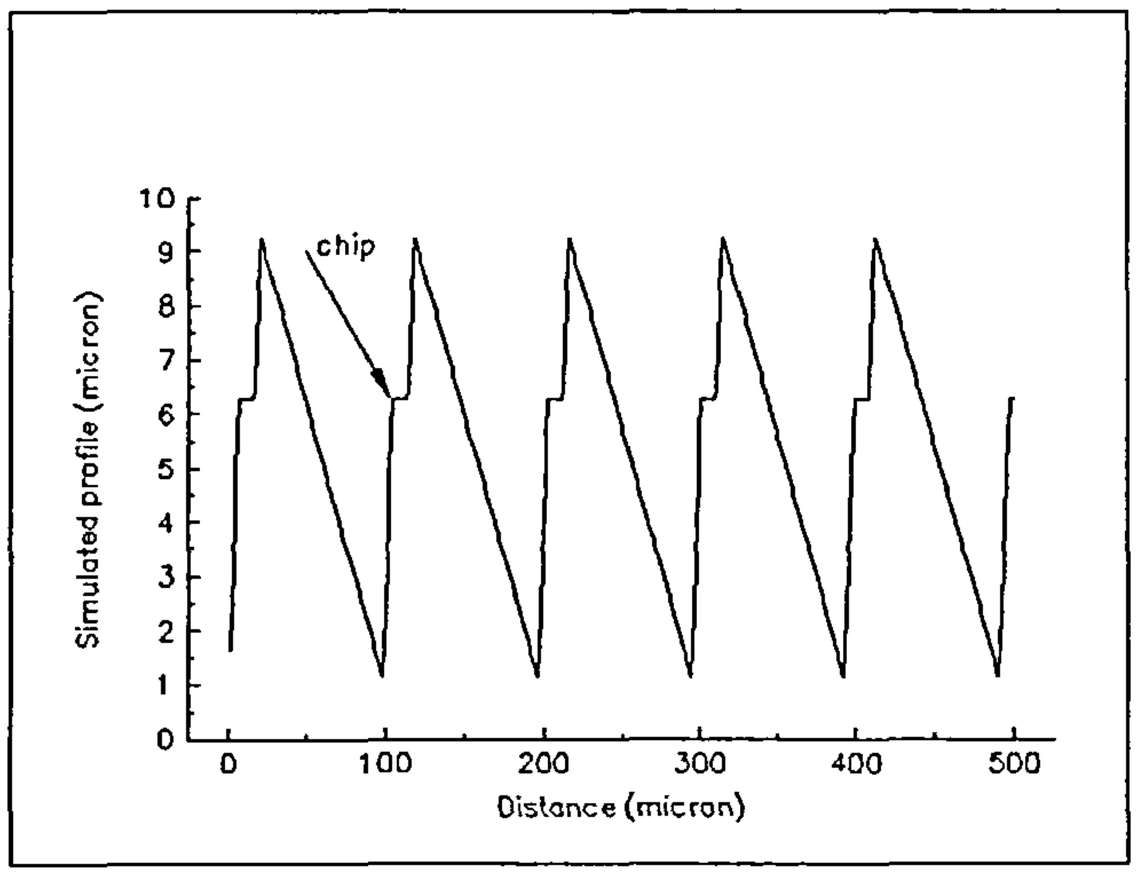

Figure 3.31 Geometric effects on the machined surface of a typical chip on the insert cutting edge.

It is to be expected that these geometric effects would be reflected in the spatial frequency spectrum of the surface produced. This is illustrated in figures 3.32a and 3.32b which show the spatial frequency spectra of a typical simulated surface generated by a worn insert and a worn, chipped insert. Both of these figures were generated by simulated inserts having the same degree of flank wear and thus the differences in the spectra result from the presence of a chipped cutting edge.

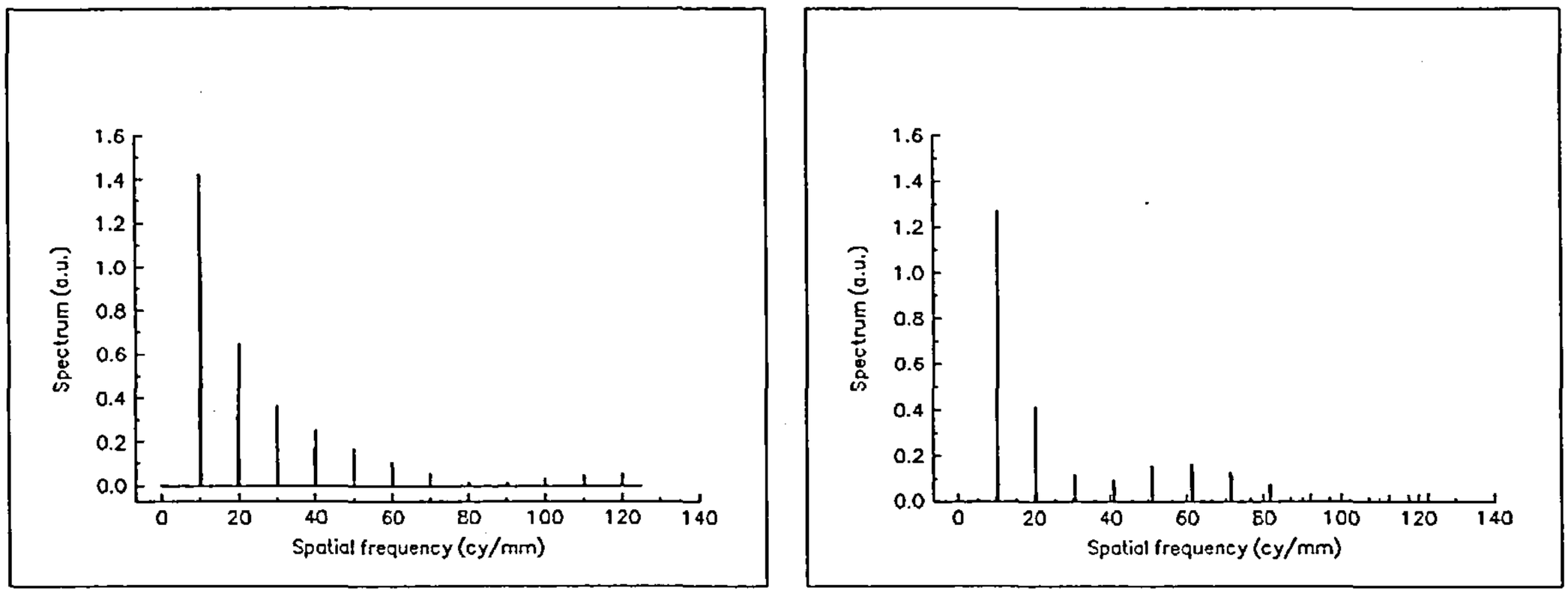

Figure 3.32 Spatial frequency spectra of simulated surfaces (a) wear parameter 6, (b) wear parameter 6 with chipped insert.

The effects of a chipped insert on the simulated surface were investigated by initiating a small chip in the insert cutting edge at a time when 40% of the insert life had been exhausted (observations made during machining tests suggest that this is a reasonable assumption) and then allowing the chip to grow until such a time that the chip occupied the length of the cutting edge. The results of this simulation are shown in figure 3.33.

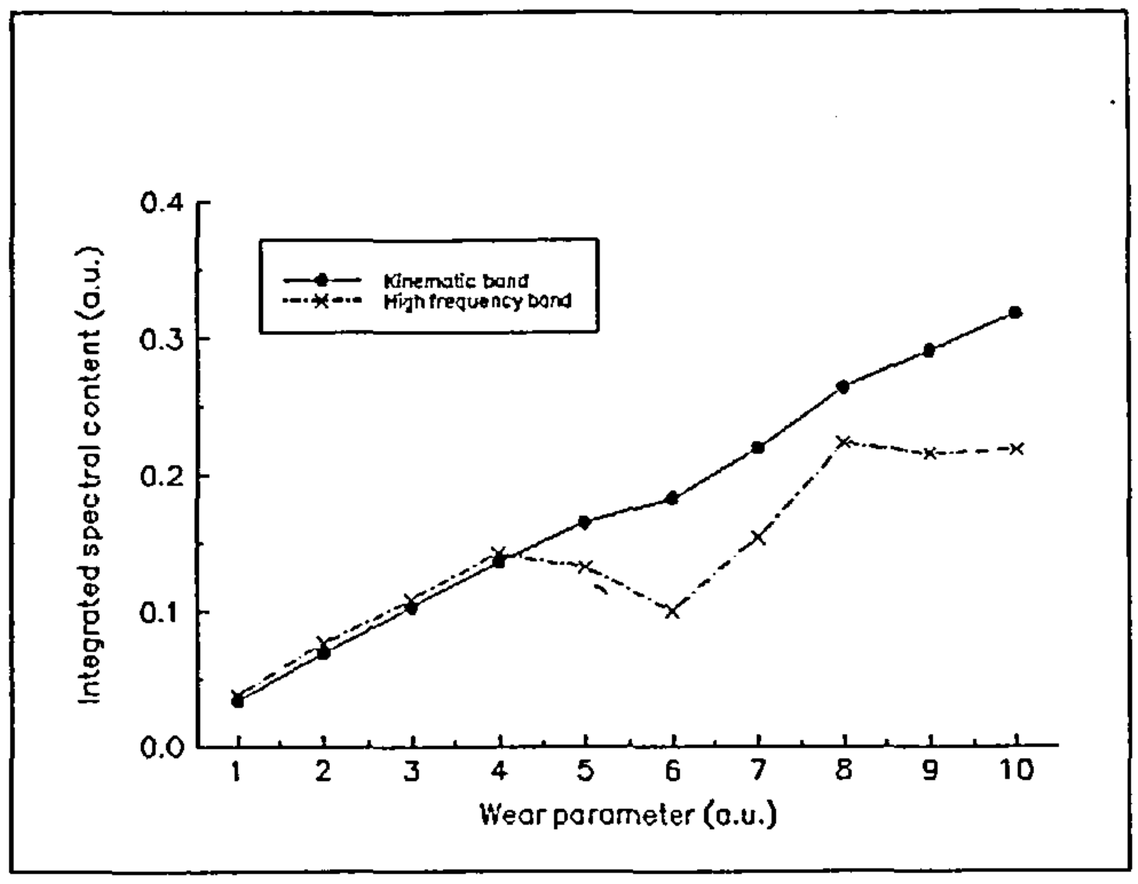

Figure 3.33 Variation in integrated spectral content of the simulated surface profile as flank wear increases combined with a cutting edge chip growth

Comparison of figure 3.33 with 3.30 shows that the presence of the growing cutting edge chip disrupts the smooth progression of the integrated spectral content in the high frequency band. It has a similar although lesser effect on the integrated spectral content in the kinematic band. It is of interest to note that as the chip length increases both the kinematic band and high frequency band integrated spectral contents revert to their unchipped characteristics. This may be explained by the fact that as the chip increases in length it is effectively worn away and the original cutting edge is replaced by a new cutting edge slightly displaced from the original.

In summary the effect of increased flank wear on the milled surface is expected to cause a progressive increase in the kinematic band spectral content of the surface. The high frequency band spectral content is anticipated to increase linearly with flank wear in the initial stages of wear thereafter the rate of change of this quantity with flank wear will decrease until the spectral content reaches a constant value. If, in addition to flank wear, a growing chip appears on the cutting edge the smooth progression of the integrated spectral content in both frequency bands will be interrupted until such time as the chip itself is essentially worn away from the edge. This will be tested experimentally and the results are reported in chapter 5 and discussed in chapter 8.

3.3 Acoustic emission and tool wear

Several sources of acoustic emission (AE) arising during the intermittent cutting process have been recognised [3.19],[3.20],[3.21] Table 3.3 lists these sources with some of their characteristics.

	Source Description	AE Type
(a)	Initial impact as the insert enters the workpiece	Burst
(b)	Shearing of the parent material of the workpiece during the cutting process	Continuous
(c)	Rubbing between the chip and the rake face and between the newly created surface and the flank face.	Continuous
(d)	Chip breakage and entanglement	Burst
(e)	A final impact caused by the relaxation of forces as the insert exits the workpiece	Burst
(f)	Insert failure	Burst

Table 3.3 Description of AE sources in machining processes.

It may be argued that the continuous AE emissions are really only a train of burst type emissions which occur so closely in time that it is impossible to separate them into individual bursts. However for this work the above classification will be used. A brief discussion of each of these sources is given below.

All these sources of AE are located in the cutting zone close to the cutting edge of the insert and AE signals are known to carry information regarding the wear state of the insert [3.6]. Kannatey-Asibu and Dornfeld [3.22] identify several properties of the AE signal which may be used to monitor the wear state of the inserts. Table 3.4 gives a brief description of these features.

	Feature	Comment
(a)	Threshold count	Does not work well with continuous emissions [3.23]
(b)	Amplitude distribution	Better suited to continuous emissions [3.24]
(c)	RMS	Useful for burst and continuous emissions [3.23]
(d)	Frequency spectra	Useful for continuous emissions but may require specialised transducers if deconvolution of transducer characteristics is to be avoided. [3.12]

Table 3.4 Acoustic emission features used in tool wear monitoring.

In this work the availability of a novel fibre optic AE transducer [3.8] which possesses wide flat frequency response to beyond 1 MHz enabled measurements of the frequency content of AE signals to be made. The signal from the same transducer could be used to provide a measure of the rms of the AE signal as described in chapter 4 and hence in this work the correlation between rms AE and tool wear was also investigated.

3.3.1 Entry impact

The magnitude of the entry impact is spindle speed dependent, increasing as rotational speed increases. It may also be argued that it is dependent on insert geometry as the effective feed per tooth varies with flank wear altering the 'quality' of initial contact with between the insert and workpiece.

The impact may be modelled by an impulse. The subsequent AE signature of the impulse would be seen as a burst exhibiting ring-down phenomena with frequency and decay rate determined by the elastic and damping properties of the workpiece material.

3.3.2 Cutting process

In this section of the thesis the models described by equations 3.19 to 3.56 were developed in the references [3.12], [3.19], [3.22] and [3.26]. It was decided however, by the present author, that the use of the original workpiece material data used by Hu et al [3.26] should be replaced by the constitutive equations developed in references [3.30] and [3.33]. These models were then used to calculate the variation of rms AE and mean frequency of AE with insert wear.

RMS AE and metal cutting parameters

The major source of AE during metal cutting is the plastic deformation associated with chip formation [3.19]. AE generation occurs in three zones in orthogonal metal cutting: the primary zone containing the shear plane, a secondary zone containing the chip/rake face interface and a tertiary zone containing the flank/workpiece interface. The AE generated in the primary zone is related to the energy required to shear the work piece material. The AE arising in the secondary zone originates in shearing processes and slipping processes. The slipping process generates AE through frictional rubbing. In the tertiary zone AE is generated by rubbing as described below. These zones are illustrated in figure 3.34

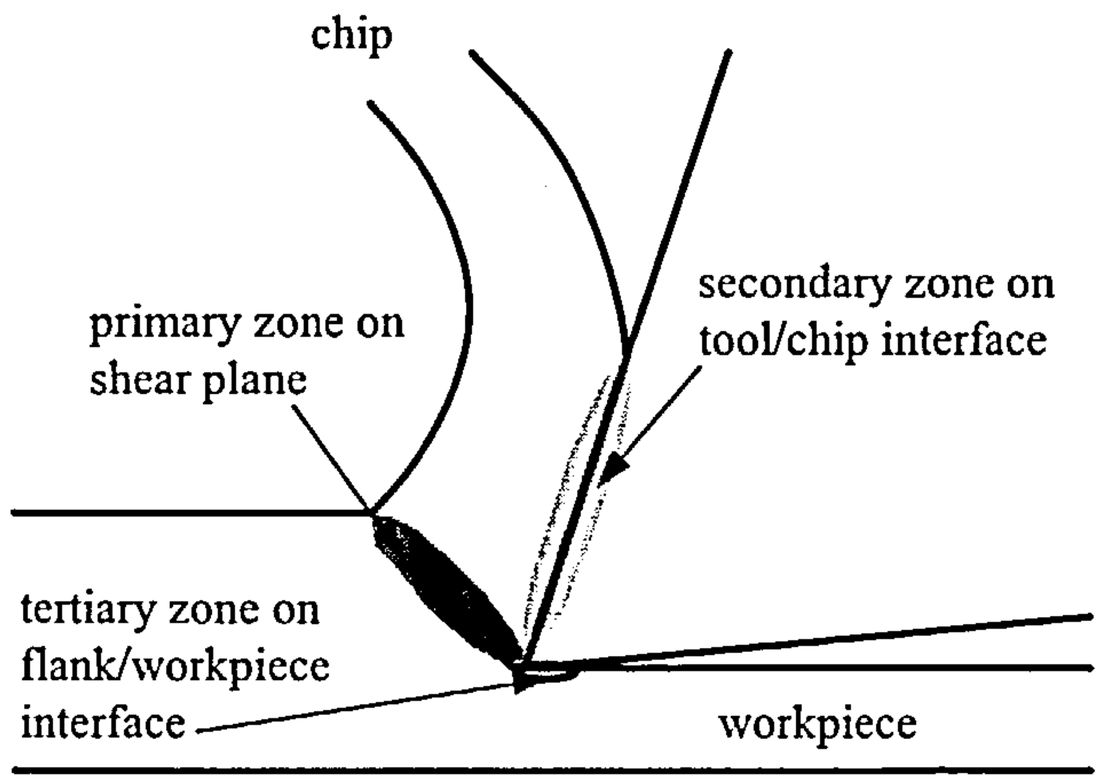

Figure 3.34 Zones of AE generation in orthogonal cutting.

Kannatey-Asibu and Dornfeld [3.22] have investigated the relationship between rms AE and cutting geometry. Briefly their work relates the definition of the rms value of the AE signal to the power of the signal and thence to the power consumed in deforming the workpiece material. From the definition of the rms value of a signal

$$P = \frac{dE}{dt} \propto (rms)^2 \qquad (3.19)$$

where P is the power of the signal and E is the energy of the signal. If the material being deformed is subject to a constant applied stress and strain rate, the rate of work of plastic deformation $\dot{W}$ is given by

$$\dot{W} = V\dot{\varepsilon}\sigma \tag{3.20}$$

where V is the volume of material undergoing deformation

$\dot{\varepsilon}$ is the strain rate

σ is the applied stress.

If it is assumed that this work rate is proportional to the power of the AE signal which it produces, then the following relationship between the rms of the AE signal and the work rate of plastic deformation results.

$$(rms)^2 = C_1 V\dot{\varepsilon}\sigma \tag{3.21}$$

where C_1 is a constant of proportionality.

In the primary zone where the average shear stress is assumed constant and using the well-known expressions for shear velocity, U_s, shear strain rate, $\dot{\gamma}$, and shear zone volume, V_s from Shaw [3.17]

$$U_s = \frac{\cos\alpha}{\cos(\phi - \alpha)} U \tag{3.22}$$

$$\dot{\gamma} = \frac{\cos\alpha}{\cos(\phi - \alpha)} \frac{U}{\Delta y} \tag{3.23}$$

$$V_s = \frac{t}{\sin\phi} b\Delta y \tag{3.24}$$

where ϕ is the shear plane angle

α is the rake angle

t is the undeformed chip thickness

b is the depth of cut

U is the cutting speed

Δy is the thickness of the shear zone.

equation 3.20 may be re-written to give the work rate of shear deformation $\dot{W}_s$ in the primary zone

$$\dot{W}_s = bt\tau_1 \frac{\cos\alpha}{\sin\phi\cos(\phi - \alpha)}U \tag{3.25}$$

where τ_1 is the flow stress in shear in the primary deformation zone.

In the secondary zone the chip sticks for part of its motion over the rake face of the insert and is subject to shear deformation and for the remaining part of its motion it slides until it loses contact with the insert. In the sticking region equation 3.20 may be re-written to give the work rate in shear $\dot{W}_{c1}$ on the rake face

$$\dot{W}_{c1} = \tau_2 b l_1 U_c \tag{3.26}$$

where τ_2 is the flow stress in shear in the secondary deformation zone

l_1 is the length of the sticking region

U_c is the chip velocity.

Again from Shaw [3.17]

$$U_c = \frac{\sin\phi}{\cos(\phi - \alpha)}U \tag{3.27}$$

which leads to an expression for the work rate in the deformation region

$$\dot{W}_{c1} = \tau_2 b l_1 \frac{\sin\phi}{\cos(\varphi - \alpha)}U \tag{3.28}$$

In the sliding region of rake face contact, the work rate is related to the friction force between the chip and the velocity of the chip over the rake face. Kannatey-Asibu and Dornfeld [3.22] demonstrated that although the normal stress distribution on the rake face is non-uniform and the actual of contact area between the chip and the rake face varies it is possible to derive an expression for the sliding friction force on this face

$$F = \frac{\tau_2 b(l - l_1)}{3} \tag{3.29}$$

where l is the total length of the chip/tool contact region.

The work rate in this region $\dot{W}_{c2}$ may then be obtained by multiplying equation 3.29 by the chip velocity

$$\dot{W}_{c2} = \frac{\tau_2 b(l - l_1)}{3} U_c = \frac{\tau_2 b(l - l_1)\sin\phi}{3\cos(\phi - \alpha)} U \tag{3.30}$$

Thus the total work rate $\dot{W}_c$ in the secondary zone from both sliding and sticking is given by the sum of $\dot{W}_{c1}$ and $\dot{W}_{c2}$ .i.e.

$$\dot{W}_c = \tau_2 b l_1 \frac{\sin\phi}{\cos(\phi - \alpha)} U + \frac{\tau_2 b(l - l_1)\sin\phi}{3\cos(\phi - \alpha)} U = \frac{\tau_2 bU(l + 2l_1)\sin\phi}{3\cos(\phi - \alpha)} \tag{3.31}$$

From equations 3.21, 3.25 and 3.31 it is possible to obtain a relationship between the rms of the AE signal and the mechanical parameters of machining for the primary and secondary zones.

$$(rms)^2 = (C_1 bU)\left[\frac{\tau_1 t\cos(\alpha)}{\sin(\phi)\cos(\phi - \alpha)} + \frac{\tau_2(l + 2l_1)\sin(\phi)}{3\cos(\phi - \alpha)}\right] \tag{3.32}$$

Blum and Inasaki [3.19] have investigated AE generation in the tertiary deformation zone resulting from the flank wear land. They concluded that AE generated in this zone was related to friction. Based on their work Carolan et al [3.11] modified equation 3.32 to take account of the effects of this tertiary zone frictionally generated AE:

$$(rms)^2 = C_1 bU\left[\frac{\tau_1 t\cos(\alpha)}{\sin(\phi)\cos(\phi - \alpha)} + \frac{\tau_2(l + 2l_1)\sin(\phi)}{3\cos(\phi - \alpha)} + C_2\tau_3 V_b\right] \tag{3.33}$$

where C_2 permits an unknown ratio of sticking to sliding at the tool/workpiece interface.

V_b is the length of the flank wear land.

Frequency content of AE signal and metal cutting parameters

Carolan et al [3.12] showed that in metal cutting the maximum in the frequency spectrum of a wave created by a group of migratory dislocations is proportional to the product of the strain ε and strain rate $\dot{\varepsilon}$ experienced by the workpiece.

$$f \propto \dot{\varepsilon}\varepsilon \tag{3.34}$$

If it is assumed that the mean frequency in the spectrum associated with the group of dislocations is related to the maximum frequency and deformation in the primary zone, where most of the AE is generated [3.12], is considered a relationship between the shear strain, γ, the shear strain rate $\dot{\gamma}$, and the mean frequency, $\bar{f}$, may be developed.

$$\bar{f} \propto \dot{\gamma}\gamma \tag{3.35}$$

If the well known expressions [3.17] for shear strain

$$\gamma = \frac{\cos\alpha}{\sin\phi\cos(\phi-\alpha)} \tag{3.36}$$

and shear strain rate

$$\dot{\gamma} = \frac{\cos\alpha}{\cos(\phi-\alpha)}\frac{U}{\Delta y} \tag{3.37}$$

are substituted into equation 3.35 an expression for the dependence of mean frequency on the geometric properties of the cutting process results

$$\bar{f} \propto \frac{\cos^2(\alpha)}{\sin(\phi)\cos^2(\phi-\alpha)}\frac{U}{\Delta y} \tag{3.38}$$

where α is the rake angle

ϕ is the shear plane angle

U is the cutting speed

Δy is the width of the shear zone

If it is assumed that Δy does not change with tool wear and that the cutting speed is constant equation 3.38 may be used to demonstrate how the mean frequency in the AE spectrum varies with changes in tool geometry brought about by tool wear. The shear plane angle ϕ will be altered by changes in the equilibrium of forces at the cutting edge brought about by changes in, for example, the local rake angle. This will in turn result in changes in the strain rates and in the temperatures in the three zones. In order to calculate the effects of geometrical changes an iterative procedure similar to that used by Young et al [3.3] and Hu et al [3.26] may be used.

Cutting geometry and acoustic emission

An inspection of equations 3.33 and 3.38 shows that both the rms value of the AE signal and its frequency content depend to some extent on the shear plane angle and the insert rake angle. It is known that the shear plane angle will vary with the insert rake angle [3.3],[3.26],[3.27].

The models of Young [3.3] and Hu [3.26] are based on earlier work by Oxley and enable the prediction of cutting forces, temperatures and shear plane angle from a knowledge of the workpiece material flow stress, workpiece material thermal properties and the cutting conditions. In this work this model will be used to predict the variation of shear plane angle with rake angle. Figure 3.35 shows the arrangement of the forces considered in this model.

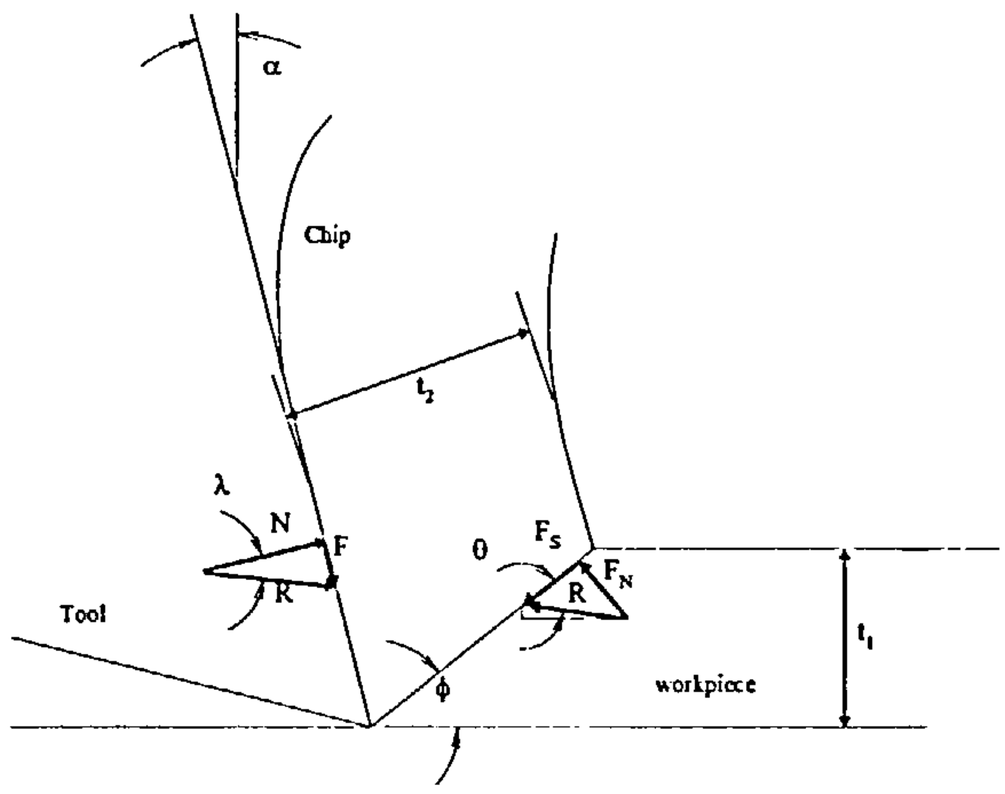

Figure 3.35 Forces in orthogonal cutting.

The force N is the normal force acting on the tool/chip interface, force F is the friction acting along this interface and together these forces produce the resultant force R acting on the interface making an angle λ with the normal force. Since the chip is assumed to be in equilibrium the resultant cutting force on the shear plane is equal and opposite to the resultant force on the tool/chip interface. F_s is the shearing force along the shear plane and the angle between the resultant cutting force and the shearing force is θ. F_n is the component of the resultant cutting force perpendicular to the shear plane. α is the rake angle of the tool.

In order to obtain the shear plane angle the model investigates the stress distributions on the tool/chip interface and the shear plane with reference to a varying shear plane angle and the workpiece properties. It is then assumed that the resultant forces on the chip applied on the shear plane and the tool/chip interface are in equilibrium and the shear plane angle is chosen accordingly. An initial estimate of the shear plane angle and the shear plane temperature is made and from this the shear strain is calculated according to equation 3.36 and the shear strain rate according to equation 3.37. The flow stress σ may then be calculated from the stress/strain relationship

$$\sigma = \sigma_1 \varepsilon^n \tag{3.39}$$

where σ_1 is the stress corresponding to unit strain

ε is the strain

n is a strain hardening index.

σ_1 and n are assumed to be functions of a velocity-modified temperature, T_{mod} which is introduced to compensate for the fact that stress/strain data is usually obtained for strain rates far lower than those involved in metal cutting [3.28]

$$T_{\text{mod}} = T\left(1 - \nu \log\left(\frac{\dot{\varepsilon}}{\dot{\varepsilon}_0}\right)\right) \tag{3.40}$$

where T is the temperature of the shear plane in kelvin

ν is a material constant taken to be 0.09 [3.26]

$\dot{\varepsilon}$ is the uniaxial strain rate

$\dot{\varepsilon}_0$ is a reference value of strain rate taken to be 1 per sec.[3.26]

The strain at the shear plane is related to the shear strain by the expression

$$\varepsilon = \frac{\gamma}{\sqrt{3}} \tag{3.41}$$

and the strain rates are related by

$$\dot{\varepsilon} = \frac{\dot{\gamma}}{\sqrt{3}} \tag{3.42}$$

In the work of Young et al [3.3] and Hu et al [3.26] the relationships between σ_f and velocity-modified temperature and between strain hardening index and velocity-modified temperature were obtained from experimental data published by Oyane et al. However Lei et al [3.29] state that a reliable material constitutive equation is a basic requirement for use with this model. A constitutive equation results from attempts to fit curves to experimentally measured data and the coefficients of the resulting equations are dependent upon the material for which the experiments were performed. Valentin et al [3.30] examine two of the most commonly used formulations of these constitutive equations. The first of these is the Johnson-Cook relationship

$$\sigma = \left(A + B\varepsilon^n\right)\left(1 + C\ln(\dot{\varepsilon})\right)\left(1 - T^{*m}\right) \tag{3.43}$$

where A, B, C, n and m are material constants

$$T^* = \frac{T - T_r}{T_m - T_r}$$

T is the absolute temperature of the deformed material

T_r is room temperature

T_m is the melting point of the material

For the steels used in this work T^* may be approximated by $T^* = \Delta T / 1500$

where ΔT is the temperature rise resulting from the material deformation.

Meyer et al [3.33] give values for these constants for two different steels $A = 1029$, $B = 739$, $C = 0.04$, $n = 0.25$, $m = 0.56$ for a 25CrMo4 steel and $A = 59$, $B = 1184$, $C = 0.07$, $n = 0.13$ and $m = 0.54$ for a 30CrNiMo8 steel. The equations resulting from use of these constants are

$$\sigma = \left(1029 + 739\varepsilon^{0.25}\right)\left(1 + 0.04\ln\left(\dot{\varepsilon}\right)\right)\left(1 - \left(\frac{\Delta T}{1500}\right)^{0.56}\right) \tag{3.44}$$

and

$$\sigma = \left(59 + 1184\varepsilon^{0.13}\right)\left(1 + 0.07\ln\left(\dot{\varepsilon}\right)\right)\left(1 - \left(\frac{\Delta T}{1500}\right)^{0.54}\right) \tag{3.45}$$

The second of the formulations examined by Valentin et al [3.30] was the Zerrilli-Armstrong relationship given by

$$\sigma = \left(C_2 + C_5\varepsilon^n\right)\left(1.13 - 0.000445T\right) + C_1\exp\left[\left(-C_3 + C_4\ln\left(\dot{\varepsilon}\right)\right)T\right] \tag{3.46}$$

where the C_i are material constants.

Valentin et al quote the following values of the constants for a chromium-molybdenum steel

$C_1 = 710$, $C_2 = 140$, $C_3 = 0.006$, $C_4 = 0.0004$ and $C_5 = 340$.

In their work Meyer et al [3.31] found that equations 3.44 and 3.45 did not fit their experimental data well. Their experiments were carried out at temperatures much lower than those experienced in metal cutting. Valentin et al [3.30] found that the Johnson-Cook relationships provided a good match to experimental data only in a small range of strain rates nevertheless the equations were easy to implement. Valentin et al obtained a reasonable fit to their experimental data with the Zerrilli-Armstrong relationship but they reported difficulties in predicting the temperature rise to be expected in metal deformation. However the Oxley model for predicting forces etc. is an iterative model and problems were experienced in achieving convergence in the temperature calculations using the original Oxley data. This was considered to be as a result of the non-linearities

in the data as shown in figures 3.36a and 3.36b. The flow stresses predicted by the Oxley data, the Johnson-Cook relationship and the Zerrilli-Armstrong relationship are temperature, strain and strain rate dependent. Figure 3.36a shows the variation of flow stress with temperature at relatively low strain and strain rate and figure 3.36b shows the variation at high strain and strain rate. It can be seen that equation 3.45 gives the closest agreement with the original Oxley data whilst avoiding the discontinuities associated with that data. Although the data presented are for steels of differing composition equation 3.45 will be taken in what follows as being representative of a typical mild steel.

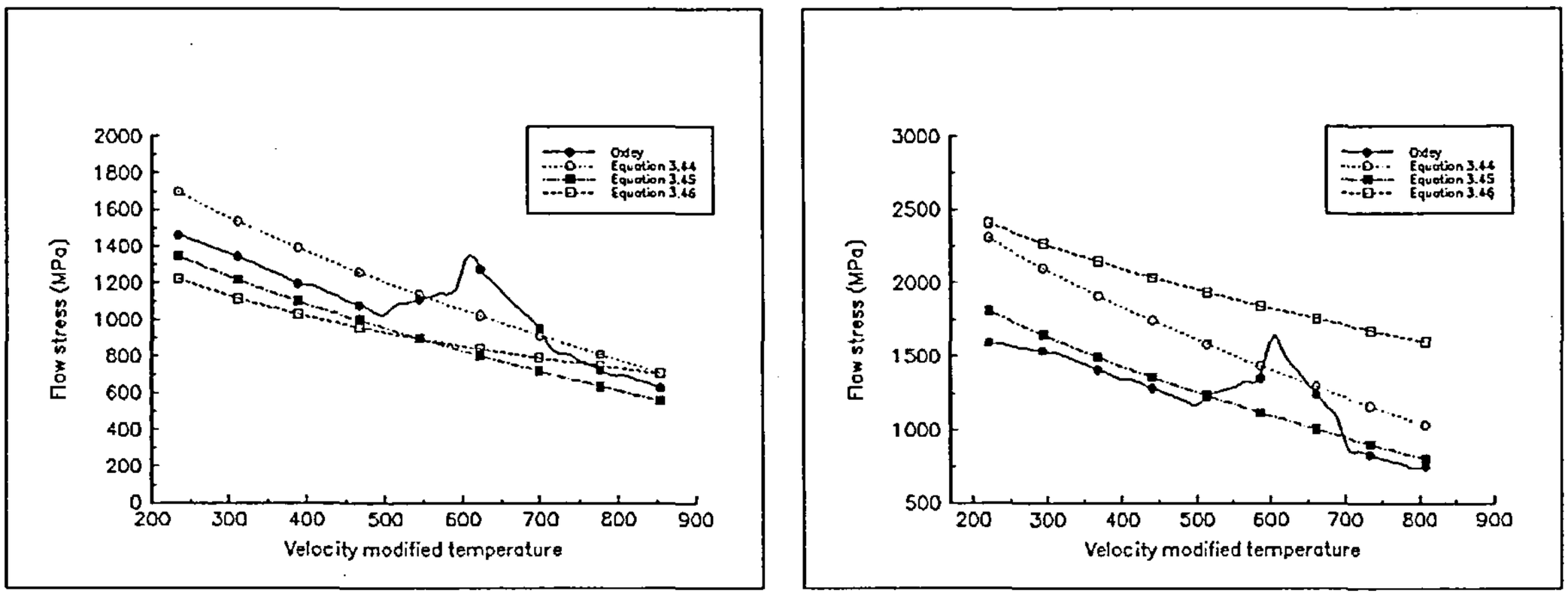

Figure 3.36 Predicted flow stress variation with temperature for (a) strain = 5, strain rate = 300/sec, (b) strain = 30, strain rate = 900/sec.

Having obtained the flow stress σ for the material it is possible to estimate the shear flow stress k_{sp} on the shear plane from

$$k_{sp} = \frac{\sigma}{\sqrt{3}} \tag{3.47}$$

and hence the shearing force F_s on the shear plane becomes

$$F_s = k_{sp} A_{sp} \tag{3.48}$$

where A_{sp} is the area of the shear plane.

From a knowledge of the shear force on the shear plane it is possible to estimate the temperature rise on the shear plane by considering the work rate of the shear force

$$\Delta T_{sp} = \frac{1-\beta}{\rho S t_1 w} \frac{F_s \cos\alpha}{\cos(\phi - \alpha)} \tag{3.49}$$

where ρ is the density of the workpiece material

S is the specific heat of the workpiece material

β is the proportion of the heat conducted into the workpiece.

It is then possible to calculate a new value of the shear plane temperature T_{sp} from

$$T_{sp}^2 = T_{sp}^1 + \Delta T_{sp} \tag{3.50}$$

where T_{sp}^2 is the new estimate of the shear plane temperature

T_{sp}^1 is the previous estimate of shear plane temperature

This exercise is then iterated until the shear plane temperature converges to a difference of less than 1% between successive estimates of the shear plane temperature. From the shearing force it is possible to estimate the resultant force R acting on the shear plane using (figure 3.35)

$$R = \frac{F_s}{\cos\theta} \tag{3.51}$$

Using the equilibrium condition for the chip the friction force F between the chip and the tool may be calculated

$$F = R\sin\lambda \tag{3.52}$$

From this the resolved shear stress at the tool/chip interface τ_{int} may be assessed

$$\tau_{\text{int}} = \frac{F}{hl} \tag{3.53}$$

where h is the width of the cut and l is the tool/chip contact length.

A similar iterative process to that described above is carried out to determine the temperature of the chip at the tool chip interface using the friction work as the heating source rather than the shearing work as was required for the shear plane temperature. The temperature rise in the chip ΔT_c is calculated from

$$\Delta T_c = \frac{F \sin\phi}{\rho S t_1 w \cos(\phi - \alpha)} \tag{3.54}$$

Again following convergence of the chip temperature to within 1% it is possible to estimate the flow stress σ on the tool/chip interface using equation 3.45 and then the shear flow stress on the tool/chip interface k_{chip} may be expressed

$$k_{chip} = \frac{\sigma}{\sqrt{3}} \tag{3.55}$$

Both τ_{int} and k_{chip} act along the tool/chip interface and both are dependent on the shear plane angle ϕ. If these calculations are repeated for a range of possible values of ϕ, the equilibrium condition requires that the true value of shear plane angle is that value which makes the shear flow on the tool/chip interface equal to the resolved shear stress on the interface. i.e.

$$\tau_{\text{int}} = k_{chip} \tag{3.56}$$

Figures 3.37a and 3.37b show the variation of these two properties with shear plane angle. Figure 3.37b clearly shows the effects of convergence problems which led to equation 3.45 being used in preference to the original data used by Oxley.

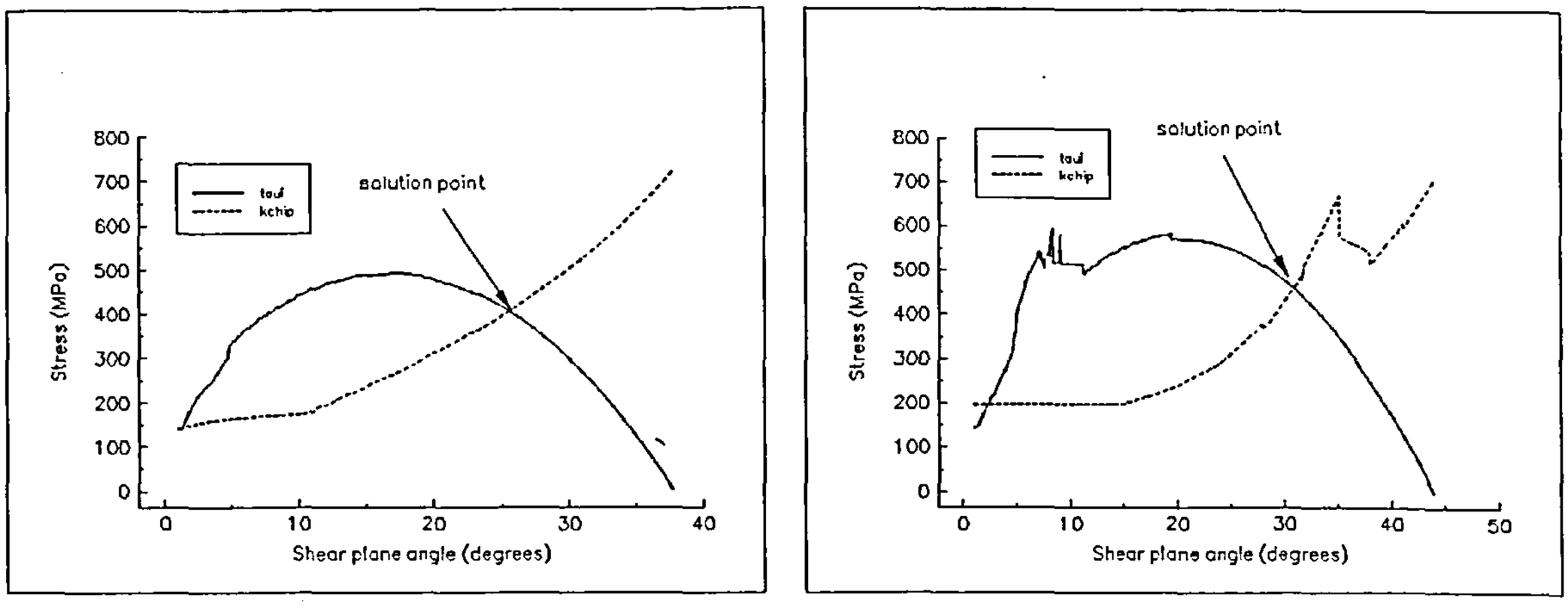

(a) (b)

Figure 3.37 Variation of shear flow stress and resolved shear stress on the chip/tool interface with shear plane angle. (a) equation 3.45, (b)original Oxley data.

The solution points indicated in figures 3.37a and 3.37b are the shear plane angles at which equation 3.56 is satisfied.

AE variation with wear

From the foregoing it can be seen that the relationship between tool wear and rms AE is complex. Increases in flank wear land length are expected to produce an increase in rms AE in a manner which varies with the square root of V_b in the absence of rake angle variations (equation 3.33) which may result from crater wear. However in the presence of rake angle variations the changes in rms AE will depend on which of terms 1 and 2 or term 3 in equation 3.33 is dominant. This will be determined by the initial rake angle of the insert and the material properties of the workpiece. Figure 3.38 shows the variation of the first two geometric terms of equation 3.33 for cutting the *representative* mild steel discussed above.

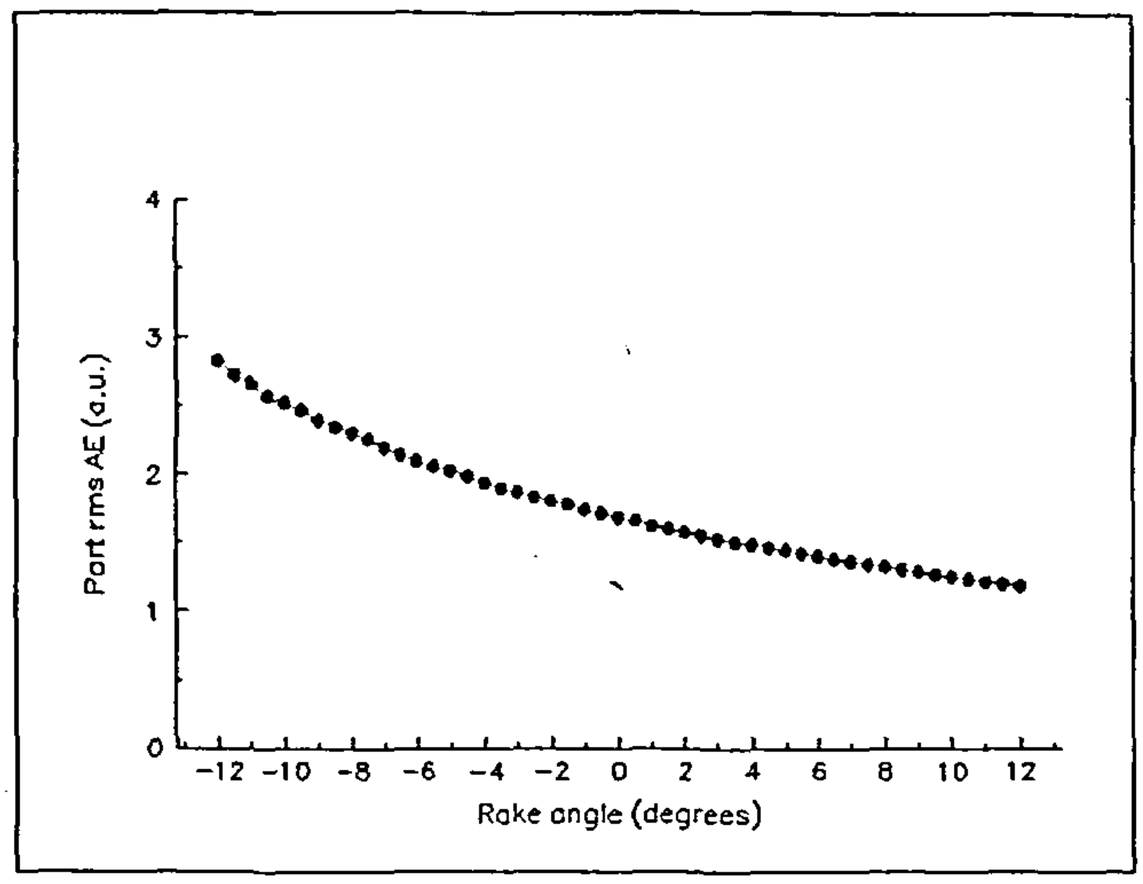

Figure 3.38 Variation in geometric terms of equation 3.33 with rake angle

Equation 3.38 shows the effect on mean frequency of changes in rake angle. Figure 3.39 shows the variation in this function with rake angle for three different cutting speeds and it may be seen that an increase in rake angle results in a reduction in the mean frequency of the AE signal.

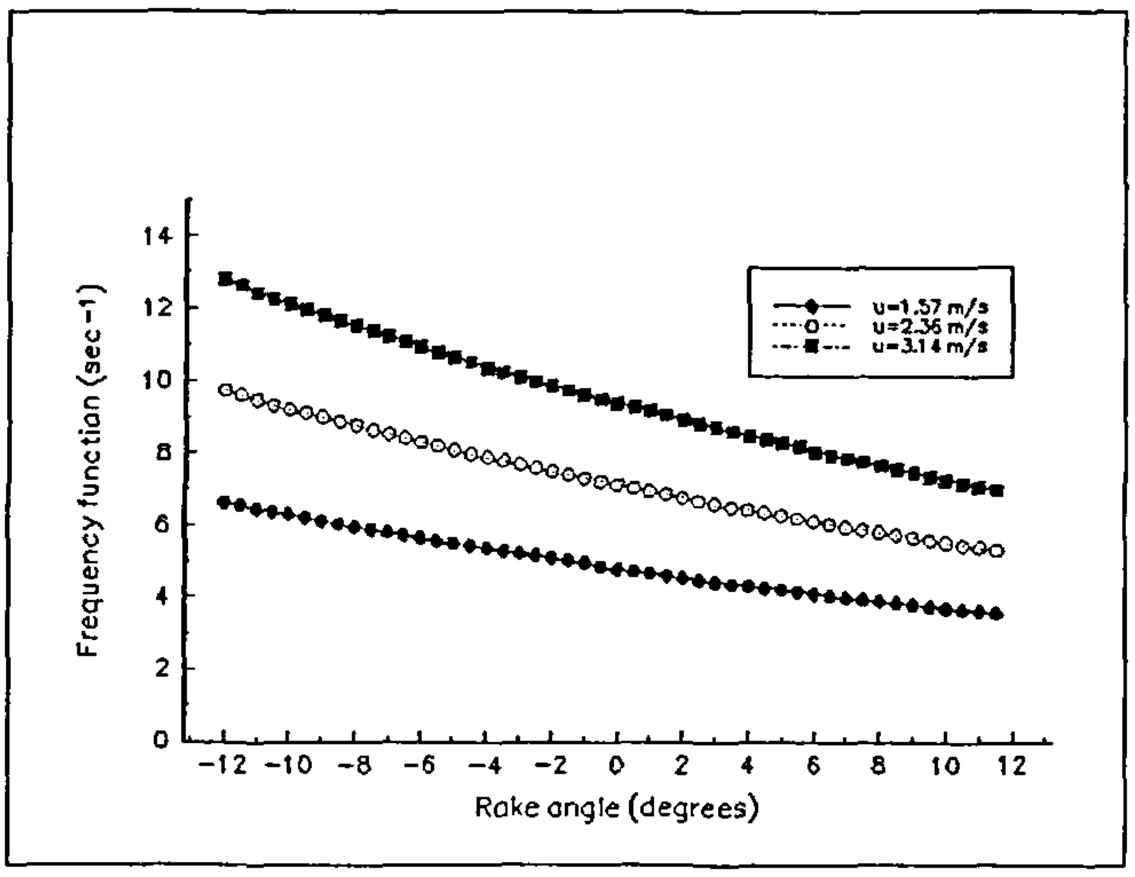

Figure 3.39 Variation in frequency function with rake angle for three cutting speeds

Variations in local rake angle are brought about by complex changes in the crater wear [3.25] and these bear a complex relationship to the flank wear experienced by the inserts. It should be noted that figures 3.38 and 3.39 show the variations in AE properties resulting from changes on the rake face of the insert. Changes on the relief face (flank

wear) will effect the rms AE (equation 3.33) but will not directly effect the frequency content of the AE signal (equation 3.38). Carolan et al [3.25] investigated the variation in the angle between the rake face and the cutting edge and the length of the flank wear land, V_b. when cutting annealed En24 mild steel with a negative rake cutter when crater wear was present. Their findings are shown in figure 3.40.

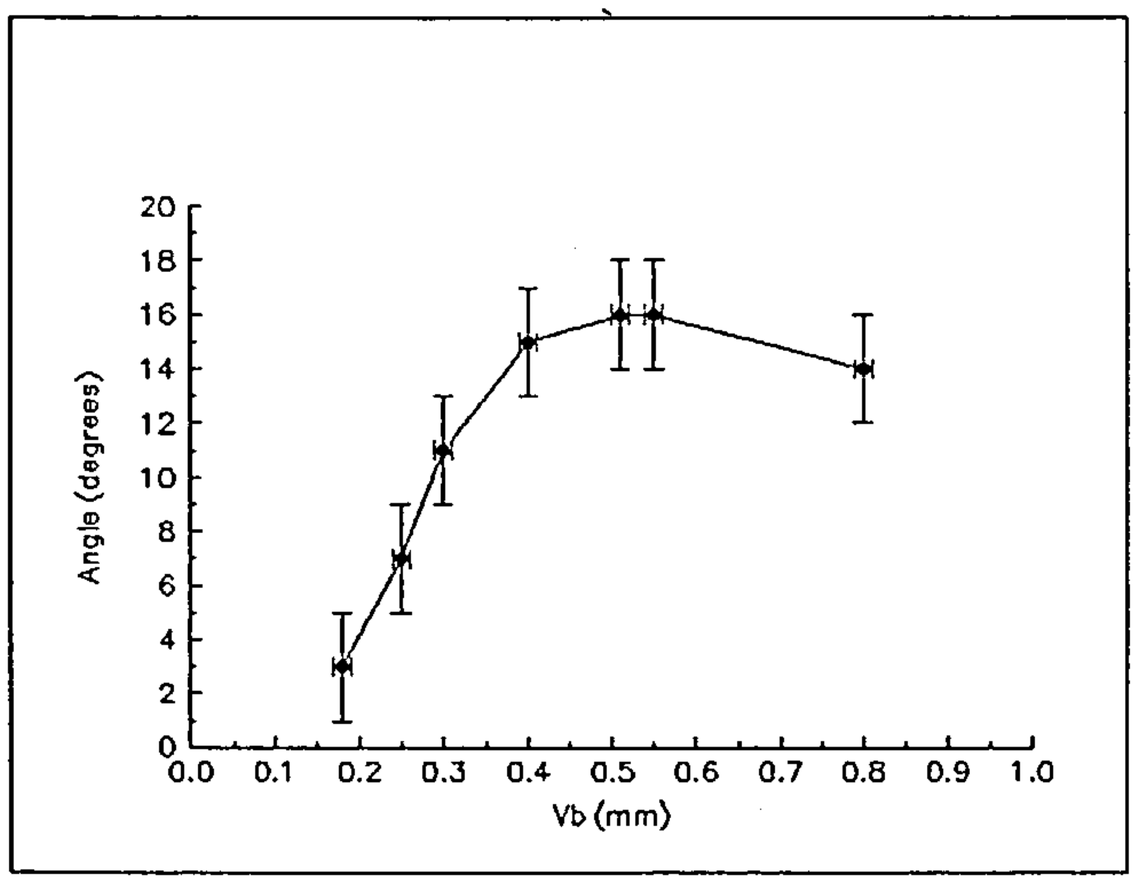

Figure 3.40 Variation in angle between the rake face and the cutting edge with flank wear land length, V_b (from [3.25]).

It can be seen that the relationship between these two parameters is linear until the cutting edge begins to deteriorate when the flank wear land is approximately 0.4 mm long. This would cause the effective local rake angle at the cutting edge to increase until the insert approached the end of its life. Beyond a flank wear land length the cutting edge appears to deteriorate and the effective rake angle would begin to decrease. It could be argued that insert chipping also have a similar consequence for the local rake angle. If this effect is considered in conjunction with figure 3.38 it can be seen that in the initial phases of wear the two geometric terms of the rms AE expression (equation 3.33) would be expected to decrease until edge erosion or edge chipping occurred after which they would increase. This would be accompanied by an increase in the rms AE which is proportional to the square root of the flank wear land length for all values of V_b. If the local rake angle variation described above is considered together with figure 3.39 it can be seen that in the early stages of wear the mean frequency of the AE signal is anticipated to reduce until such times as edge deterioration or chipping occurs after which an increase in mean frequency should result.

In the absence of crater wear the local rake angle will be invariant and the rms AE signal is predicted to increase with the square root of the length of the flank wear land. Similarly the mean frequency in the AE signal is expected to be constant in the absence of rake angle effects. It can be seen from this that changes in the mean frequency of the AE signal may be taken as indicative of crater wear and/or of insert chipping whilst changes in rms AE may be taken as an indicator of insert flank wear and/or chipping. In both properties of the AE signal an increase in either or both indicates that the insert is approaching the end of its useful life.

3.3.3 Rubbing sources

AE generated by rubbing and friction is recognised as coming from two related sources, asperity collision with the insert and deformation of those asperities [3.32]. Jiaa and Dornfeld [3.33] investigated a relationship, first proposed by Diei, between the rms AE signal and the rate of frictional energy dissipation in metal to metal sliding contact. Their work confirmed that the Diei equation described accurately the generation of AE from rubbing sources. The expression relates rms AE to sliding velocity, contact area and material properties as shown:

$$rms = \left(k\eta A_a \tau_s V\right)^{m/2} \tag{3.57}$$

where k and m are constants that depend on the AE measuring system and material properties of the contacting pair.

η is a constant function of surface roughness and elastic properties of the contacting pair.

A_a is the apparent area of contact

τ_s is the shear strength of the interfacial material

V is the sliding velocity

If we translate this to a face milling environment it may be argued that in the flank/workpiece contact zone (tertiary zone) the area of contact is approximately proportional to the length of the flank wear land, the constant of proportionality being the

width of the flank wear land or depth of cut b. Equation 3.57 may be re-written in terms of the flank wear land length V_b:

$$rms = \left(KbV_b\tau_s V\right)^{m/2} \tag{3.58}$$

where K is a constant = $k\eta$ in equation 3.57

If it is assumed that m should be taken as unity in this expression it can be seen that equation 3.58 is similar to the third term in equation 3.33 and this suggests that the contribution of the flank wear land to rms AE is indeed that of a rubbing source.

3.3.4 Chip breakage and entanglement

Chip entanglement in the cutter is essentially a random event and it is unlikely that changes in insert geometry would exhibit a correlation with AE from this source. Therefore it will not be considered further in this work.

3.3.5 Exit shock

The AE generated on disengagement of the insert is generated by the sudden relaxation of the cutting forces. It is of similar form to the entry impact and may be modelled in a similar fashion as a series of impulses. The amplitude of the AE pulse is related to tool wear through the cutting forces which increase as tool wear progresses.

3.4 Summary

In this chapter the theoretical problems associated with the modelling of the effects of insert wear on surface finish and acoustic emission generated in face milling have been considered. The relevant literature has been reviewed in some detail. This has provided the basis for simulations of the consequences of insert wear for surface profile and AE.

The surface profile model required the calculation of the cutting forces generated during milling which were then related to deflections of the tool holder. The frequency domain properties of the simulated surface profile resulting from the deflected tool holder were used to demonstrate the effects of tool wear. The changes in AE resulting from insert

wear were modelled through the dependency of acoustic emission on strain, strain rate and cutting geometry. The predictions of these models were illustrated using examples of single point and eight point cutting.

The conclusions drawn from these simulations showed that, if progressive wear of the insert occurs, a progressive increase in the energy content of the kinematic spatial frequency band is to be expected. The energy content of the high frequency band will increase progressively in the early stages of wear but will approach a steady value in the later stages of wear. However if insert chipping accompanies progressive insert wear it is anticipated that the smooth trends in both of the spatial frequency bands will be disrupted.

The AE model indicates that, in the presence of local rake angle variations, the rms AE signal will initially reduce until edge deterioration sets in after which the rms signal will increase. Similarly local rake angle variations are expected to result in reductions in AE mean frequency until cutting edge deterioration results in an increase in this quantity. In the absence of local rake angle variations it is anticipated that the rms AE will increase in a manner which is proportional to the square root of the length of the flank wear land length. Under these circumstances the model suggests that the mean frequency will remain unchanged as flank wear progresses. Thus it may be concluded that rms AE variations are indicative of flank wear and changes in the mean frequency of the AE signal are indicative of crater wear.

These results will be tested against the observations from sets of systematic tool wear experiments reported in the following three chapters.

3.5 References

3.1) N.N. Zorev trans H.S.H. Massey. "Metal Cutting Mechanics", Pergamon Press, Oxford, 1966

3.2) W.R. DeVries. "Analysis of Material Removal Processes", Springer-Verlag, New York, 1992

3.3) Hong-Tsu Young, P. Mathew and P.L.B. Oxley. "Predicting cutting forces in face milling". International Journal of Machine Tools and Manufacture, 34(1994), 771-783.

3.4) D.J. Whitehouse. "Handbook of surface metrology", I.O.P. publishing, Bristol, 1994.

3.5) E. Emel and E. Kannatey-Asibu. "Acoustic emission monitoring of the cutting process - Negating the influence of varying cutting conditions". Transactions of the ASME, Journal of Engineering Materials and Technology, 113(1991), 456 - 464.

3.6) E.N. Diei and D.A. Dornfeld. "Acoustic emission sensing of tool wear in face milling". Transactions of the ASME, Journal of Engineering for Industry, 109(1987), 234 - 240.

3.7) A.E. Diniz, J.J. Liu and D.A. Dornfeld. "Correlating tool life, tool wear and surface roughness by monitoring acoustic emission in finish turning". Wear, 152(1992), 395 - 407.

3.8) R. McBride, T.A. Carolan, J.S. Barton, S.J. Wilcox, W.K.D. Borthwick and J.D.C. Jones. "Detection of acoustic emission in cutting processes by fibre optic interferometry". Measurement Science Technology, 4(1993), 1122 - 1129.

3.9) Anselmo Eduardo Diniz, José Caldeirani Filho. "Influence of the relative positions of tool and workpiece on tool life, tool wear and surface finish in the face milling process". Wear, 232(1999), 67 - 75.

3.10) Rajeev Kapoor and Sia Nemat-Nasser. "Determination of temperature rise during high strain rate deformation". Mechanics of Materials, 27(1998), 1 - 12.

3.11) T.A. Carolan, S.R. Kidd, D.P. Hand, S.J. Wilcox, P. Wilkinson, J.S. Barton, J.D.C. Jones and R.L. Reuben. "Acoustic emission monitoring of tool wear during the face milling of steels and aluminium alloys using a fibre optic sensor Part 1: energy analysis". Proceedings of the Institution of Mechanical Engineers, Part B, 211(1997), 299-309.

3.12) T.A. Carolan, S.R. Kidd, D.P. Hand, S.J. Wilcox, P. Wilkinson, J.S. Barton, J.D.C. Jones and R.L. Reuben. "Acoustic emission monitoring of tool wear during the face milling of steels and aluminium alloys using a fibre optic sensor Part 2: frequency analysis". Proceedings of the Institution of Mechanical Engineers, Part B, 211(1997), 311-319.

3.13) Dae Kyun Baek, Tae Jo Ko and Hee Sool Kim. "A dynamic surface roughness model for face milling". Precision Engineering, 20(1997), 171-178.

3.14) Janusz Cieloszyk, Wieslaw Olszak and Janusz Skrodzewicz.. "Influence of the geometry of cutting action on surface formation in face milling". PD-vol. 64-5, Engineering Systems Design and Analysis, Volume 5, ASME 1994.

3.15) H.J. Fu, R.E. DeVor, S.G. Kapoor. "A mechanistic model for the prediction of the force system in face milling operations". Transactions of the ASME, Journal of Engineering for Industry, 106(1984), 81-88.

3.16) Dell K. Allen and Leo Alting, "Mechanical Mass Reducing Family A-2: Cutting, Abrading and Shearing". Published by the CAM Software Research Laboratory, Brigham Young University, Provo, Utah, U.S.A. 1985.

3.17) M.C. Shaw. "Metal Cutting Principles", Oxford University Press, New York, 1989.

3.18) P. Wilkinson, R.L. Reuben, J.D.C. Jones, J.S. Barton, D.P. Hand, T.A. Carolan, S.R. Kidd. "Surface finish parameters as diagnostics of tool wear in face milling". Wear, 205,(1997), 47-54.

3.19) T. Blum and I. Inasaki. "A study on acoustic emission from the orthogonal cutting process". Transactions of the ASME, Journal of Engineering for Industry, 112,(1990), 203-211.

3.20) R. Du, D. Yan, M.A. Elbestawi. "Time-frequency distribution of acoustic emission signals for tool wear detection in turning", 4th World Meeting on Acoustic Emission and 1st International Conference on Acoustic Emission in Manufacturing, The American Society for Nondestructive Testing, Columbus, OH, USA, 1991, pp269-285.

3.21) J.A. Rice and S.M. Wu. "On the feasibility of catastrophic cutting tool fracture prediction via acoustic emission analysis", Transactions of the ASME, Journal of Engineering for Industry, 115,(1993), 390-398.

3.22) E. Kannatey-Asibu Jr. and D.A. Dornfeld. " Quantitative relationships for acoustic emission from orthogonal metal cutting", Transactions of the ASME, Journal of Engineering for Industry, 103,(1981), 330-340.

3.23) C.B. Scruby. "An introduction to acoustic emission", Journal of Physics E: Scientific Instrumentation, 20,(1987), 946-953.

3.24) T. Blum, I. Suzuki and I. Inasaki. "Development of a condition monitoring system for cutting tools using an acoustic emission sensor", Bulletin of the Japanese Society of Precision Engineers, 22,(1988), 301-308.

3.25) T.A. Carolan, D.P. Hand, J.S. Barton, J.D.C. Jones, P. Wilkinson and R.L. Reuben. "Assessment of tool wear in milling using acoustic emission detected by a fiber-optic interferometer". Transactions of the ASME, Journal of Manufacturing Science and Engineering, 118(1996) 428-433.

3.26) R.S. Hu, P. Mathew, P.L.B. Oxley and H.T. Young. "Allowing for end cutting edge effects in predicting forces in bar turning with oblique machining conditions". Proceedings of the Institution of Mechanical Engineers, Part C, 200(1986) 89-99.

3.27) E. Shamoto and Y. Altintas. "Prediction of shear angle in oblique cutting with maximum shear stress and minimum energy principles". Transactions of the ASME, Journal of Manufacturing Science and Engineering, 121,(1999), 399-407.

3.28) W.F. Hastings, P. Mathew and P.L.B. Oxley. "A machining theory for predicting chip geometry, cutting forces etc. from work material properties and cutting conditions". Proceedings of the Royal Society of London, A 371,(1980), 569-587.

3.29) S. Lei, Y.C. Shin, F.P. Incropera. "Material constitutive modeling under high strain rates and temperatures through orthogonal machining tests". Transactions of the ASME, Journal of Manufacturing Science and Engineering, 121,(1999), 577-585.

3.30) T. Valentin, P. Magain, M. Quik, K. Labibes and C. Albertini. "Validation of constitutive equations for steel". Journal de Physique IV, 7(1997), 611-616.

3.31) L.W. Meyer, K. Seifert and S. Abdel-Malek. "Behaviour of quenched and tempered steels under high strain rate compression loading". Journal de Physique IV, 7(1997), 571-576.

3.32) Musa K. Jouaneh, Richard Lemaster and Frank C. Beall. "Study of acoustic emission generation in sliding motion". Journal of Acoustic Emission, 10(1992), 83-89.

3.33) C.L. Jiaa and D.A. Dornfeld. "Experimental studies of sliding friction and wear via acoustic emission signal analysis". Wear, 139(1990), 403-424.

Chapter 4

The Milling Experiments

This chapter describes the series of milling tests carried out in the experimental part of this work. A description of the apparatus employed is given followed by a discussion of the test materials used and of the experimental procedure pursued. The generation of acoustic emission and the production of sample engineering surfaces was accomplished using a Wadkin V-5 Machining Centre. The acquisition of acoustic emission signals was achieved either via a conventional resonant AE transducer or via a novel fibre optic interferometric AE transducer transmitting signals to two CompuScope 220 digital sampling oscilloscopes, one resident in a Cambridge Micro Computers PC 486-50 and the other in a DCS PC 286 which had been up-graded to PC 486-SX format. The preserved test surfaces were profiled at a later date using either a Talysurf-120 stylus instrument or a Zygo non-contacting surface analyser.

The justification for these particular tests lay in the need to perform a standard cutting operation (face milling, finishing cut) on a range of materials in common usage in engineering practice in order to measure acoustic emission generated during cutting throughout the life of the milling inserts. These tests also produced engineering surfaces for investigation into correlations between surface features and insert life. The face milling process was chosen as an example of an interrupted cutting process which is common in manufacturing but which presents a more complex AE signal and surface finish pattern than the simpler un-interrupted processes such as turning. In some experiments the problems of multi-point cutting were removed by using a single insert in the tool. Finishing cuts were employed throughout the tests to avoid the complications of large scale ambient vibrations associated with roughing cuts and to economise on material consumption during the tests.

4.1 The Wadkin V5-10 Machining Centre

All the milling experiments were performed on this machine which is equipped with a toolchanger magazine with a capacity for 30 tools. It is a three-axis computer numerically controlled machining centre with traverses of 1000 mm, 500 mm and 600 mm (780 mm without pallets) in the X- (longitudinal), Y- (lateral) and Z- (vertical) directions respectively. The spindle is operated by a DC motor of maximum power 18 kW giving a spindle speed range of 50 - 5500 rev/min. The actual power delivered to the spindle varies with spindle speed up to 900 rev/min after which it remains constant at 18 kW. It can supply a feed rate of up to 10 m/min and possesses a cutting capacity of 160 cm^3/min when processing mild steel. The positional accuracy on all three axes is +/- 25 μm with a repeatability of +/- 13 μm.

4.2 The Cutting Tools

In all these experiments the process involved was the simple one of face milling blocks of differing materials with identical plan dimensions. Two tool holders were used to enable a range of cutting geometries to be investigated. The diameter of each tool holder was 100 mm and both were capable of carrying eight inserts although in some cases both were used to fly cut (single point cutting) the specimen materials. The tool holder types were (a) SECO 220.74 possessing a cutting rake angle of -7° and a lead angle of 75° (hereafter referred to as the negative rake cutter) and (b) SECO 220.13 with a cutting rake of +12° and a lead angle of 45° (referred to as the positive rake cutter). The negative rake tool was necessary for machining the harder materials used in these tests.

Only one type of insert was employed for tests using the negative rake cutter. This was the SECO type SNKN of grade S25M. This insert was designed by the manufacturer with a wiper flat intended to produce a good surface finish, the grade being determined by the material to be machined.

Three types of insert were used in conjunction with the positive rake cutter. The relatively soft annealed steel was machined using SECO type SEKN-AFN grade S25M inserts which have a rounded cutting edge. The harder quenched & tempered steel specimens were processed using the SECO type SEKN-AFTN grade S25M inserts possessing identical geometry to the -AFN inserts but with a reinforced cutting edge. In order to

machine the stainless steel specimens, SECO type SEKN-AFTN grade S10M inserts were selected on the manufacturers' recommendation as being more suitable for processing this material.

4.3 The Test Materials

All the milling experiments were performed on blocks of material with identical plan dimensions, the width of these blocks being 60 mm and their length being 250 mm, the depth of each block being unimportant save that there was enough material to perform the tests. Typical depths were 100 mm.

The materials were chosen to provide a comprehensive range of machinability and specific cutting energy. This resulted in a wide range of wear types including chipping. Tests were performed on En24 steel in two conditions, fully softened in the annealed condition with a measured Vickers hardness (H_V) of 280 and quenched and tempered to BS639 V condition. Additionally tests were carried out on an austenitic stainless steel type 304.

4.4 The Acoustic Emission Transducers and Signal Conditioning

4.4.1 The Piezo-electric Instruments

Two piezo-electric AE transducers were used in these experiments, both being PZT based sensors. The first group of tests were performed using a Dunegan Endevco D9201A transducer. It has a relatively flat frequency response for this type of transducer and adequate sensitivity for the metal cutting process. The second series of milling tests were carried out using a Physical Acoustics Corporation D9203B transducer. Its calibration curve is shown in Figure 4.1. This instrument is similar to the D9201A but it possess greater sensitivity over a frequency range of 100 - 625 kHz.

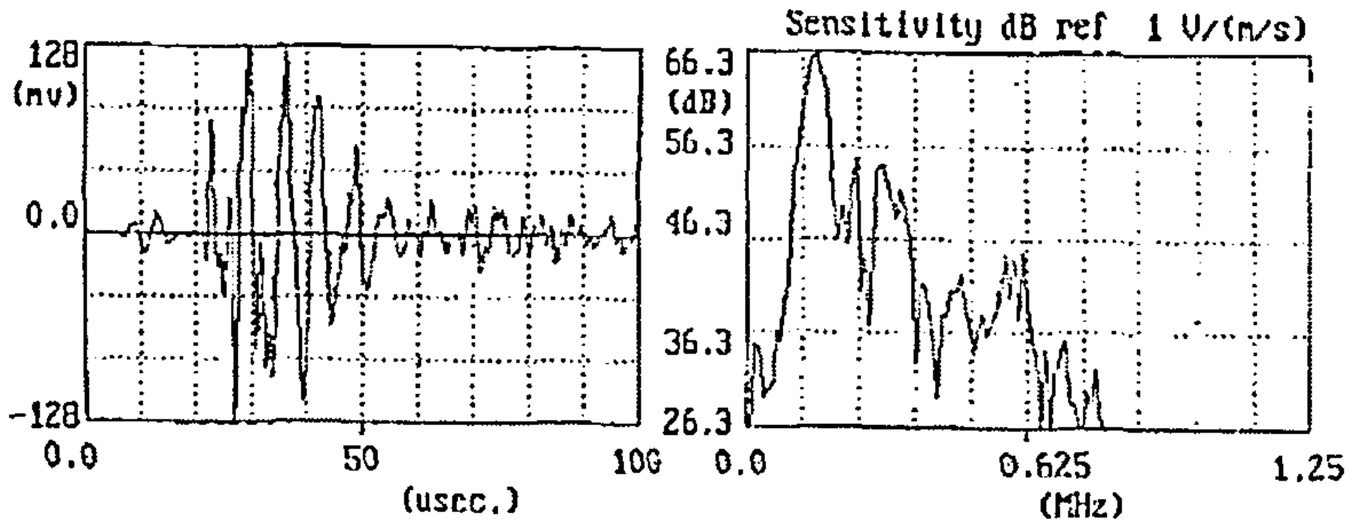

Sensor Manufacturer	PAC	Peak Frequency (KHz)	146.5
Model/Type	D9203B	Center Frequency (KHz)	170.8
Serial Number	50	Peak_Peak Voltage (mv)	255.
Calibration Date	02/04/92	Rise Time (usec)	16.1
Nominal Frequency (KHz)	175	Fall Time (usec)	50.
Peak of Spectrum (dB)	66.28	Number of Cycles	26.

Figure 4.1 Calibration for Physical Acoustics Corporation D9203B piezo electric AE transducer

The output from the AE sensors was amplified before acquisition by means of a Physical Acoustics Corporation 1220A preamplifier. This amplifier provides switchable gains of 40 dB or 60 dB and was supplied with a Butterworth bandpass filter of bandwidth 100 kHz - 1200 kHz (3 dB points).

The output from the preamplifier was then sampled by the CompuScope data acquisition board as described in section 4.5. It was also passed to an RMS processing unit from which was derived the RMS of the AE signal. This signal was sampled as described in section 4.5. The RMS processing unit was capable of operating on four channels simultaneously although in this work only two channels were used. The channels were arranged to have one with an averaging time constant of 0.5 msec, two with time constants of 250 msec and one with a variable time constant from 2.5 μsec to 250 msec. All the channels had a maximum bandwidth of 1 MHz. The two channels selected used time constants of 0.5 msec to process signals from the piezo-electric sensor and the fibre optic sensor described in section 4.4.2. The processing unit was limited in that only signal levels greater than one volt will have an RMS calculated on the full bandwidth of the unit as a result of the automatic gain control of the system circuitry which increased the gain of small signals typically less than 100 mV. During metal cutting the signal levels did not drop below this value and thus the circuitry only limited the bandwidth of the noise.

4.4.2 The Fibre Optic AE Sensor

This device based on a fibre optic Michelson interferometer was designed and tested as part of a joint project, which was funded by the SERC ACME Directorate, between the Departments of Physics and Mechanical Engineering at Heriot Watt University [4.1],[4.2],[4.3]. Figure 4.2 shows a schematic diagram of this instrument.

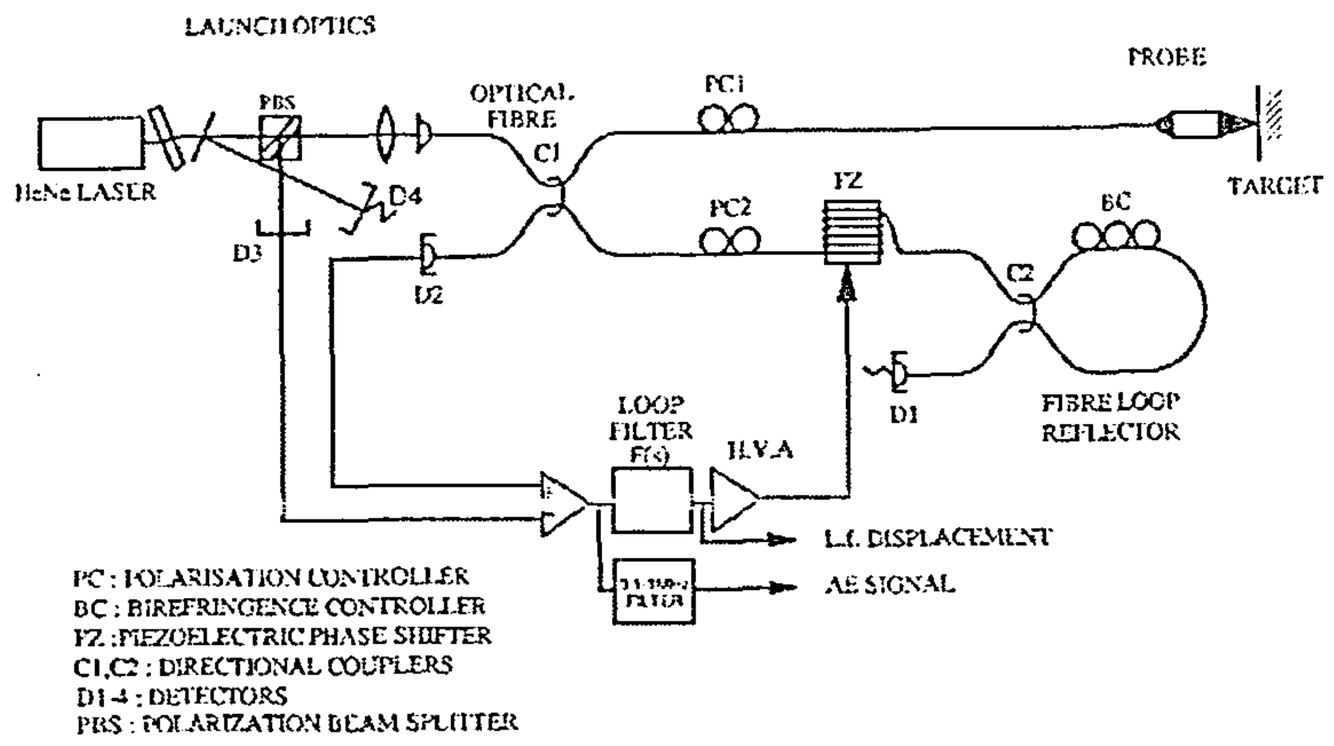

Figure 4.2 Schematic diagram of the fibre optic AE transducer after Carolan [4.4]

Coherent (laser) light is introduced into a single mode optical fibre by means of a microscope objective. The light is then split equally into the reference and signal arms of the interferometer using a directional coupler, the fibre optic analogue of a beam splitter. The signal arm consists of a length of single mode fibre spliced onto several metres of highly birefringent (hi-bi) fibre which makes the instrument insensitive to mechanical bending of the signal arm. Light emerging from the signal arm fibre is focused onto the test specimen by a graded index lens. Reflected light from the target is coupled back into the fibre. Light in the reference arm of the instrument is directly reflected from the fibre loop reflector. The reflected light from both arms is re-combined at the fibre coupler where interference occurs. A portion of the resultant wave is then detected by the detector D2. The interference of light causes the light intensity at D2 to vary periodically as

$$I = I_o\left(1 + V\cos\phi\right) \tag{4.1}$$

where V is the visibility of the interference pattern and ϕ is the optical phase difference between the signal arm and the reference arm. If the distance between the end of the signal arm probe is altered by an amount x as a result of, for example, vibratory motion in

the target, the optical path length in the signal arm will change and this will result in a phase change of $4\pi x/\lambda$ where λ is the wavelength of the source light. It is the intensity change corresponding to the phase change which the detector observes. The instrument is designed to measure target motions of the order of nanometres at frequencies in excess of 100 kHz (AE waves) in the presence of large amplitude, (of the order of mm) low frequency (less than 10 kHz) ambient vibrations. Rejection of these low frequency vibrations is achieved by a piezo-electric servo system which stretches the reference arm in response to the unwanted signals. The differences in optical path lengths between the signal and reference arms at low frequencies are thus compensated whilst the response to the high frequency AE signals is retained.

The version of the instrument used in this work employed a laser diode of wavelength 780 nm as source. The focused spot size on the target was 40 μm with the probe located at a working distance of 20 mm from the surface. The resolution of the instrument was 50 pm over a bandwidth of 0.1 - 1.0 MHz. The bandwidth of the piezo-electric servo used to reject low frequency signals was 11 kHz and its tracking range was 0.3 mm. A comparison of the performance of the fibre optic AE transducer with the conventional piezo-electric AE transducer when presented with an impulsive event (Hsu-Nielsen test) is shown in figure 4.3. The Hsu-Nielsen test involves the breakage of a standard length (2 mm) of 0.3 mm diameter 2H pencil lead on a test surface and the measurement of the resultant acoustic wave. Figure 4.3 clearly shows the resonant characteristics of the piezo-electric transducer whilst the fibre optic transducer only registers the passage of the primary AE wave and its subsequent reflections from the edges of the test surface.

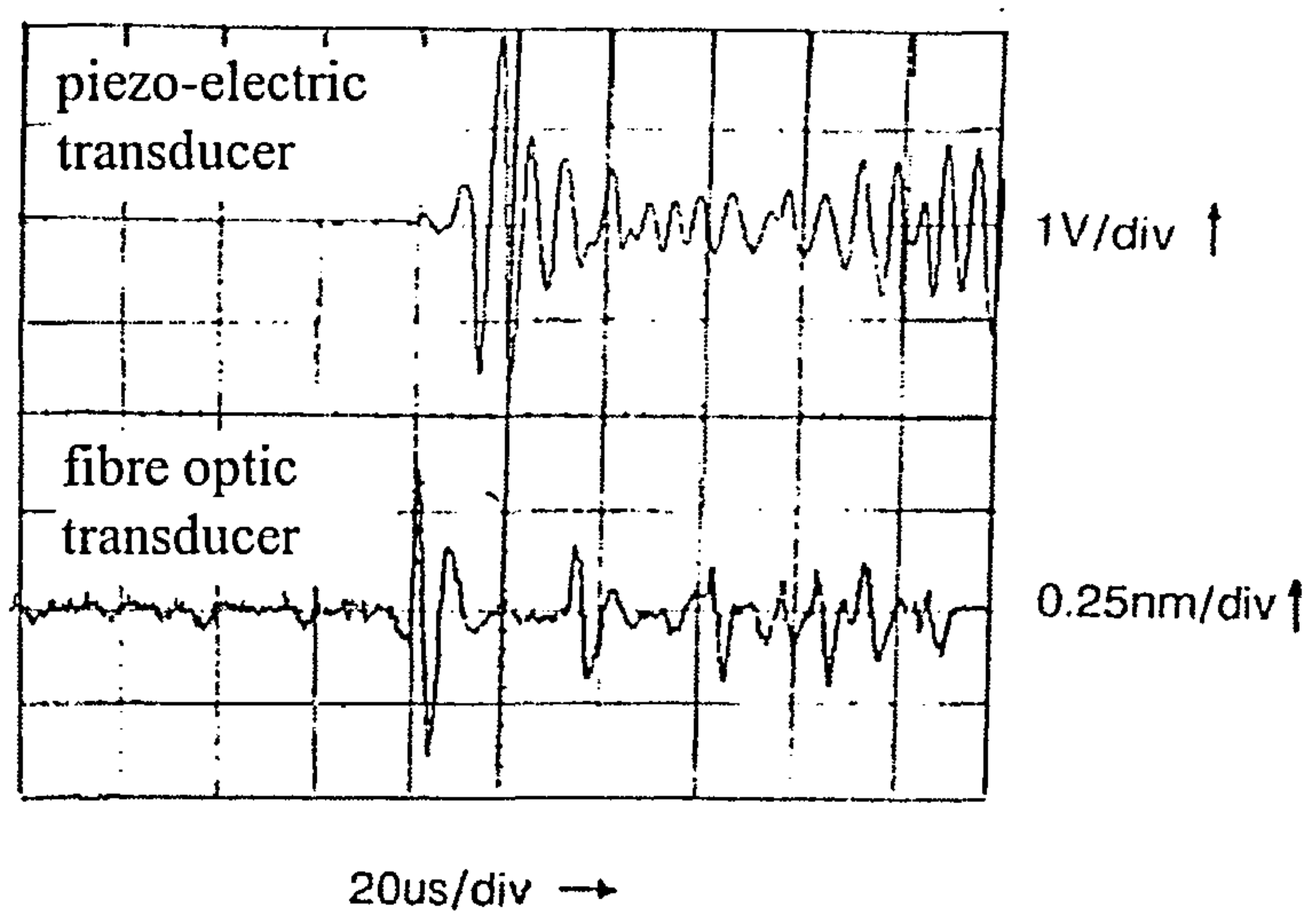

Figure 4.3 Comparison of fibre optic AE transducer with piezo electric AE transducer following impulsive event.

4.5 The AE Data Acquisition System

The AE data were acquired through two CompuScope 220 data acquisition boards located in two distinct personal computers. These boards possess 256 kbytes of on board memory and can operate at a maximum sampling rate of 40 MHz. However for the applications described in this work the available 256 kbytes of memory were split equally between two channels to enable data from both the piezo-electric and fibre-optic transducers to be collected. Each channel uses an 8-bit analogue/digital converter. The unprocessed AE signals were sampled at a rate of 5 MHz giving a record length of 25.6 msec and the RMS AE signals were sampled at a rate of 5 kHz giving a record length of 25.6 sec.

The board operates by cyclically filling on-board buffers until a trigger signal is received. At this point the process is stopped and data is stored in an internal buffer. The buffer may then be down-loaded to the hard disc of the PC in which the board is resident. This data is thus available for later processing.

4.6 The Measurement of Tool Wear

In all the tests described in this work the indicator of insert wear was taken to be the length of the flank wear land, V_b. An insert was considered to be at the end of its life when V_b exceeded 0.7 mm.

In the early series of tests the wear land was measured at intervals with the aid of a charge coupled device (CCD) camera which produced a magnified image of the insert on a television monitor. The magnification factor of ten achieved by this system produced a resolution of 0.01 mm for the measurement of flank wear.

The later tests employed a Hilger and Watt engineer's microscope to measure the flank wear land. This microscope has a small table with X- and Y- co-ordinate travels of 25 mm in total and makes use of two micrometers both of which allow a practical resolution of 0.005 mm.

4.7 The Impact Test Instrumentation

This instrumentation was used to ascertain the natural frequencies of the head stock of the Wadkin Engineering Centre in the feed direction. The apparatus consisted of a Bruel & Kjaer type 8202 impact hammer equipped with a Bruel & Kjaer type 8200 force transducer. Three tips were provided with this hammer, one of rubber, one of plastic and one of steel which cause excitation of different frequency ranges in the test specimen. For this work the rubber tip exciting a frequency range of 0 - 500 Hz was used. The response of the head stock was measured using a D.J. Birchall A/02 general purpose piezo-electric accelerometer. A D.J. Birchall type CA/01 two channel charge amplifier was used in conjunction with the hammer and the accelerometer. Processing of the signals from the two sensors was performed by means of a Spectral Dynamics SD 380 spectral analyser operating in its transfer function mode.

4.8 Experimental Procedure

4.8.1 Milling Experiments

The procedure employed in all of the milling experiments was essentially the same for each of the metallic specimens, differing only in the required cutting conditions for each individual material. The machining process in all cases was that of face milling with a finishing cut to a depth of 0.5 mm. Every test block was pre-trimmed to the nominal dimensions of 250 mm (long) x 60 mm (wide) x 100 mm (deep) to ensure sufficient depth of material for cutting during the test and a similar plan area for each specimen. One end face of each test specimen was diamond polished to a mirror finish using 6 μm diamond paste. This ensured sufficient reflectivity from the specimen for a usable signal/noise ratio to be obtained from the fibre optic AE transducer.

The test blocks were mounted on the machine tool bed using one of the two system vices. The second vice was used to hold the fibre optic probe at a nominal distance of 10 mm from the reflective surface of the test block and the block position was then finely adjusted to give a focused laser beam spot on that surface. The piezo-electric AE transducer was mounted on the workpiece vice as close to the workpiece as possible to minimise the number of interfaces traversed by the AE wave and yet avoid mechanical damage to the transducer from the cutting process.

The machining tests proper used either single point or 8-point cutters depending on the material being processed. Table 4.1 gives a detailed summary of the materials processed, the inserts employed and the cutting conditions used in the tests.

Material	Cutting tool	Cutting conditions
En 24 annealed	8-point Positive rake S25M	Feed/tooth = 0.1 mm Cutting speed = 300 m/min Spindle speed = 955 rev/min Feed = 764 mm/min
En24 annealed	8-point Positive rake S25M	Feed/tooth = 0.22 mm Cutting speed = 200 m/min Spindle speed = 637 rev/min Feed = 1146 mm/min
En24 annealed	8-point Negative rake S25M	Feed/tooth = 0.1 mm Cutting speed = 300 m/min Spindle speed = 955 rev/min Feed = 764 mm/min
En24T annealed	8-point Negative rake S25M	Feed/tooth = 0.026 mm Cutting speed = 300 m/min Spindle speed = 955 rev/min Feed = 200 mm/min
En24 annealed	Single point Negative rake S25M	Feed/tooth = 0.1 mm Cutting speed = 300 m/min Spindle speed = 955 rev/min Feed = 96 mm/min
En24 quenched & tempered	8-point Positive rake S25M	Feed/tooth = 0.1 mm Cutting speed = 260 m/min Spindle speed = 828 rev/min Feed = 662 mm/min
En24 quenched & tempered	8-point Negative rake S25M	Feed/tooth = 0.1 mm Cutting speed = 100 m/min Spindle speed = 318 rev/min Feed = 254 mm/min
En24 quenched & tempered	8-point Negative rake S25M	Feed/tooth = 0.1 mm Cutting speed = 200 m/min Spindle speed = 637 rev/min Feed = 510 mm/min
Stainless steel type 304	Single point Positive rake S10M	Feed/tooth = 0.1 mm Cutting speed = 200 m/min Spindle speed = 637 rev/min Feed = 64 mm/min

Table 4.1 Summary of materials, cutting tools and cutting conditions used in the milling experiments.

Each test began with new inserts and a series of cuts were taken from the test specimens until the length of the flank wear land, V_b, exceeded 0.7 mm, the normally accepted indicator (ISO 3685) for the end of insert life. At intervals during the tests unprocessed AE and rms AE were recorded from both the interferometric transducer and the resonant transducer. Immediately following this the cutter was dismounted from the machine tool

and the values of V_b for each insert were recorded thus providing a history of the progressive wear of the inserts. The cut surfaces produced in the cutting process were preserved for further analysis when changes in flank wear land lengths of approximately 0.1 mm occurred.

Figure 4.4 shows a diagram of the general experiment arrangement for all of the tests performed in this work.

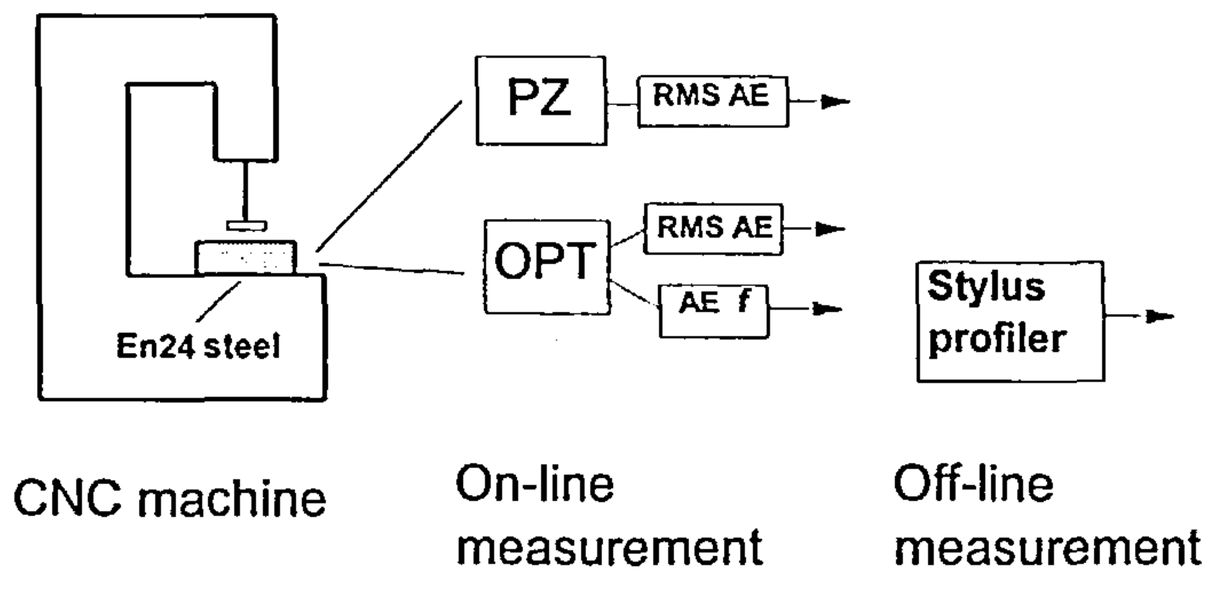

Figure 4.4 General arrangement of experimental tests

4.8.2 Determination of Headstock Natural Frequencies

In chapter 3 it was shown that the machined surface resulting from the milling process was dependent on the stiffness of the machine tool used in the process. It was proposed that the dominant stiffness in the system was that exhibited by the headstock and that an estimate of that stiffness could be obtained from a knowledge of the lowest natural frequency of the headstock/cutter combination. The headstock natural frequencies were determined from an impact test using the B & K instrumented hammer and the David Birchall accelerometer as noted earlier. The accelerometer was affixed to the headstock of the Wadkin machining centre with its sensitive axis aligned with the x-axis of the machine tool. Signals from both the accelerometer and the hammer were transmitted to the Spectral Dynamics SD 380 frequency analyser which determined the transfer function of the headstock. The transfer function was determined from an average of 16 consecutive

impacts applied to the headstock. A graphical display of a typical transfer function in the range 0-500 Hz is shown in figure 4.5. From this figure it can be seen that the principal natural frequencies in this range in the feed direction (x-axis) of the machine tool are 75 Hz and 90 Hz. These values are consistent with those obtained by Wilcox [4.5] from a frequency response test on the same machine. The transfer functions will be discussed in further detail in chapter 5.

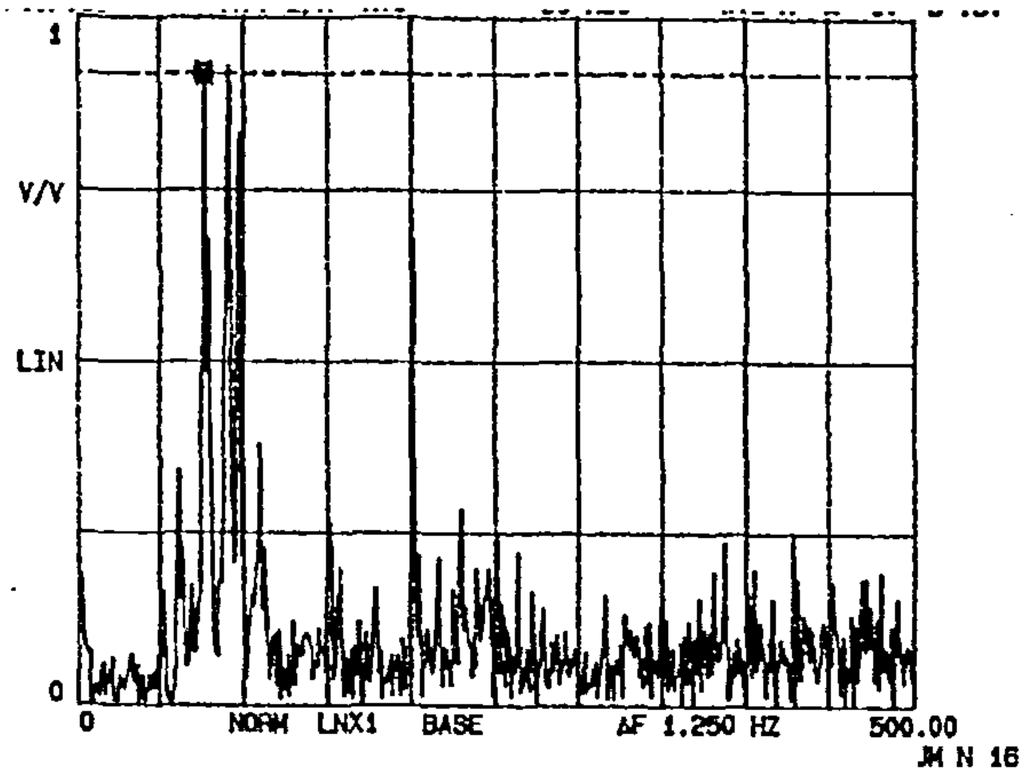

Figure 4.5 Typical transfer function for WADKIN headstock in range 0-500 Hz

4.9 The Surface Finish Data Acquisition System

4.9.1 Stylus Instrumentation

Surface profile data for the harder metallic specimens, was obtained through the use of a Rank Taylor Hobson Talysurf 5-120 surface texture measuring system. This instrument employs a stylus of tip diameter 2μm to traverse the specimen surface and provide an analogue electrical signal equivalent to surface profile which may then be processed by the system to provide such parameters as R_a or which may be transmitted to a chart recorder through an amplifier of (known) variable gain.

In this work the stylus was held immobile whilst the specimen surface was traversed under it by a computer controlled motorised stage at a rate of 1 mm/sec thus providing greater stability in the traverse speed than was available from the built-in Talysurf traversing unit. This was necessary to ensure confidence in the subsequent frequency

domain analyses carried out on the data. The surface profile data was sampled from the recorder output socket located on the rear panel of the system processor which delivered 1 volt per 25.4 mm of chart recorder deflection this equating to 2.36 volts FSD. This signal was recorded by a CompuScope 220 data acquisition board set to sample the data at a rate of 5 kHz. The memory depth used by the data acquisition board was determined by the available scan length of the surface, 128 kbytes corresponding to 26.2 mm at the set sample rate.

4.9.2 The Zygo Instrument

The stylus instrument discussed in section 4.9.1 gives a measure of the surface profile in only one particular region of the workpiece. In order to provide a three dimensional view of parts of the machined surfaces a non-contacting surface structure analyser, located in the University of Edinburgh Department of Mechanical Engineering, was used.

This instrument was a Zygo New View 100 3D Imaging Surface Structure Analyser. It is a scanning white light interferometer which is equipped with six objective lenses providing a range of magnifying powers from 2.5x to 100x. The principle of operation of the instrument is that incoming white light is split into two beams in the interferometer, one beam being passed to a reference surface and the other to the test surface. Following reflection at these surfaces the beams are recombined in the instrument where they produce the light and dark fringe patterns characteristic of optical interference. A CCD camera attached to a precision translation stage then constructs a three dimensional interferogram of the surface which is then stored in computer memory. This interferogram is then transformed into a 3D image through frequency domain processing. In this work the 2.5x objective was used.

The use of the 2.5x objective resulted in a field of view on the test surface of 2.82 x 2.11 mm. The CCD array density for the camera used in this application was 320 x 240 with a pixel size of 11 x 11 μm. The lateral resolution achieved with this configuration was 4.87 μm and the spatial sampling was 8.8 μm. The vertical resolution was 0.1 nm. Eight bit digitisation was employed in the sampling of the interferogram.

4.9.3 The Differential Optical Probe

A second objective of the SERC ACME funded project mentioned in section 4.4.2 was to design, construct and test a non-contacting fibre optic probe capable of profiling machined surfaces inter-operationally and in-situ. The non-contacting nature of this instrument made it ideal for profiling the softer aluminium surfaces without dismounting them from the machine tool [4.6],[4.7]. The device, which makes use of two focused laser beams, is a development of a single spot probe designed and used to make absolute profile measurements from machined surfaces in earlier work[4.8].

The mode of operation of the instrument is based on an extrinsic Michelson interferometer, where fibre optic components are used to form an instrument capable of operating in practical environments. Figure 4.6 shows a schematic of the instrument and figure 4.7 shows more detail of the operation of the probe shown in figure 4.6.

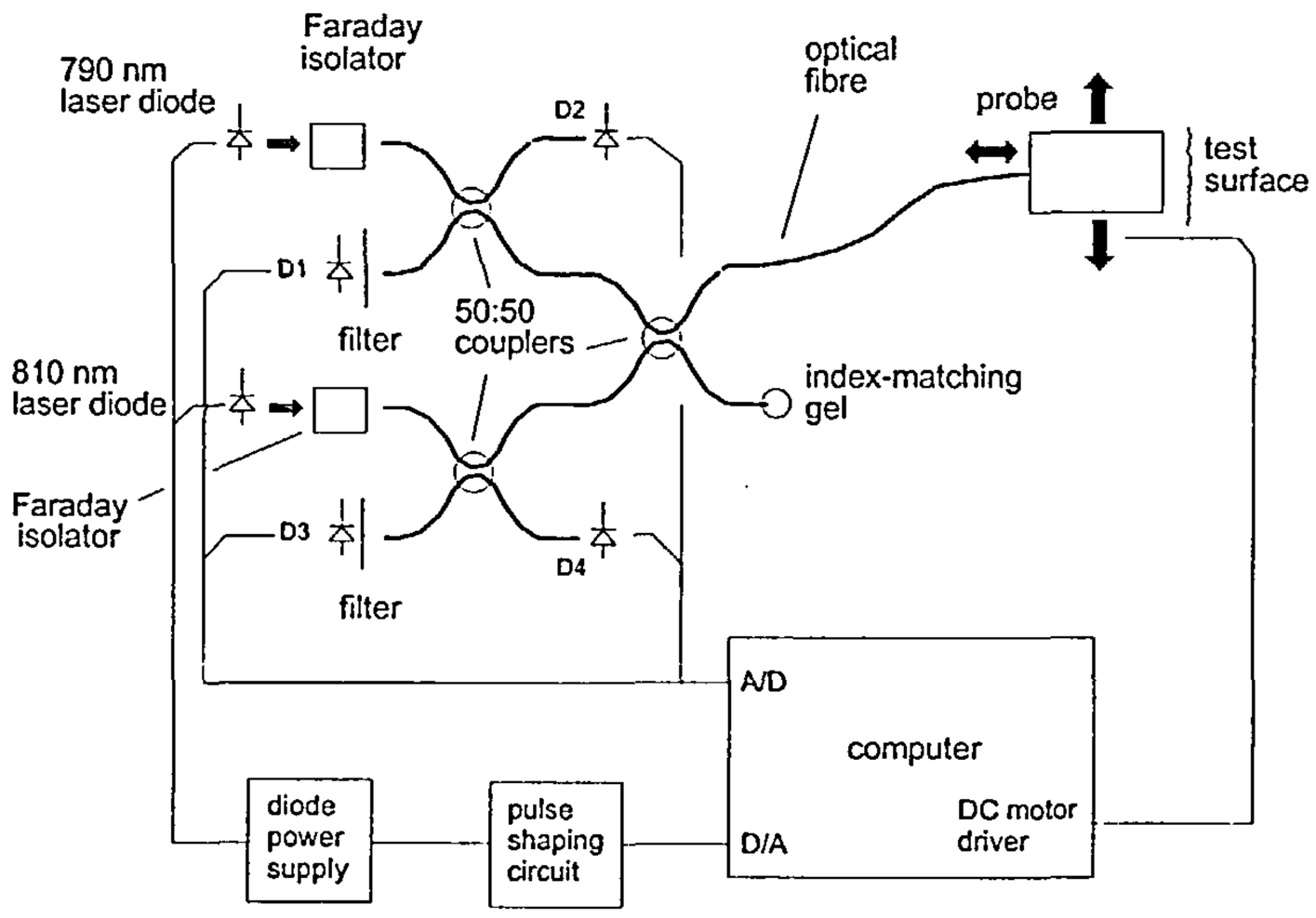

Figure 4.6 Schematic diagram of the fibre optic surface profile instrument

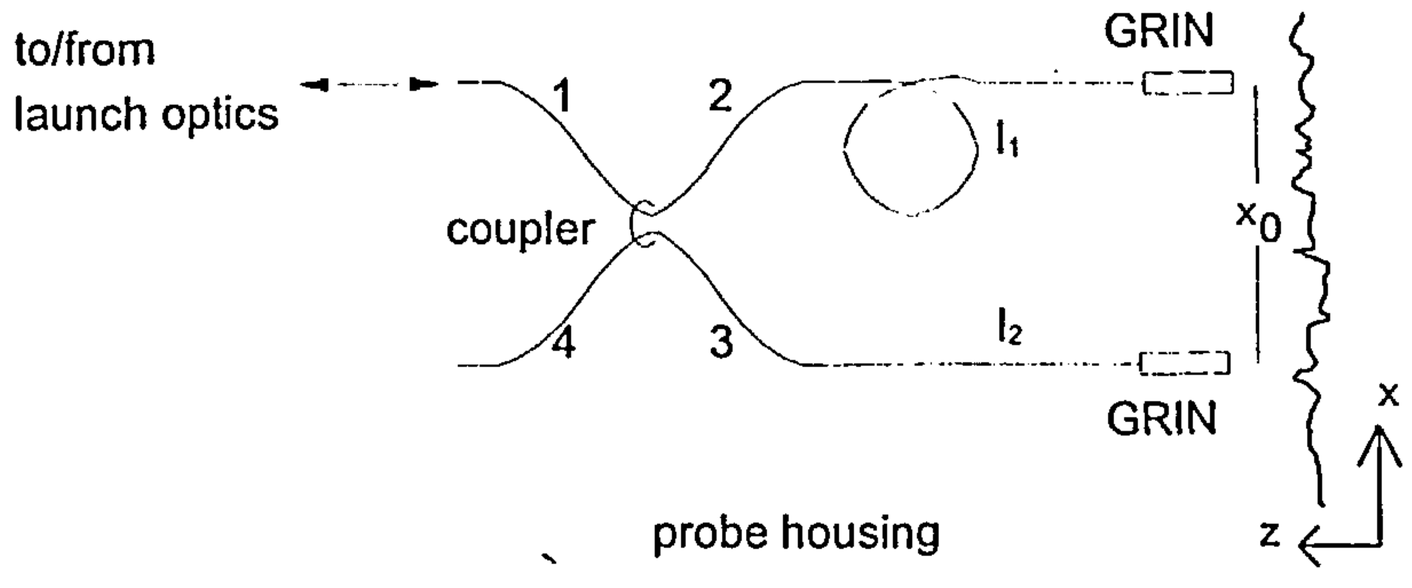

Figure 4.7 Detail of fibre optic probe shown in figure 4.6

A laser beam is used to measure the optical path length difference l_1 - l_2 by interferometry, with a resolution in the nm range (comparable with a stylus profiler). The path lengths l_1 and l_2 are derived from the test surface, thus generating a 'differential' profile as the surface is scanned. Whilst an absolute surface profile is more readily interpreted, this differential instrument has the practical advantage of being insensitive to whole-body out-of-plane motion (which affects equally l_1 and l_2). Although it is difficult to reconstruct an absolute profile from the differential one, or to derive easily quantities such as R_a, it is straightforward to interpret the differential profile in the spatial frequency domain.

The differential profile may be interpreted as follows. With reference to figure 4.7, the differential profile is given by

$$l_\delta(x) = l_1 - l_2 = l(x) - l(x - \delta x) \qquad (4.2)$$

where l(x) is the absolute profile and δx is the separation between the laser beams. Denoting the spatial frequency by k, the spectra for the differential and absolute profiles are L_δ(k) and L(k) respectively, where

$$L_\delta(k) = \left(1 - e^{-ik\delta x}\right)L(k) \qquad (4.3)$$

This transfer function suppresses spatial frequencies that are integral multiples of 1/δx. However, when probing a surface of broad spectral composition, the integrated spectral content over a spatial frequency range δk >>1/δx in the differential profile is still

representative of that in the absolute profile. Thus differential probe measurements could be used in the same way as the absolute profiles obtained the stylus instrument.

The instrument used in this work employed a lens to surface working distance of 2 mm with two focused spots of diameter 7 μm and separation 3 mm. The wavelengths of the laser diodes used in this instrument gave a measurement range of ±8 μm.

4.10 Summary

In this work face milling experiments were conducted, using both multi-point and single point cutters, on annealed En24 steel, quenched and tempered En24 and type 304 stainless steel. Measurements of the AE generated during the cutting process were made using a fibre optic AE sensor and a conventional piezo-electric AE transducer. Surface profile measurements were taken from a set of machined surfaces which had been preserved at intervals during the experiments using a stylus profilometer. The lengths of the wear lands of the inserts were measured with an engineer's microscope when the experiments were temporarily stopped to allow the preservation of the machined surfaces. Chapter 5 describes the results obtained from the surface profile measurements and shows correlations between tool wear state as measured by the length of the insert wear land length and the spatial frequency content of the machined surface. Chapter 6 discusses the correlations between tool wear state and the AE measurements made during the machining process. These two approaches to the problem of tool wear monitoring are integrated in chapter 7 where the use of artificial neural networks is discussed.

4.11 References

4.1) D.P. Hand, T.A. Carolan, J.S. Barton, J.D.C. Jones. "Extrinsic Michelson interferometric fibre optic sensor with bend insensitive downlead", Optics Communications, 97 (1993) 295-300

4.2) J.S. Barton, "Making measurements with optical fibres", Physics Education, 29 (1994) 151-154.

4.3) R. McBride, T.A. Carolan, J.S. Barton, S.J. Wilcox, W.K.D. Borthwick, J.D.C. Jones. "Detection of acoustic emission in cutting processes by fibre optic interferometry", Measurement Science and Technology, 4 (1993) 1122-1128.

4.4) T.A. Carolan. "Acoustic emission detected by fibre optic interferometry". PhD Thesis, Heriot Watt University, Edinburgh, 1994.

4.5) S.J. Wilcox. "Cutting tool condition monitoring using multiple sensors and artificial intelligence techniques on a computer numerical controlled milling machine." Ph.D. Thesis, Heriot Watt University, Edinburgh, 1992.

4.6) P. Wilkinson, R.L. Reuben, J.D.C. Jones, J.S. Barton, D.P. Hand, T.A. Carolan, S.R. Kidd. "Surface finish parameters as diagnostics of tool wear in face milling". Wear, 205,(1997), 47-54.

4.7) S.R. Kidd, D.P. Hand, T.A. Carolan, J.S. Barton, J.D.C. Jones. "Measurement aspects of surface form using an optical differential height measurement technique". Measurement Science and Technology, 7(1996) 1579-1582.

4.8) D.P. Hand, T.A. Carolan, J.S. Barton, J.D.C. Jones. "Profile measurement of optically rough surfaces by fibre optic interferometry", Optics. Letters 18 (1993) 1361-1363

Chapter 5

Surface Finish Data Processing and Results

This chapter describes the data processing applied to the data obtained from the experimental tests discussed in chapter 4. The results derived from this processing are introduced but discussion is withheld until chapter 8.

All the acoustic emission data and the surface finish data were recorded and stored on computer disc via the CompuScope CS220 digital sampling oscilloscope. This process employed 8-bit analogue/digital converters and resulted in the data being stored in 8-bit binary format. In order to simplify subsequent data processing this binary data was converted to ASCII format, as required, using proprietary software supplied by the manufacturer of the digital sampling oscilloscope.

5.1 Evolution of wear

Many tool management schemes require tool or insert changes after an elapsed cutting time corresponding to a calculated tool life. Often this tool life is calculated from an equation such as the extended Taylor tool life equation [5.1].

$$T = KV^{\alpha} f^{\beta} h^{\gamma} V_{b\max}^{\delta} \qquad (5.1)$$

where T is the life of the tool

V is the cutting speed

f is the feed rate

h is the depth of cut

V_{bmax} is the maximum flank wear

K, α, β, γ, δ are empirical constants

The constants in this equation are obtained empirically, often from machining tests using single point tools. The results of these tests have then been applied to other machining

processes [5.1]. However when applied to interrupted cutting processes such as single point or multi-point face milling the predicted tool life must be interpreted conservatively. It is also apparent that as the tests from which the constants in equation 5.1 are derived are based on progressive wear tests, discontinuous wear such as chipping or tool failure cannot be taken into consideration when predicting tool life from such equations. This may result in unacceptable product quality which would not be readily identified in an automated machining environment. Conservative use of tool life equations may also result in uneconomically short tool replacement times with inserts being replaced before having reached the end of their useful lives. Similarly, use of the tool life equations with multi-point face milling cutters takes no account of uneven insert wear caused by axial and radial runout. This is illustrated in Figure 5.1a which shows the evolution of flank wear (V_b) for each insert with cut number, which is synonymous with cutting time since all cutting parameters were maintained at constant values throughout the test, when machining annealed En24 with an eight point, negative rake cutter. Figure 5.1b shows the evolution of average flank wear (mean V_b) for the same cutter with the variation in V_b across the inserts shown as error bars.

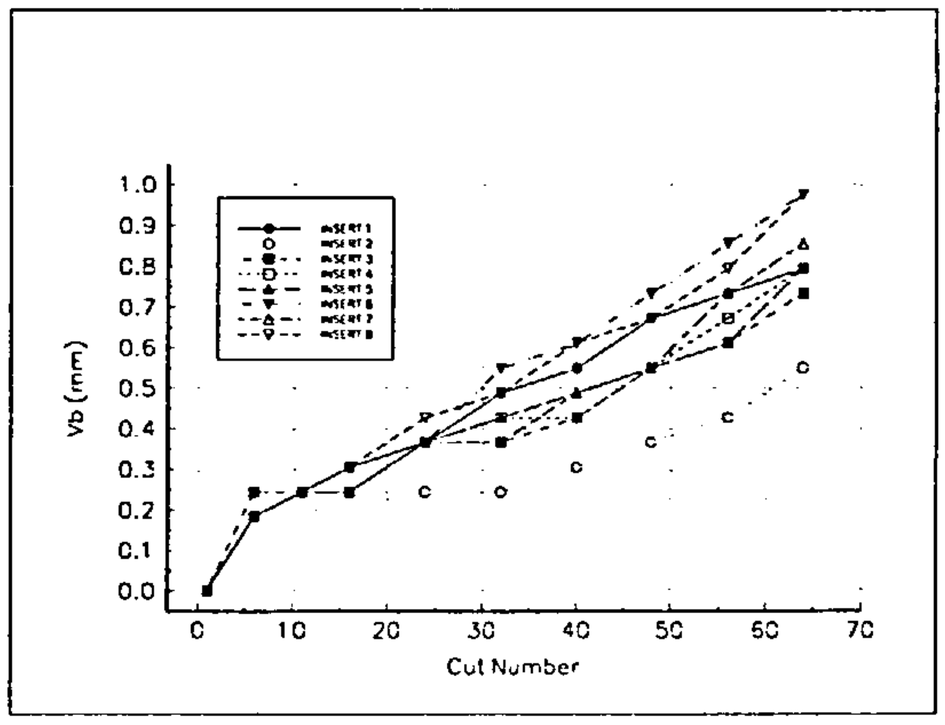

Figure 5.1a Typical variation in V_b with cut number.

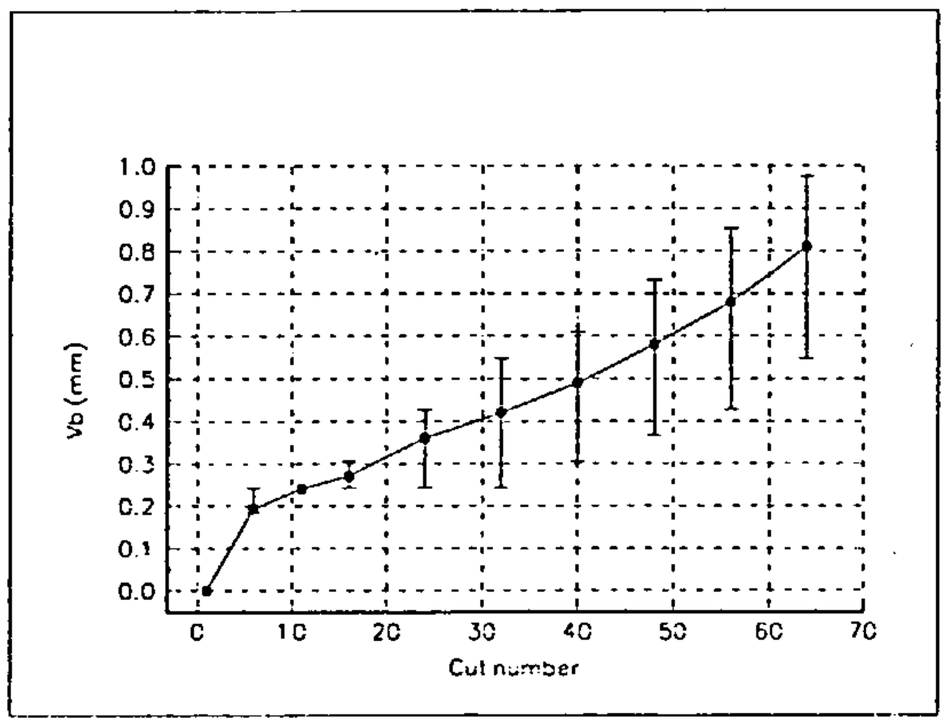

Figure 5.1b Typical variation in mean V_b with cut number.

From these figures it may be noted that towards the end of the test there are considerable differences in the wear states of the inserts as measured by V_b. In particular insert 2 shows a much lower wear rate than the others and it might be imagined that this insert is working less hard than the others as a result of radial runout. Figure 5.1b shows the classic wear curve [5.2] used to estimate tool life and if tool life were predicated on such a

curve as this the tool would be considered to be exhausted at cut 58 based on a maximum allowable value of V_b of 0.7 mm. Figure 5.1b also shows that at least one of the inserts is worn out by cut 48. This might be expected to cause some deterioration in product quality before the tool were to be changed. Clearly tool life equations will not provide sufficiently detailed information to enable tool changing in an automated system at an economically acceptable rate. It is necessary therefore to examine aspects of the cutting process itself to extract information which would enable appropriate tool changes to be made.

5.2 Surface finish

The quality of a machined component is usually assessed by the dimensional tolerances to which it is manufactured and the surface finish which is achieved during the manufacturing process. Dimensional tolerances are important in assembly and surface finish is of importance in establishing and maintaining the functionality of the component and in achieving an aesthetic appearance. For example surface finish is important in components which are intended to retain lubricants, in optical components and in heat transfer applications. As surface finish is affected by the wear state of the machine tool which produced the surface it is reasonable to include a surface finish parameter in a tool wear monitoring system.

The texture of a machined surface may be considered to be made up of roughness components superimposed on waviness components [5.3], [5.4]. The roughness elements result from the production process and the waviness elements arise from such factors as machine deflections, chatter and vibrations. It may be expected that, as the insert wears, changes in both the waviness and the roughness components of the profile will occur. Geometric changes on the flank of the insert, such as grooving, will be impressed onto the generated surface and will be observed as a change in its roughness characteristics. In addition, insert wear causes an increase in the cutting force experienced by the tool [5.5] which in turn will increase the tool deflections and be reflected in the waviness components of the profile. Figure 5.2a shows a surface profile generated by machining annealed En24 using an eight point, negative rake cutter using new inserts whilst Figure

5.2b shows a surface profile generated by the same cutter and material but employing worn inserts. The changes in roughness component of the surfaces can be seen easily.

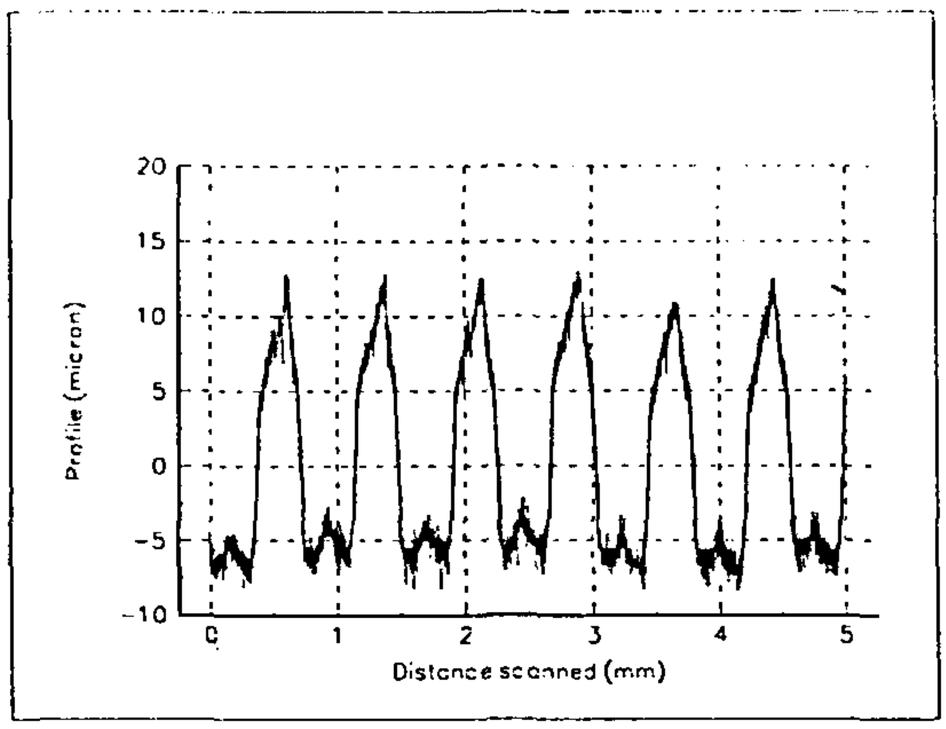

Figure 5.2a Surface profile generated by new inserts cutting annealed En24

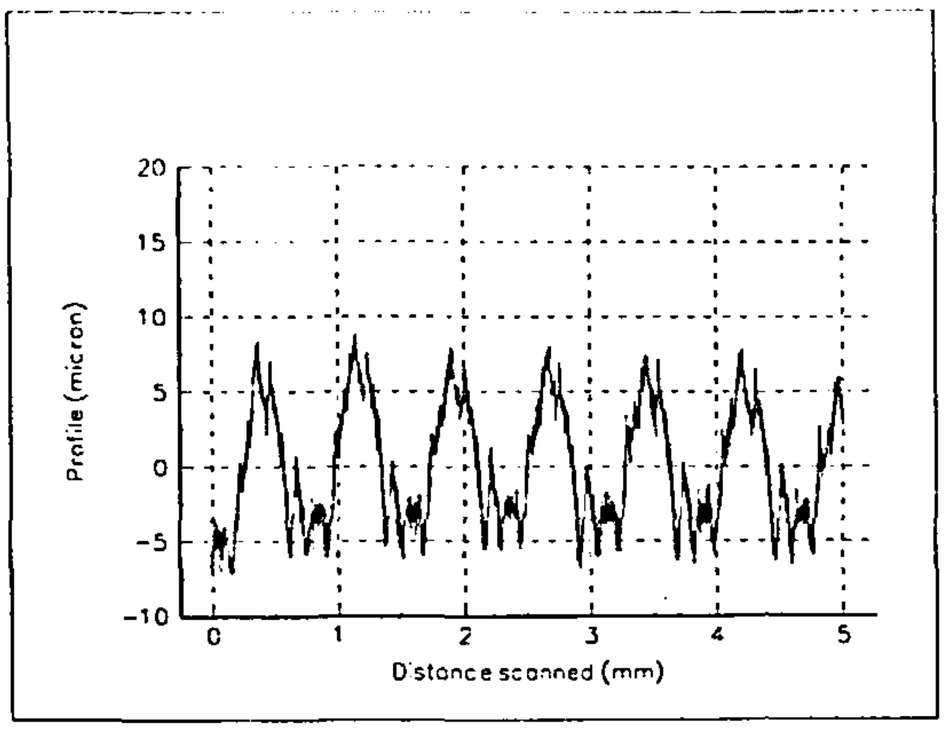

Figure 5.2b Surface profile generated by worn inserts cutting annealed En24

Figures 5.3a and 5.3b show a longer scan of both of these surfaces clearly demonstrating the changes in waviness constituent of the surfaces.

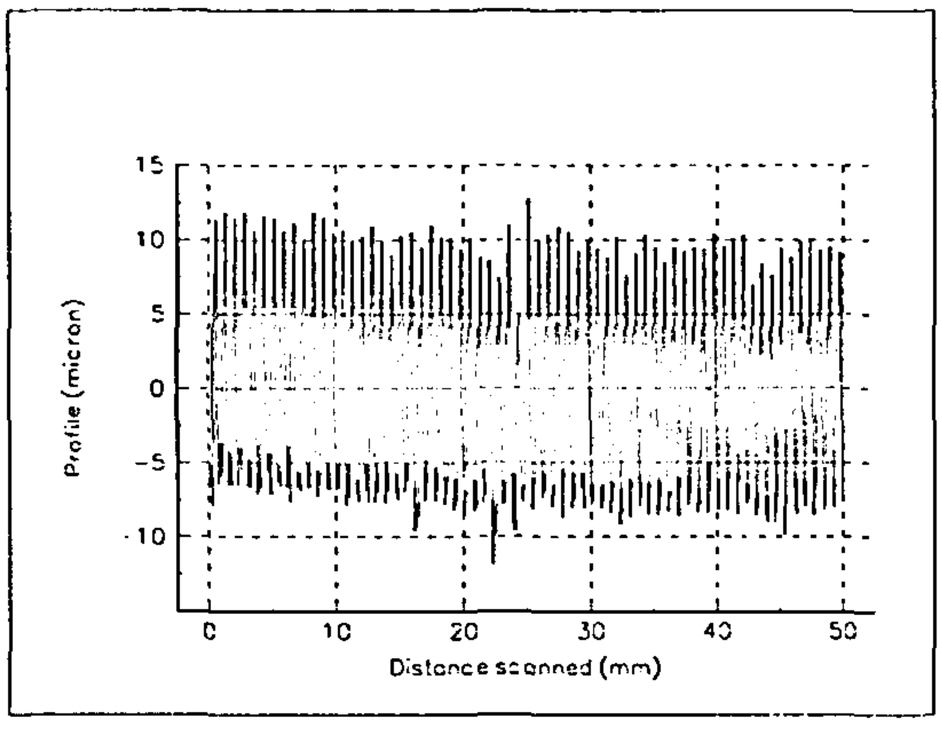

Figure 5.3a 50 mm length of machined surface corresponding to fig 5.2a

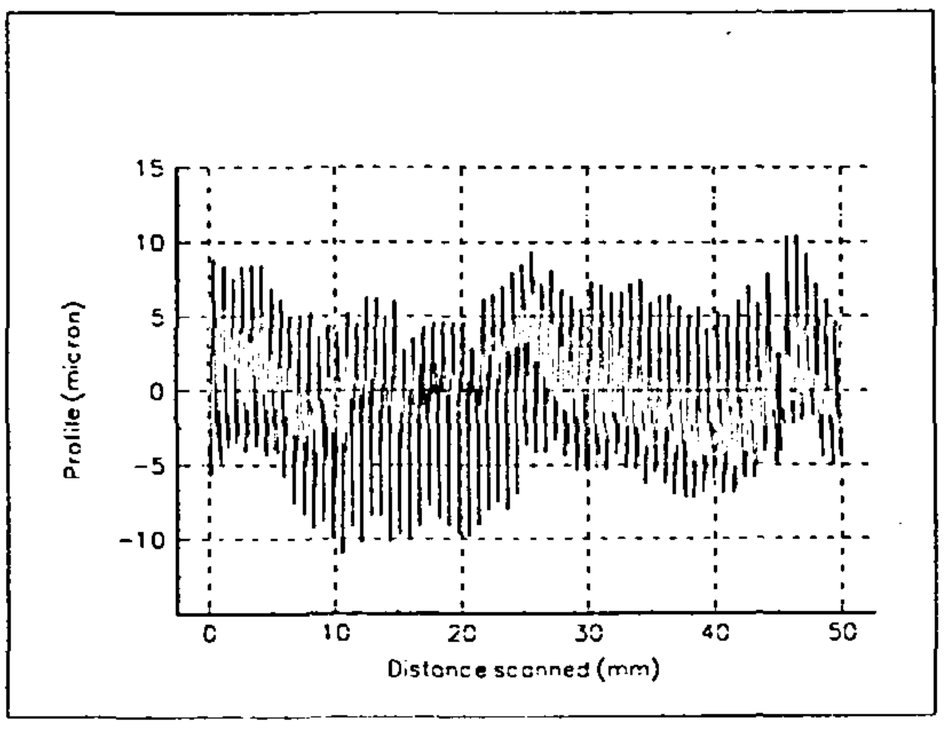

Figure 5.3b 50 mm length of machined surface corresponding to fig 5.2b

As discussed in chapter 3, it has long been of interest to predict surface finish from a specified tool geometry and cutting conditions. Many investigators have developed models of the cutting process. These range from an assumption that the tool is rigid and that the cutter produces a series of tracks in the surface determined by the kinematic

relationship between the tool and work-piece [5.6] to models which include the dynamics of the tool [5.7].

Assessment of surface texture may be made from profile measurements taken by a contacting profilometer. Conventional measures of surface texture are obtained from amplitude parameters such as R_a, R_z and R_t or from spacing parameters such as peak spacing S_m. The most commonly usèd of these parameters is the centre line average R_a and this parameter will be investigated in the following.

5.2.1 Centre line average R_a

R_a is the arithmetic average value of the departure of the of the profile from the profile centre line throughout the measurement length. Mathematically:

$$R_a = \frac{1}{n}\sum_n |y_i| \qquad (5.2)$$

where y_i is the distance of the profile at sample point i from the centre line and n is the total number of sample points. Figure 5.4 illustrates this terminology.

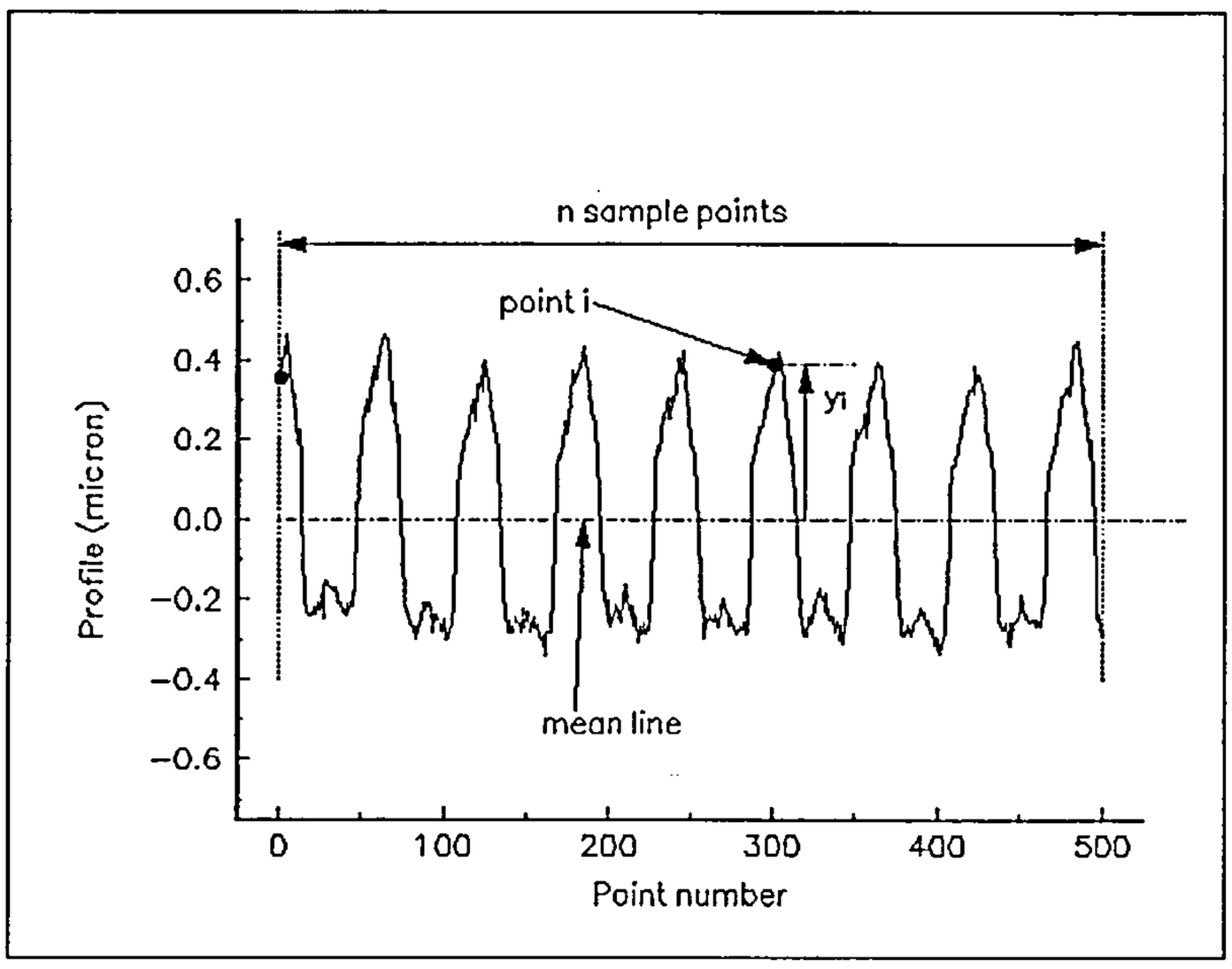

Figure 5.4 Terminology used in calculating R_a

The use of R_a (and of all single number parameters) as a means of characterising a surface is limited. It is possible for several surfaces with identical departures from the centre line

of the surface but of differing character as shown in Figure 5.5 to exhibit the same value of R_a.

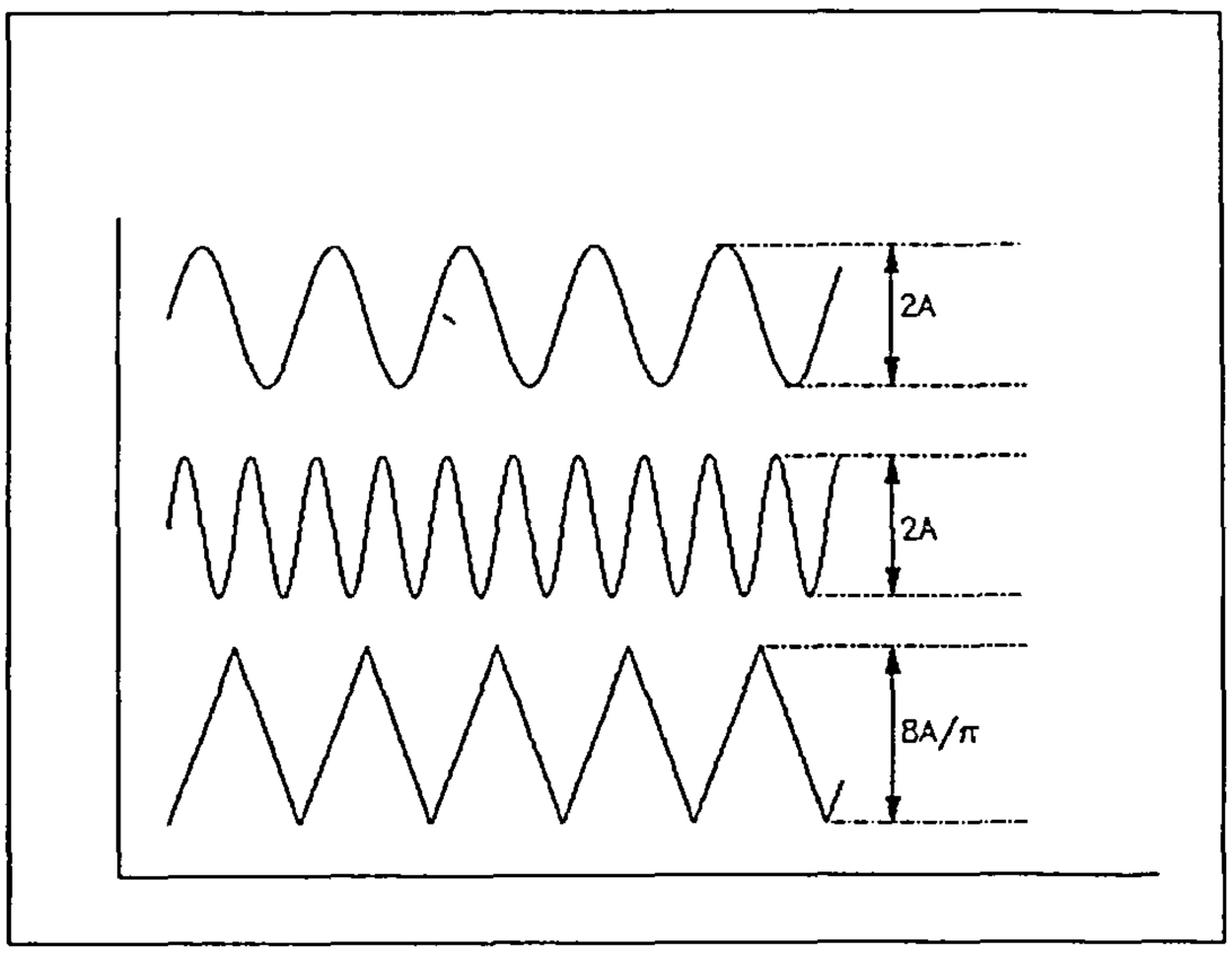

Figure 5.5 Profiles with differing characteristics but all with a value of R_a of $2A/\pi$

Additionally the value of R_a may vary with location on the machined surface and it is usual to take measurements from several positions on the surface and to quote an average value of R_a for the entire surface. This is demonstrated in Figure 5.6a which shows R_a values plotted against V_b from two locations on a surface produced by multi-point, positive rake milling of annealed En24 and Figure 5.6b which shows similar R_a data from a surface produced by fly-cutting annealed En24 with a negative rake tool.

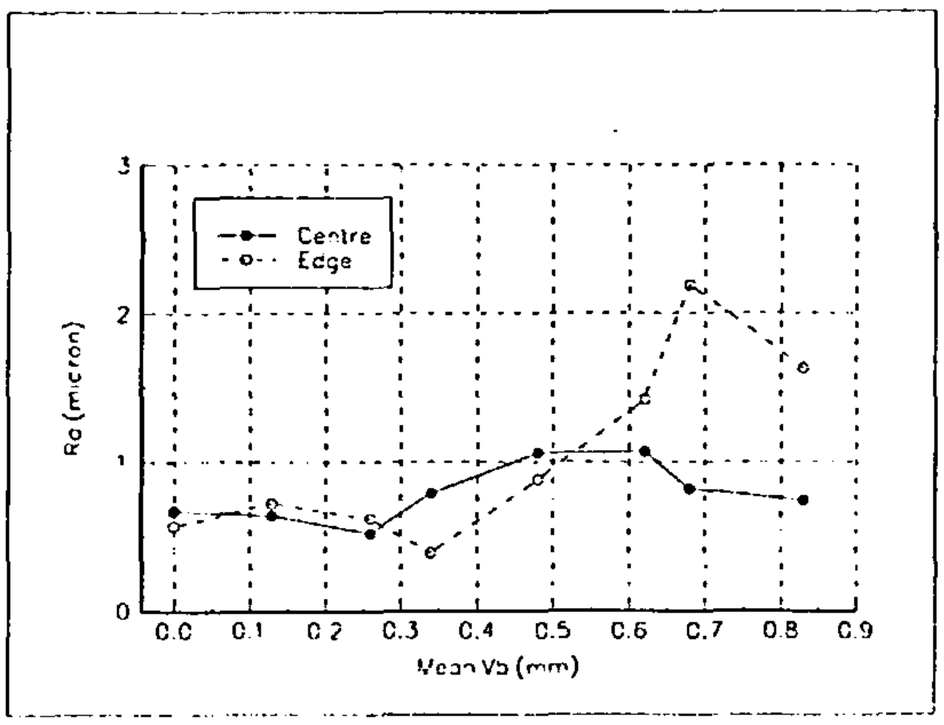

Figure 5.6a R_a vs mean V_b from 2 locations on surfaces produced by multi-point milling of En24

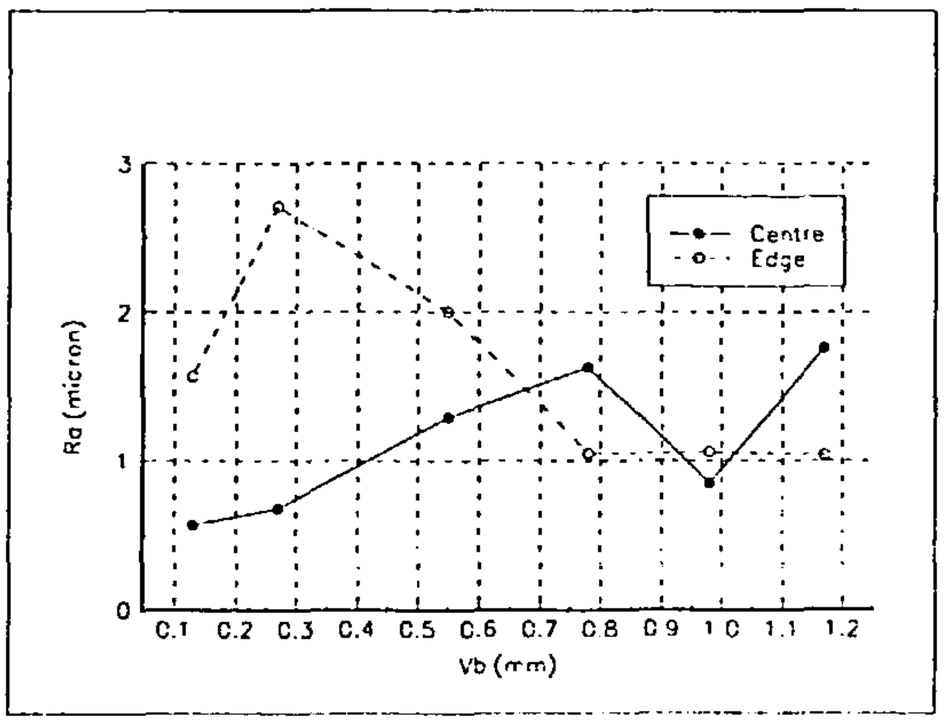

Figure 5.6b R_a vs V_b from 2 locations on surfaces produced by single point milling of En24

As a result of this it has been shown that single number parameters do not correlate with V_b, the length of the flank wear land of the insert [5.8]. This is confirmed by the author's own observations on surfaces generated in the wear tests described in chapter 4. In this work the value of R_a was calculated over 200k points extracted from profilometer records of length 256k points. This represented a physical length of 40.96 mm on each surface. This length is greater than that which is customarily used in measuring R_a where the normal maximum cut-off length is 8.0 mm. However for the purposes of this work which examines the spatial spectral content of the machined surface profile the increased scan length was considered to be more representative of the surfaces. Figure 5.7 shows the variation in R_a calculated from a scan of the centre line of the test pieces with V_b for a range of tests employing eight point, tools and Figure 5.8 which depicts the variation of R_a with V_b for tests using single point tools.

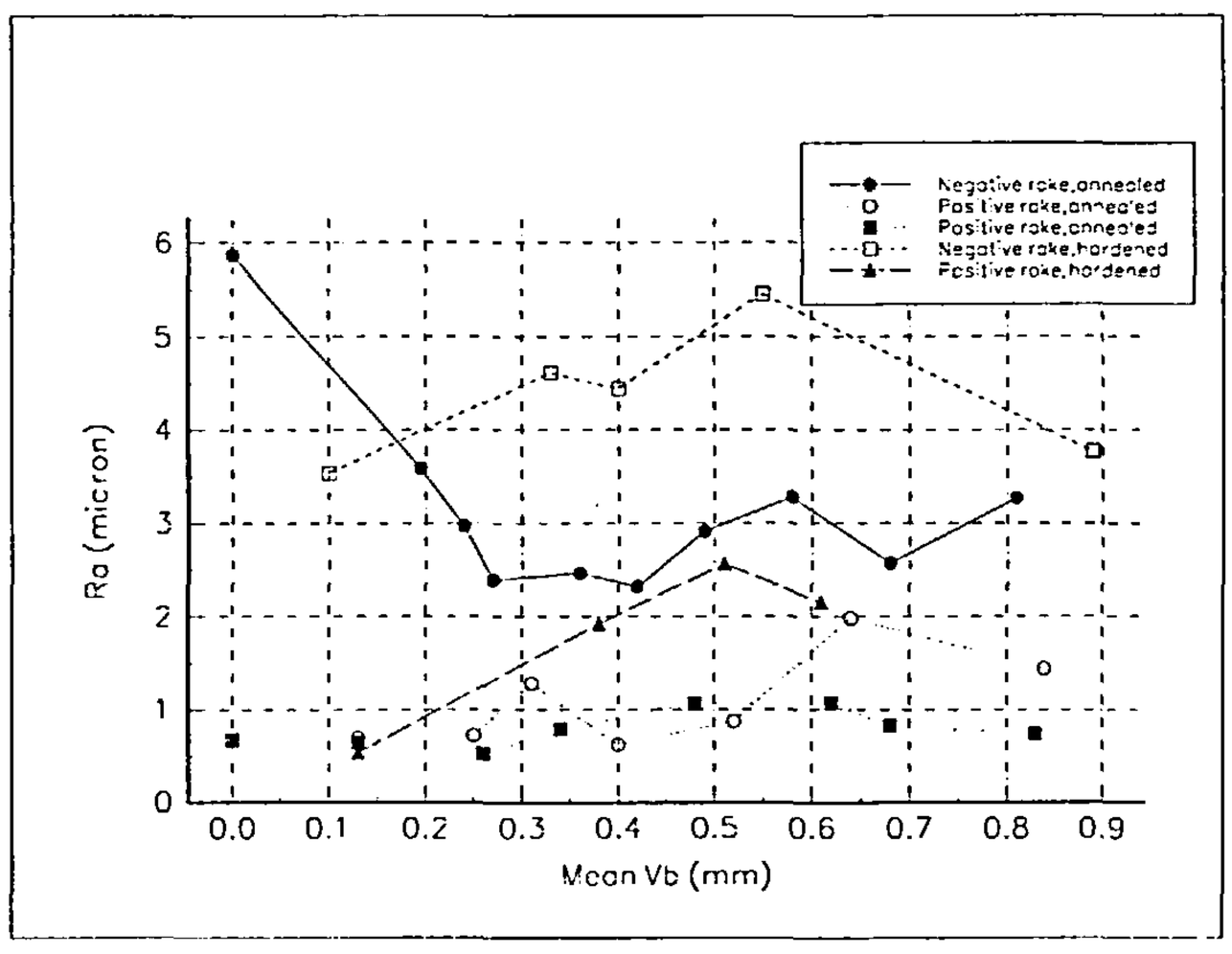

Figure 5.7 Variation of R_a with mean V_b for eight point, negative & positive rake cutters machining both annealed and hardened En24

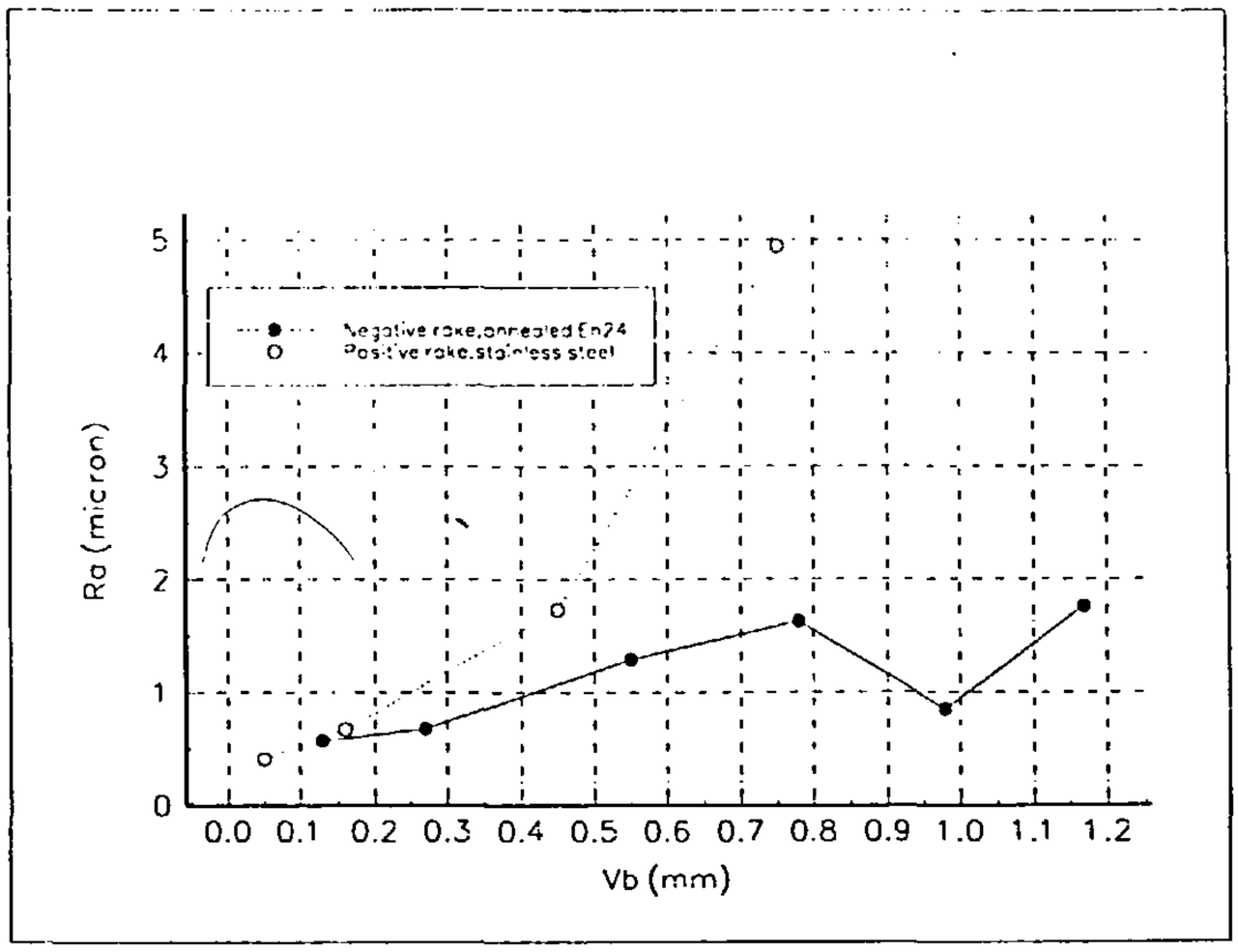

Figure 5.8 Variation of R_a with V_b for single point, negative & positive rake cutters machining annealed En24 and stainless steel

5.2.2 Spectral analysis of surfaces

As was stated in the introduction, the texture of a machined surface is made up of a roughness component superimposed on a longer wavelength waviness component. The source of the longer wavelength component is in machine vibrations and the roughness element arises from the cutting tool profile and its movement relative to the cut surface. Other factors which may be expected to affect the machined profile are random variations in micro-hardness in the work-piece which may produce forced vibrations of the tool, progressive and discontinuous changes in the insert geometry such as flank wear or chipping and the presence of a built up edge.

It is possible to identify three spatial frequency bands which may be associated with effects of the machining process. A *low frequency band* up to but excluding the frequency associated with spindle rotation (the feed per revolution), a *kinematic band* including the frequencies associated with feed per revolution and feed per tooth and a *high frequency band* with spatial frequencies greater than those associated with feed per tooth [5.9]. The kinematic band and the high frequency band are identified in Figure 5.9b which shows the spatial frequency spectrum for the surface shown in Figure 5.9a. In this work the spatial frequency associated with the feed per tooth was 10 mm^{-1} and that associated with the

feed per revolution lay in the range 1.25 mm^{-1} to 10 mm^{-1} depending on the number of inserts being used in the milling cutter. Thus the kinematic frequency band was arbitrarily identified as occupying the spatial frequency range 0.75 mm^{-1} to 11 mm^{-1}. The low frequency band is taken to contain those frequencies lower than the lowest of the kinematic band frequencies.

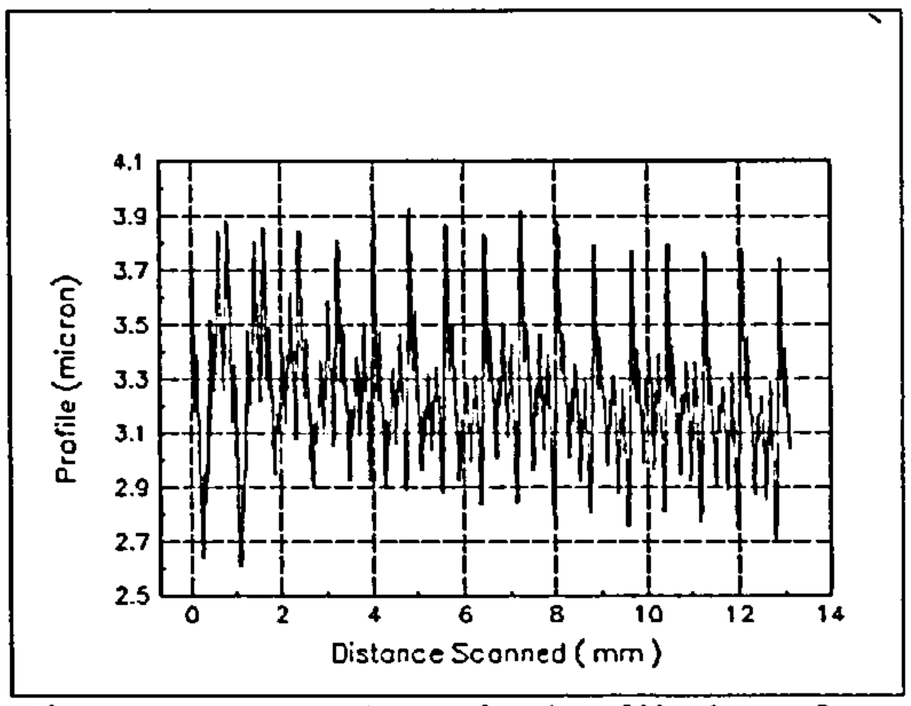

Figure 5.9a A typical milled surface

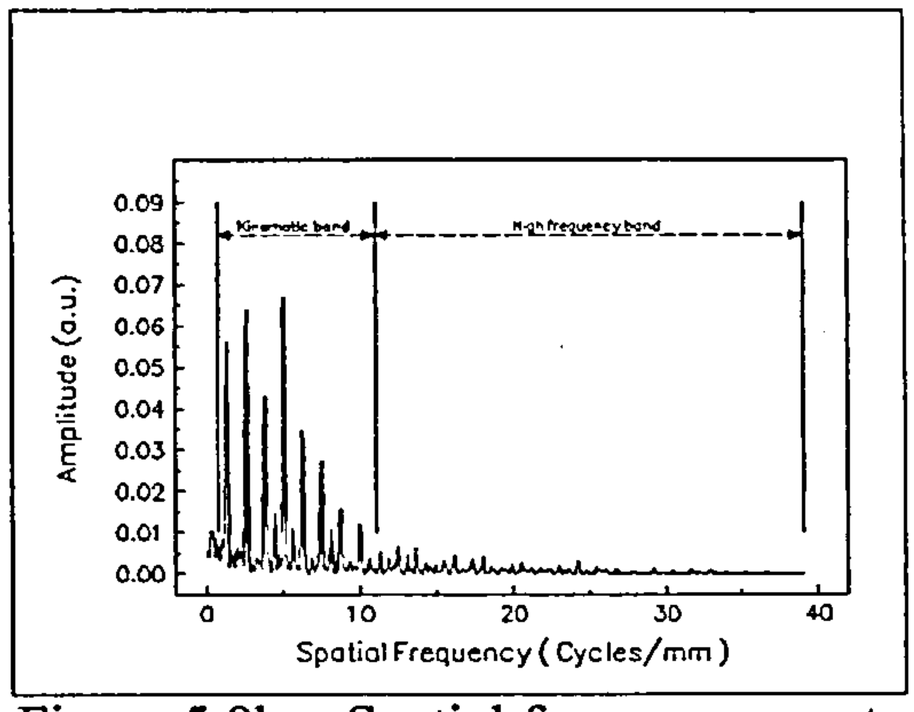

Figure 5.9b Spatial frequency spectrum of the surface shown in Figure 5.9a identifying the kinematic and high frequency bands

Since changes in the wear state of the inserts produce changes in the cutting forces and insert geometry it is reasonable to expect that such changes will be reflected in each of these frequency bands.

The fundamental kinematic effect is the feed per tooth. In practice, radial and axial variations in tool set are possible and this makes multi-point milling more complicated than single point milling. Similarly wear or chipping of one or more inserts will alter the machined profile. Wear affects the profile in several ways. Flank wear will introduce higher frequency variations in the profile as a result of grooves forming on the wiping face of the insert and alterations in the wiping angle. The expected consequences of this are a transfer of spectral energy out of the kinematic band and into the high frequency band. In multi-point cutting chipping, of one or more inserts may alter the balance within the kinematic band whereas in single point cutting this event would enhance the high frequency band of the spectrum. Insert wear also manifests itself in the machined surface through the medium of increased cutting forces which will tend to increase spindle deflections. The resultant vibrations will either be free, in which case the associated

frequencies will be around those of the head stock, or forced in which case the vibration frequencies will be those of the kinematic band. The free vibrations will tend to enhance the energy in the low frequency band whilst the forced vibrations will alter the energy in the kinematic band.

A measure of the energy in each of the frequency bands was taken to be represented by the "integrated spectral content" of the surface profile. Spatial frequency spectra were produced for each profile following which selected bands within the spectra were integrated to give the required frequency band energies. Each profilometer record consisted of 256k points taken over scan lengths of 52.4 mm. The records were averaged over 64 points and then every 32^{nd} point was selected, resulting in 8k points in each data set. The data sets were processed in batches of 2k points to produce three spatial spectra, each separated by 1k points. Thus the spectra were obtained from three locations on the surfaces each of length 13.1 mm and each separated from its nearest neighbour by 6.55 mm. These spectra were integrated over the frequency bands corresponding to the kinematic and high frequency regions identified above. Figure 5.10a shows an example of the averaged spatial frequency spectrum obtained from a surface produced by 8-point positive rake milling of annealed En24 when the mean value of V_b for the cutter was 0.13 mm. Figure 5.10b shows an example of the spatial frequency obtained from a surface generated by the same process but with a mean V_b of 0.84 mm.

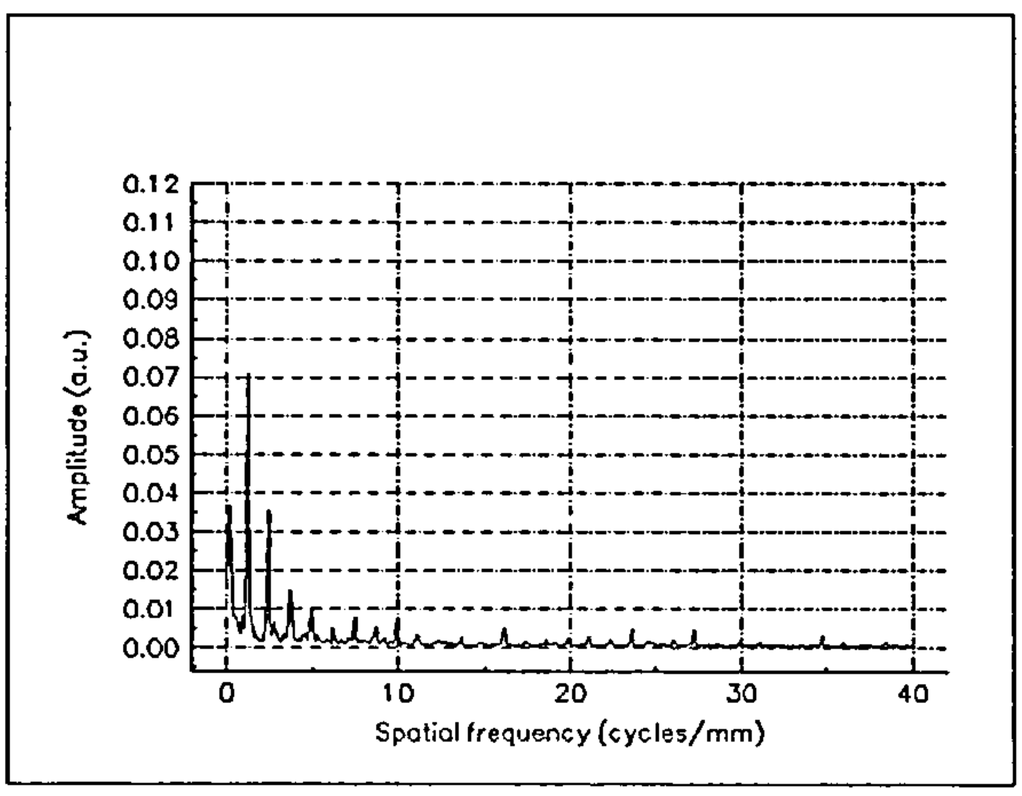

Figure 5.10a Spatial frequency spectrum of a surface generated by 8-point cutting with new inserts

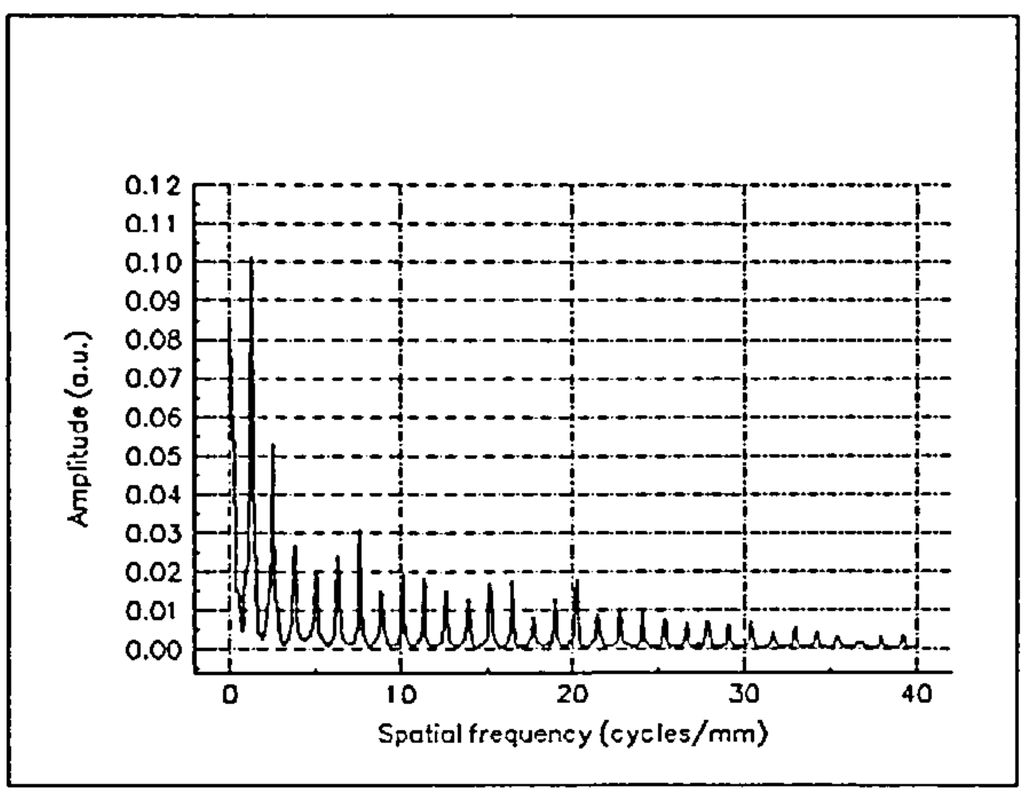

Figure 5.10b Spatial frequency spectrum of a surface generated by 8-point cutting with worn inserts

The differences between the two spatial frequency spectra are clearly visible.

In order to produce the low frequency data the 256k points of each profilometer record were averaged over 512 points and then every 512th point was selected giving a data set of 512 points. The data sets were then processed to give spatial frequency spectra from which the high frequency content had been filtered. The spectra were integrated over the low frequency band defined above to give the energy content in the low frequency band. Figure 5.11a shows the results of this processing for the case corresponding to the conditions of Figure 5.10a and Figure 5.11b shows the results for the case corresponding to the conditions of Figure 5.10b.

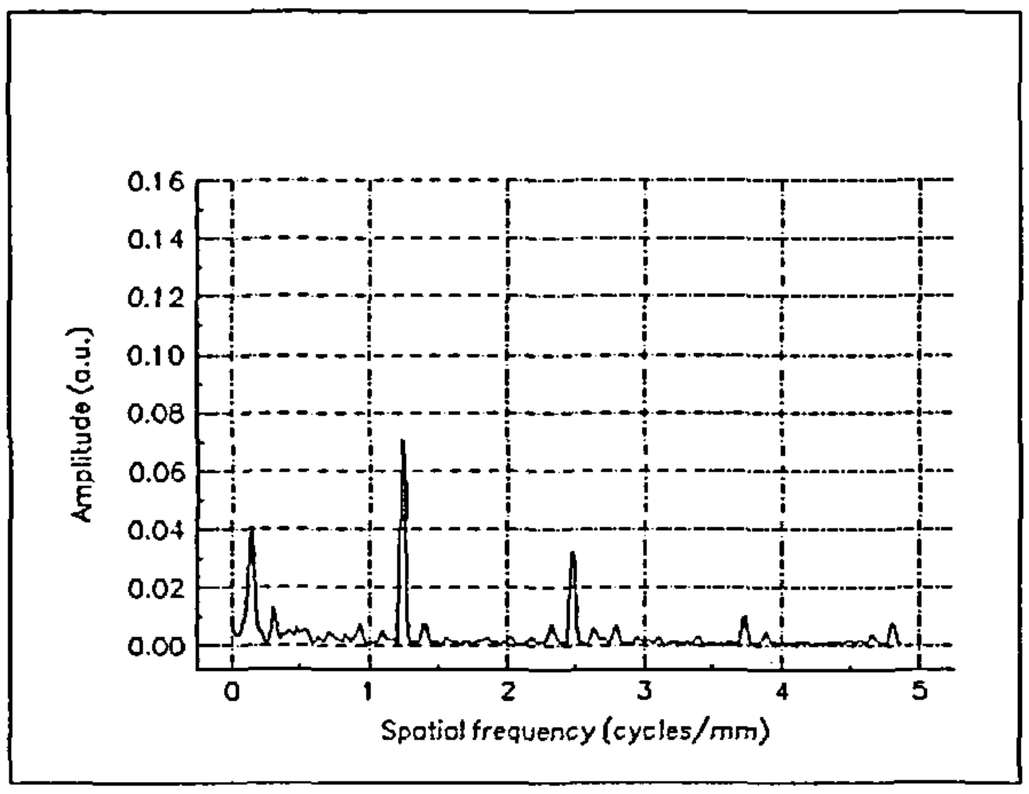

Figure 5.11a Low spatial frequency spectrum corresponding to Figure 5.10a

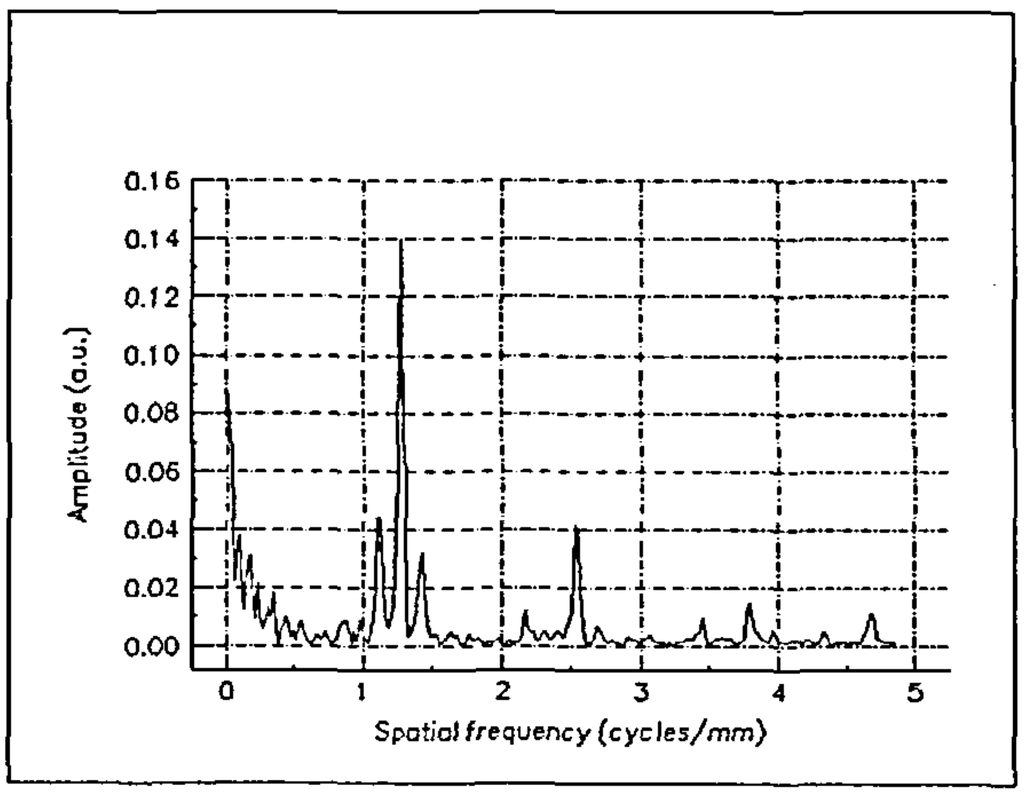

Figure 5.11b Low spatial frequency spectrum corresponding to Figure 5.10b

Again the differences between the two spectra are clearly visible.

Positive rake cutting of annealed En24

Figure 5.12 shows the variation in spectral band energies, for the three frequency bands, with the mean length of the flank wear land, V_b, when cutting annealed En24 with an 8-point tool. The general trend of the spectral energies is to increase with V_b. A local minimum in the values of spectral energies in both the high frequency band and the kinematic band is observable at a value of V_b of 0.26 mm. This is accompanied by a local maximum in the low frequency band spectral energy. These turning points in the data coincided with the chipping of one of the inserts. This chipping developed during the

seven cuts which were made on the test block between the measurement of V_b as 0.26 mm and the previous measurement of V_b.

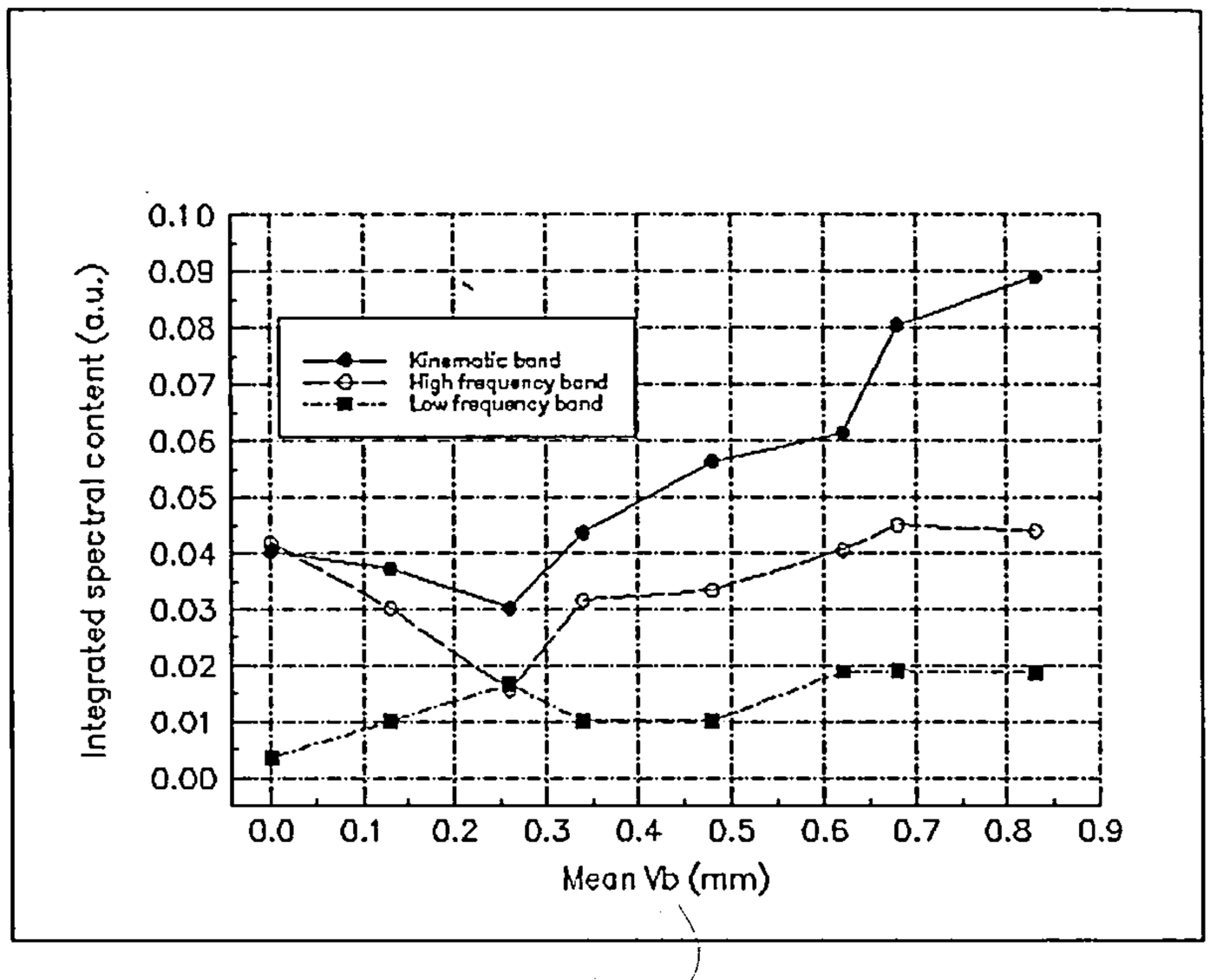

Figure 5.12 Variation of integrated spectral content in three frequency bands with mean V_b for 8-point positive rake cutting of annealed En24

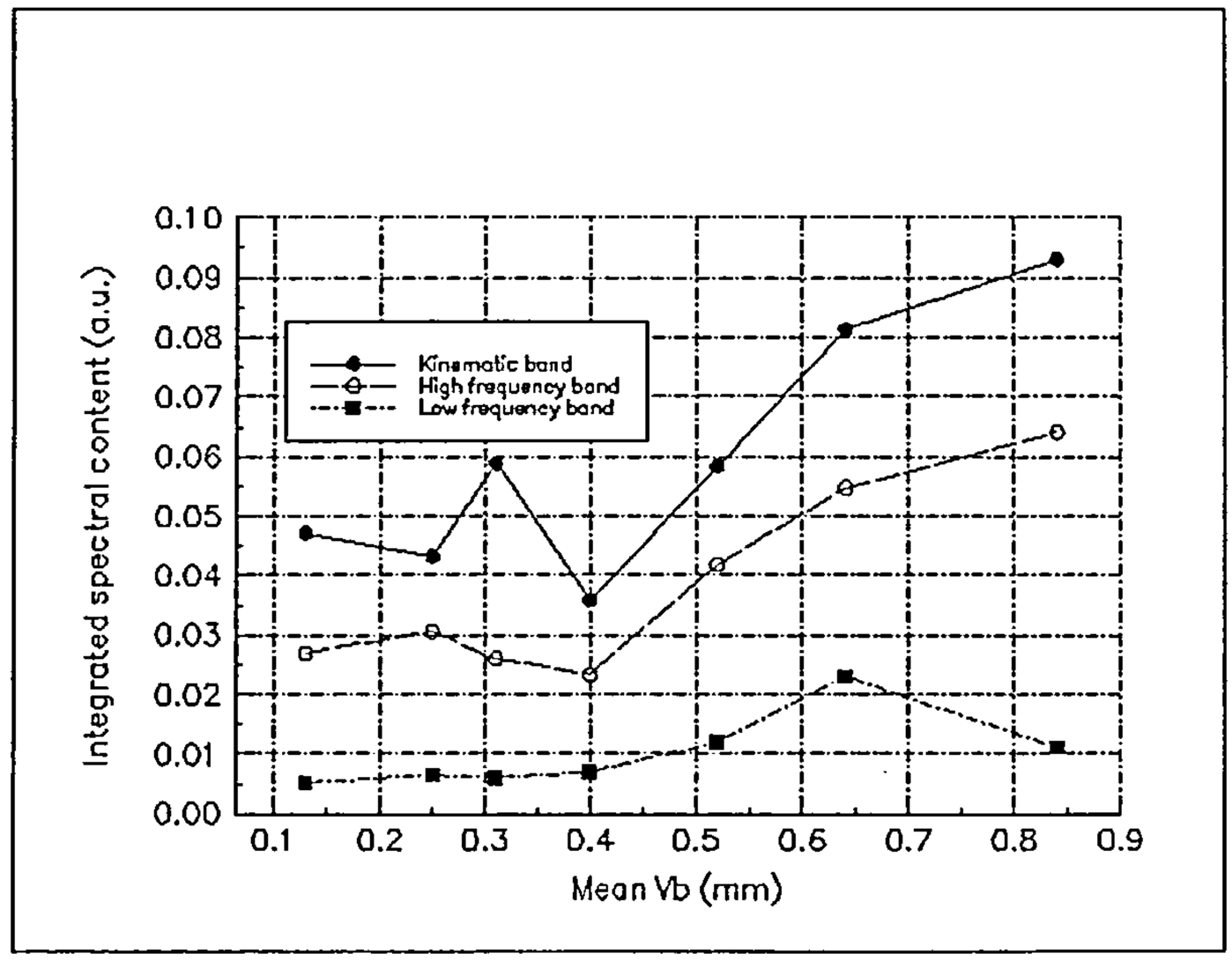

Figure 5.13 Variation of integrated spectral content in three frequency bands with mean V_b for 8-point positive rake cutting of annealed En24. Second experiment.

Figure 5.13 shows the variation in integrated spectral content with V_b for a second series of tests on annealed En24 using an 8-point, positive rake cutter. The same general trend of increasing spectral energy with V_b is observable. Again local minima in the high

frequency band and kinematic band occurred, on this occasion at a value of V_b of 0.4 mm. There is, however, no apparent local maximum in the low frequency band energy. The local minima coincided with chipping of insert 1.

Negative rake cutting of annealed En24

Figure 5.14 shows the variation of integrated spectral content with mean V_b obtained from surfaces generated by 8-point, negative rake cutting of annealed En24.

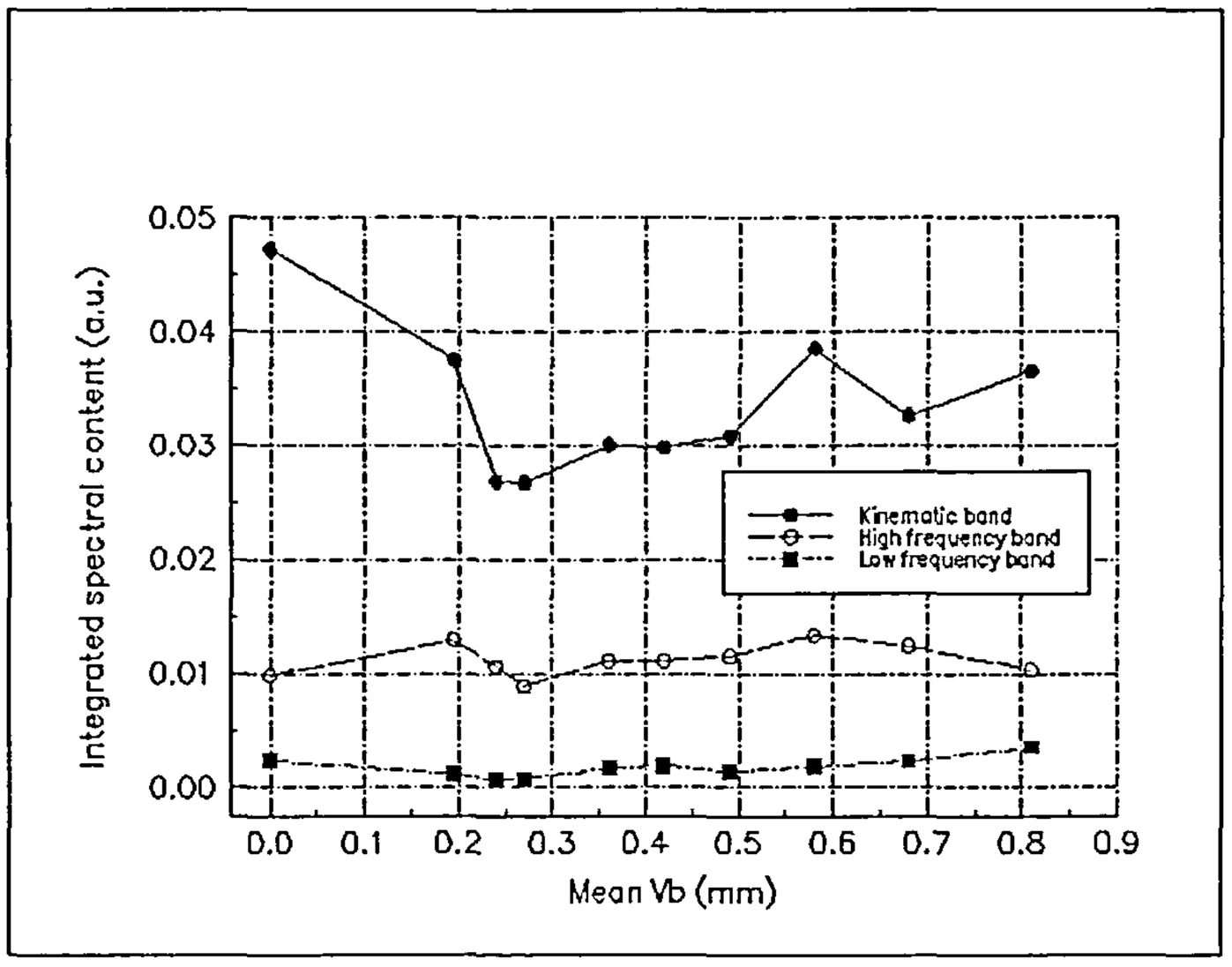

Figure 5.14 Variation of integrated spectral content in three frequency bands with mean V_b for 8-point negative rake cutting of annealed En24

As in the previous cases the general trend of integrated spectral content with V_b is to increase. Local minima in the high frequency and kinematic bands are apparent, in this case accompanied by a local minimum in the low frequency content of the surface. There was no evidence of insert chipping in this test however the variation of V_b with cut number during this test revealed that uneven wear of the inserts was occurring especially in the early stages of insert wear as shown in Figure 5.1b.

Figure 5.15 is a graph of variation in integrated spectral content versus V_b derived from surfaces generated by milling annealed En24 with a single point, negative rake cutter.

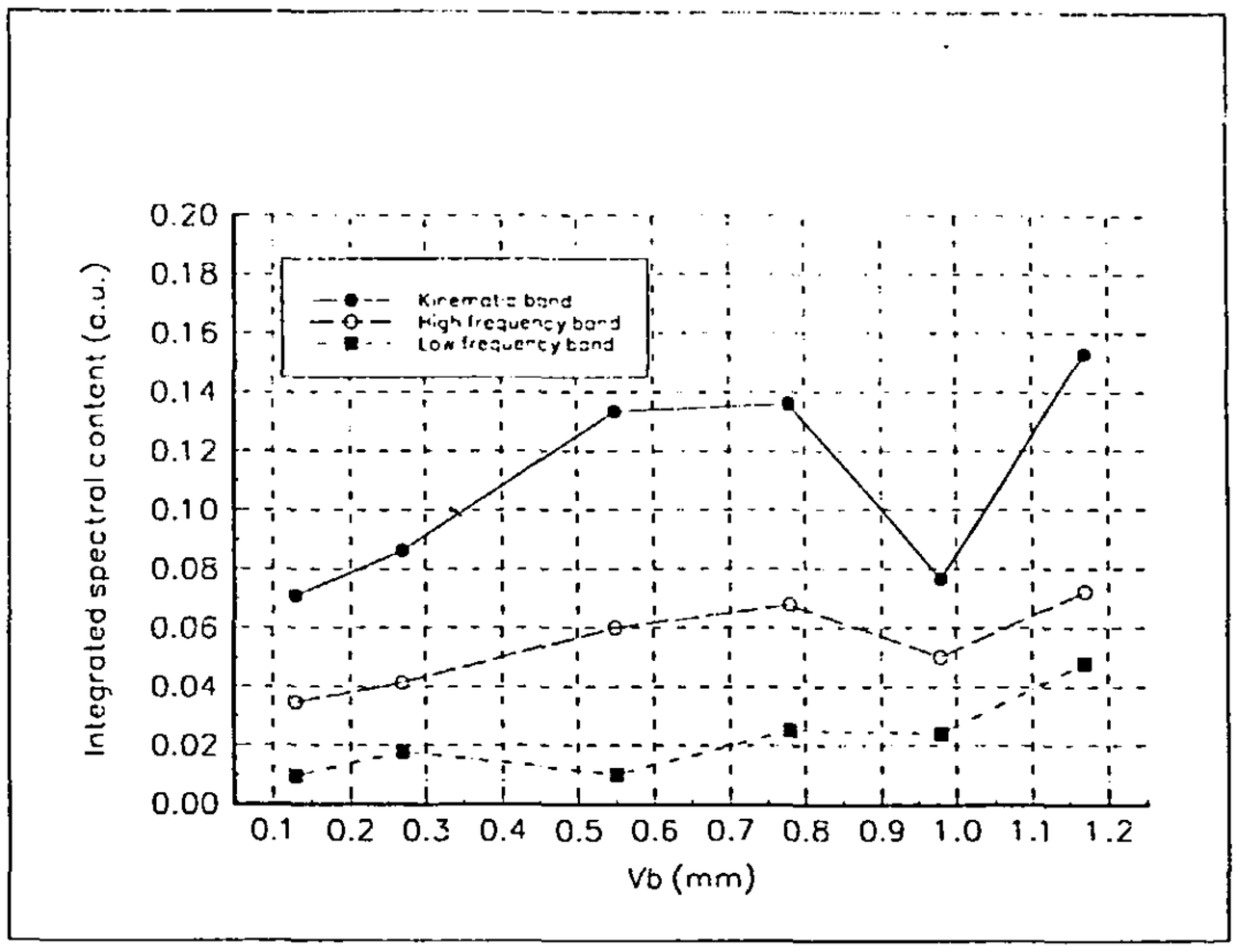

Figure 5.15 Variation of integrated spectral content in three frequency bands with V_b for single point negative rake cutting of annealed En24

Again the trend in all three spatial frequency bands is for the integrated spectral content to increase with V_b. Comparison of Figure 5.15 with Figure 5.14 shows that, following the initial uneven wear patterns for the multi-point cutter i.e. when mean V_b exceeds 0.24 mm, the shapes of the graphs are similar. Figure 5.15 shows some of the characteristics which have been associated with insert chipping in the previous section except that local minima are observed in integrated spectral content for all of the spatial frequency bands under discussion at a value of V_b of 0.98 mm rather than in only the high frequency and kinematic bands. No evidence of insert chipping was present however changes in the insert cutting edge and flank were detected when measuring the length of the flank wear land to be 0.55 mm and again at a value of 0.78 mm. The edge and flank had acquired a groove wear pattern which when impressed on the cut surface would be expected to increase the high frequency content of the surface energy.

Positive rake cutting of quenched and tempered En24

Figure 5.16 shows a plot of the variation of integrated spectral content with mean V_b from surfaces produced by 8-point, positive rake cutting of hardened En24

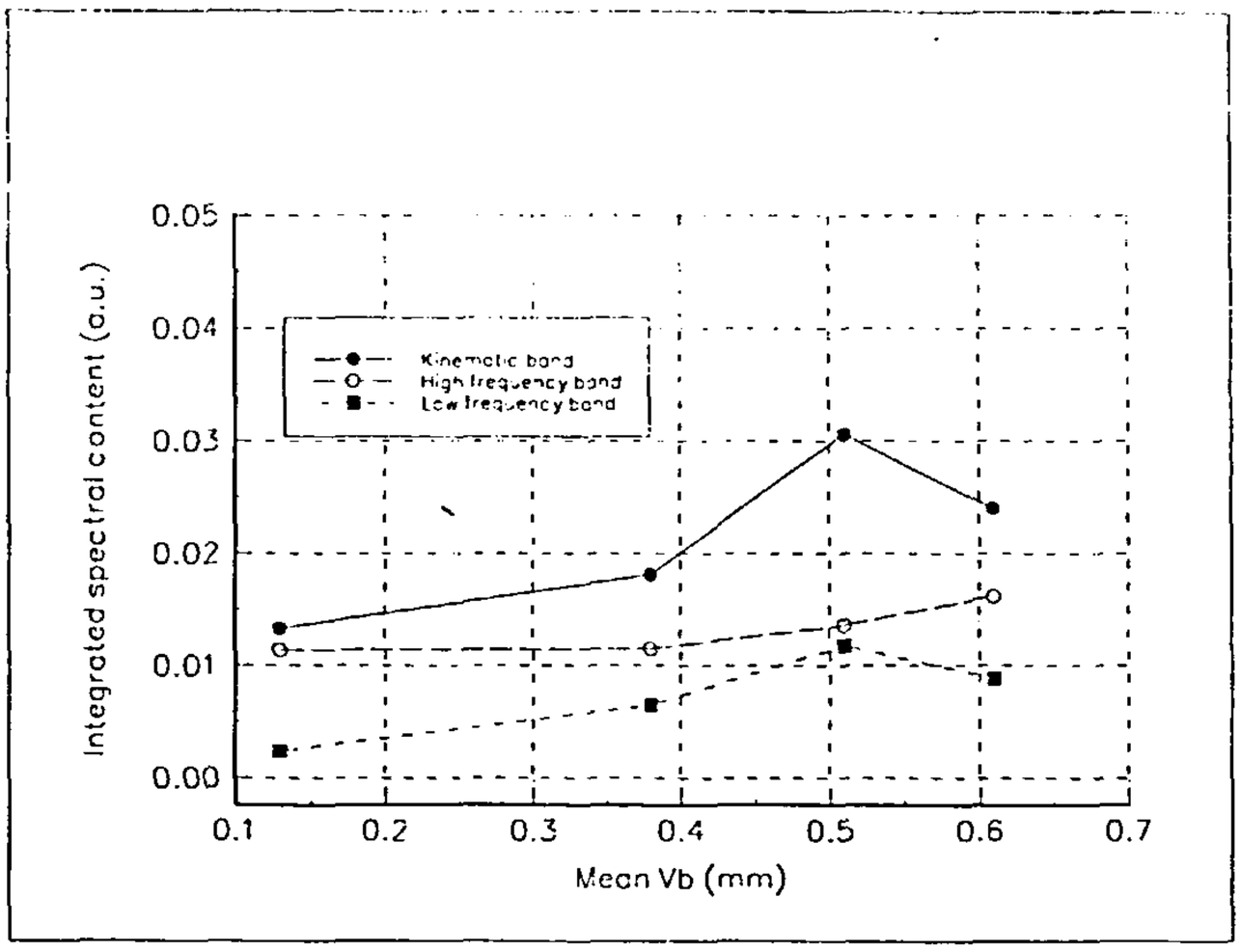

Figure 5.16 Variation of integrated spectral content in three frequency bands with mean V_b for 8-point positive rake cutting of quenched & tempered En24

The general trend of the integrated spectral content in all of the spatial frequency bands is to increase with wear. Insert chipping was present during this series of tests. Insert 7 was observed to be chipped at cut number 40 corresponding to a value of V_b of 0.51 mm. This is accompanied by a fall in the kinematic band content of the surface. Contrary to the observations following insert chipping when cutting annealed En24, the high frequency band was unaffected and a reduction in the low frequency band was detected. As in all the experiments in this work, attempts were made to reduce the axial runout of the inserts before the tests were commenced but uneven wear of the inserts was noticed throughout the test. For example at cut number 40 (the cut number at which insert chipping was noted) the range in wear land length was from 0.35 mm to 0.67 mm.

<u>Negative rake cutting of quenched and tempered En24</u>

Figure 5.17 shows the change in integrated spectral content obtained from surfaces produced by 8-point negative rake cutting of quenched and tempered En24 steel. This experiment was characterised by an unusually high rate of wear for the inserts, the tool being worn (mean V_b = 0.89 mm) out after 16 cuts. The general characteristics of this graph are similar to those of Figure 5.14 in which the softer annealed En24 was also cut by an 8-point negative rake cutter. There is an increase in the integrated spectral content

in the high and low spatial frequency bands with wear land length and the trend of the kinematic band is to increase with V_b. There was no evidence of insert chipping although at the end of the tests insert 8 displayed a much longer wear land (1.04 mm) than the remaining seven inserts (average 0.87 mm)

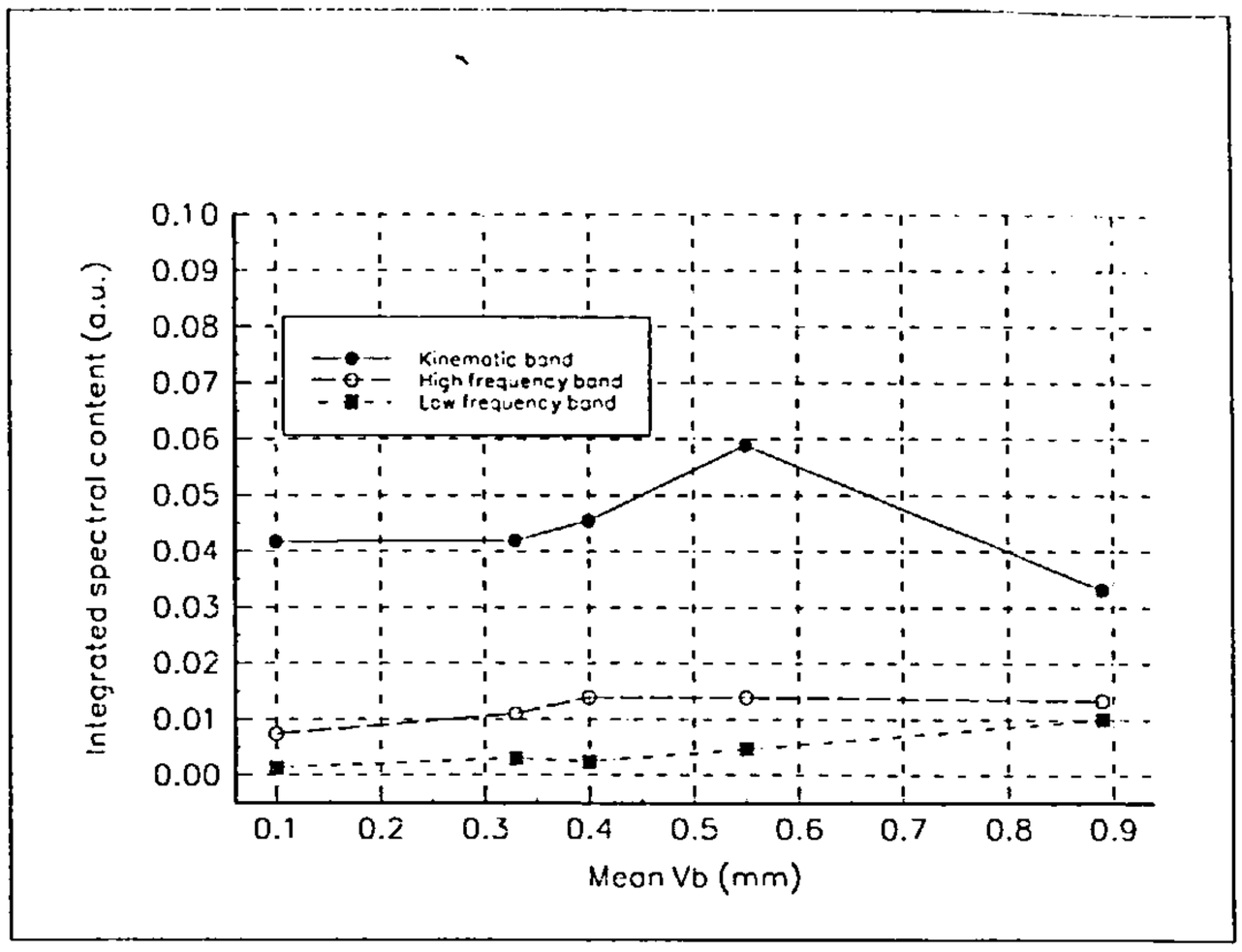

Figure 5.17 Variation of integrated spectral content in three frequency bands with mean V_b for 8-point negative rake cutting of quenched & tempered En24

Single point cutting of stainless steel

Figure 5.18 shows the change in integrated spectral content obtained from surfaces produced by single point positive rake cutting of stainless steel. The energy associated with all of the spatial frequency bands is seen to increase with wear land length. These characteristics are similar to those exhibited by the positive rake cutting of annealed En24 as shown in Figures 5.12 and 5.13 and by the positive rake cutting of quenched and tempered En24 as shown in Figure 5.16. Although there was no evidence of tool chipping in these tests the insert exhibited notch wear. This effect is not detectable in the spectral content of the machined surfaces.

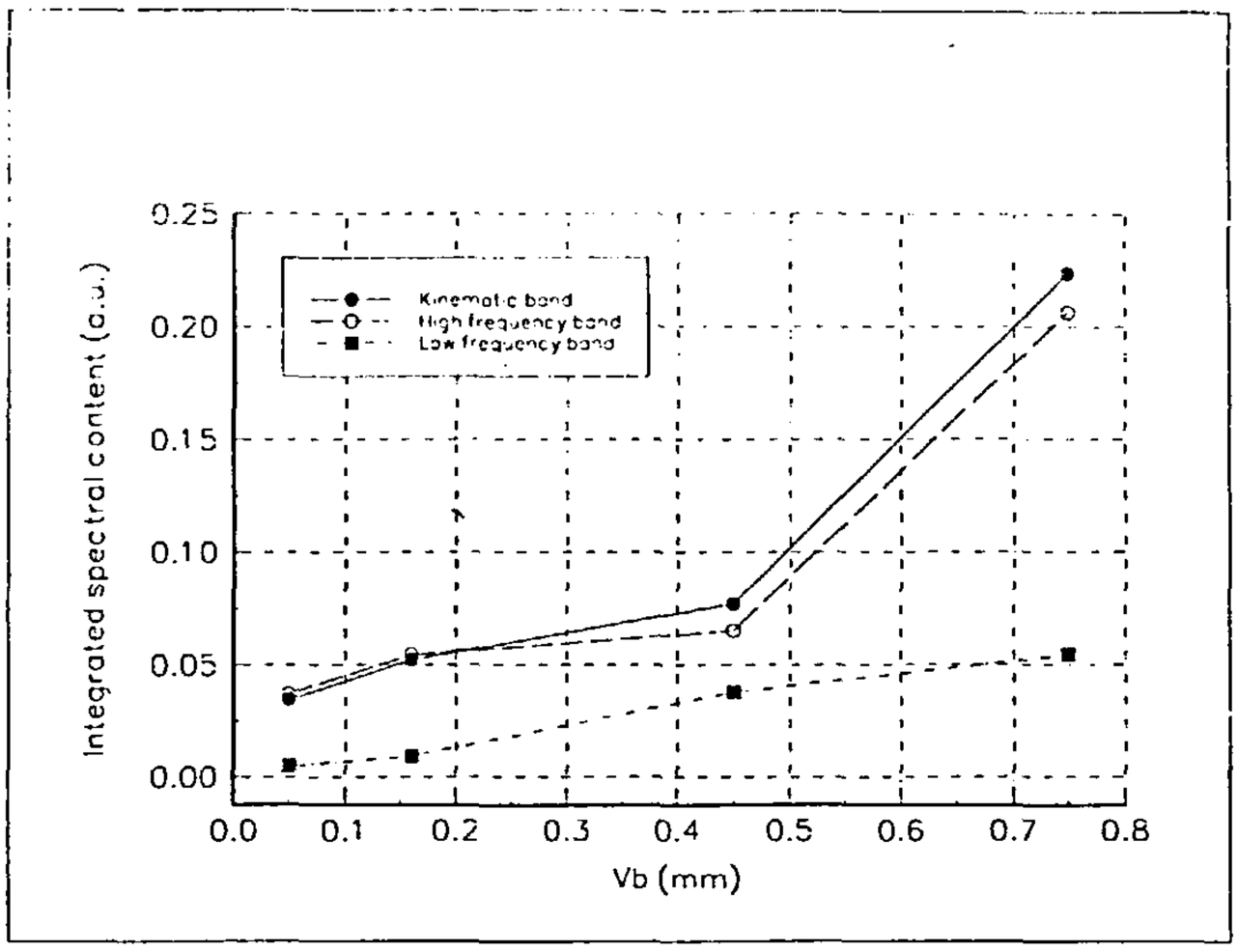

Figure 5.18 Variation of integrated spectral content in three frequency bands with V_b for single point positive rake cutting of stainless steel.

<u>General observations on surface spectral content</u>

By comparing Figures 5.12, 5.13, 5.16 and 5.18 it may be seen that the geometry of the cutter is more important than the workpiece material in determining the way in which the spectral content of the machined surfaces varies with tool wear when using positive rake cutters. It can be seen that this variation has a similar characteristic for both single-point and multi-point cutting.

Comparison of Figures 5.14, 5.15 and 5.17 also suggests that the geometry of the cutter has a dominant effect on the variation of integrated spectral content with wear. It may be seen that in the case of negative rake cutters the kinematic band is most sensitive to tool wear.

Examination of Figures 5.12, 5.13 and 5.16 indicates that the integrated spectral content of a machined surface may be used to detect insert chipping during the cutting process.

5.2.3 Fractal analysis

A geometric object is said to be *self similar* if it may be considered to be made up of rescaled copies of itself and the scaling factor is the same in all directions. If the scaling

factor varies with direction the object is said to be *self affine* [5.10]. There are several techniques available for calculating the fractal dimension of self similar and self affine signals [5.11], [5.12], [5.13], [5.14], [5.15]. These techniques may be loosely classified as geometrical, statistical and spectral methods. The geometrical procedures include divider and box counting methods [5.14], [5.16] statistical techniques incorporate variogram methods, relative dispersion methods and structure function methods [5.15] and the spectral approach uses an application of the FFT to arrive at a fractal dimension [5.12]. In this work the spectral approach to fractal dimension was not used as it was considered to give no more information than that already gained in the spectral analysis of the surfaces described in section 5.2. Two methods were used in this work to calculate the fractal dimension of the machined surfaces: the divider method and the structure function method. These will be discussed in turn.

The divider dimension

This method is based on a technique used originally to determine the true lengths of cartographic features. In its simplest implementation a pair of dividers, set at a known width ε, is walked along the profile under investigation and the number of steps n(ε) required to cover the profile is counted. The length of the profile at this divider setting L(ε) is then given by

$$L(\varepsilon) = n(\varepsilon) \times \varepsilon$$

If the width of the divider were to be reduced and the process repeated, the length of the profile at the new divider setting would be estimated in exactly the same way but in general the new length estimate would differ from the original estimate. A repeat of this exercise using a systematic reduction in divider width would reveal the relationship between apparent profile length and measurement scale. It is observed that the estimated length of the profile is a function of the divider setting or measurement scale [5.17], [5.18], [5.14]. A power law relationship exists between the estimated profile length and the measurement scale [5.19] given by

$$L(\varepsilon) = L_o \varepsilon^{1-D} \tag{5.3}$$

Where L_o is a constant with the dimensions of length and D is the fractal dimension of the profile. Equation 5.2 may be expressed as

$$\log(L(\varepsilon)) = \log(L_o) + (1 - D)\log(\varepsilon) \tag{5.4}$$

A plot of $\log(L(\varepsilon))$ against $\log(\varepsilon)$ will reveal the fractal dimension in the form of the slope β of the linear portion of the plot. Thus

$$D = 1 - \beta \tag{5.5}$$

If the dimension D of the profile lies in the range 1<D<2 (i.e. the dimension D exceeds the topological dimension of the profile), the profile meets the minimum requirement to exhibit fractal properties.

The form of the curve (Richardson plot) is as shown in Figure 5.19

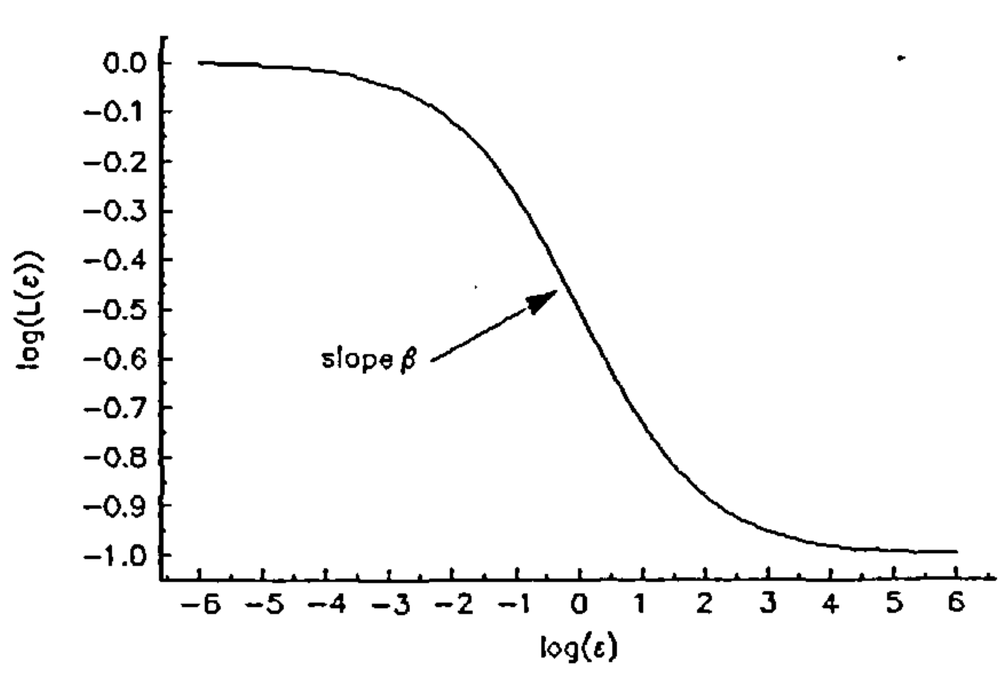

Figure 5.19 Log of estimated length (L(ε)) vs Log of measurement scale (ε)

From equation 5.2 it would be expected that this figure should be a straight line however in practice features of the measurement system cause it to deviate from linearity at both ends of the measurement scale. The data from which the fractal dimension is to be extracted is a discrete data set which has a fixed interval between data points. As the measurement scale approaches the length of this interval, the sampled points appear to be part of a straight line and under these conditions the apparent profile ceases to be fractal

[5.20]. Similarly as the measurement length approaches the total length of the data set the apparent profile again ceases to be fractal. Den Outer et al [5.20] have suggested that these two effects mean that the divider method cannot discriminate between data sets of low fractal dimension and data sets of fractal dimension equal to unity.

Inevitably a non integer number of divider steps will be required to cover the data set and this will result in the generation of a remainder length. The disposal of this remainder is the major problem in determining the fractal dimension from the divider method. It is generally recommended that the remainder be included in the estimation of apparent profile length [5.14]. In this work the remainder is included and is calculated as the geometrical length of the remaining profile as determined by the remaining points.

In order to test the algorithm which carried out the estimation of surface fractal dimension it was initially applied to the Koch curve shown in Figure 5.20. This curve is generated from a series of straight line manipulations and possesses a theoretical fractal dimension of 1.26 [5.10].

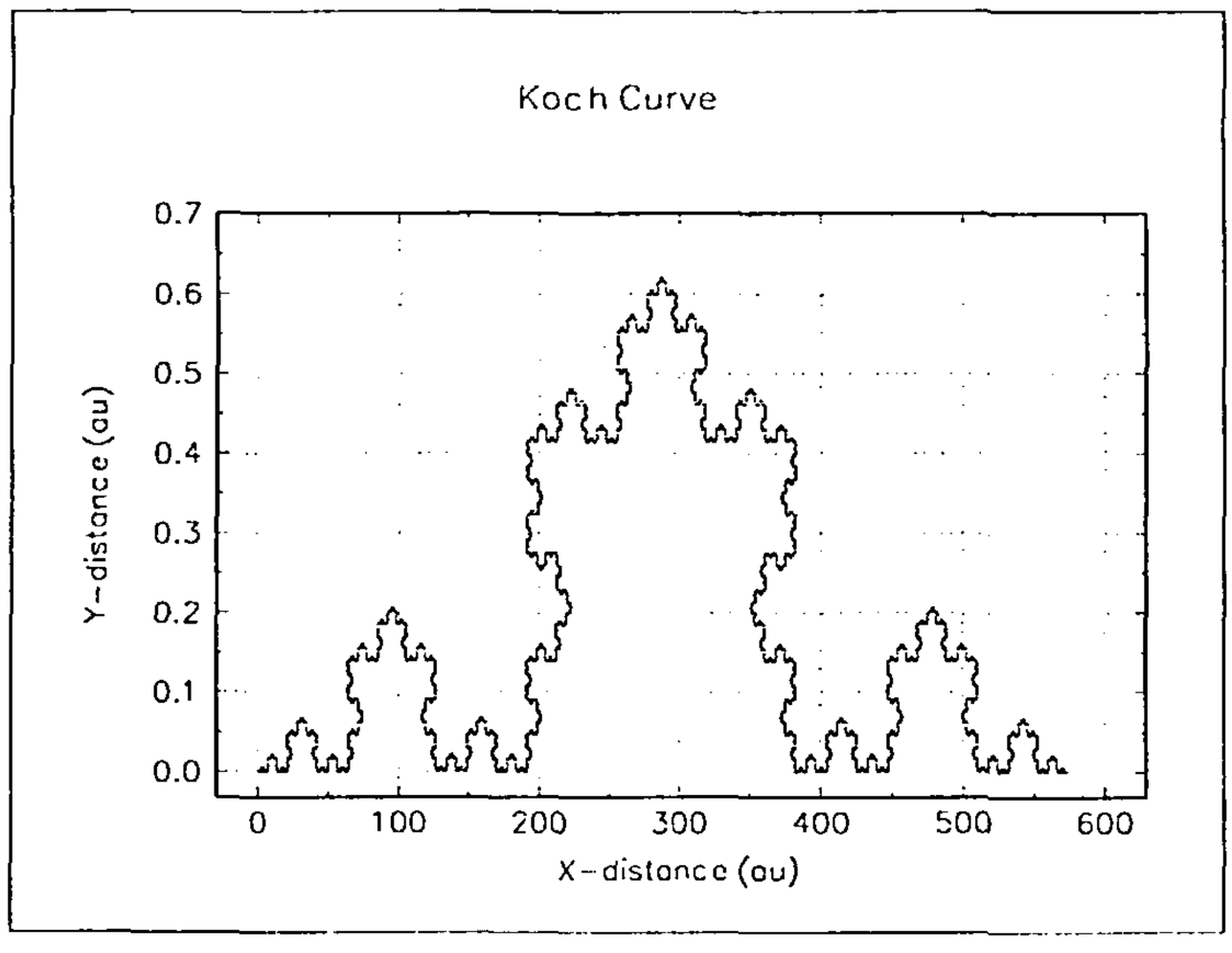

Figure 5.20 The Koch curve

The Richardson plot generated by stepping the dividers through the curve is shown in Figure 5.21a and the linear portion of the Richardson plot, from which the fractal dimension of the Koch curve is determined, is shown in Figure 5.21b.

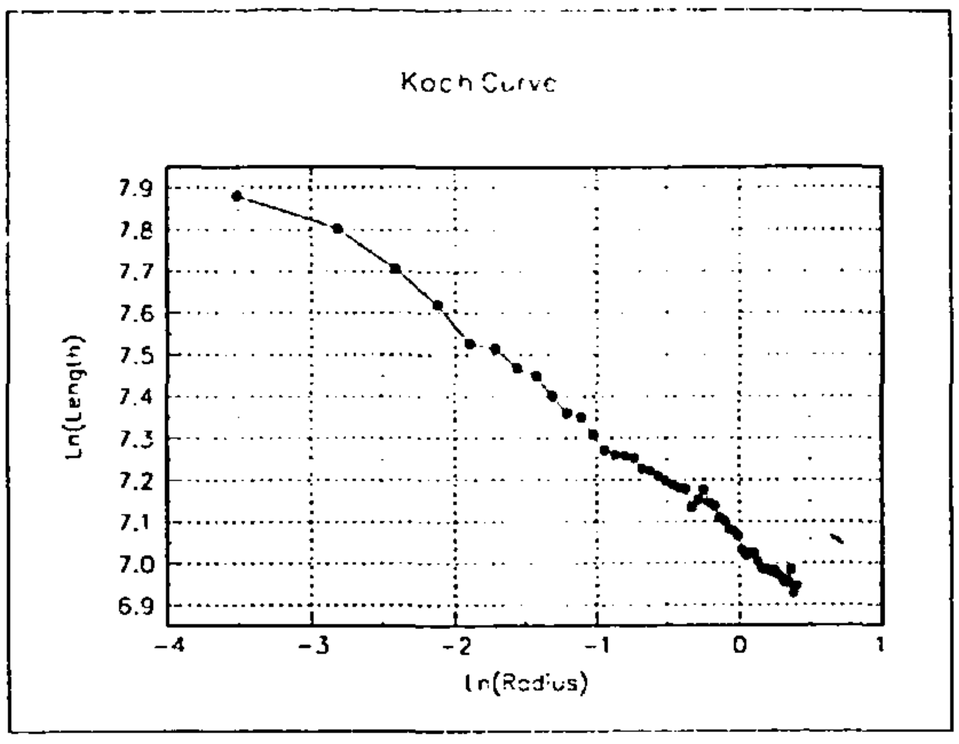

Figure 5.21a Richardson plot from Koch curve

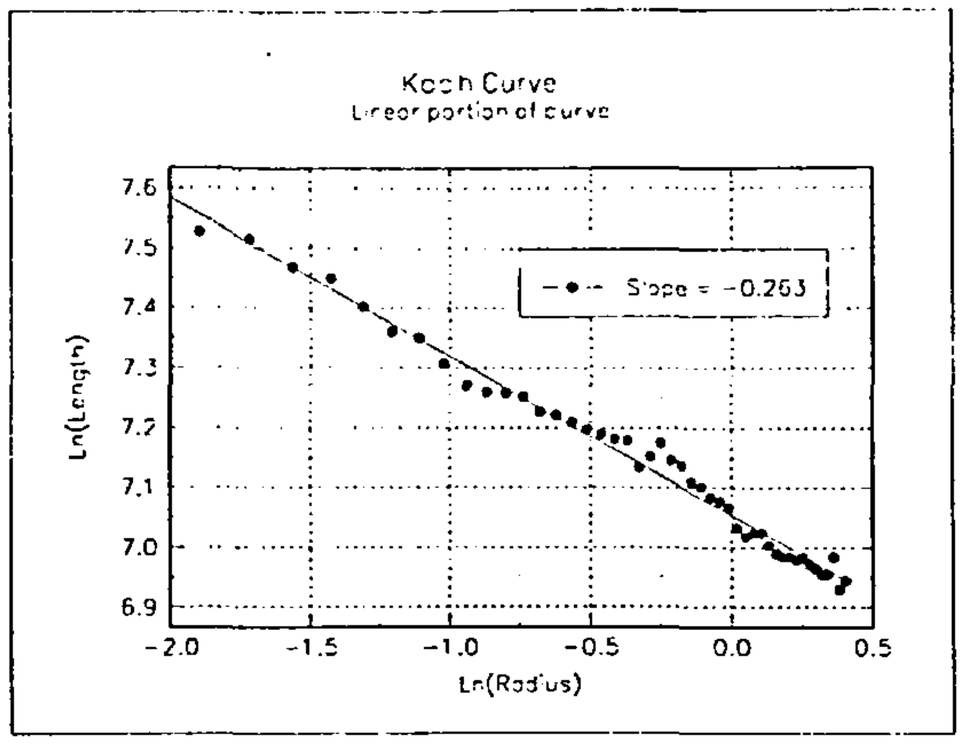

Figure 5.21b Linear portion of Figure 5.21a

From equation 5.4 it can be seen that the estimated fractal dimension of the Koch curve is 1.263. Hence we can conclude that the divider computation is validated for this known fractal curve.

A systematic investigation into the variation of divider fractal dimension of the machined surface profiles with wear land length, V_b, was carried out. Figure 5.22 shows a typical Richardson plot obtained during this investigation. The steps varied in length from $5x10^{-5}$ mm (below the minimum information level associated with the point separation) to $2.5x10^{-3}$ mm (12.5 times the minimum information level) at which point the fractal character of the profiles ceased. The total length of profile consisted of 204800 points which was equivalent to a physical length of 41 mm.

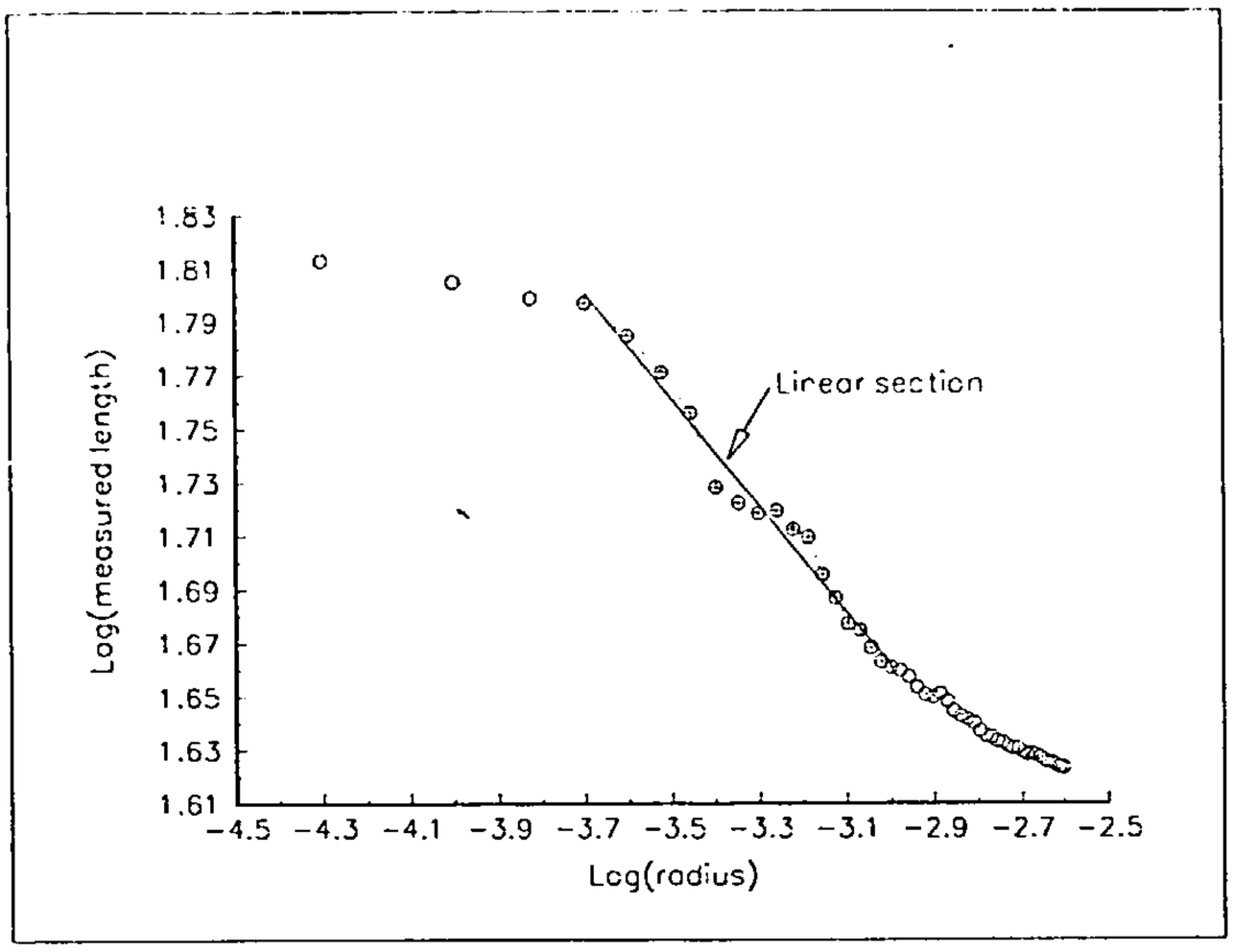

Figure 5.22 Typical Richardson plot generated from a real surface

The points in the plot designated by a cross within a circle denote the linear range from which the fractal dimension of the surface was extracted. All the Richardson plots produced displayed similar characteristics to those of Figure 5.22. The slopes of the linear portions of the Richardson plots were calculated using a least squares linear regression on the appropriate points. The error in calculation of this slope associated with the scatter of points about the linear portion of the plot were to taken to be indicative of the error in calculating the fractal dimension. These errors are indicated in the following plots of divider fractal dimension vs wear land length as error bars.

Positive rake cutting of annealed En24

Figures 5.23 and 5.24 show the variation of divider fractal dimension with V_b obtained from two series of experiments employing identical cutting conditions when cutting annealed En24 steel. The surfaces from which these data were extracted were created using the 8-point arrangement of the cutting tool.

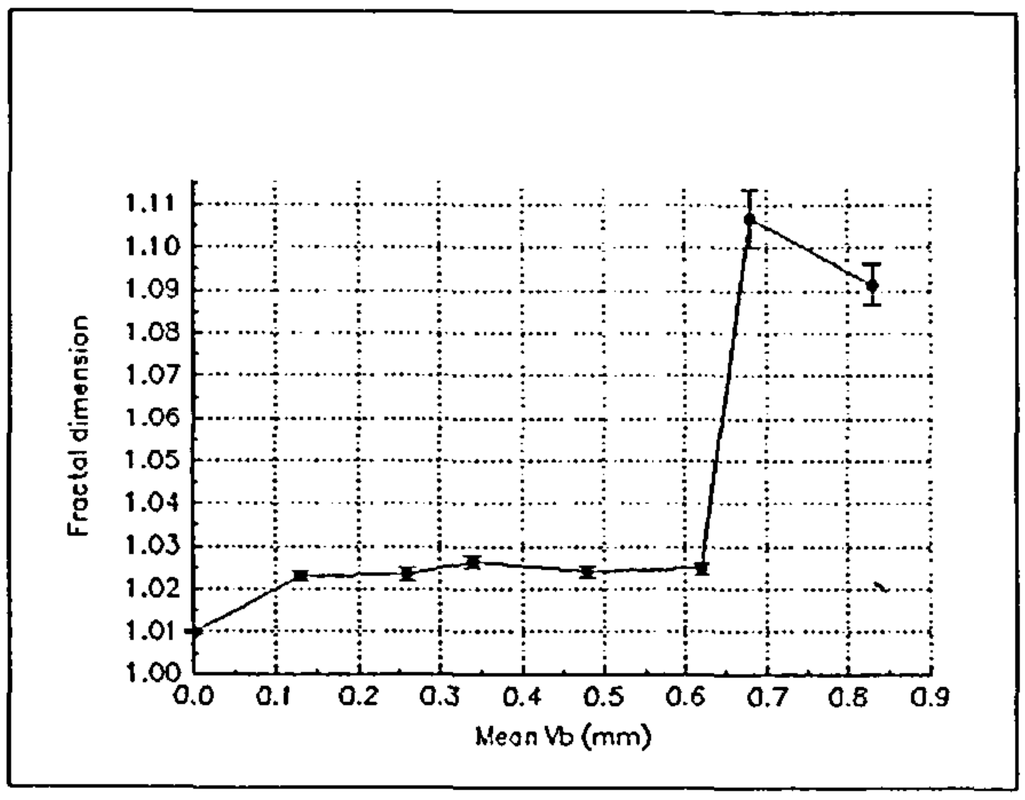

Figure 5.23 Divider fractal dimension vs mean V_b for 8-point positive rake cutting of annealed En24

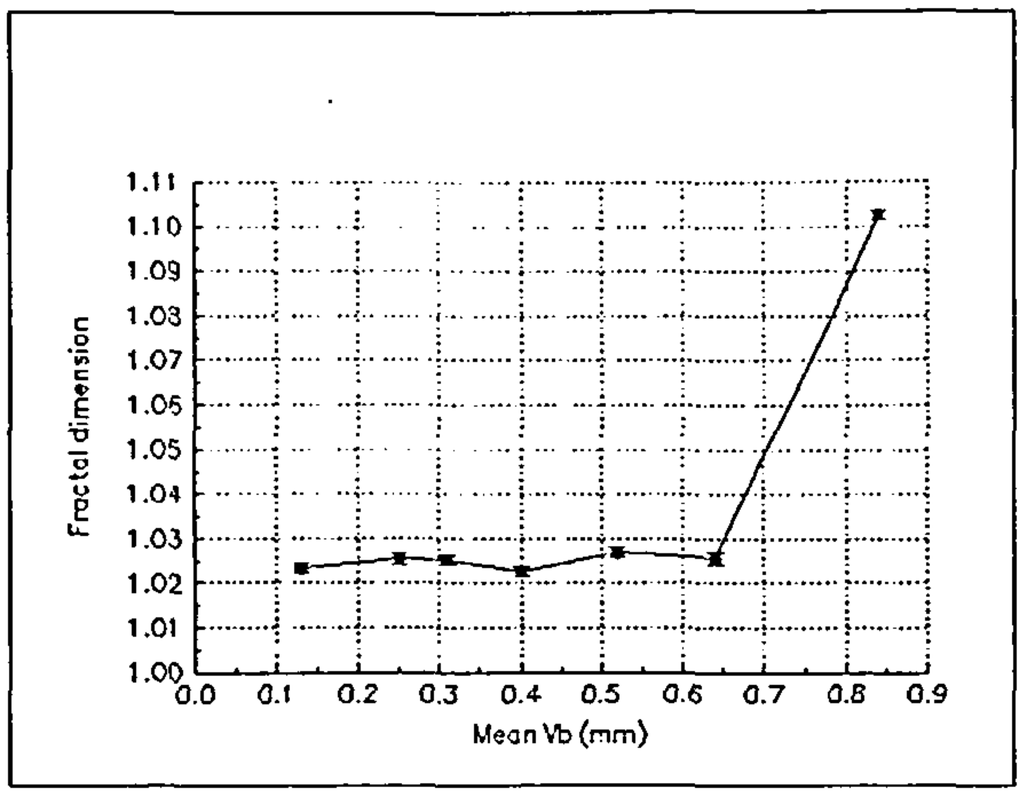

Figure 5.24 Divider fractal dimension vs mean V_b for 8-point positive rake cutting of annealed En24, second test.

Both of the figures show little variation in fractal dimension until the length of the wear land exceeds 0.8 mm when there is a steep rise. It should, however be noted that the total range of variation in fractal dimension is small.

Although insert chipping events are known to have occurred when the mean wear land length was equal to 0.4 mm in the test represented by Figure 5.23 and at a value of mean V_b of 0.26 mm for the test shown in Figure 5.24, there is no change in divider fractal dimension at these values of V_b. Thus in this case the divider dimension will not indicate insert chipping occurrences.

Negative rake cutting of annealed En24

Figure 5.25 shows the variation of fractal dimension with V_b exhibited by a set of surfaces produced by 8-point, negative rake cutting of annealed En24.

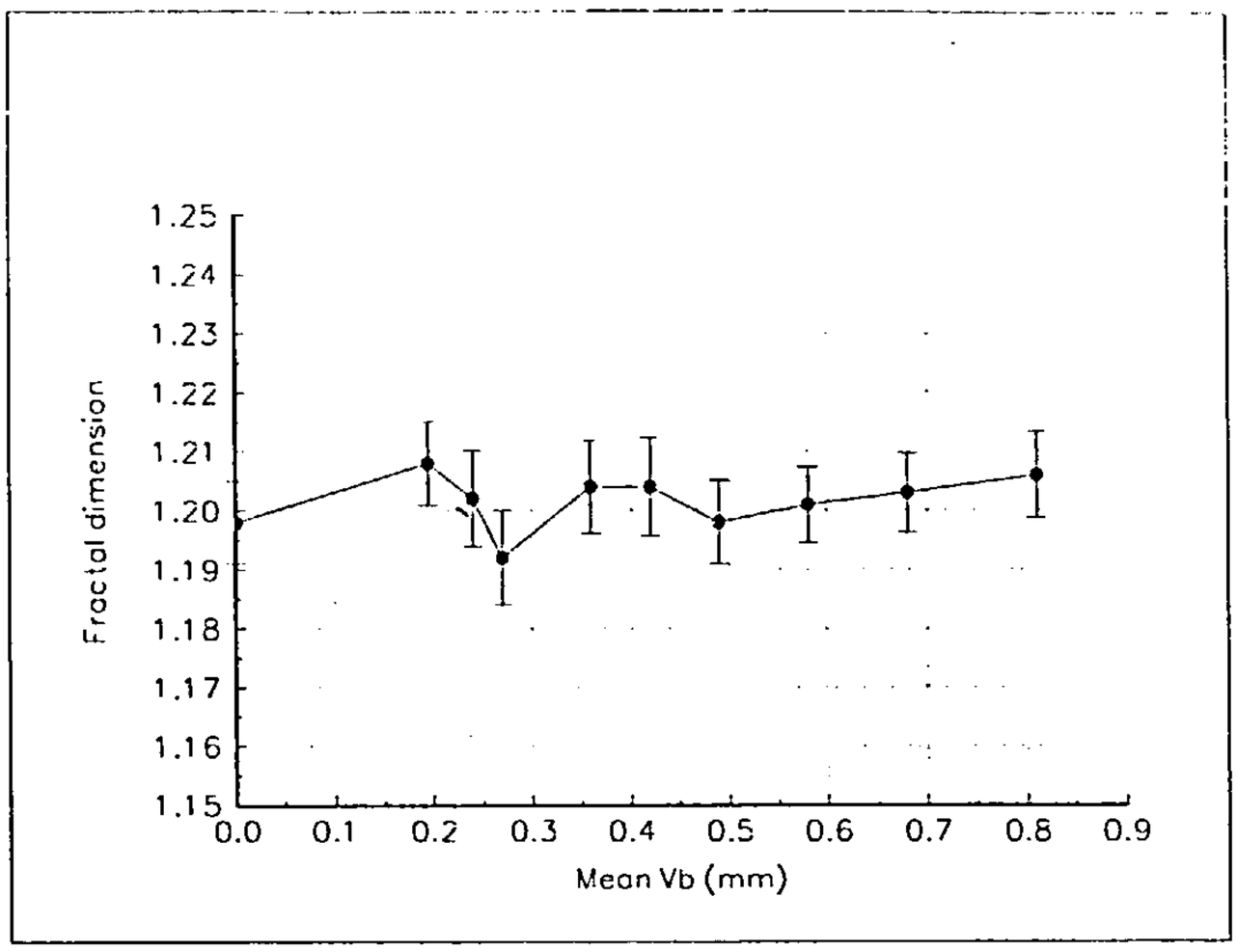

Figure 5.25 Divider fractal dimension vs mean V_b for 8-point negative rake cutting of annealed En24

It can be seen that although the trend of the graph shows an increase in fractal dimension with wear land length, the increase is small and lies within the error in the estimation of fractal dimension.

Figure 5.26 shows the change in fractal dimension with wear land length for a series of surfaces generated by single point, negative rake cutting of En24.

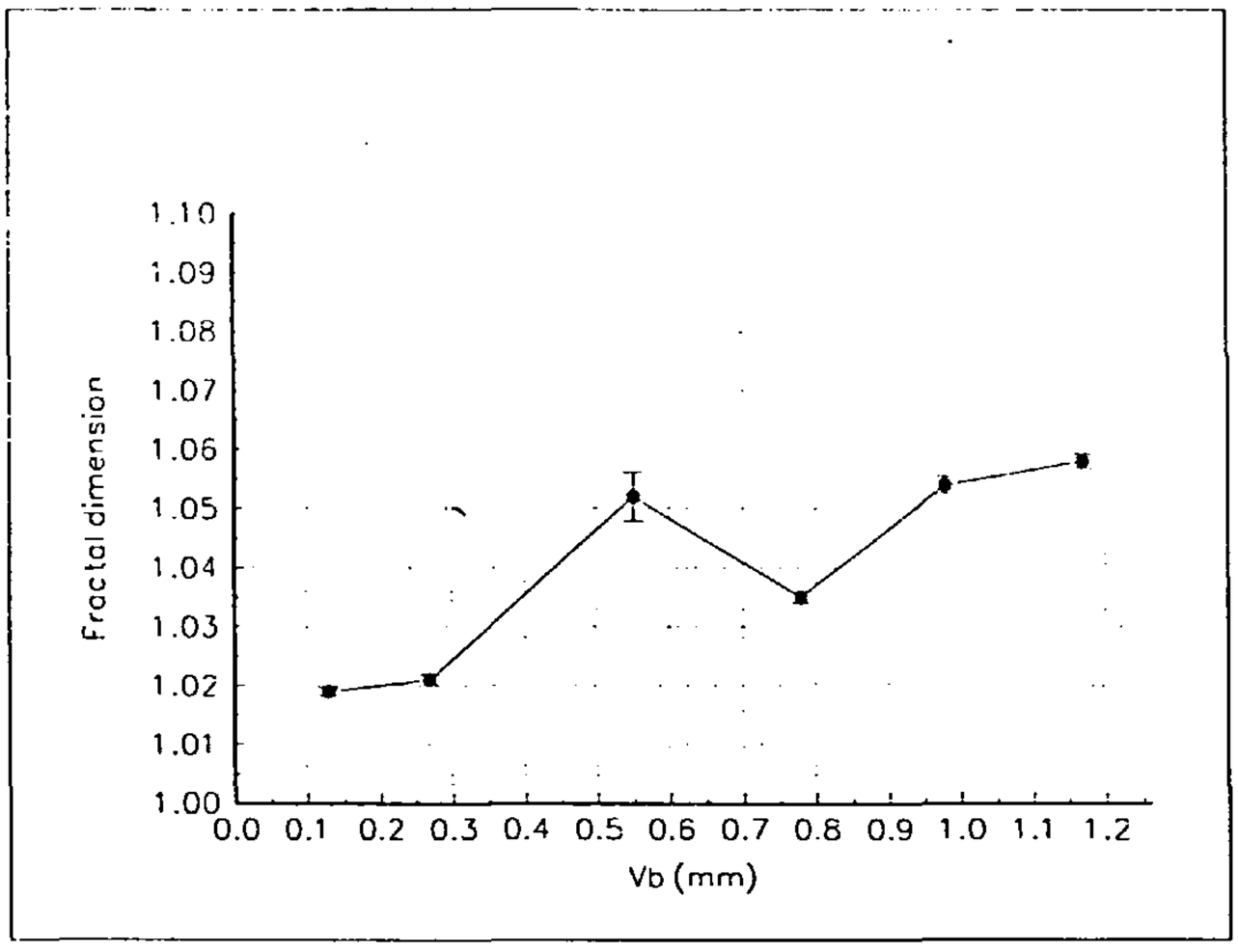

Figure 5.26 Divider fractal dimension vs V_b for single point negative rake cutting of annealed En24

From this figure it can be seen that there is an increase in fractal dimension with V_b although it is again small. That the increase is more marked for single point cutting than for 8-point cutting suggests that the complexities of multi-point cutting associated with such errors as radial and axial runout mask the more subtle changes in fractal dimension associated with tool wear.

Positive rake cutting of quenched and tempered En24

Figure 5.27 shows a modest increase in fractal dimension with wear land length when cutting hardened En24 with a positive rake cutter carrying eight inserts.

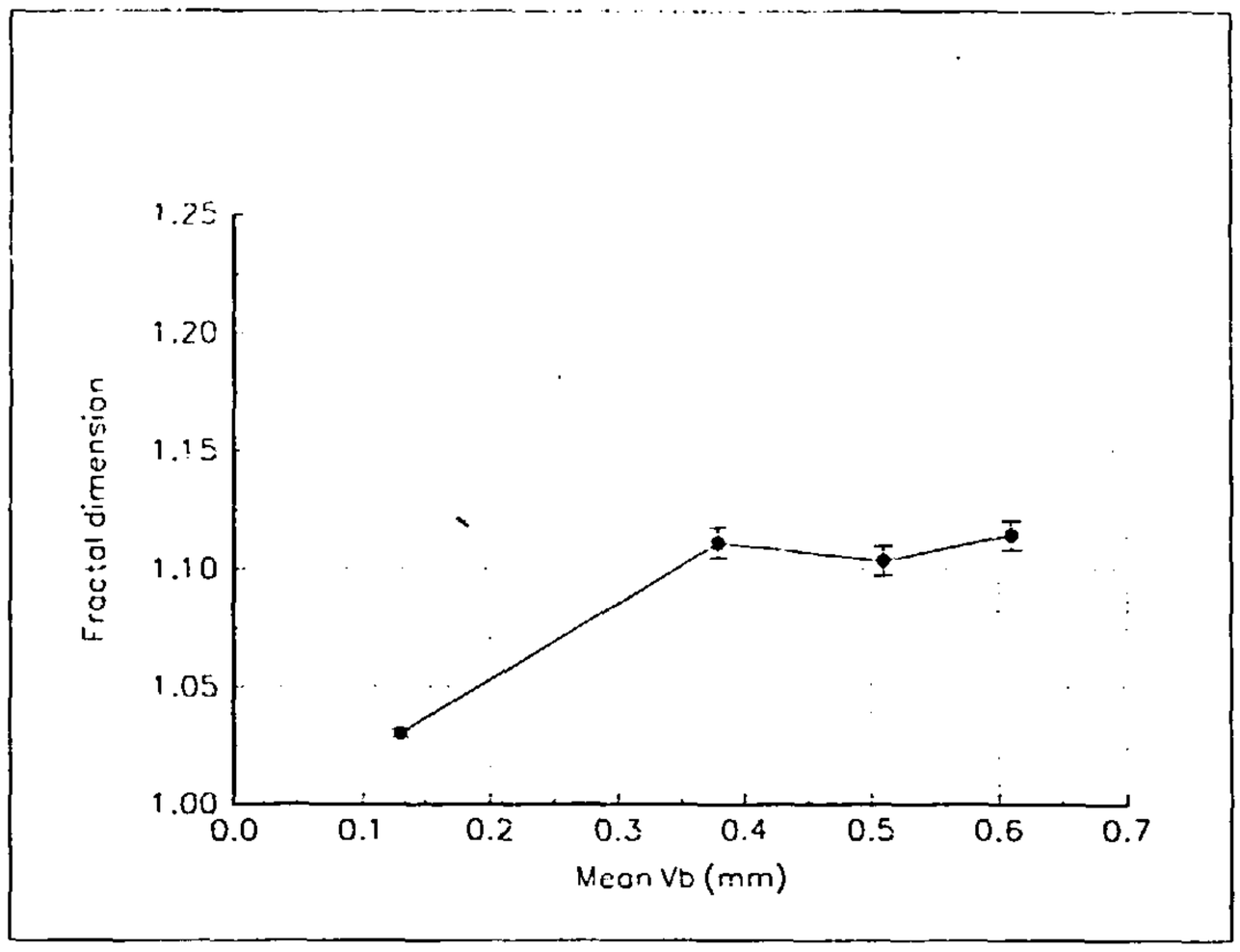

Figure 5.27 Divider fractal dimension vs mean V_b for 8-point positive rake cutting of quenched & tempered En24

The increase in fractal dimension of the machined surface over the tool life is clearly shown in this figure. Comparison of this figure with Figure 5.23 and Figure 5.24 shows that the divider fractal dimension is an indicator of tool wear in positive rake cutting of En24 in both its annealed and hardened states.

There is no clear indication that an insert chipping event occurred in this test prior to the mean V_b value reaching 0.51 mm. Therefore the divider dimension will not indicate such events in this case.

Negative rake cutting of quenched and tempered En24

Figure 5.28 illustrates the variation in fractal dimension with V_b when cutting quenched and tempered En24 with an eight point negative rake cutter employing identical cutting conditions to those of the previous section.

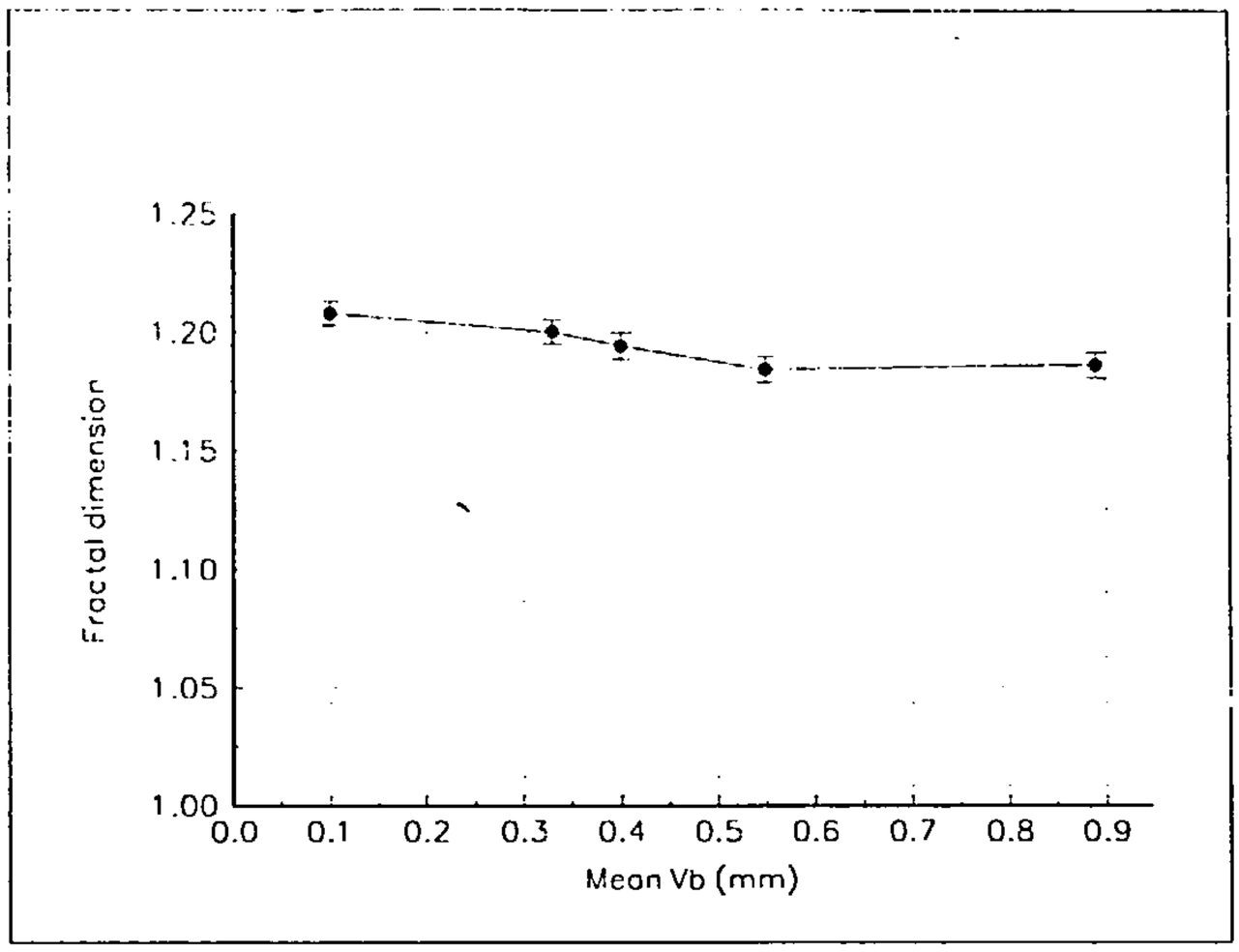

Figure 5.28 Divider fractal dimension vs mean V_b for 8-point negative rake cutting of quenched & tempered En24

It can be seen that there is a minor reduction in fractal dimension as the tool wears in this case however this variation is almost contained within the margin of error involved in the calculation of the fractal dimension. Comparison of this figure with Figure 5.25 indicates that there is little variation in divider fractal dimension with tool wear for negative rake cutting of either annealed or quenched and tempered En24.

Positive rake cutting of stainless steel

Figure 5.29 shows the variation in fractal dimension associated with single point, positive rake cutting of stainless steel. The increase in fractal dimension with V_b is obvious from this figure. If this figure is compared with Figures 5.23, 5.24 and 5.27 it will be observed that the overall change in fractal dimension over the life of the cutter is approximately of the same magnitude for each process but that the increase is monotonic in the case of single point cutting. This suggests again that the intricacies of multi-point cutting may obscure some of the subtle changes in machined surface properties resulting from tool wear effects.

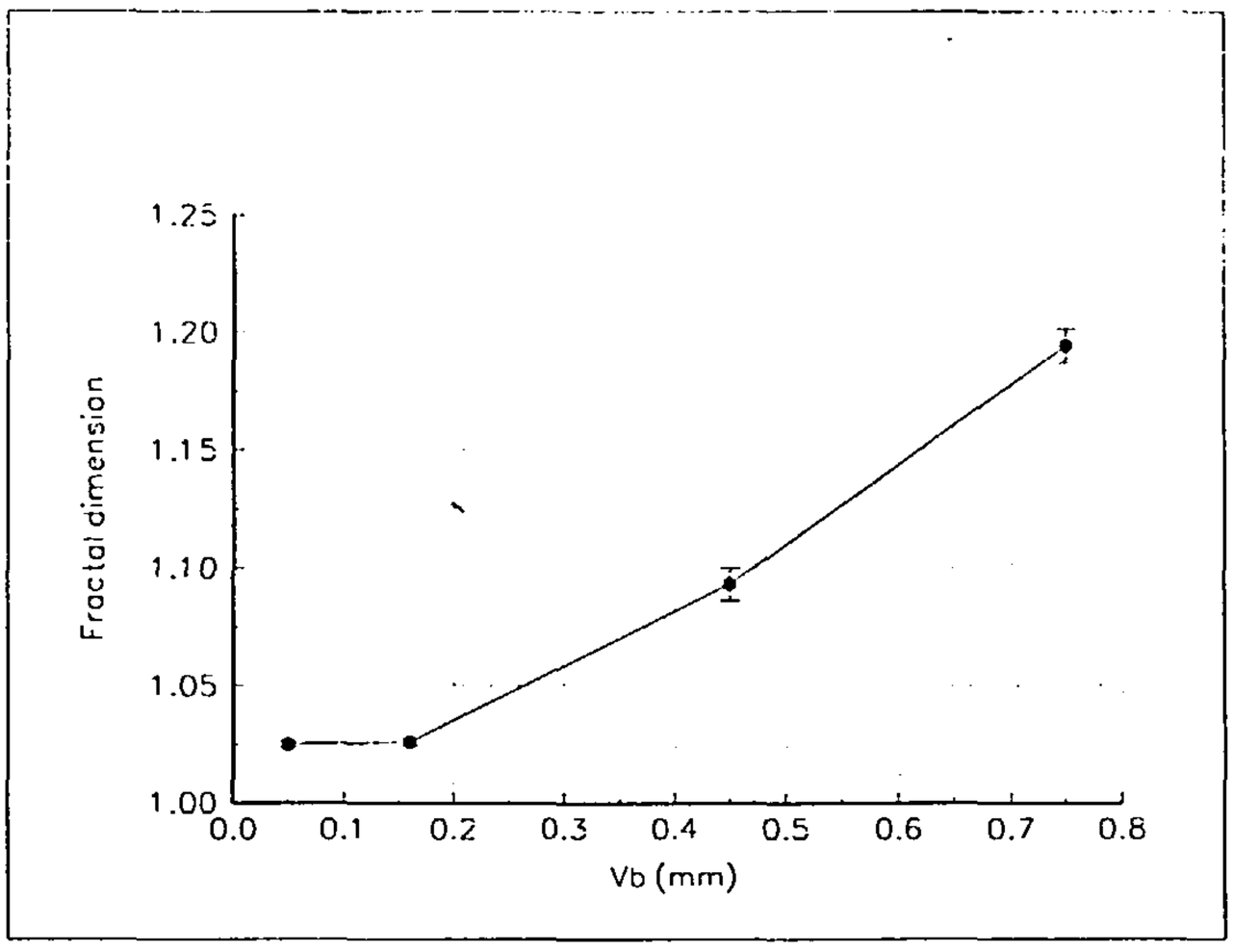

Figure 5.29 Divider fractal dimension vs V_b for single point positive rake cutting of stainless steel En24

General observations on divider fractal dimension

From the foregoing it may be seen that divider fractal dimension varies with wear land length when the cutting process employs a positive rake cutter. It may also be seen that, within the range of materials tested, the work-piece material has a minimal effect on this variation. However, when a negative rake cutter is employed, there is little variation in divider fractal dimension with tool wear.

It must be remembered that there are misgivings in the literature about applying the divider technique to data sets of low fractal dimension [5.20] and that the technique is only applicable to self affine data sets with care [5.21]. However Brown and Savary applied the technique successfully to describing the texture of a ground surface[5.22] and Brown et al used to carry out a fractal analysis of a turned surface[5.23]. In the light of this techniques which are applicable to both self similar and self affine profiles were investigated.

The structure function dimension

The structure function is defined by the expression

$$S(\tau) = \left\langle \left[Z(x+\tau) - Z(x) \right]^2 \right\rangle \qquad (5.6)$$

where Z(x) is the deviation of the profile from its mean line at location x, τ is a displacement in the x-direction and the angular brackets indicate an averaging process. If the sample interval used in the surface measuring process is Δx the value of τ becomes

$$\tau = n\Delta x, \ (n = 1,2,3,.....)$$

where n is the number of data points in the interval τ.

The data set from which the values of Z(x) are extracted consists of N equally spaced digitised values representing a physical length of L. We may express the values of Z(x) as

$$Z(x) = Z_i, \ (i = 1,2,3,.....N)$$

The structure function may now be expressed

$$S(\tau) = S(n\Delta x) = \left\langle \left[Z(x+n\Delta x) - z(x) \right]^2 \right\rangle \qquad (5.7)$$

whence

$$S(\tau) = \frac{1}{N-n} \sum_{i=1}^{N-n} (Z_{i+n} - Z_i)^2 \qquad (5.8)$$

If the surface is fractal, a plot of the logarithm of the structure function against the logarithm of the sample interval will be a straight line of slope β. The fractal dimension D is related to this slope by the expression [5.8]

$$D = \frac{4-\beta}{2} \qquad (5.9)$$

Sayles and Thomas [5.24] carried out a detailed investigation into the use of the structure function to characterise rough surfaces although Whitehouse [5.8] claims to have first established the usefulness of the function in defining machined surfaces. Thomas and Thomas [5.25] applied the structure function to self affine data sets and showed that the fractal characteristic of machined surfaces was not scale invariant and that different fractal behaviour may occur at different scales. Changes in fractal dimension with scale would result in several straight line portions of the log-log plot. He and Zhu [5.16] applied the

structure function technique to lapped and shaped Babbitt alloy surfaces and observed two distinct regions of fractal behaviour at two length scales in the case of the lapped surfaces. They attributed these regions to two different causes, microfracture and plastic deformation, occurring during the lapping process.

In this work the structure function was initially evaluated using 132k points representing a physical surface length of 26.2 mm with intervals on the x axis ranging from 2 to 2048 points. However it was found that using 16 k points corresponding to a physical length of 3.3 mm with the same intervals altered the estimated fractal dimension by less than 2% in all cases. This considerably reduced the computing effort required to calculate the structure function and in what follows these shorter sample lengths and intervals were used.

Figure 5.30 shows a typical plot of log(structure function) vs log(sample interval) obtained from these calculations.

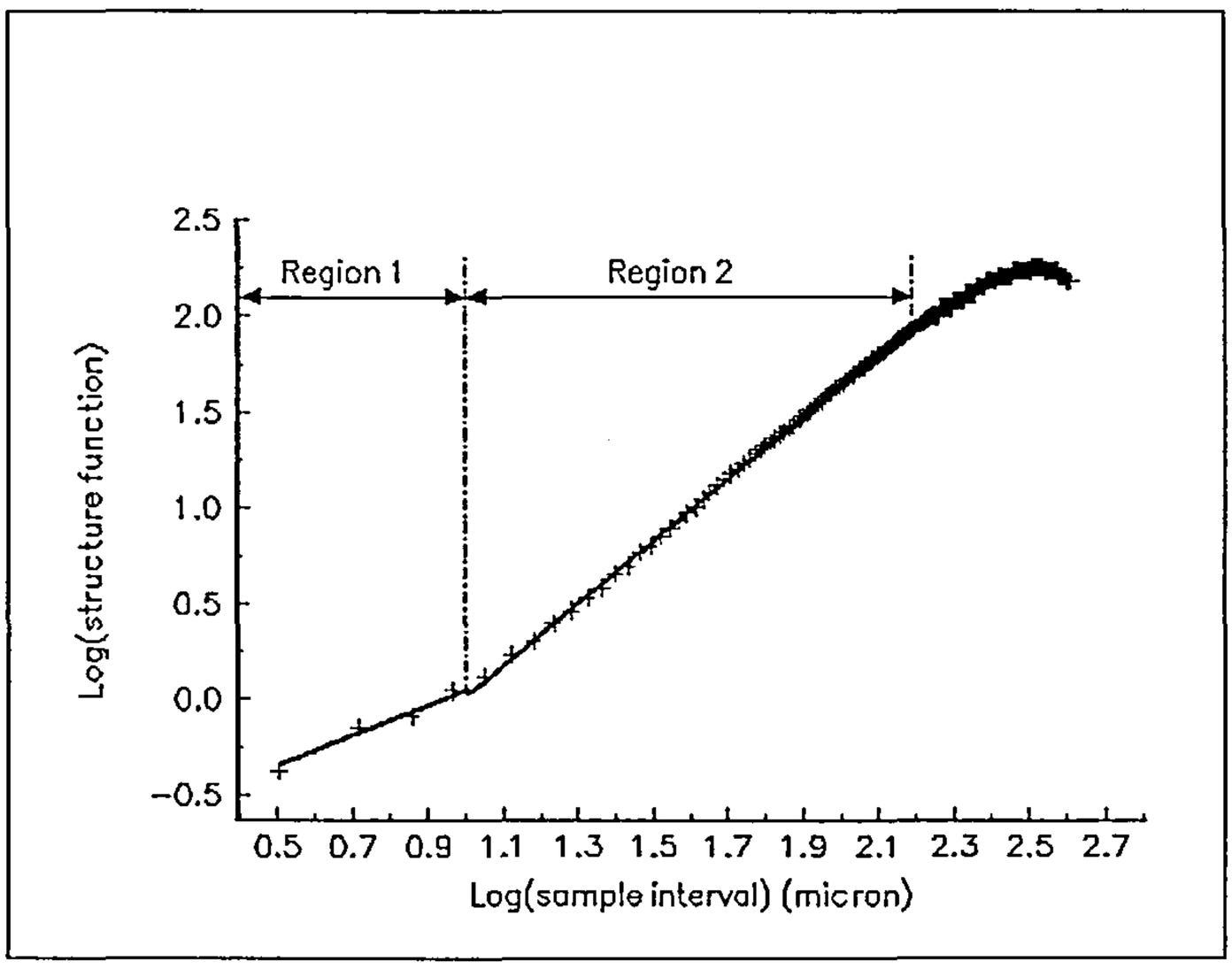

Figure 5.30 Log(structure function) vs log(sample interval) for a typical milled surface.

From this it can be seen that the milled surfaces exhibit bi-fractal behaviour as shown in the regions of the figure designated 'Region 1' and 'Region 2'. It might be argued that the milling process is so complex that several sub-processes such as rubbing, plastic deformation etc., are occurring and that multi-fractal behaviour would be expected. It is as

a result of this that bi-fractal characteristics are observed. It was not the purpose of this work to examine fractal generation processes in detail and further investigation would be required in this area to establish the true source of the bi-fractal nature of the surfaces. The fractal dimensions in the following graphs were extracted from both of the regions exhibited in figures of the type Figure 5.30 and their variations with wear land length V_b are labelled accordingly. The error bars displayed in the figures were determined as the errors in calculating the slopes of the log-log curves in both regions of the plots.

Positive rake cutting of Annealed En24

Figures 5.31a and 5.31b illustrate the variation in structure function fractal dimension when cutting annealed En 24 with an 8-point, positive rake cutter

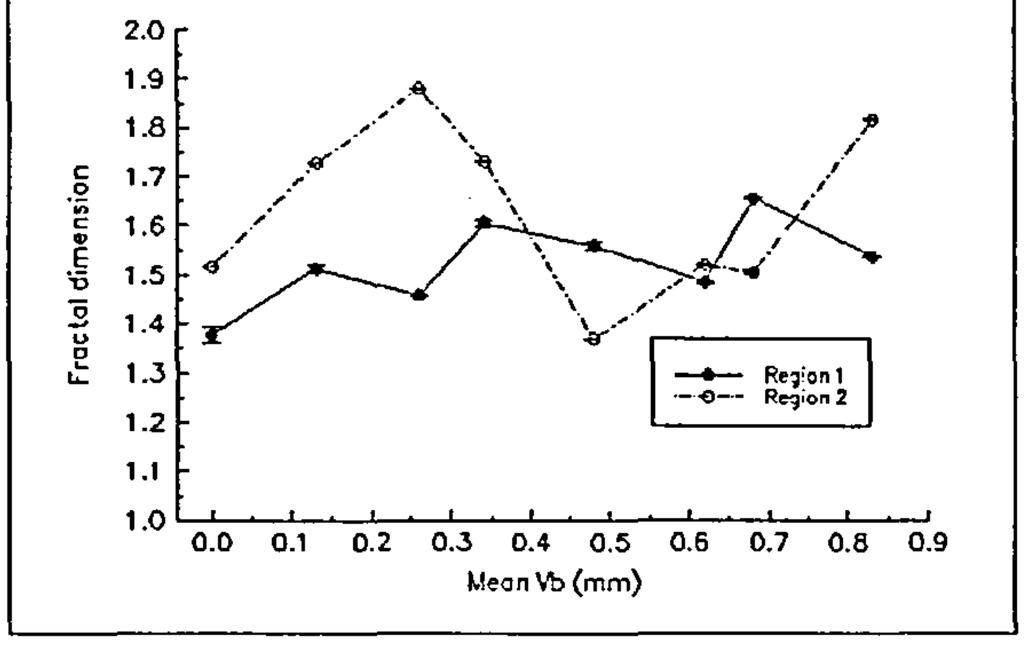

Figure 5.31a Structure function fractal dimension vs mean V_b for 8-point positive rake cutting of annealed En24.

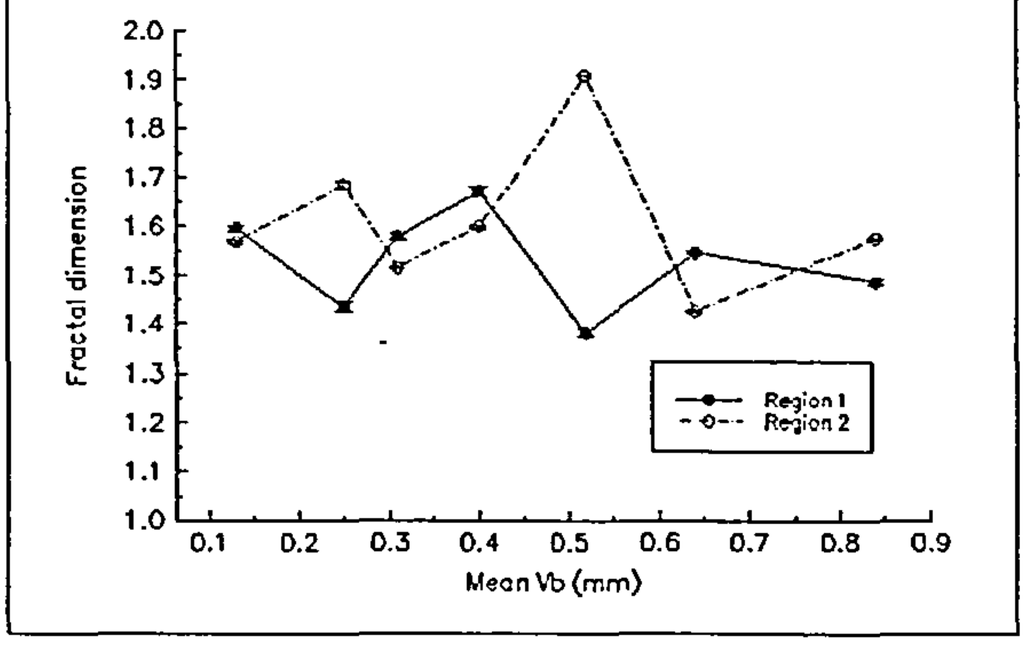

Figure 5.31b Structure function fractal dimension vs mean V_b for 8-point positive rake cutting of annealed En24. Second test.

It can be seen from these figures that there is no structure to the variation in structure function fractal dimension with wear in these cases. Comparison of these figures with Figures 5.23 and 5.24 which show the variation in divider fractal dimension suggests that, although the divider technique does not reveal the bi-fractal nature of the surfaces, it may be of more use in indicating tool wear. However the small range in divider dimension variation must be noted.

There is a maximum divergence between the fractal dimensions from region 1 and region 2 in Figure 5.31a at a value of V_b of 0.26 mm. This coincided with a chipping event on one of the inserts of the cutter. A similar divergence in fractal dimension is shown in Figure 5.31b at a wear land length of 0.52 mm. Although this does not coincide with a chipping event it follows a chipping event noted at the previous measurement of wear land length.

Negative rake cutting of Annealed En24

Figure 5.32 shows the variation in structure function dimension with mean wear land length when milling annealed En 24 with an 8-point negative rake cutter.

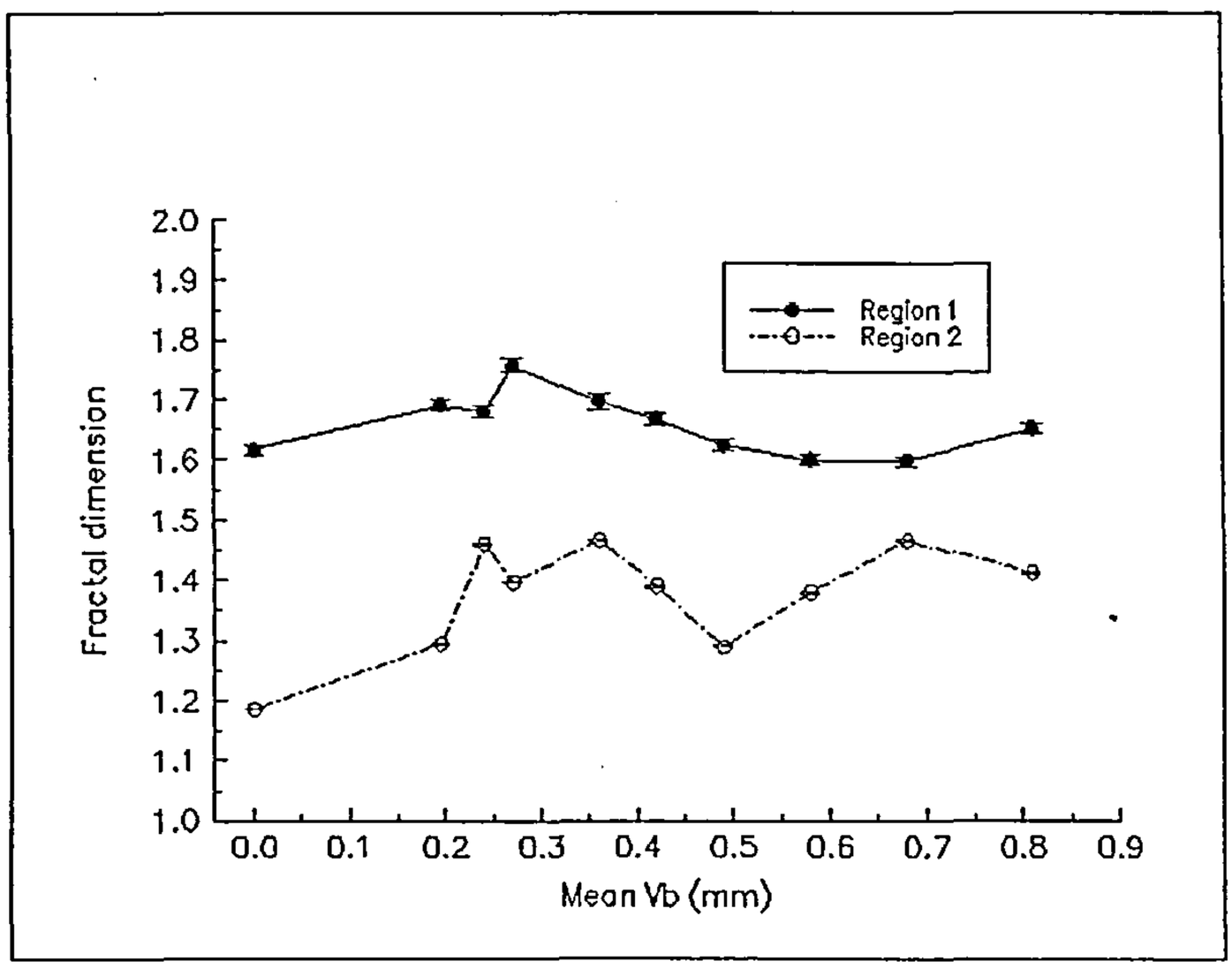

Figure 5.32 Structure function fractal dimension vs mean V_b for 8-point negative rake cutting of annealed En24.

It can be seen that there is only a small variation in structure function fractal dimension with V_b in either region. The fractal dimension in region 2 displays a rising trend with wear and comparison with Figure 5.26 shows that the shape of the divider dimension variation is similar to those of Figure 5.32.

Figure 5.33 shows the change in structure function fractal dimension with wear for single point negative rake cutting of annealed En24.

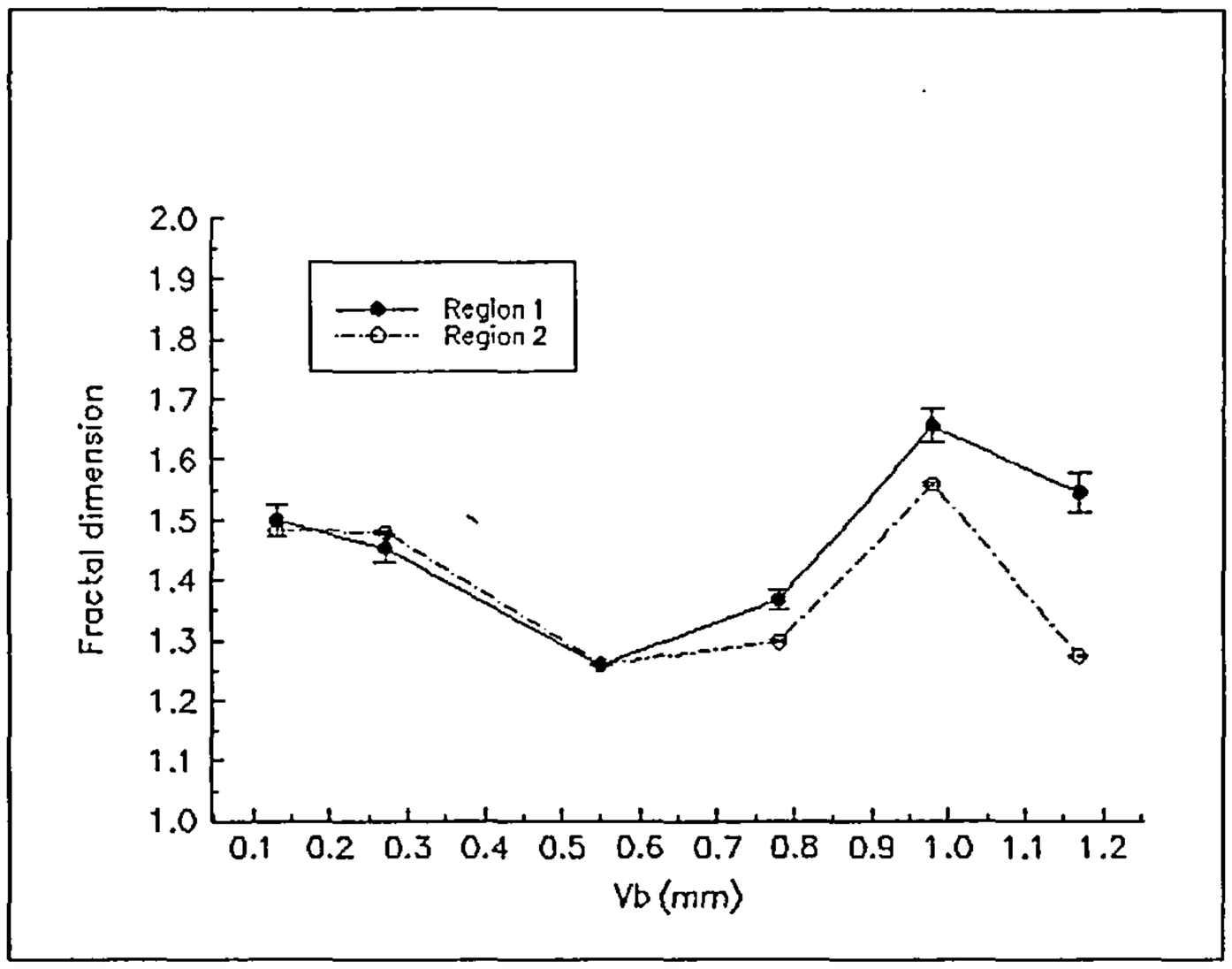

Figure 5.33 Structure function fractal dimension vs mean V_b for single point negative rake cutting of annealed En24.

This shows that the surface generated in this process is only weakly bi-fractal as the fractal dimensions in both regions are almost identical. This suggests that the bi-fractal nature of the surfaces results from the vagaries of multi-point cutting such as errors in setting the inserts. It should again be noted that the overall variation in structure function fractal dimension is inconclusive in attempting to predict tool wear.

Positive rake cutting of quenched and tempered En24

Figure 5.34 shows the variation in structure function fractal dimension with V_b for 8-point cutting of quenched & tempered En24.

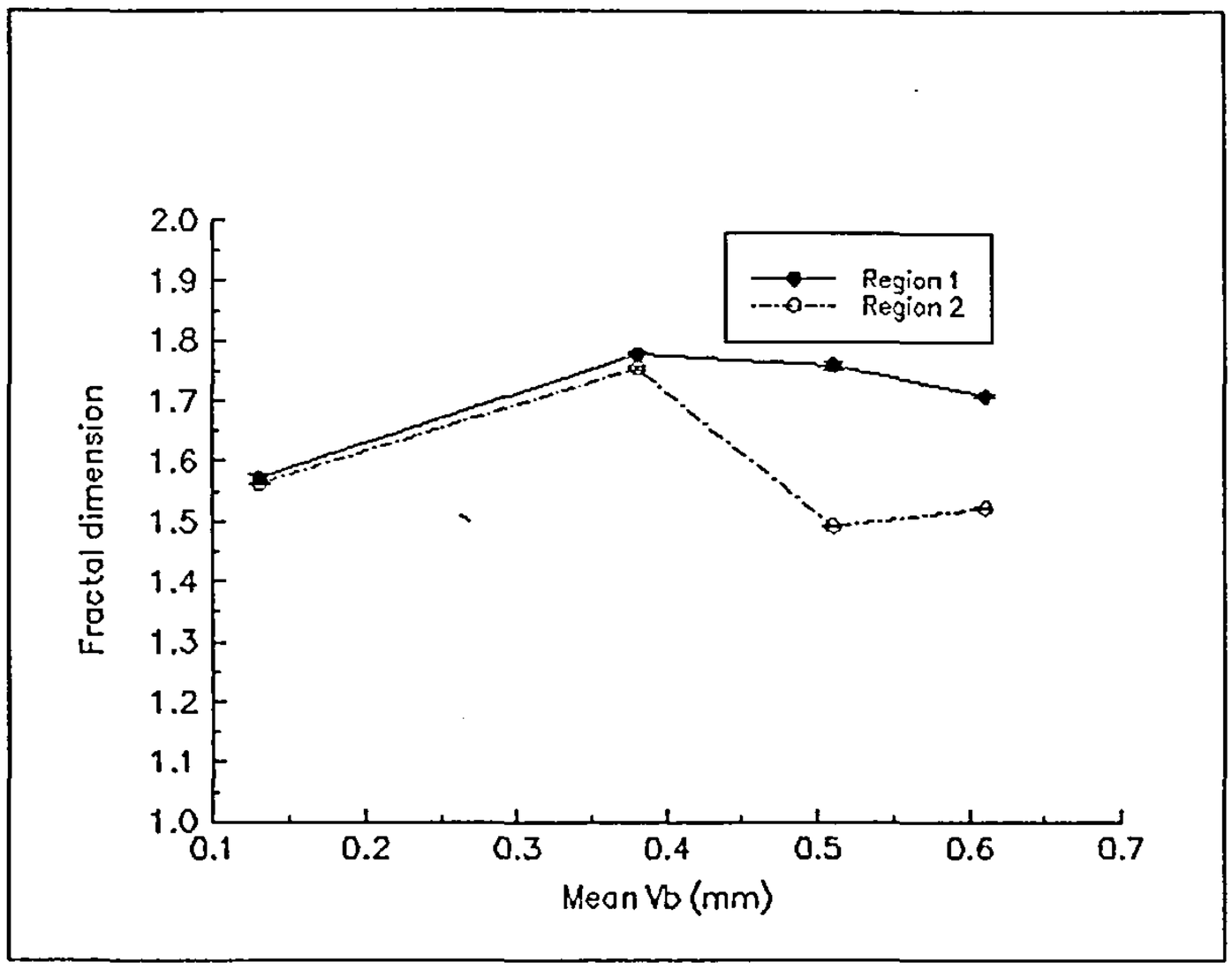

Figure 5.34 Structure function fractal dimension vs mean V_b for 8-point positive rake cutting of quenched & tempered En24.

Contrary to the previous experiments, the variation in structure function fractal dimension in region 1 shows a smooth change with tool wear. However experience with the other experiments using the 8-point positive rake cutter suggests that this result is most likely to be attributable to the lack of data points between V_b values of 0.13 mm and 0.38 mm. The change in structure function fractal dimension with V_b in region 2 does not reflect the variation observed in region 1.

It may also be observed that the bi-fractal nature of the surfaces does not become apparent until the mean wear land length has achieved a value of 0.51 mm at which point the divergence between the fractal dimension in the two regions reaches a maximum. As with chipping events in other experiments, this maximum divergence occurred concurrently with a chipping event on one of the inserts.

Negative rake cutting of quenched and tempered En24

Figure 5.35 demonstrates the change in structure function fractal dimension as tool wear developed when cutting quenched and tempered En24 with an 8-point negative rake tool.

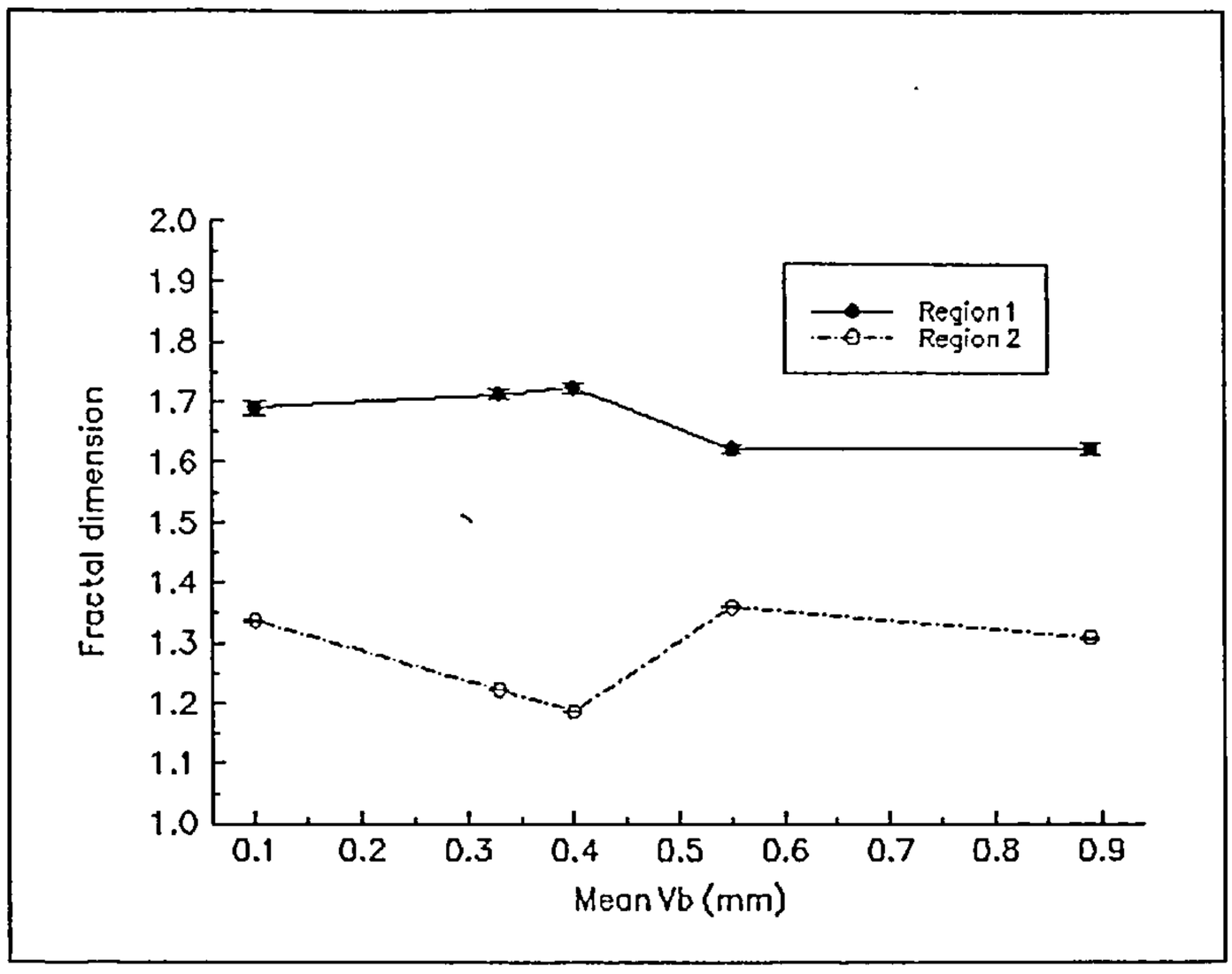

Figure 5.35 Structure function fractal dimension vs mean V_b for 8-point negative rake cutting of quenched & tempered En24.

From this figure it can be seen that the structure function fractal dimension does not change in either region 1 or region 2 with progressive wear when cutting hardened En24 with a negative rake tool.

Positive rake cutting of stainless steel

Figure 5.36 shows the variation in structure function fractal dimension with insert wear for single point cutting of stainless steel.

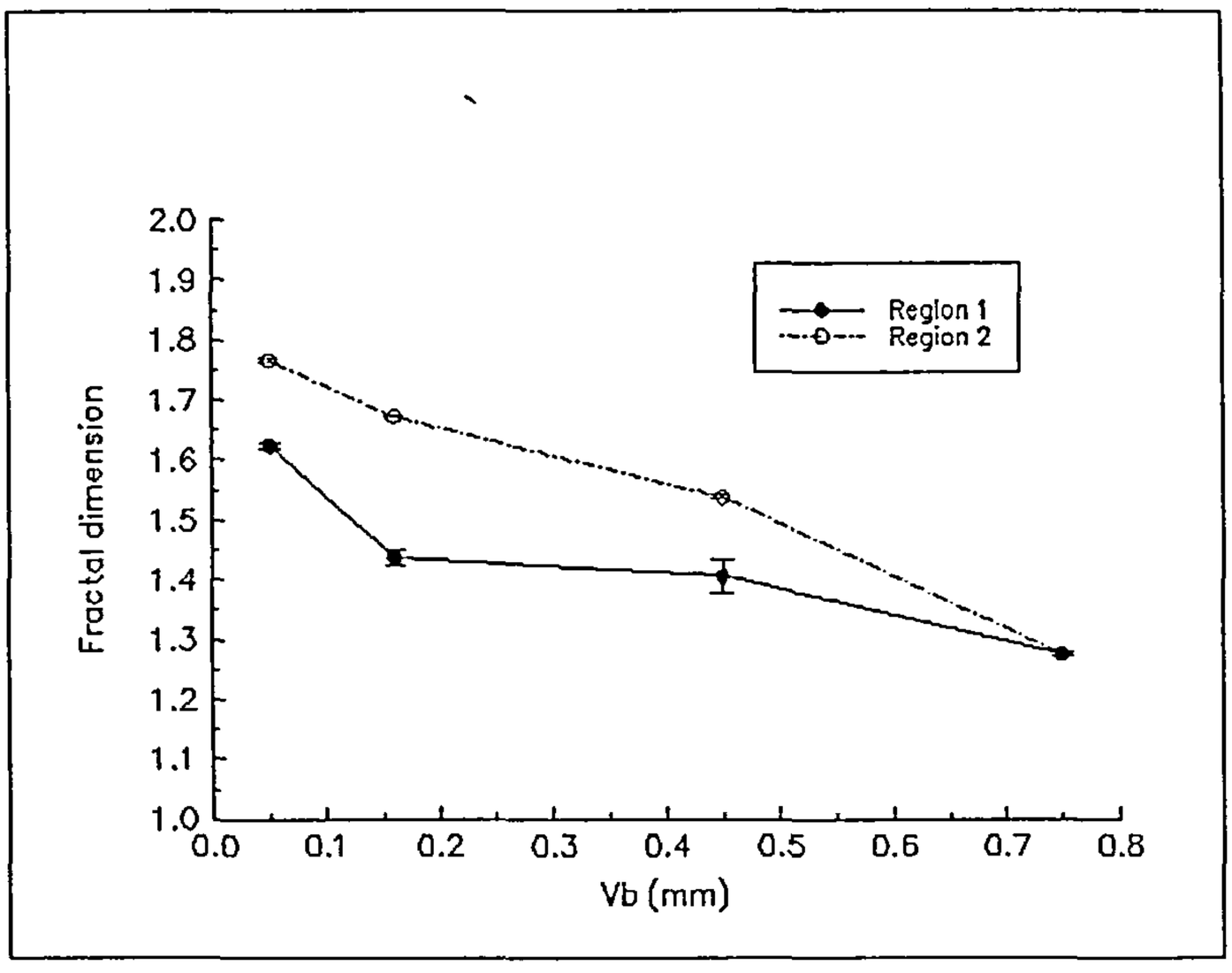

Figure 5.36 Structure function fractal dimension vs mean V_b for single point positive rake cutting of stainless steel.

The bi-fractal nature of these surfaces was not well defined on the log-log plots from which the structure function fractal dimensions were extracted. As tool wear progressed the fractal dimension in both regions converged until at the end of tool life the surfaces exhibited mono-fractal behaviour. It may be noted that the fractal dimension reduced with increasing V_b, indicating that in this case the structure function could be used to monitor tool wear.

General observations on structure function fractal dimension

The structure function fractal dimension has been used successfully to characterise machined surfaces [5.16], [5.25] in other fields of investigation. However the foregoing demonstrates that changes in the character of these surfaces resulting from progressive changes in cutting insert geometry are not reflected in the structure function fractal dimension.

He and Zhu [5.15] showed that it was possible to recognise different mechanisms of surface processing in lapping from the bi-fractal nature of the surfaces investigated. It has been shown that sudden changes in insert geometry as a result of insert chipping are illuminated by the bi-fractal nature of the surfaces as evidenced by the divergence of the fractal dimensions in the two regions of fractal behaviour observed.

5.3 Machine tool natural frequencies

As has been stated in chapter 4, the cutting inserts used in these experiments employed a wiping flat to improve the machined surface finish provided that the feed per tooth is less than 1.5 mm. The feed per tooth used in this work ranged from 0.1 mm to 0.2 mm per tooth and from a purely geometric view the resultant surface would be expected to be featureless. Figure 5.37 shows the geometry of the an insert used in the negative rake cutter.

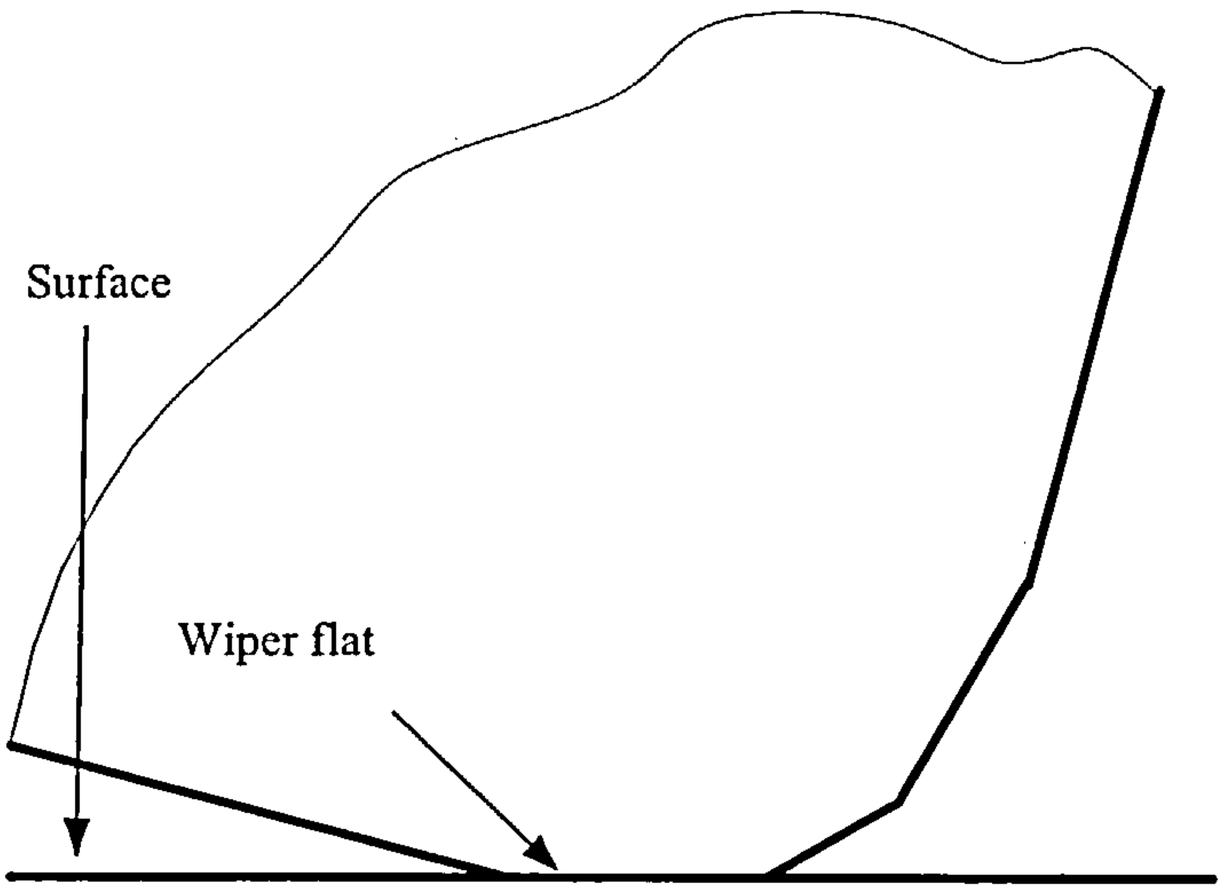

Figure 5.37 Wiper flat location

Since the generated surfaces are clearly not featureless as demonstrated by Figures 5.2a and 5.2 b and Figures 5.3a and 5.3b, the generation mechanism of the surfaces must be more complex than a simple geometric argument. Forces associated with the cutting process will produce both static deflections and a forced vibration response in the cutter. Of these the influence of forced vibration is more severe than that of the static deflection [5.26]. The effects of the forces may be considered in three mutually perpendicular directions, the feed or x-direction, the depth or z-direction and the y-direction which is perpendicular to the plane containing the x- and z- directions. Baek et al [5.26] state that

relative motion in the y-direction plays no part in generating the surface profile. Therefore an investigation into the natural frequencies of the machine tool and the cutter in both the x- and z- directions was carried out. An impulse technique was used to measure the natural frequencies. David Birchall type A/02 accelerometers were placed on the cutter with their sensitive axes parallel to the x- and z- directions as shown in Figure 5.38. A Bruel & Kjaer type 8202 impact hammer was then used to deliver a series of impacts to the cutter in the x- and z- directions.

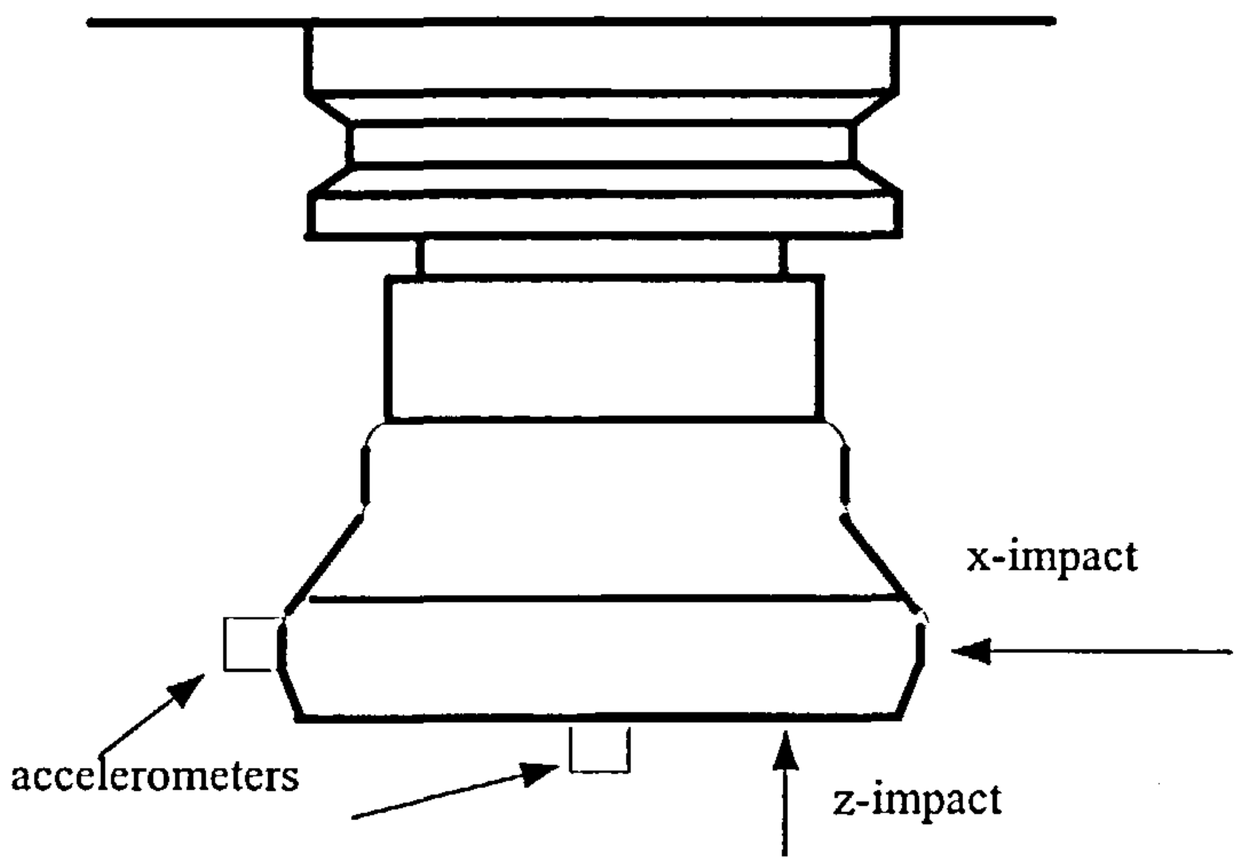

Figure 5.38 Accelerometer locations for impact tests on cutter.

The signals from the accelerometers and impact hammer were analysed by a Spectral Dynamics SD380 signal analyser operating in transfer function mode.

Figure 5.39 shows the transfer function obtained for the cutter in the feed direction. The figure indicates that the first three natural frequencies are contained in the range 0 to 4.0 kHz. The two higher natural frequencies are in the ratios 2.5:1 and 3.8:1 to the first natural frequency. It is well known [5.27] that the first three natural frequencies of a cantilever beam with ideal fixing are in the ratio 2.5:1 and 4.2:1. This strongly suggests that the natural frequencies shown in Figure 5.39 are the first three cantilever modes of the cutter. It is to be expected that the major forcing frequencies on the cutter will be in a range contained by spindle speed at the lower extremity (> 5 Hz)and tooth passing frequency at the upper extremity (<85 Hz) and consequently the cantilever modes are unlikely to be excited during the cutting processes described in this work.

Figure 5.40 shows the transfer function of the cutter in the z-direction. As was to be expected the cutter is much stiffer in the z-direction than the x-direction. This is demonstrated by the existence of only one natural frequency in the range 0 to 4.0 kHz. This frequency of 2850 Hz is again well outside the range of forcing frequencies associated with cutting.

To provide further information about the natural frequencies of the machine tool the impact tests were repeated with the accelerometers attached to the machine tool frame rather than the cutter with their sensitive axes parallel to the feed and vertical directions. It was intended to investigate the existence of natural frequencies in the range associated with cutter forcing frequencies (< 500 Hz).

Figure 5.41 shows the transfer function of the machine tool in the x-direction and in the range 0 to 500 Hz. From this it is clear that natural frequencies between 75 and 90 Hz and at 200 Hz exist but that they are well damped in comparison with the cantilever modes of the cutter.. However in machining processes these may be excited by frequencies in the cutting frequency range. Similarly Figure 5.42 shows the transfer function of the machine tool in the z-direction. This confirms the existence of natural frequencies at 32.5 Hz and 268 Hz which again may be excited by cutting forces.

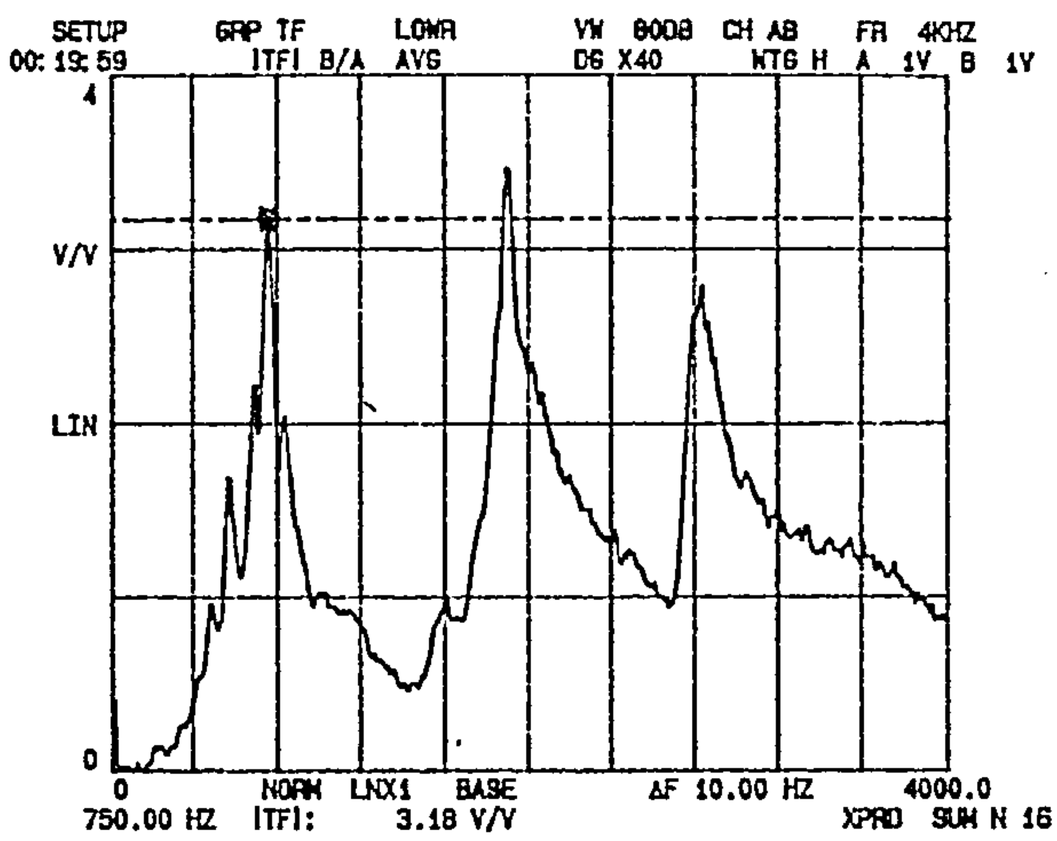

Figure 5.39 Transfer function of cutter in the feed direction in the range 0 to 4 kHz

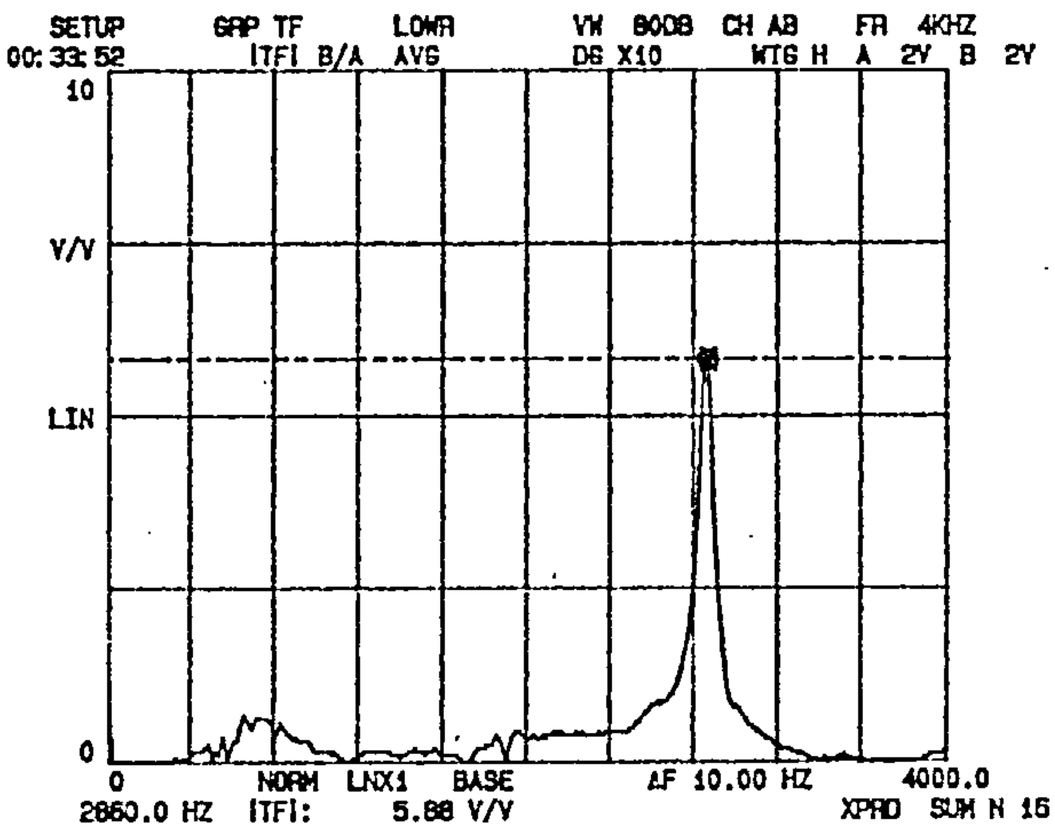

Figure 5.40 Transfer function of cutter in the z - direction in the range 0 to 4 kHz

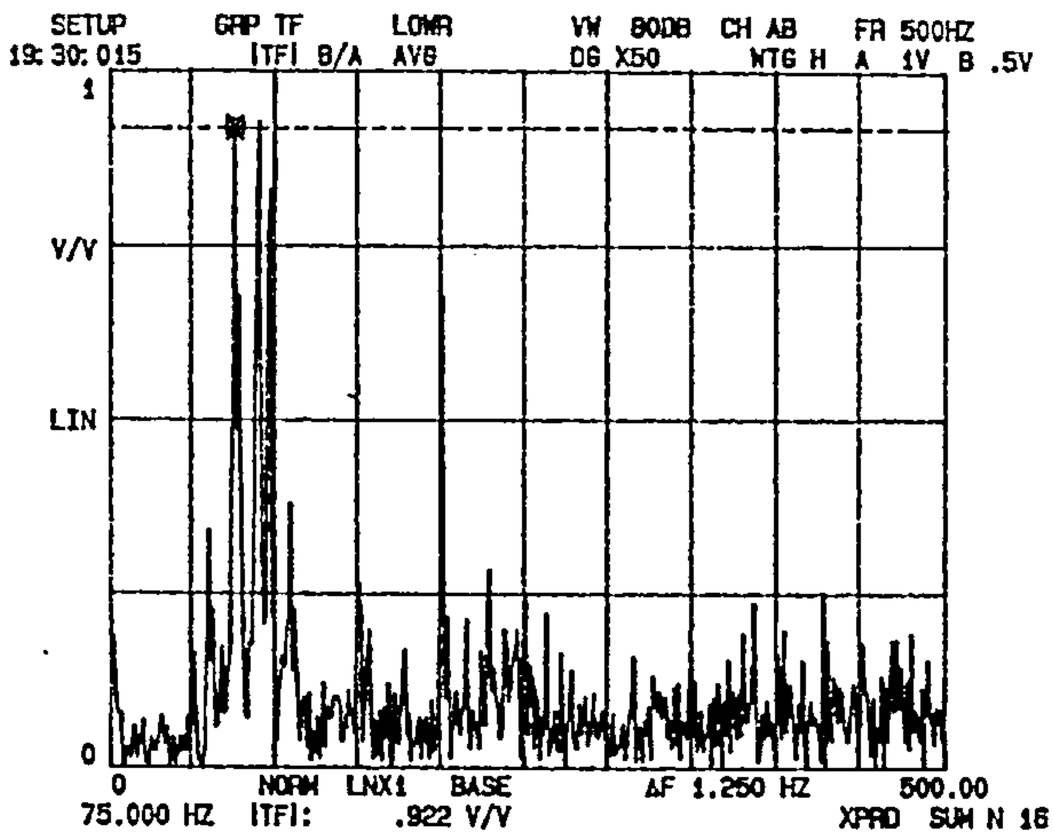

Figure 5.41 Transfer function of cutter in the feed direction in the range 0 to 500 Hz

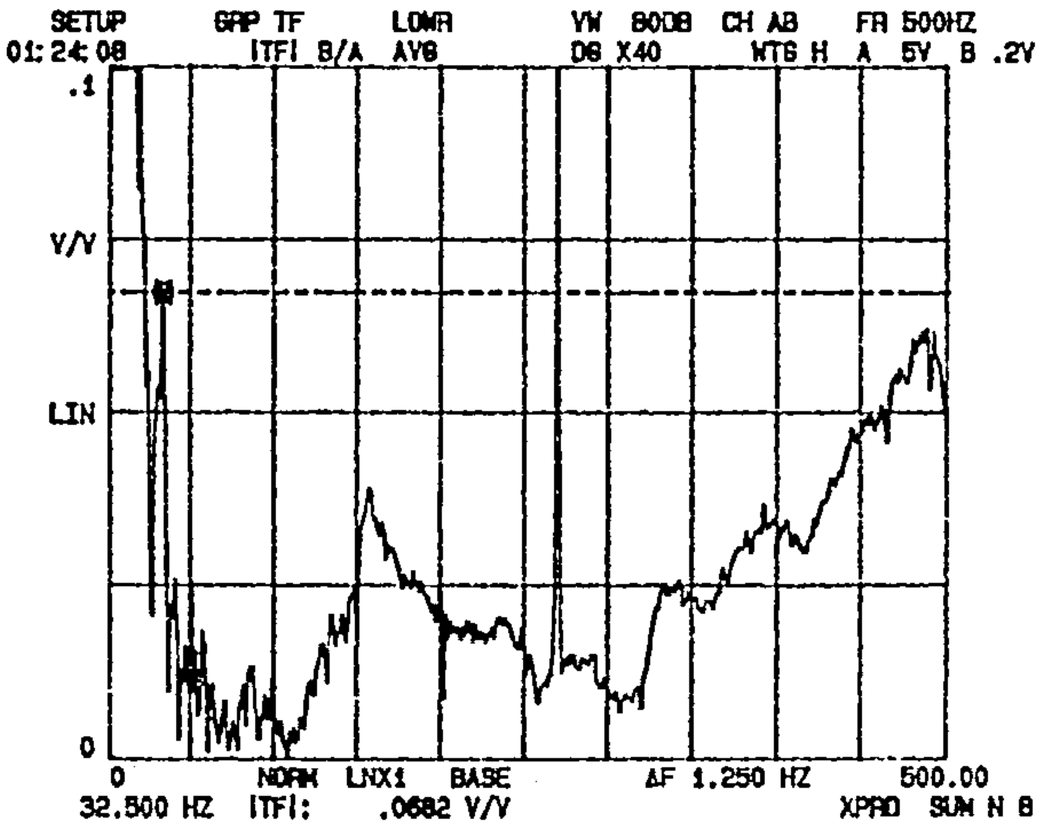

Figure 5.42 Transfer function of cutter in the z - direction in the range 0 to 500 Hz

It is of course possible that the table of the machine tool will experience vibrations associated with defects in the lead screw and the slideways and it is the relative motion between the cutter and the workpiece attached to the table which will generate the observed surface profile. To investigate this a series of tests at varying feed rates was carried out with two accelerometers attached to the table, one to measure vibrations in the feed direction and one to measure vibrations in the z-direction. The results of these tests suggests that no significant vibrations of the table were present. The signals generated by both accelerometers when the table was in motion were indistinguishable from the noise present in the accelerometer signals when the table was stationary.

5.4 Conclusions

It has been shown that conventional measures of surface roughness such as centre line average values (R_a) do not correlate with either progressive tool wear or with sudden insert failure such as chipping.

The spatial spectral content of milled surfaces may be used to monitor tool wear and insert chipping in both single point and multi-point cutting. This was observed from the behaviour of the spatial spectral energy content of the surfaces in three distinct frequency bands; a high frequency band containing frequencies above tooth passing, a kinematic band containing frequencies between tooth passing and spindle frequencies and a low frequency band containing frequencies below spindle speed.

The milled surfaces studied have all demonstrated fractal characteristics and those characteristics have been quantified by a fractal dimension parameter. The divider fractal dimension was only sensitive to tool wear when cutting with the positive rake cutter and the work-piece material had a minimal effect on this sensitivity. The divider dimension was not susceptible to changes occurring as a result of insert chipping.

The structure function revealed the bi-fractal nature of the machined surfaces. The structure function fractal dimension did not change with progressive tool wear however the divergence in fractal dimension in the two fractal zones indicated that insert chipping had occurred.

Impulse testing of the machine tool showed that damped natural frequencies existed within the range of machining frequencies characteristic of the milling process.

5.5 References

5.1) A.L.B. Dos Santos, M.A.V. Duarte, A.M. Abrao, A.R. Machado. "An optimisation procedure to determine the coefficients of the extended Taylor's equation in machining". International Journal of Machine Tools and Manufacture, 39,(1999), 17 - 31.

5.2) W.R. DeVries, "Analysis of Material Removal Processes", p94, Springer-Verlag, New York, 1992

5.3) "Method for the assessment of surface texture, Part 1, Method and instrumentation" BS 1134: Part 1: 1972.

5.4) "Method for the assessment of surface texture, Part 2, General information and guidance" BS 1134: Part 2: 1972.

5.5) N.N. Zorev trans H.S.H. Massey. "Metal Cutting Mechanics", Pergamon Press, Oxford, 1966

5.6) M.C. Shaw, Metal Cutting Principles, Oxford University Press, New York, 1984

5.7) S. Smith and J. Tlusty, "An overview of modelling and simulation of the milling process". Transactions of the ASME, Journal of Engineering for Industry, 113,(1991), 169 - 175.

5.8) D.J. Whitehouse, "Handbook of surface metrology", I.O.P. publishing, Bristol,1994.

5.9) P. Wilkinson, R.L. Reuben, J.D.C. Jones, J.S. Barton, D.P. Hand, T.A. Carolan, S.R. Kidd. "Surface finish parameters as diagnostics of tool wear in face milling". Wear, 205,(1997), 47-54.

5.10) H.M. Hastings and G. Sugihara. "Fractals: a users guide for the natural sciences", p.19, Oxford University Press, New York, 1993.

5.11) J. Theiler. "Estimating fractal dimension". Journal of the Optical Society of America, 7, (1990), 1055-1073.

5.12) J.R. Carr and W.B. Benzer. "On the practice of estimating fractal dimension", Mathematical Geology, 23,(1991) 945-958.

5.13) H.E. Schepers, J.H.G.M. van Beek, J.B. Bassingthwaite. "Four methods to estimate the fractal dimension from self-affine signals", IEEE Engineering in Medicine and Biology, (1992), 57-71.

5.14) B. Klinkenberg. "A review of methods used to determine the fractal dimension of linear features", Mathematical Geology, 26,(1994), 23-46.

5.15) J.C. Russ. "Fractal Surfaces", 27-55, Plenum Press, New York, (1994)

5.16) L. He, J. Zhu. "The fractal character of processed metal surfaces", Wear,208,(1997), 17-24.

5.17) R. Andrle. "Estimating fractal dimension with the divider method in geomorphology", Geomorphology,5,(1992), 131-141

5.18) K. Develi and T. Babadagli. "Quantification of natural fracture surfaces using fractal geometry", Mathematical Geology,30,(1998), 971-998.

5.19) B.B. Mandelbrot. "Fractals: Form, Chance and Dimension", p 32, W.H. Freeman (1977).

5.20) A.Den Outer, J.F. Kaashoek, H.R.G.K. Hack. "Difficulties with using continuous fractal theory for discontinuity surfaces", International Journal of Rock Mechanics, Mineral Science and Geomechanics Abstracts, 32,(1995), 3-9.

5.21) A. DeSantis. "A direct divider method for self-affine fractal profiles", Geophysical Research Letters, 24,(1997), 2099-2102.

5.22) C.A. Brown and G. Savary. "Describing ground surface texture using contact profilometry and fractal analysis", Wear, 141,(1991), 211-226.

5.23) C.A. Brown, W.A. Johnsen, R.M. Butland. "Scale-sensitive fractal analysis of turned surfaces", Annals of the CIRP, 45,(1996), 515-518.

5.24) R.S. Sayles and T.R. Thomas. "The spatial representation of surface roughness by means of the structure function", Wear, 42,(1977),

5.25) T.R. Thomas and A.P. Thomas. "Fractals and engineering surface roughness", Surface Topography, 1,(1988), 143-152.

5.26) D.K. Baek, T.J. Ko and H.S. Kim. "A dynamic surface roughness model for face milling", Precision Engineering, 20,(1997), 171-178

5.27) W.T. Thomson "Theory of vibration with applications: fourth edition", p.510, Chapman & Hall, London, 1993.

Chapter 6

Acoustic Emission Data Processing and Results

This chapter describes the results obtained from the acoustic emission experiments discussed in chapter 4 and the subsequent data processing used to assess tool wear. The work will be concerned with an analysis of the rms acoustic emission data and with a spectral analysis of the raw acoustic emission data.

6.1 RMS Analysis

The root mean square (rms) of a time varying real signal *v(t)* is defined as

$$V_{rms} = \sqrt{\frac{1}{\tau}\int_0^{\tau} v^2(t)dt} \qquad (6.1)$$

where τ is the time interval over which the square of the signal is averaged.

Many workers have used rms characteristics of acoustic emission (AE) signals as a means of monitoring tool wear. In 1988 Roget et al [6.1] examined the application of rms AE signals to the general problem of tool condition monitoring. They concluded that although AE is sensitive to tool wear in turning and milling possible industrial applications would be limited. Not withstanding this conclusion they did accept that the technique could detect tool failure. Blum and colleagues [6.2] surveyed the different kinds of acoustic emission tool wear monitoring methods. They concluded from this survey that all the methods examined have both advantages and disadvantages but that the mode of the AE-amplitude distribution showed the best correlation with tool wear, tool chipping and workpiece chip formation processes in turning. This leads to the suggestion that a single sensor may provide the solution to tool wear monitoring problems. It must be understood that this claim is based on a limited series of turning experiments.

Diei and Dornfeld [6.3] showed that the mean rms signal increased with tool flank wear when fly-cutting with a positive rake tool. In this study the authors avoided the complications of crater wear by using inserts with a strong resistance to crater wear. They

observed that the tendency of the rms signal to increase with wear was not so marked with inserts employing artificially induced flank wear as it was for inserts which had been naturally worn. They also observed that a "settling period" was required before the increasing trend established itself. This was attributed to the initial breakdown of the insert sharp edge. Diei and Dornfeld [6.4] also showed that rms AE was susceptible to changes in cutting conditions in face milling. In the present work the cutting conditions were maintained constant for any given set of tests.

Cho and Komvopoulos [6.5] showed a correlation between AE and tool wear in turning AISI 4340 steel. In this work the authors established that the rms AE increased with insert wear during the early stages of cutting and eventually achieved a constant value towards the end of tool life. Again in turning, Messaritis and Borthwick [6.6] showed the variation of rms AE with time for various chip formation mechanisms thus confirming that one of the major sources in AE generation is chip breakage and entanglement [6.3]. They also concluded that, within the limits of their experiments, there is little difference in the rms level of the AE signal between orthogonal and semi-orthogonal cutting. It is well known [6.3] that other sources of AE lie in the shear and plastic deformation of the workpiece, the chip/tool rake face interface and the workpiece/tool flank contact. Work by Heiple et al [6.7] concludes that the major source of AE in turning AISI 4340 steel originates in the sliding friction between the flank face and the newly produced machined surface. The friction at this interface is dependent on material properties of the inserts and the workpiece thus suggesting that a change in the AE signal would be expected when different workpiece materials were cut. Heiple's results suggest that AE rms values may be used to monitor flank wear directly.

Carolan et al [6.8] demonstrated the use of a novel fibre optic transducer designed to measure AE signals in machining processes. This transducer has advantages over conventional piezo-electric AE transducers in that it has a flat frequency response to displacement, possesses an absolute calibration defined by the wavelength of the laser light used to drive the instrument and is non-contacting. In [6.8], Carolan and his co-workers demonstrated that the instrument could be used to monitor tool wear when face milling annealed En24 steel with a multi-point cutter. This work was extended by Carolan

et al [6.9], [6.10] to show that both AE rms processing and AE frequency analyses could be used to monitor tool wear.

In what follows the results obtained using the fibre optic transducer will be illustrated. The results from the piezo-electric transducer will only be used for comparison purposes since the resonant nature of its operation could be expected to contaminate the measured AE signals.

6.1.1 Data Acquisition and Processing

The fibre optic transducer described briefly in chapter 4 was used to obtain short time segments (26.2 ms) of unprocessed AE signals for frequency analysis and rms AE signals recorded over the full duration of the cut (typically 26 s). The rms signals were obtained from an analogue processor operating with an averaging time of 0.55 ms. This provided acceptable temporal resolution over the time of a tooth pass of approximately 12 ms. The rms signals were then recorded by a PC based analogue-to-digital data logging system with 128 kbyte of memory at a sampling rate of 5 kHz.

The changes in rms AE signal with tool wear can be seen clearly from a comparison of figure 6.1a which shows a portion of a typical signal obtained when cutting with a new tool with figure 6.1b which shows a typical AE signal obtained when cutting with a worn tool. The workpiece material was annealed En24 steel and a negative rake cutter carrying eight inserts was used in the generation of the AE signals shown in these figures.

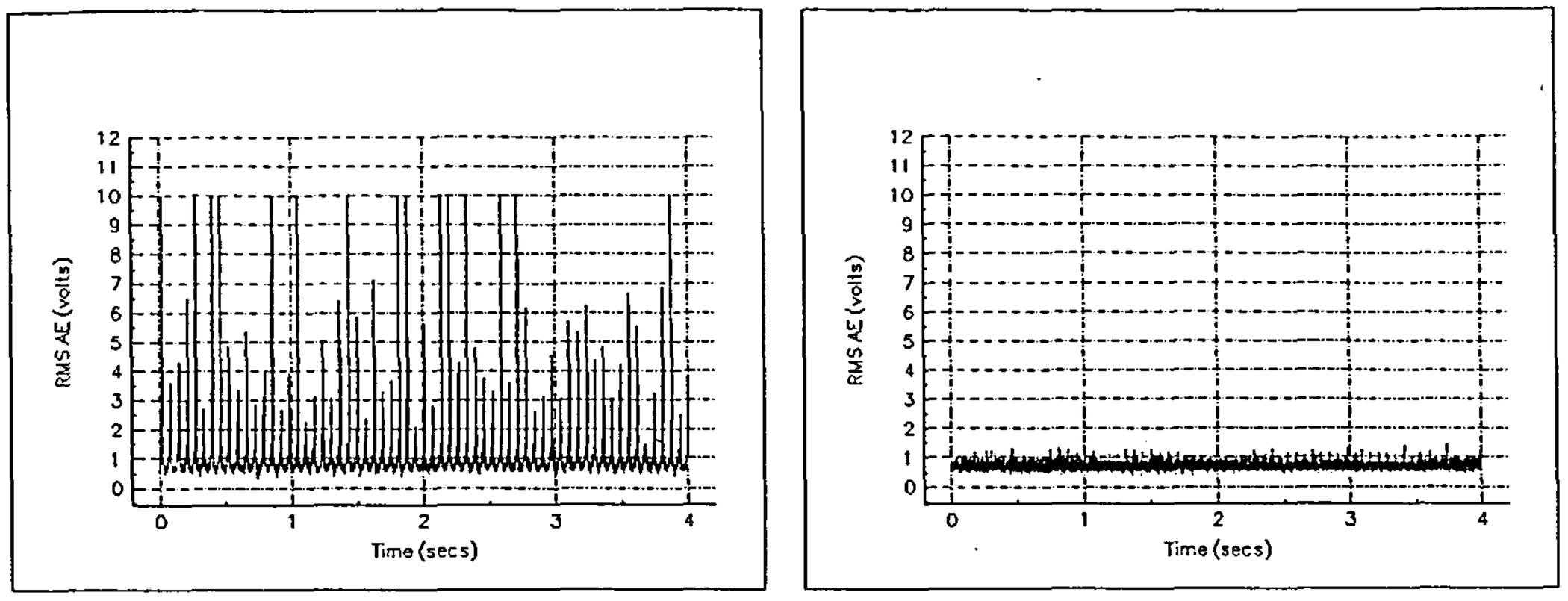

a b

Figure 6.1 Typical rms AE signals generated by 8-point milling of En24 with a negative rake cutter. a) New tool. b) Worn tool.

The large reduction in average peak height of the rms AE signal is apparent. Although this change appears to be dramatic it should be remembered that figures 6.1a and 6.1b show the rms AE signals generated by the cutter at the beginning and end of its life. It was observed that the changes between these extremes were progressive with wear as will be shown.

When milling the same material with a positive rake cutter changes were again observed in the rms AE signal as wear progressed as shown in figures 6.2a and 6.2b

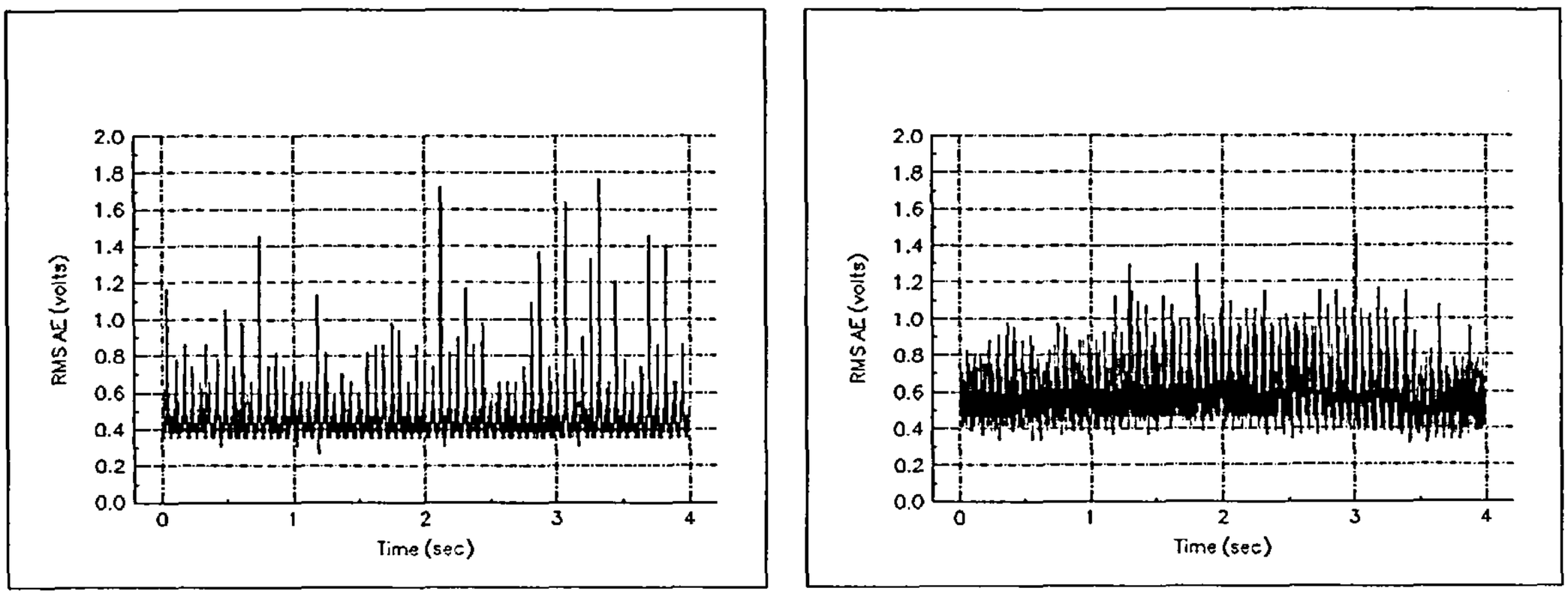

a b

Figure 6.2 Typical rms AE signals generated by 8-point milling of En24 with a positive rake cutter. a) New tool. b) Worn tool.

A change in rms response is again apparent between the two extremes of tool life. The trend in the signal was to increase in this case, a trend which was again progressive with tool wear.

The manner of the changes suggested that a simple long average rms over the cut might be an indicator of tool wear. This was achieved by digitally rms averaging the 0.55 ms rms signal over the full record length. In [6.8], Carolan et al suggested that the standard deviation of the 0.55 sec rms signal would also be a good indicator of tool wear. In the following both of these parameters will be examined in relationship to tool wear. The standard deviation data will be presented as the relative dispersion of the rms AE signal. The relative dispersion of a signal is the standard deviation of the signal normalised to its mean. This method was used by Carolan et al [6.8] as a means of comparing the performance of the two AE instruments which they used in measuring AE signals.

In the case of multi-point cutting, the AE signal is complicated by the presence of more than one insert cutting at any given time and thus by the presence of several sources of AE. Single point cutting or fly cutting eliminates these complications and generates a relatively simpler rms AE signal. This is shown in figure 6.3.

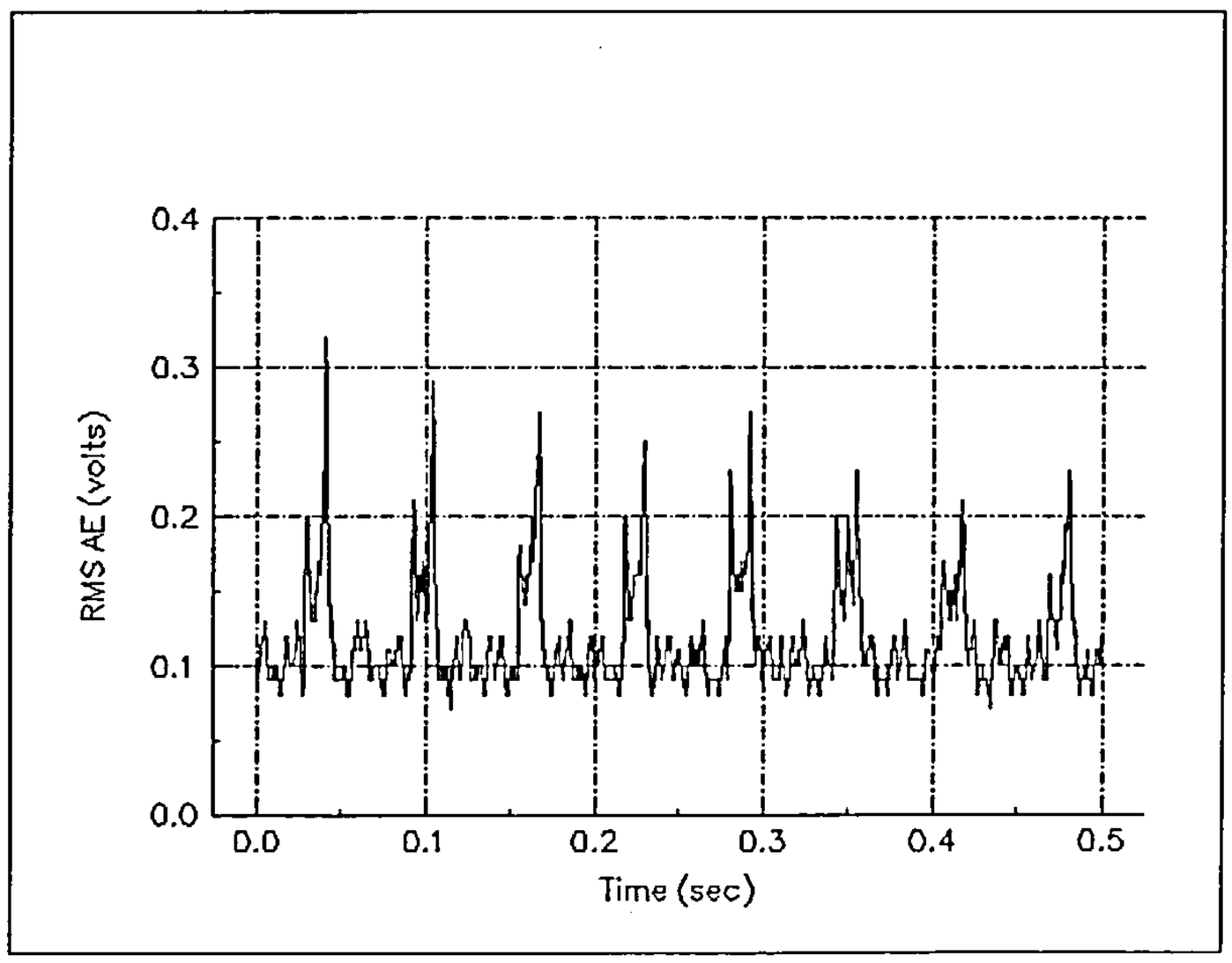

Figure 6.3 Typical rms AE signal generated when single point cutting annealed En24 with a negative rake insert.

As can be seen the AE activity is discontinuous and the tooth passing events are clearly visible. This figure is in agreement with the observations made by Diei et al [6.3] in which it was noted that peaks in AE activity occurred at tooth entry to the workpiece and at tooth exit from the workpiece. In order to characterise the AE energy associated with single point cutting the mean peak height of the AE activity associated with the tooth pass was used.

Positive rake cutting of annealed En24

Figure 6.4a shows the variation of rms AE with tool wear for positive rake cutting of annealed En24 using an eight point cutter. Figure 6.4b shows the variation in relative dispersion of the 0.55 ms AE signal with tool wear for the same tool.

The rms AE signal shows a small increase with V_b overall but this trend is interrupted by a large excursion for medium levels of wear in the range $0.3<V_b<0.7$ mm. Similarly the smooth evolution of relative dispersion with V_b is disturbed in the same region of wear. During this experiment considerable differences in wear rate between inserts occurred as illustrated in figure 6.5. The error bars in this figure indicate the range of measured values of V_b about the mean value observed at each measurement. Evolution of wear was characterised by a chip occurring at cut number 22, at which point the value of mean V_b had reached 0.26 mm, in one of the inserts which then continued to wear at a higher rate than the other inserts.

	Long time scale rms AE	Relative dispersion of rms AE
First test	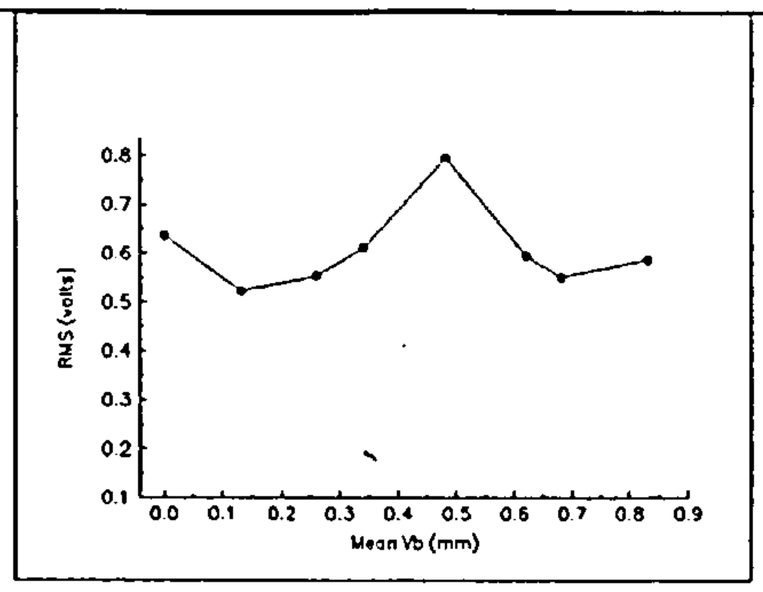	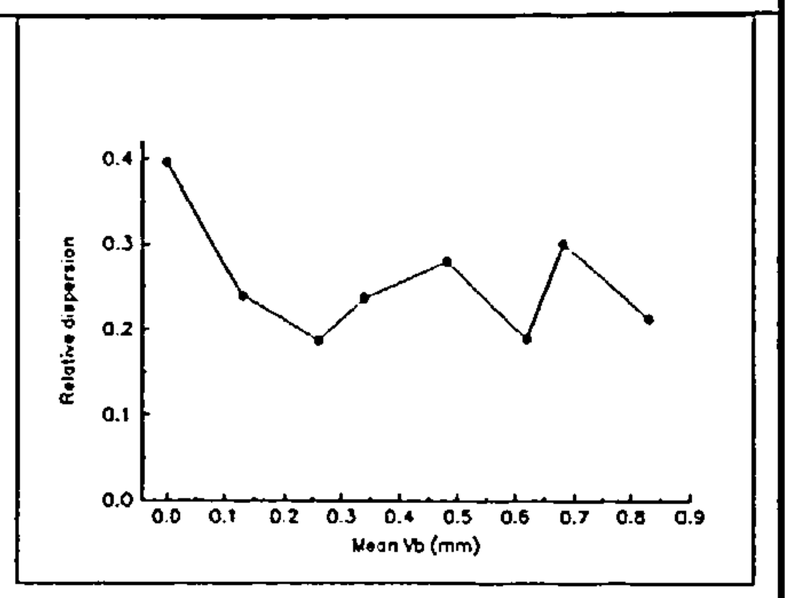
	(a)	(b)
Second test	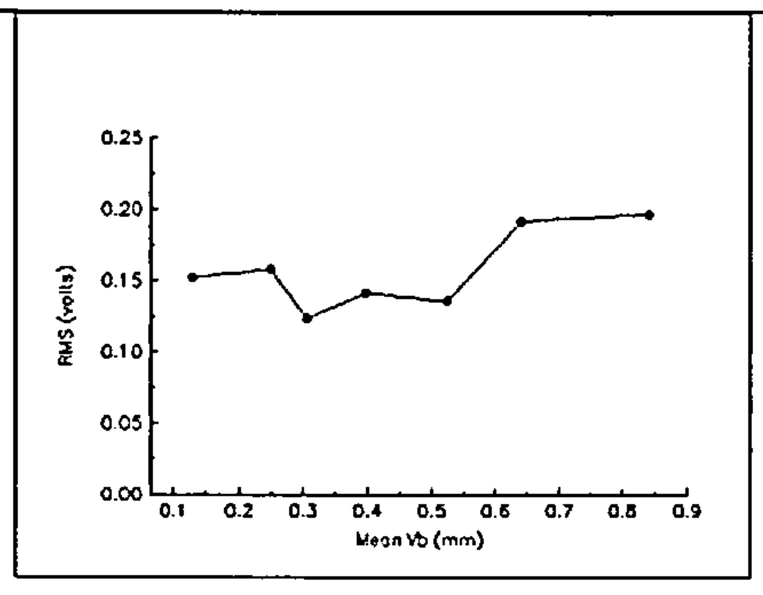	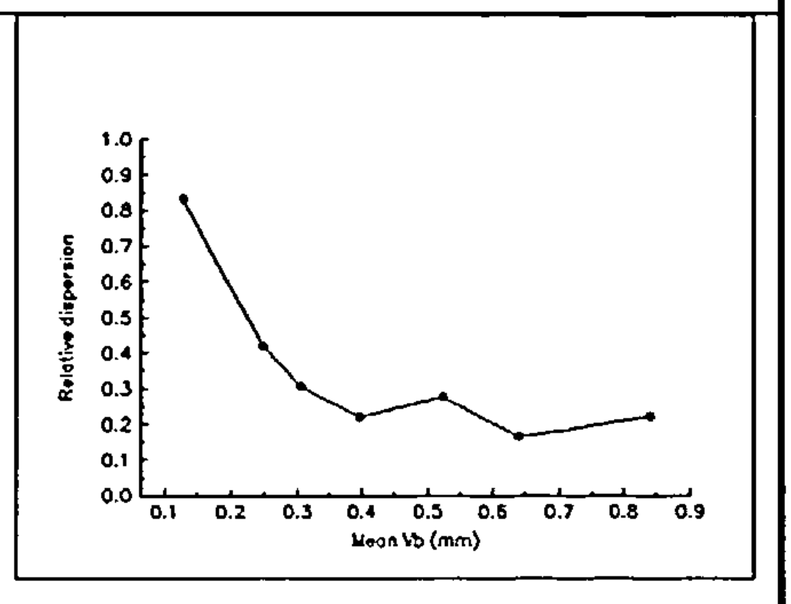
	(c)	(d)

Figure 6.4 Results obtained from 8-point positive rake cutting of annealed En24

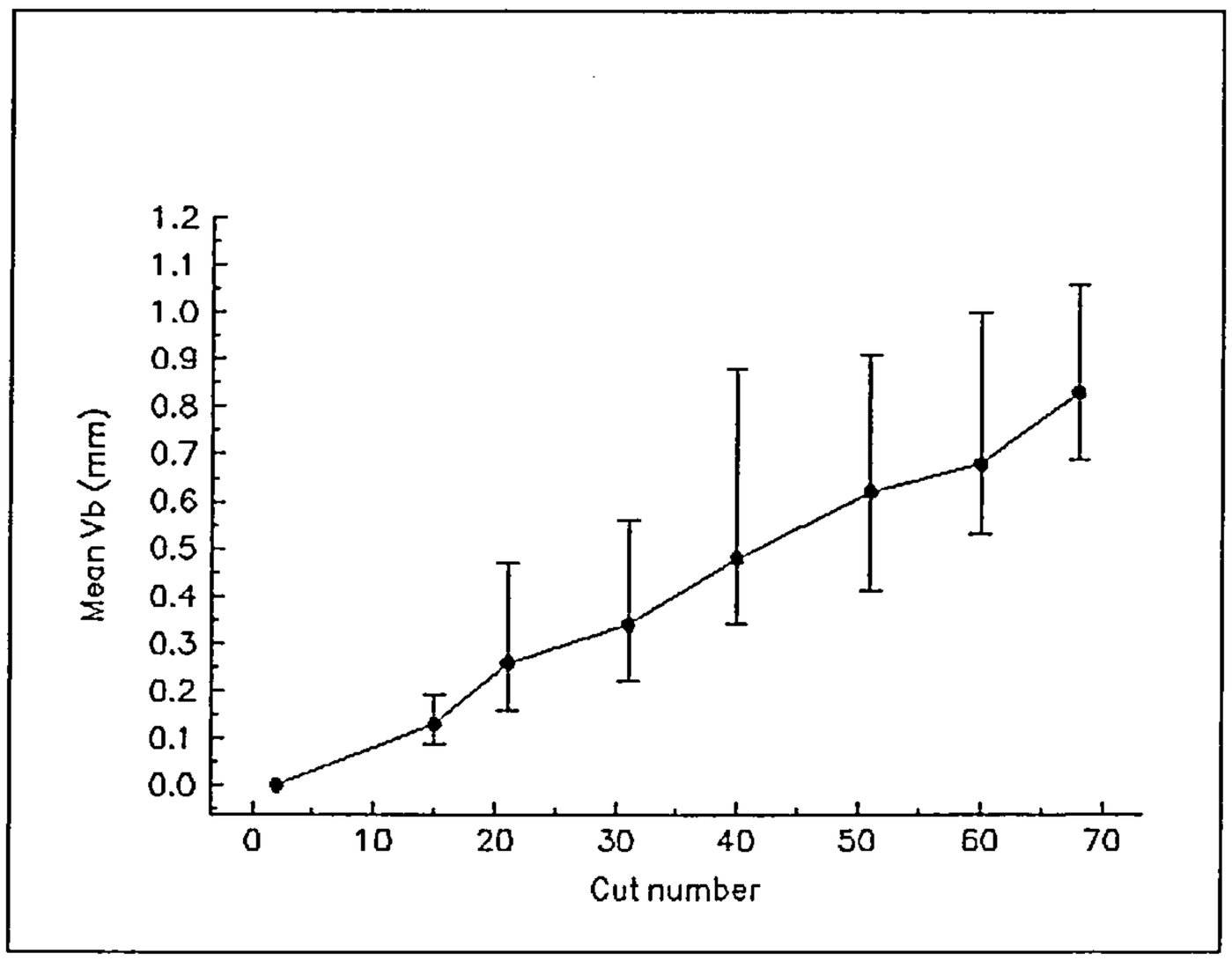

Figure 6.5 Evolution of mean flank wear land length with cut number for 8-point positive rake cutting of annealed En24.

Examination of figures 6.4a, 6.4b and 6.5 shows that the maximum divergences between the expected smooth developments of rms AE and relative dispersion of rms AE occur at a mean flank wear land length of 0.48 mm which corresponds to the measurement taken at cut number 40. This coincides with the maximum spread of measured flank wear land lengths for the individual inserts in the cutter and thus it would appear that the rms AE signal is sensitive to the changes in the detailed cutting edge geometry.

Figures 6.4c and 6.4d show the long time scale rms AE variation with mean V_b and the relative dispersion variation with V_b for an experiment involving the positive rake cutting of annealed En24. The cutting conditions were identical to the case considered previously in figures 6.4a and 6.4b.

The trend of the long period rms AE signal is to increase with insert wear as measured by the mean length of the flank wear land V_b. This is in agreement with the work by Diei and Dornfeld [6.3] and Carolan et al [6.9] although Carolan et al showed the variation in rms AE with cut number rather than V_b.

The trend of the relative dispersion of the 0.55 ms rms AE signal shows a steep reduction until it reaches an almost constant value at a mean value of V_b of 0.4 mm. This trend could be used to indicate light to medium wear of the cutter in a monitoring situation.

It was noted that an insert had chipped when the mean length of the flank wear land averaged over the whole cutter had reached 0.4 mm. It may be observed that the otherwise smooth evolutions of rms AE and relative dispersion signals are disrupted in this region of the graphs.

Negative rake cutting of annealed En24

Figure 6.6a shows the variation in long time scale rms AE with mean tool flank wear land length for negative rake cutting of annealed En24 steel when using a multi-point cutter. The tendency of the rms AE signal to decrease with increasing wear is contrary to that observed in the previous section and disagrees with reported observations by Diei and Dornfeld in milling experiments [6.3] and by Blum et al in turning experiments [6.11]. However these works were confined to positive rake cutters and in some instances to

artificial flank wear. The wear pattern in this set of experiments was characterised by uneven wear, an inevitable consequence of using naturally worn inserts, as shown in figure 6.1b but this is not reflected very strongly in figure 6.6a

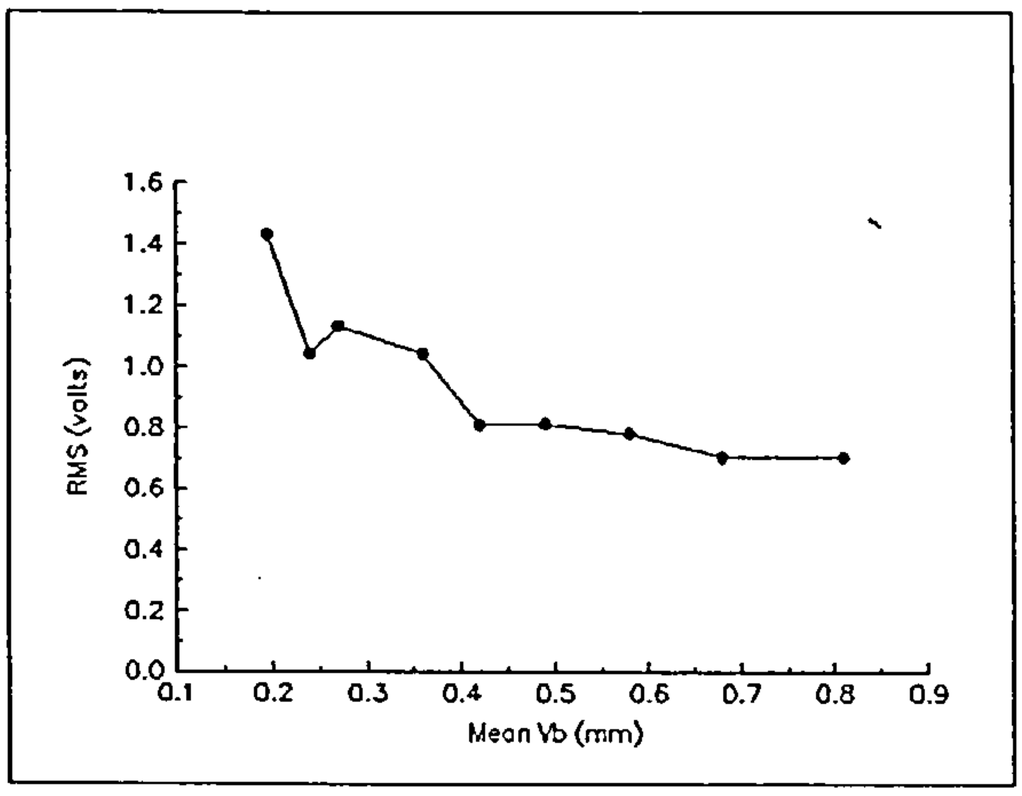

Figure 6.6a Variation in long time scale rms AE with V_b for 8-point negative rake cutting of annealed En24

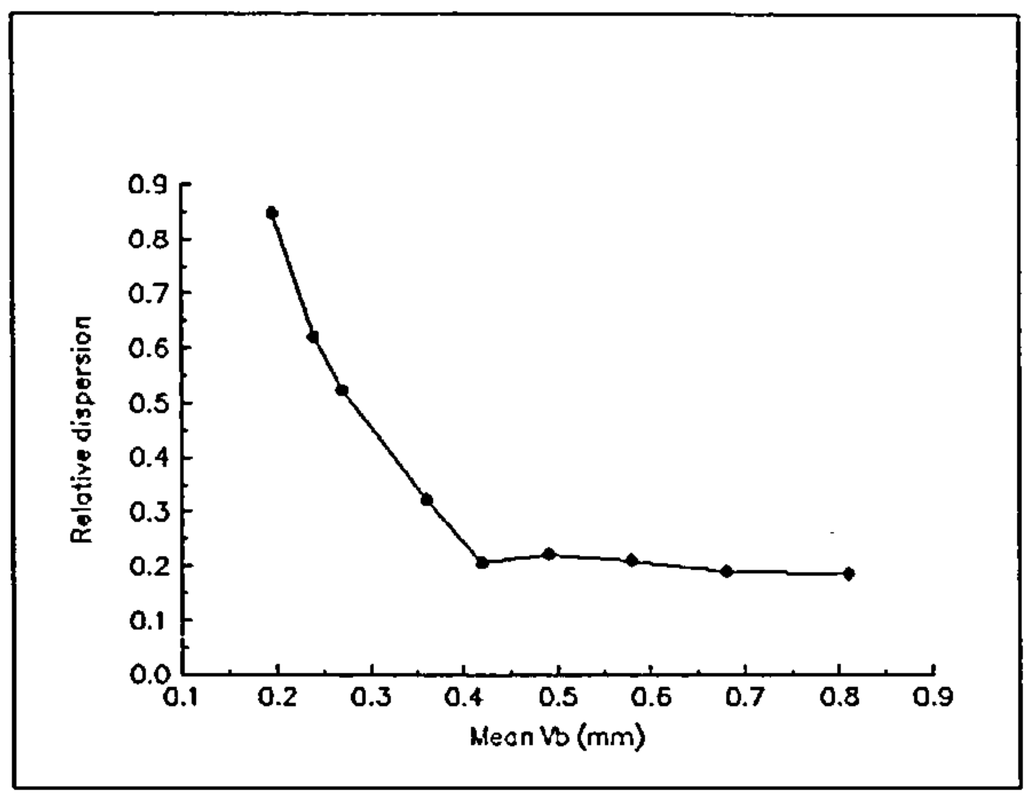

Figure 6.6b Variation in relative dispersion with V_b

The variation in relative dispersion of the rms AE signal shows a sharp reduction until a mean flank wear land length of 0.4 mm is generated beyond which the relative dispersion maintains a relatively constant value. This is similar to the effect noted in figure 6.4d.

Figure 6.7a shows the variation in mean peak rms AE with tool wear for single point negative rake cutting of annealed En24. As discussed on page 6, the mean peak rms AE is used in the case of fly-cutting since it is the most useful indicator of rms energy when the AE signal is discontinuous. In this case the variation in mean peak rms value shows an increase with flank wear land length. However figure 6.7a shows an 'initial period of instability' for values of V_b of less than 0.26 mm which exhibits a variation comparable to that reported by Diei and Dornfeld [6.3]. After this period the variation in mean peak rms AE signal is similar to that observed in figure 6.6a. It would appear from a comparison of figures 6.6a and 6.7a with figures 6.4a and 6.4c that a gross geometric effect can be observed in the variation of rms AE with tool wear. The effect appears to be that a positive rake cutter will cause the rms AE signal to increase with tool wear as measured by flank wear land length and that conversely a negative rake cutter will cause it to

decrease. However the situation is much more complex than this and several conflicting geometric effects are present as will be discussed in chapter 8.

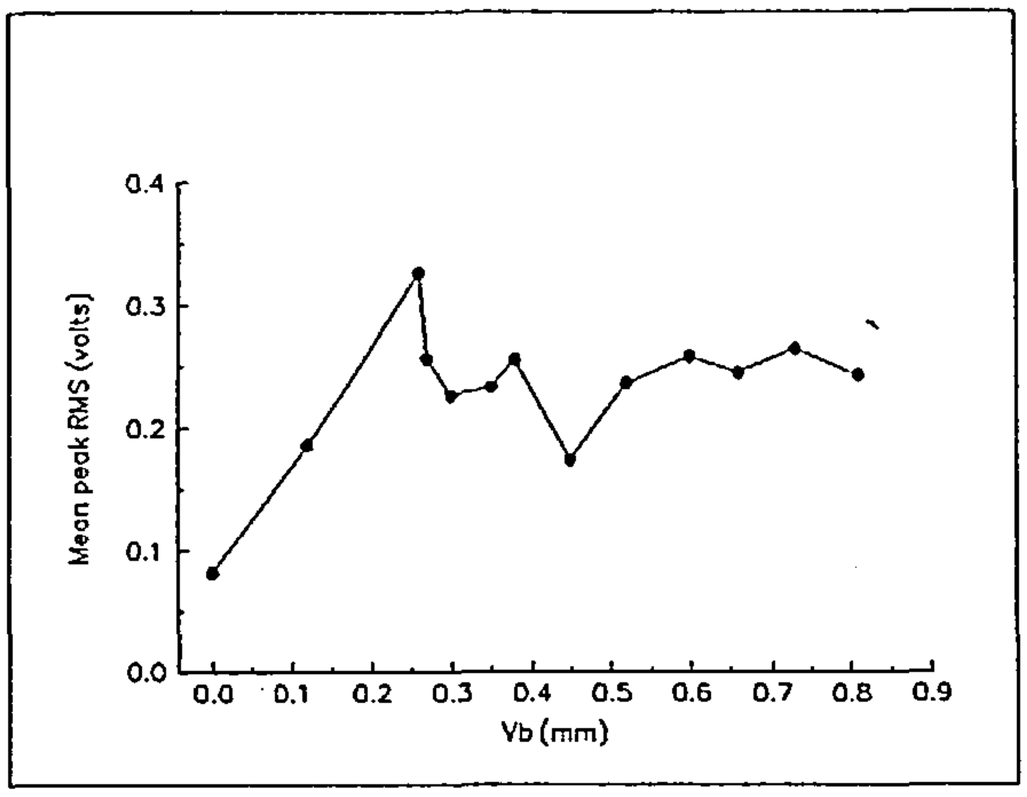

Figure 6.7a Variation in mean peak rms AE with V_b for fly-cutting of En24

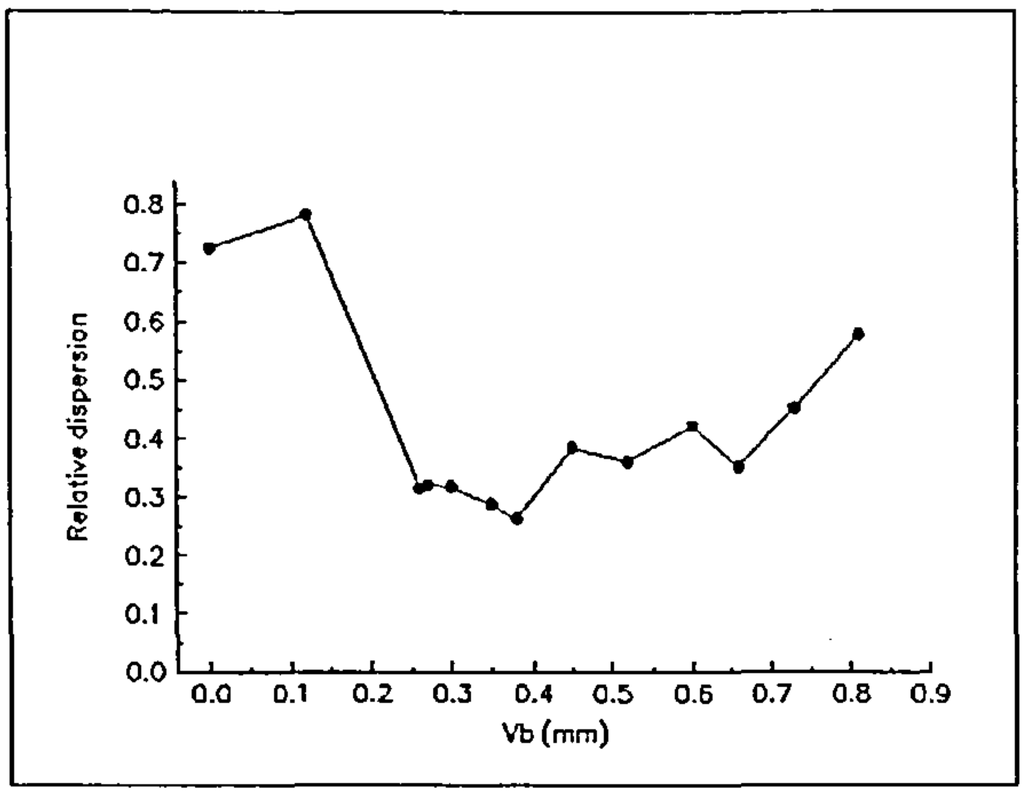

Figure 6.7b Variation in relative dispersion of AE with V_b for fly-cutting of En24.

Figure 6.7b demonstrates the variation in relative dispersion of the rms AE signal with flank wear land length. Again the trend for this parameter is a sharp decrease with wear until the value of V_b mm is approximately 0.4 mm after which value an almost constant value of relative dispersion is exhibited until a V_b value of 0.7 mm is achieved.

The increase in flank wear in this experiment was accompanied by crater wear until at a flank wear land length of 0.3 mm break through of the crater onto the flank face occurred and the cutting edge crumbled. At a value of V_b of 0.35 mm grooving of the flank face of the insert was evident. These phenomena coincide with disruptions to the smooth trends in mean peak rms of the AE signal and in the relative dispersion of the rms AE signal as shown in figures 6.7a and 6.7b.

Positive rake cutting of quenched and tempered En24

Figure 6.8a shows the evolution of long time scale rms AE with mean flank wear land length. The major trait of this figure is a steady increase in AE energy with increase in tool wear. This experiment was characterised by the chipping of several inserts as wear progressed and this is reflected in the perturbations of the curve from a smooth evolution.

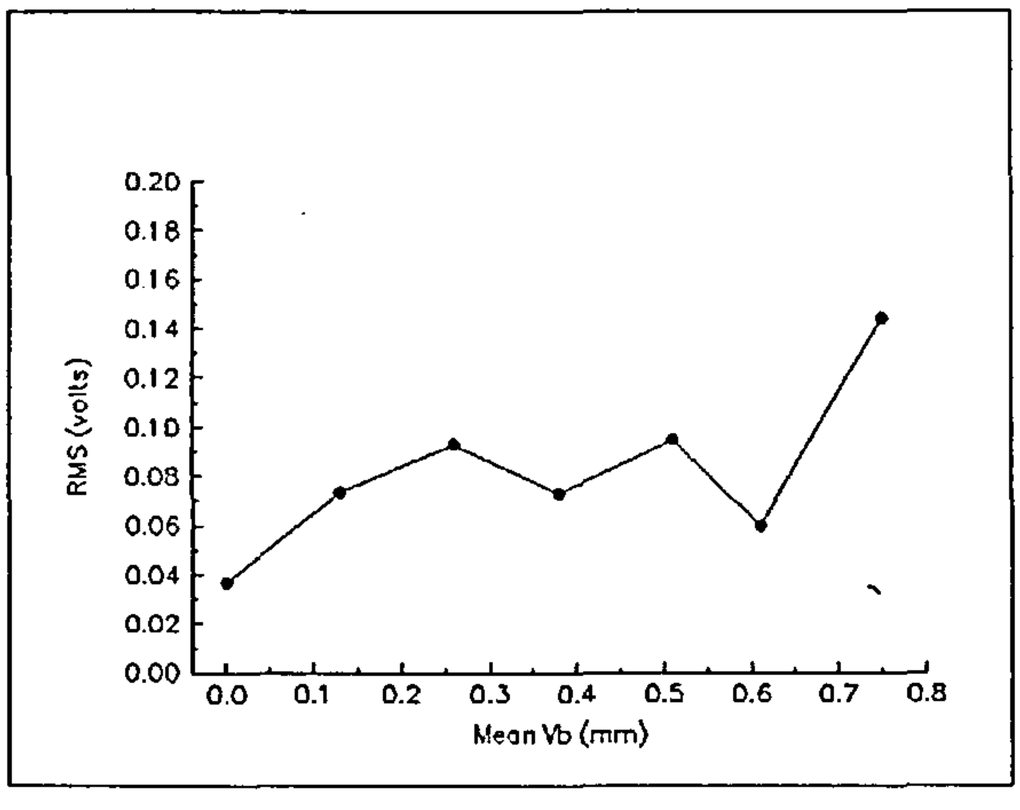

Figure 6.8a Variation in long time scale rms AE with V_b for 8-point positive rake cutting of quenched & tempered En24.

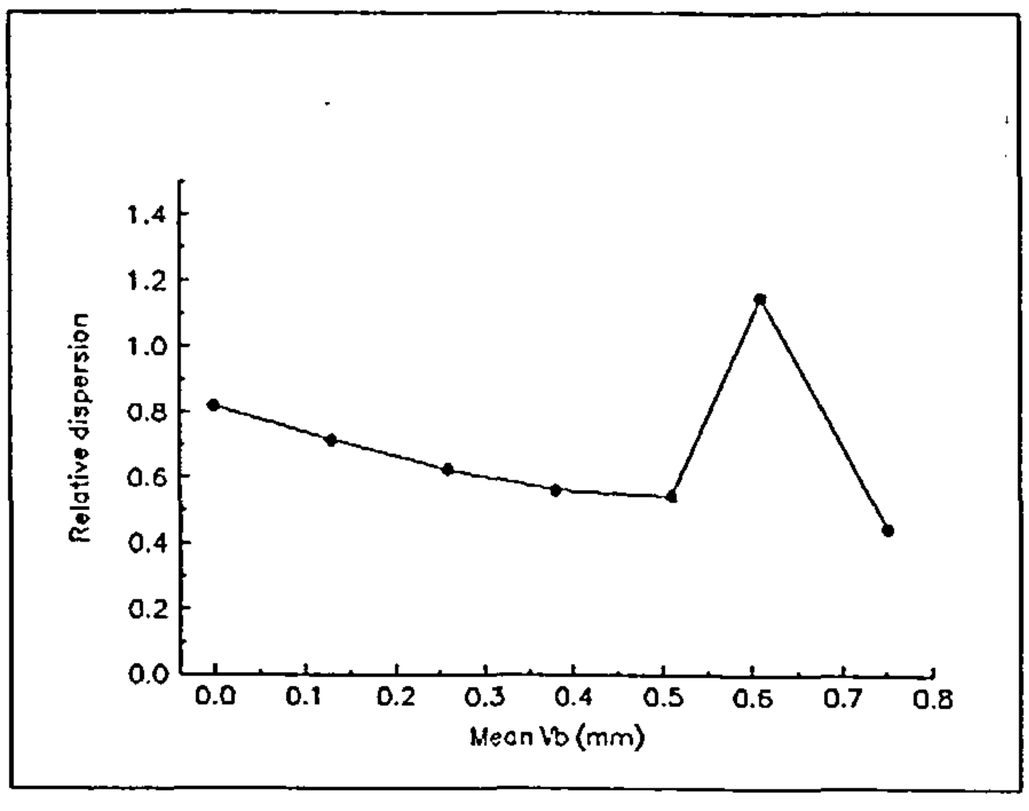

Figure 6.8b Variation in relative dispersion with V_b for 8-point cutting of quenched & tempered En24.

Figure 6.8b shows the variation of relative dispersion of the rms AE signal with mean flank wear land length. The trend of this curve is not so marked as when cutting the softer annealed En24 and the relative dispersion does not appear to reach a constant value before the end of tool life. It may also be seen that relative dispersion is not sensitive to insert chipping until several inserts have chipped at the end of the useful life of the tool.

Negative rake cutting of quenched and tempered En24

Figure 6.9a shows the change in long time scale rms AE signal with mean flank wear when cutting quenched and tempered En24 with an 8-point negative rake cutter. Similarities between this figure and figures 6.6a and 6.8a are apparent in that the gross geometric effect discussed earlier manifests itself in an initial reduction in the rms signal with wear. However as the tool wears the trend of the graph assumes the aspect of a positive rake cutter in that the rms AE increases with increasing flank wear land length. In this experiment the increase in flank wear land length was accompanied by the formation of craters on the rake faces of the inserts. The craters appeared when the mean wear land length had reached 0.23 mm (the third data point in figure 6.9a). Crater enlargement continued throughout the experiment until at a value of V_b of 0.58 mm the crater caused the cutting edge to crumble. The influence of the crater on the effective rake angle of the insert is complex as will be shown in chapter 8.

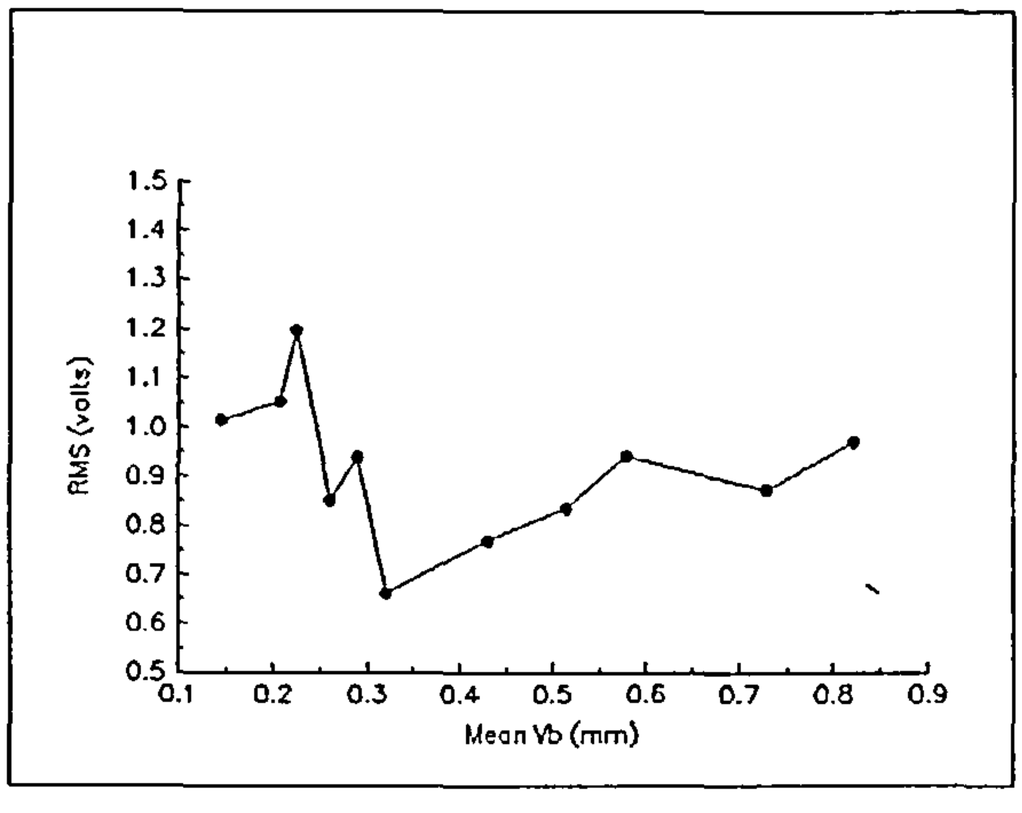

Figure 6.9a Variation in long time scale rms AE with V_b for 8-point negative rake cutting of quenched & tempered En24.

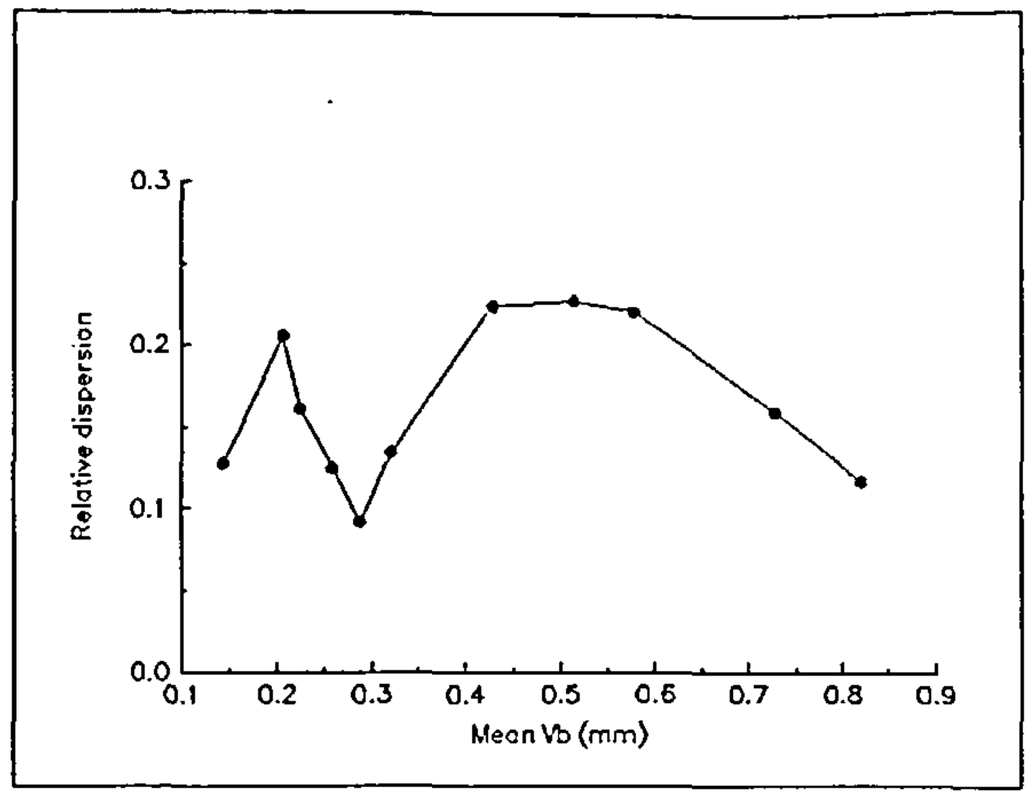

Figure 6.9b Variation in relative dispersion with V_b for 8-point negative rake cutting of quenched & tempered En24.

Figure 6.9b shows the variation in relative dispersion of the rms AE signal with mean flank wear length. Initially the trend of this graph is similar to variations in relative dispersion observed in previous experiments. However as flank wear exceeds 0.32 mm the graph exhibits characteristics inconsistent with those seen in previous graphs of relative dispersion vs flank wear land length. As has been indicated changes at the cutting edges of the inserts have been associated with a complex interaction between the flank wear land and rake face crater formation and it is to be expected that this will be reflected in the rms AE signal.

Single point cutting of stainless steel

Figures 6.10a and 6.10b show the results obtained when cutting SS304 stainless steel with a positive rake cutter carrying a single insert. The mean peak rms AE signal (figure 6.10a) displays a steady increase as wear progresses. This is in agreement with earlier results obtained from milling softer annealed En24 with a positive rake cutter. The relative dispersion of the rms AE signal exhibits an increasing trend with increasing flank wear land length.

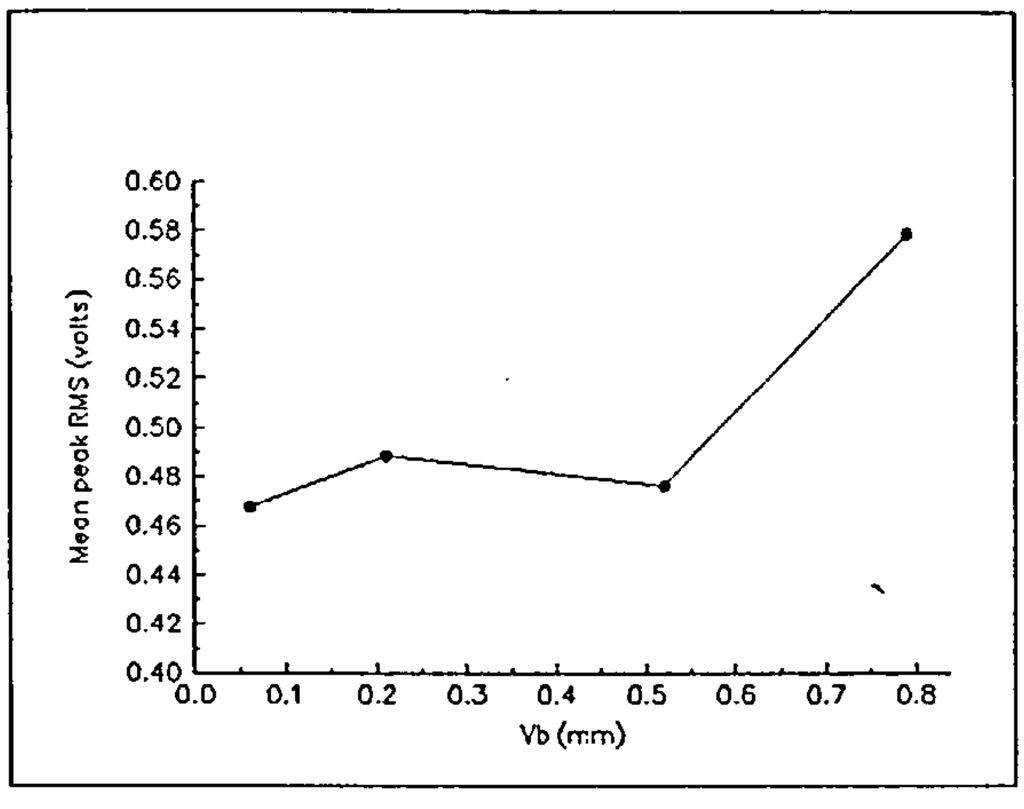

Figure 6.10a Variation in mean peak rms AE with V_b for fly-cutting of stainless steel

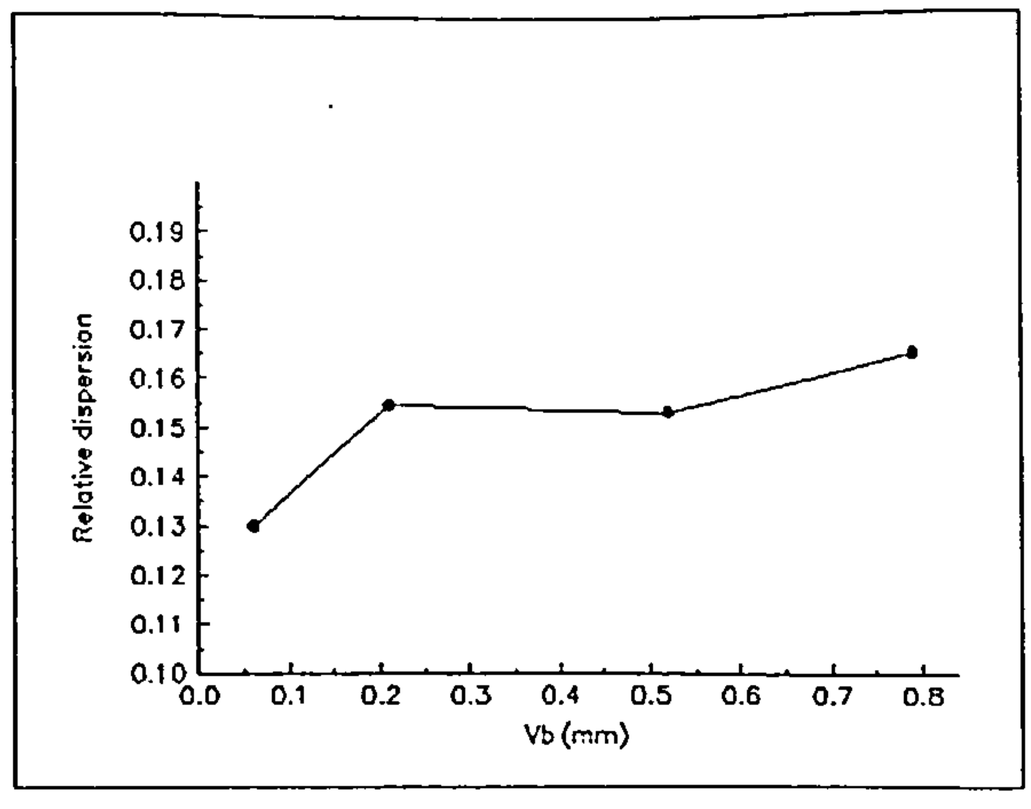

Figure 6.10b Variation in relative dispersion with V_b for fly-cutting of stainless steel.

Examination of the inserts as wear progressed showed that the normal flank wear was accompanied by notch wear which increased in both length and width as V_b increased. Figure 6.11 shows the increase in notch length and width as flank wear land length increased. The notch dimensions were measured with the aid of an engineer's microscope. The length of the notch was taken to be the maximum length of the notch from the junction of the original cutting edge with the wiper flat in a direction parallel to the original cutting edge. The width of the notch was taken to be the maximum width of the notch measured across the rake face of the insert from the line of the original cutting edge and in a direction perpendicular to the original cutting edge.

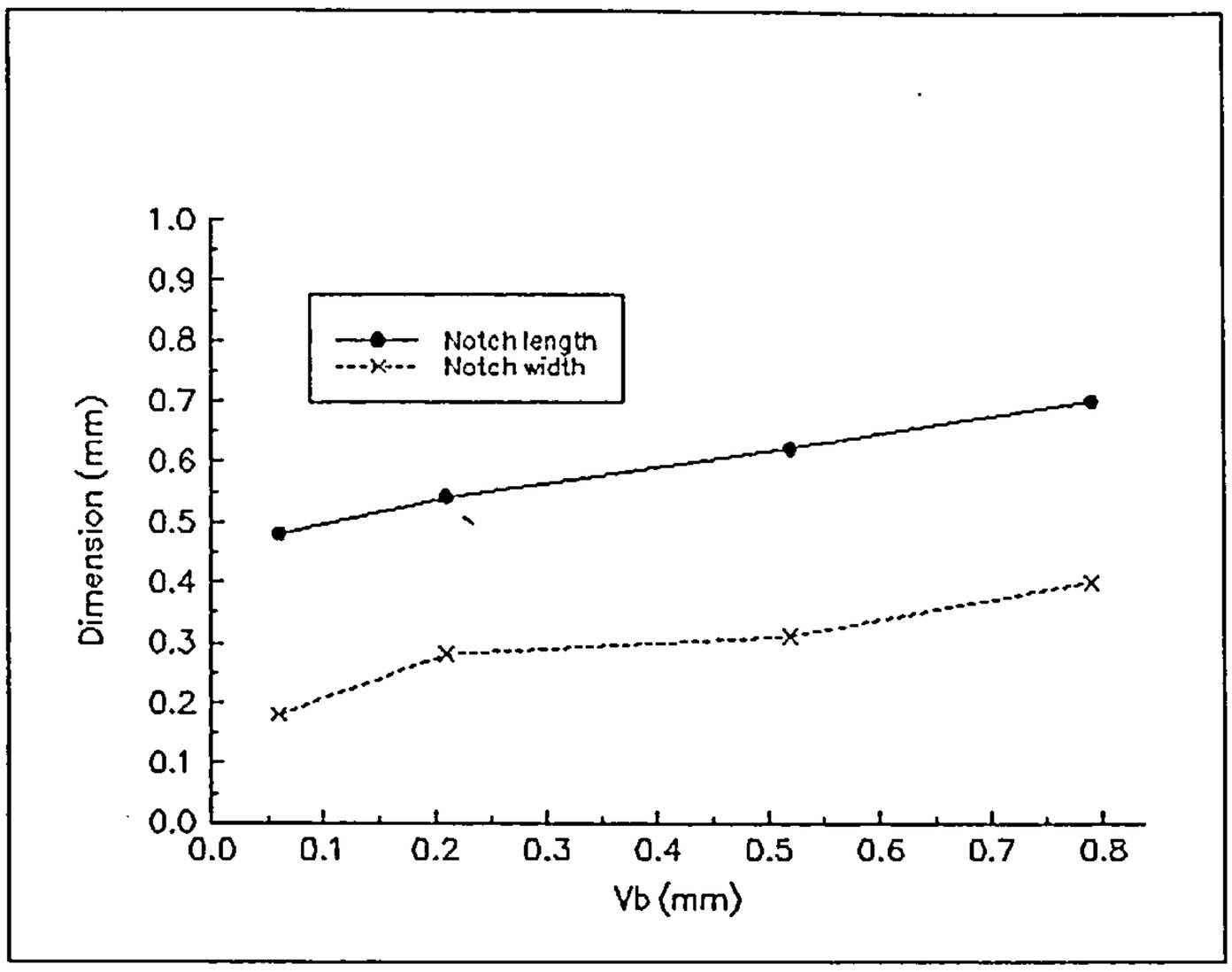

Figure 6.11 Increase in notch wear dimensions with increasing flank wear land length.

Since both measures of notch wear increase linearly with flank wear it is reasonable to use the measure of flank wear land length as the indicator of insert wear state in this case. It is of interest to observe that the shape of the graph of the notch width vs V_b curve is similar to the shape of the relative dispersion vs V_b curve. This observation is however most likely to arise from the relatively small number of points in the curves rather than from any physical correlation.

6.1.2 Spectral analysis of rms AE signal

The spectral analysis of the rms AE signal will reveal low frequency information in the rms signal which may be related to insert wear. The results of this analysis are shown in figure 6.12 for both positive rake and negative rake cutting of annealed En24. The spindle frequency (955 rev/min = 15.92 Hz) and insert passing frequency (127.3 Hz) are clearly visible in these figures. A reduction in the spectral content of the rms AE signal with wear is also apparent from these figures

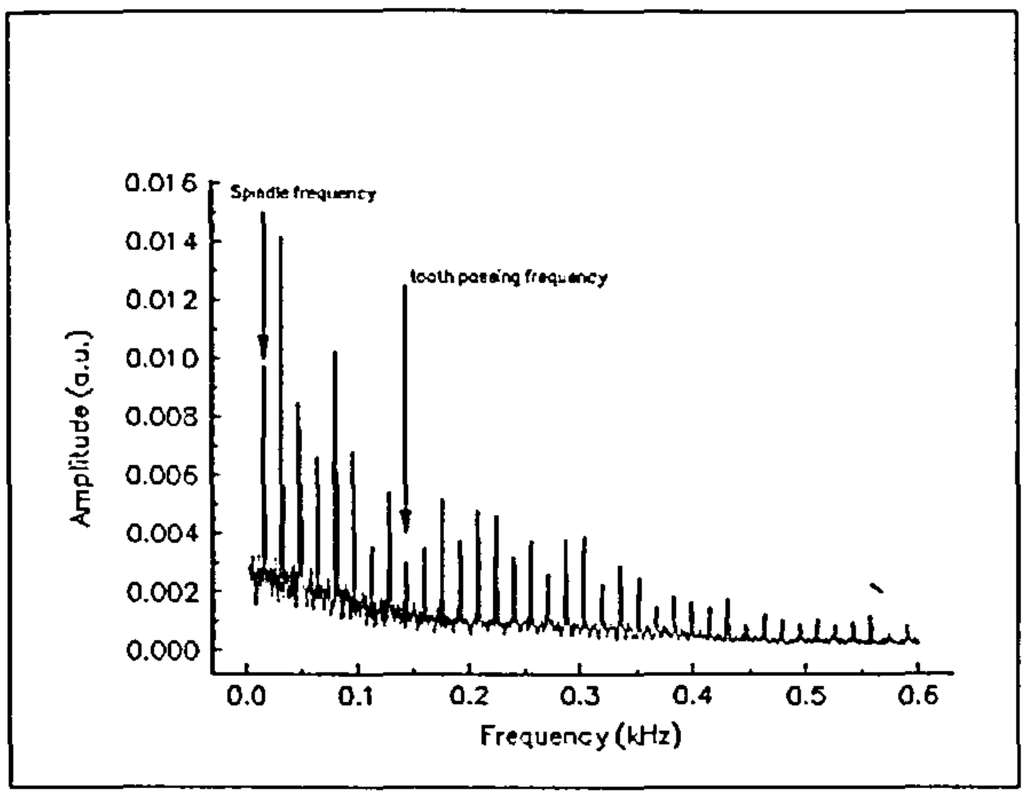

(a)

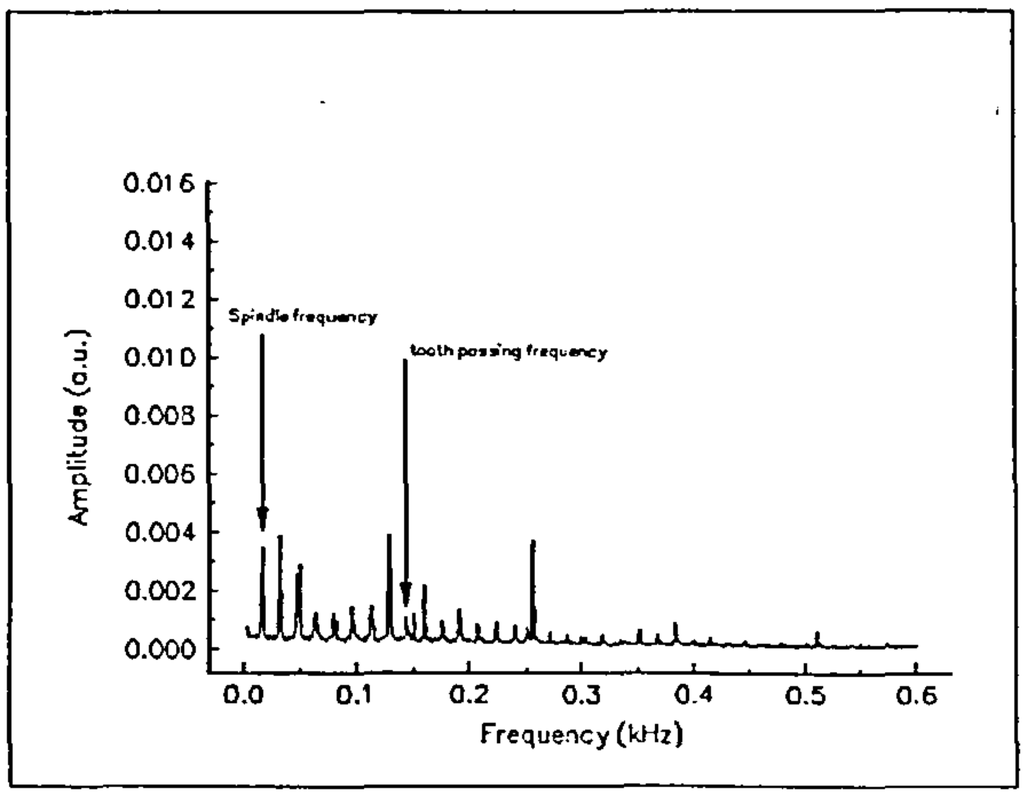

(b)

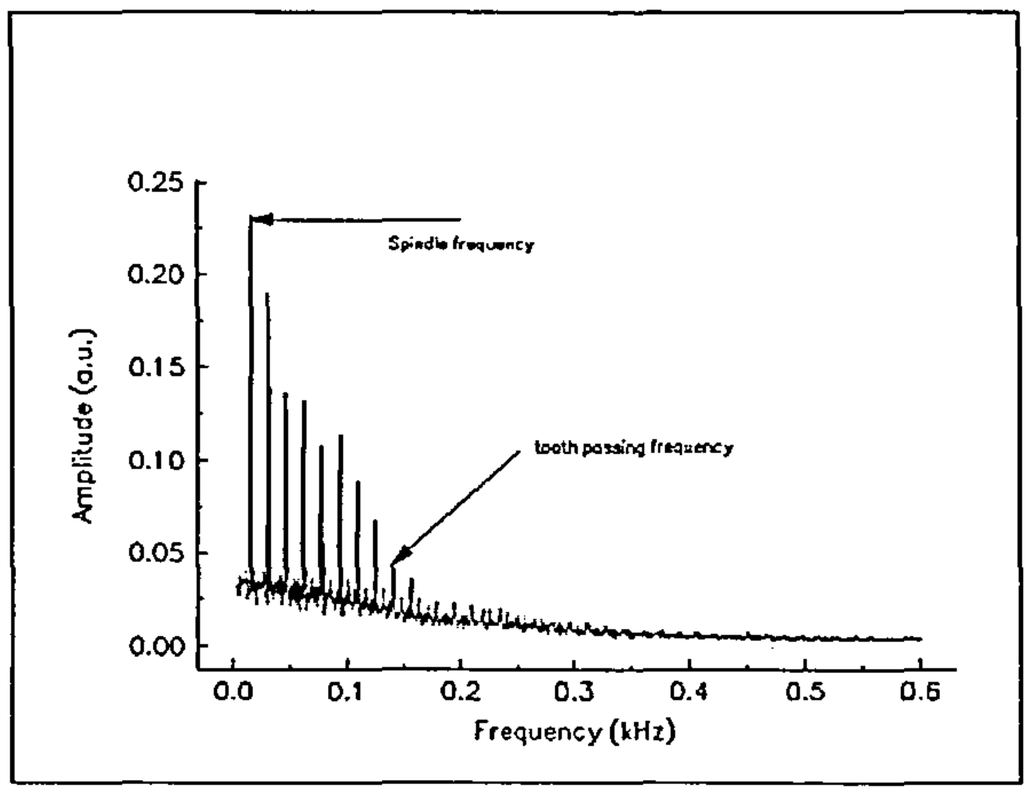

(c)

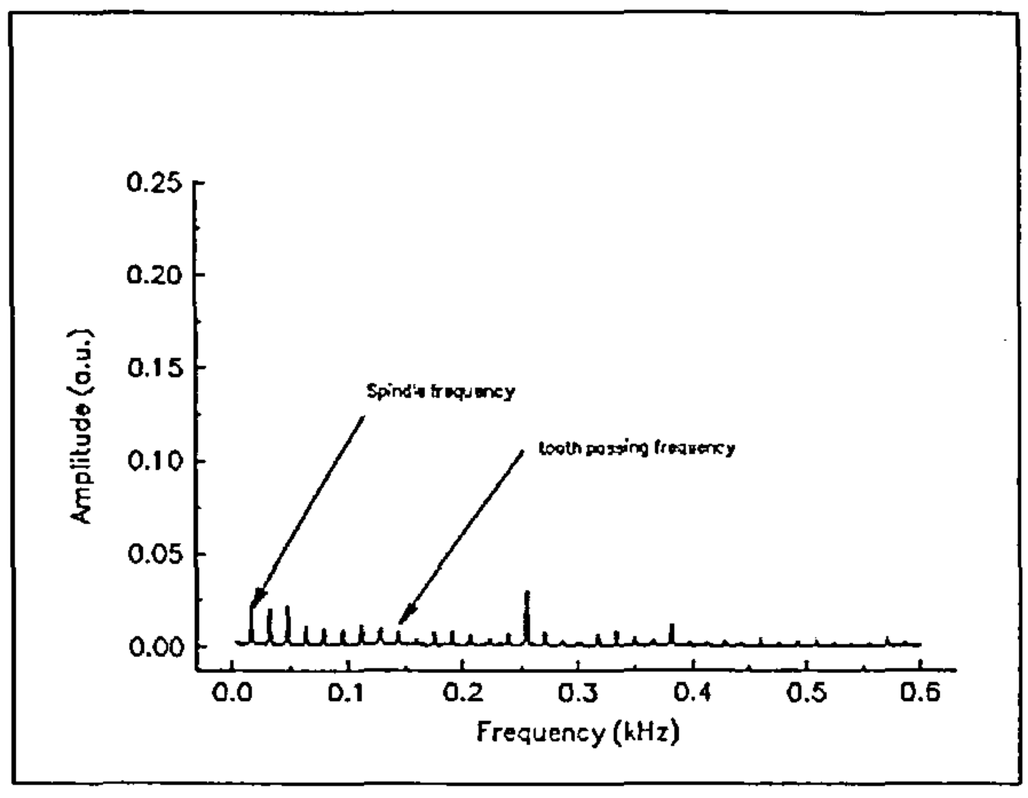

(d)

Figure 6.12 Spectrum of rms AE signals a) positive rake cutting of annealed En24 with a new insert b) positive rake cutting of annealed En24 with a worn insert c) negative rake cutting of annealed En24 with a new insert d) negative rake cutting of annealed En24 with a worn insert b)

A progressive reduction in the energy content of the rms AE signal with tool wear was observed in both experiments until the mean length of the flank wear lands reached approximately 0.3 mm. Thereafter the was little change in this parameter. In order to quantify the change in observed spectrum the integrated spectral content in the energy band 9.76 Hz to 404 Hz was calculated and plotted against mean flank wear land length. This frequency band extended from just below the spindle frequency to just above that frequency at which no significant AE activity was seen. Figure 6.13 illustrates the results of these calculations.

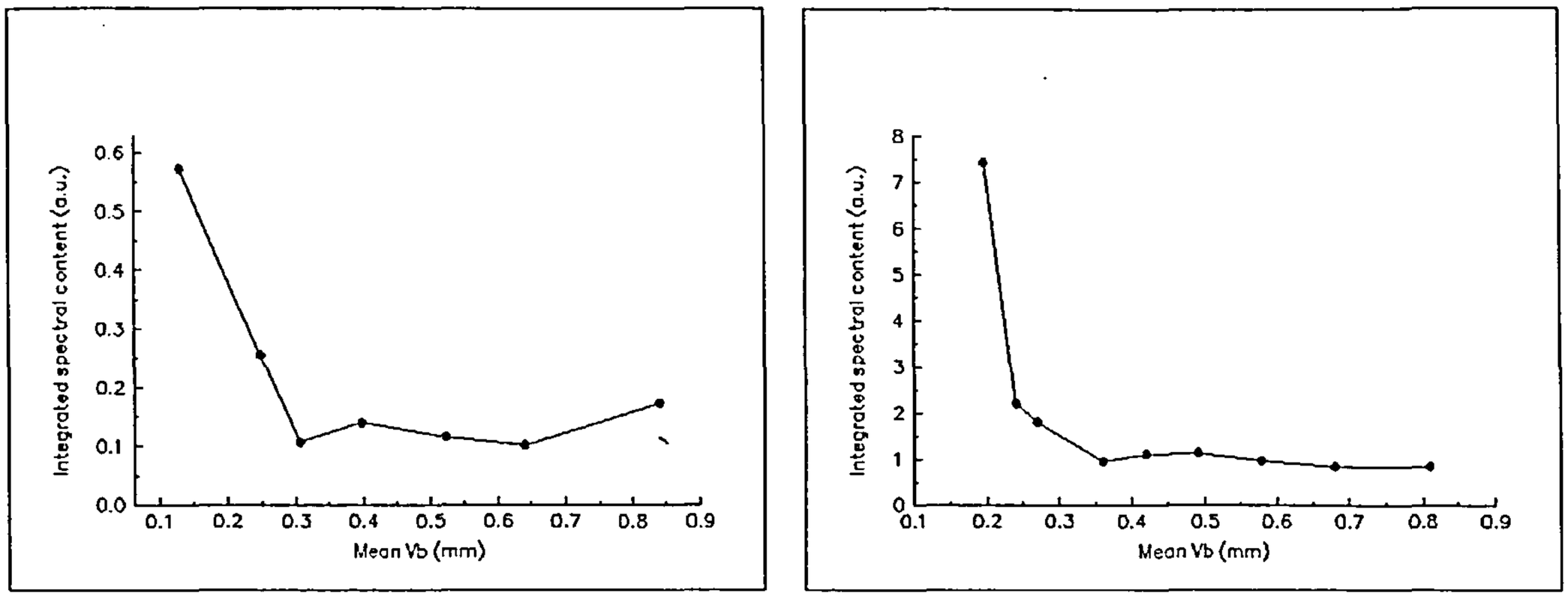

(a) (b)

Figure 6.13 Variation in integrated spectral content of rms AE signal with mean V_b when cutting annealed En24 a) positive rake cutting b) negative rake cutting

Although this parameter shows variation with insert wear before the cutter enters the medium wear stage it is unable to detect wear towards the end of the life of the cutter. It is of interest to note the similarities between these figures and figures 6.4d and 6.6b which show the variation of relative dispersion of the rms AE signal with insert wear for the same experiments. Since the spectral content of the rms AE signal shows no correlation with tool wear at large values of insert wear it will not be considered further in this work.

6.2 Frequency Analysis

Conventional piezo-electric AE transducers suffer from several disadvantages when used to measure AE signals from which spectral information is to be extracted. In order to improve sensitivity, these transducers are resonant in the frequency range of interest in AE measurement (60 kHz to 1 MHz). Thus they are unable to reproduce accurately AE signals to which they are subjected as the signal which they generate will be contaminated by the frequency response of the transducer. Since they require to be in intimate contact with some part of the machine tool on which they are deployed, the signal generated by these transducers is affected by variations in acoustic coupling between the machine tool and the transducer. These variations can arise from irregularities in the surface condition at the transducer location, changes in the amount of coupling fluid used and even subtle variations in the amount of pressure used to mount the sensor on the machine tool [6.12]. The transmission path between the site of the AE generation and the AE transducer will

also alter the nature of the signal generated by the transducer. This arises because the elastic waves which are the mechanical AE signal are subject to reflections and refractions at each mechanical interface through which they pass en route to the transducer. Most of these effects can be removed or mitigated by means of deconvolution techniques. In order to achieve this, the impulse response of the transducer may be measured by means of a pencil lead break test occurring at the tool tip. The signal generated by the transducer is then transformed into the frequency domain to give the impulse response of the transducer/transmission medium system. This may be deconvolved in the frequency domain from AE signals generated by the cutting process hence removing the unwanted aspects of the AE signal. The arrangement of the transducer/transmission path/tool system should thereafter remain undisturbed for this method to be effective. In processes such as milling which involve several moving sources of AE generation this technique is clearly impracticable. In this work the workpiece was also dismounted from the machine tool at various intervals in order to preserve the milled surfaces for later analysis as described in chapter 5. This resulted in changed transmission paths for the AE waves when new workpieces were mounted in the machine tool and in changed transmission characteristics resulting from differing tightening torques being applied to the vice holding the workpiece. As a result of this it was decided that the data obtained from interferometric AE transducer described in chapter 4 would provide more reliable results in frequency analysis than would the piezo-electric transducer. In what follows the graphs are produced using data from this source.

6.2.1 Data Acquisition and Processing

The unprocessed AE signals from the fibre optic transducer were recorded at full bandwidth using a fast data acquisition card mounted in a PC. The data acquisition card was operated at a sampling rate of 5 MHz and the full memory depth of 128 kbyte of the card was used. This enabled samples of unprocessed AE of duration 26.2 ms to be taken throughout the tool life. An FFT algorithm was used to obtain the frequency spectrum of these samples. The 128 kbyte samples were divided into 16 samples of length 8 kbyte and the spectrum of each of these sub-samples was calculated before the spectrum of the signal was produced by averaging over the 16 sub-samples. Figure 6.14a shows a typical power spectrum of the AE signal generated by a new tool and figure 6.14b shows a

typical power spectrum generated from an AE signal produced by a worn tool. In both cases the tool was an eight point negative rake cutter and the workpiece material was annealed En24 steel. The structure observed in the spectra above 600 kHz is related to the instrument noise spectrum as shown in figure 6.14c. The frequency content of the AE signal which is relevant to metal cutting has been identified as being confined to frequencies less than 500 kHz [6.10].

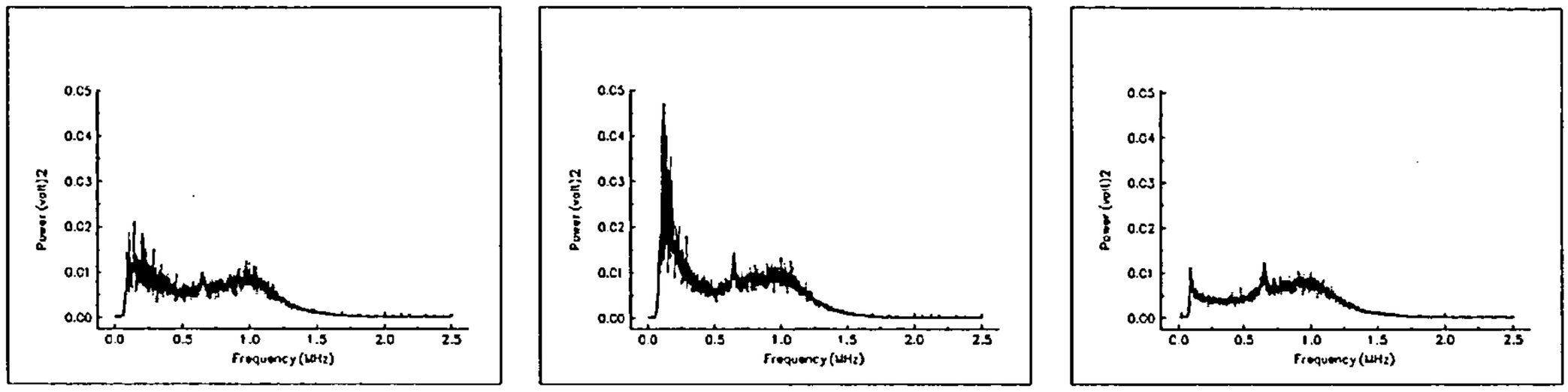

(a) (b) (c)

Figure 6.14 Typical AE spectrum produced by a) new tool, b)worn tool c) instrument noise when not cutting

Clearly changes have occurred in the AE power spectrum between the two wear states depicted here. Carolan et al [6.10] have quantified these differences in terms of the variation of mean frequency of the power spectrum with tool wear. Du et al [6.13] examined the frequency content of AE signals generated in turning and came to the conclusion that frequency effects near 100 kHz were related to shearing or plastic deformation of the work piece and frequency effects near to 300 kHz were due to friction at the tool/workpieces interfaces. They also showed that the non-stationary nature of their recorded signals made it necessary to examine the changes in the AE signal in both frequency and time. However, Rangwala and Dornfeld [6.12] investigated the use of mean frequency and standard deviation of mean frequency in assessing the effects of cutting conditions on AE generation.

The mean frequency f_m of the frequency spectrum was calculated from the expression

$$f_m = \frac{\sum_1^n P_i f_i}{\sum_1^n P_i} \qquad (6.2)$$

where P_i is the power at frequency f_i and n is the total number of points in the spectrum. The standard deviation σ of the AE frequency is given by

$$\sigma = \sqrt{\frac{\sum_1^n P_i (f_i - f_m)^2}{\sum_1^n P_i}} \qquad (6.3)$$

In the following both the mean frequency variation with V_b and the change in standard deviation of frequency with V_b will be examined.

Positive rake cutting of annealed En24

Figure 6.15a shows the variation of mean frequency and of standard deviation of frequency with mean flank wear land length when cutting annealed En24 with an eight point positive rake cutter..

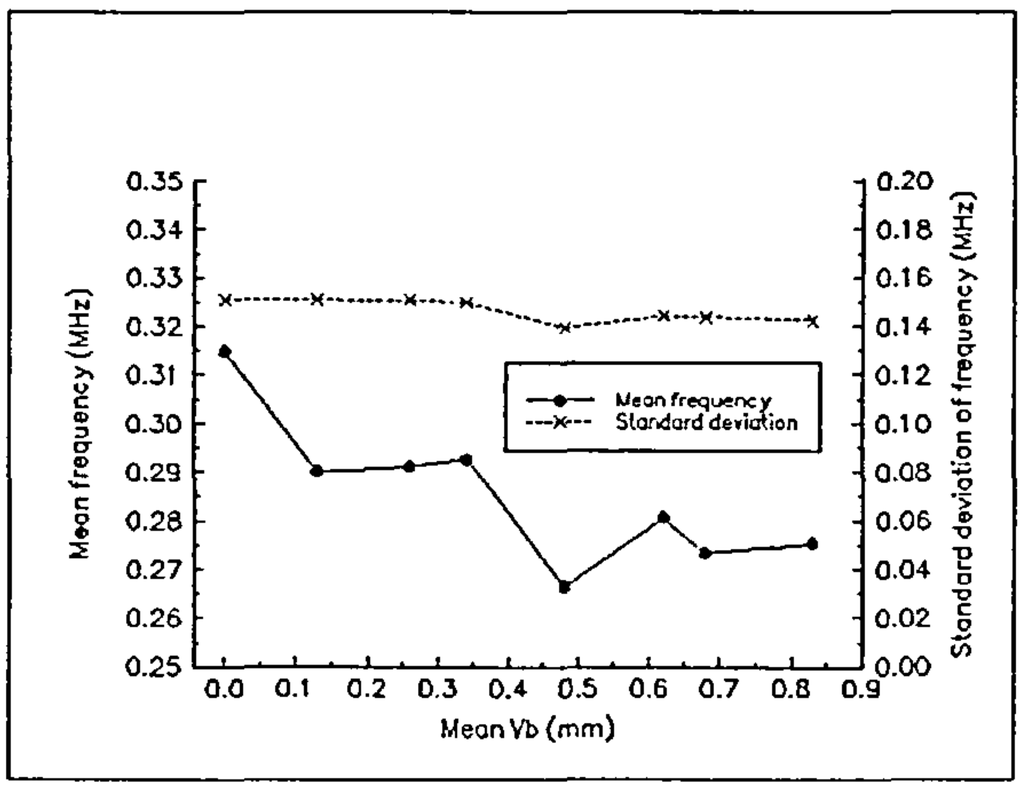

Figure 6.15a Variation of mean frequency and standard deviation of frequency with V_b for positive rake cutting of annealed En24

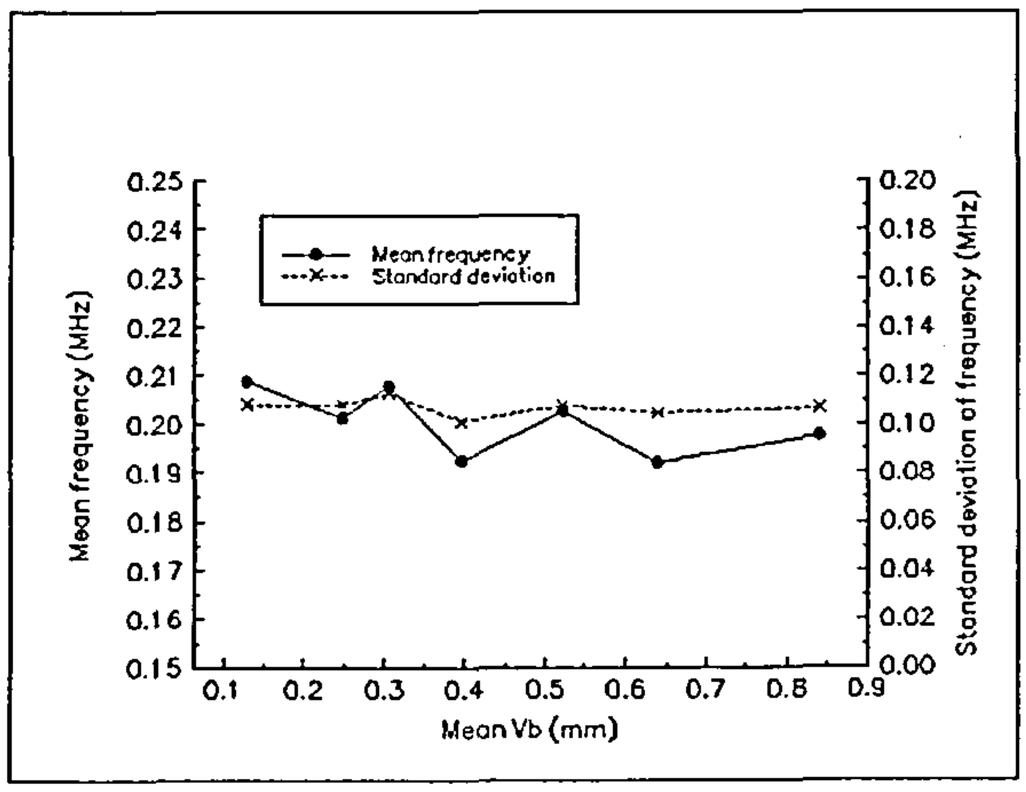

Figure 6.15b Variation of mean frequency and standard deviation of frequency with V_b for positive rake cutting of annealed En24. Second test.

The mean frequency shows a reduction with V_b indicating a movement in signal power towards the low frequency region of the spectrum as the tool wears. The data presented in this figure was obtained in the same set of experiments which provided the data for figures 6.4a and 6.4b. The effects of the chip which was observed at a mean value of V_b of 0.26 mm are evident in the disturbance in the smooth development of the mean frequency curve. The minimum in this graph corresponds to the maximum divergence of the individual flank wear land lengths from the mean flank wear land length suggesting that the mean AE frequency is sensitive to detailed insert geometry in a multi-insert cutter. The standard deviation is insensitive to changes in tool geometry in these experiments.

Figure 6.15b shows the results of a second experiment performed using the same cutting conditions as those employed to produce the data of figure 6.15a. The value of mean frequency shows a reduction over the life of the tool although this is not as marked as in the results displayed in figure 6.15a. The disturbance in the smooth variation of this graph occurs in the region of tool life in which insert chipping was observed. However, the sensitivity to a chipping event is not as clear as in the results presented in figure 6.15a. It can be seen that the standard deviation of frequency exhibits no correlation with the mean length of the flank wear land.

Negative rake cutting of annealed En24

Figure 6.16 illustrates the changes in mean frequency and standard deviation of frequency when cutting annealed En24 with an eight point negative rake cutter. The wear pattern of the inserts was uniform and no chipping events occurred in this experiment.

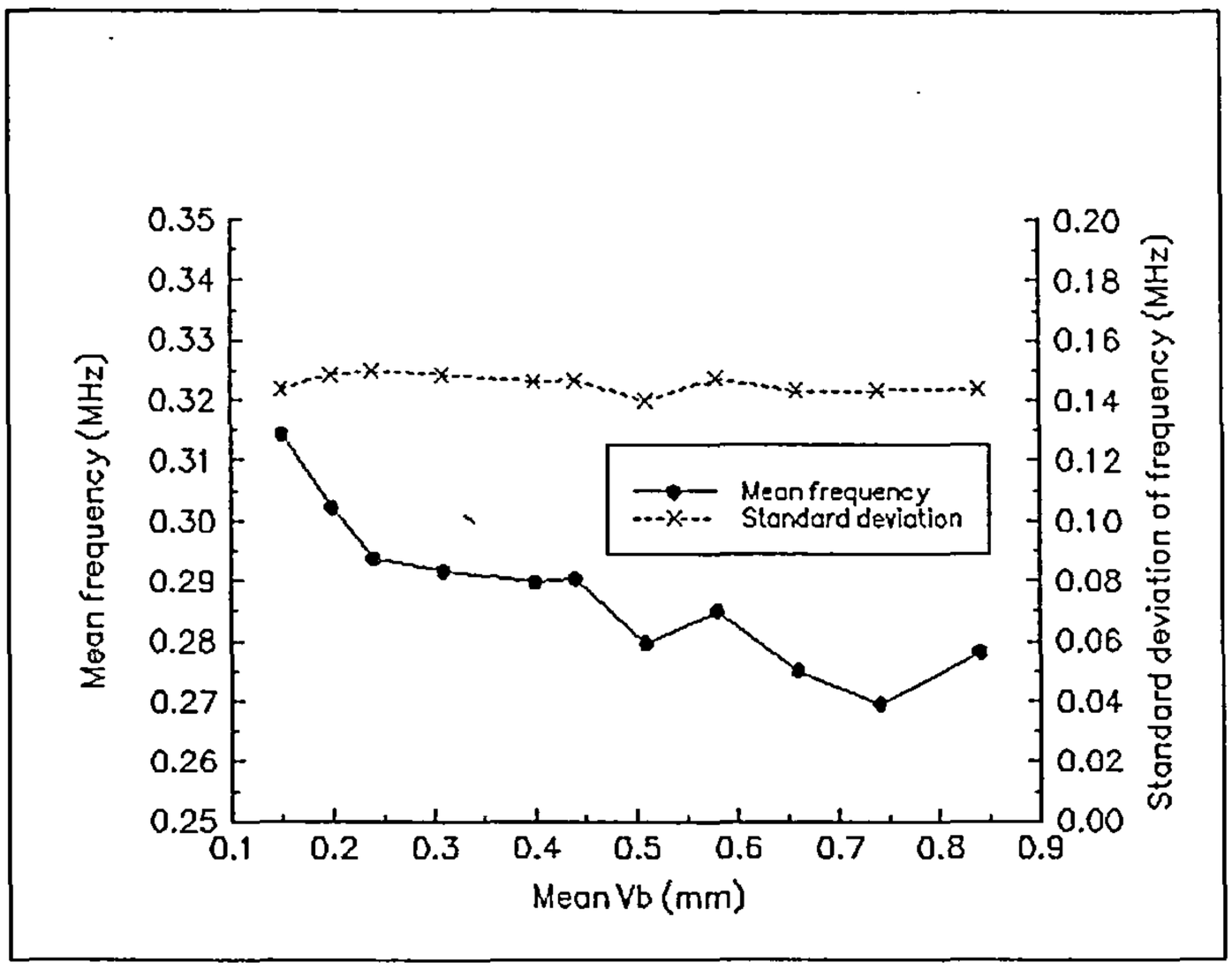

Figure 6.16 Variation of mean frequency and standard deviation of mean frequency with V_b for 8-point negative rake cutting of annealed En24.

It can be seen that the mean frequency exhibits a correlation with mean flank wear land length. The trend is for a reduction in mean frequency indicating a migration of AE power to the low frequency region of the spectrum. As in the previous case there is no relationship between standard deviation of AE frequency and tool wear as measured by the mean length of the cutter flank wear lands.

Figure 6.17 shows the variation of AE mean frequency and standard deviation of frequency with V_b obtained when cutting annealed En24 with a single insert. The trend of the mean frequency curve is to reduce with increasing wear but it is not so marked as in the case of eight point cutting of the same material. The effects of crater break through and edge crumbling which occurred at a value of V_b of 0.3 mm (section 6.1.1) are reflected in the evolution of the mean frequency graph but this is not as clear as in the rms AE data.

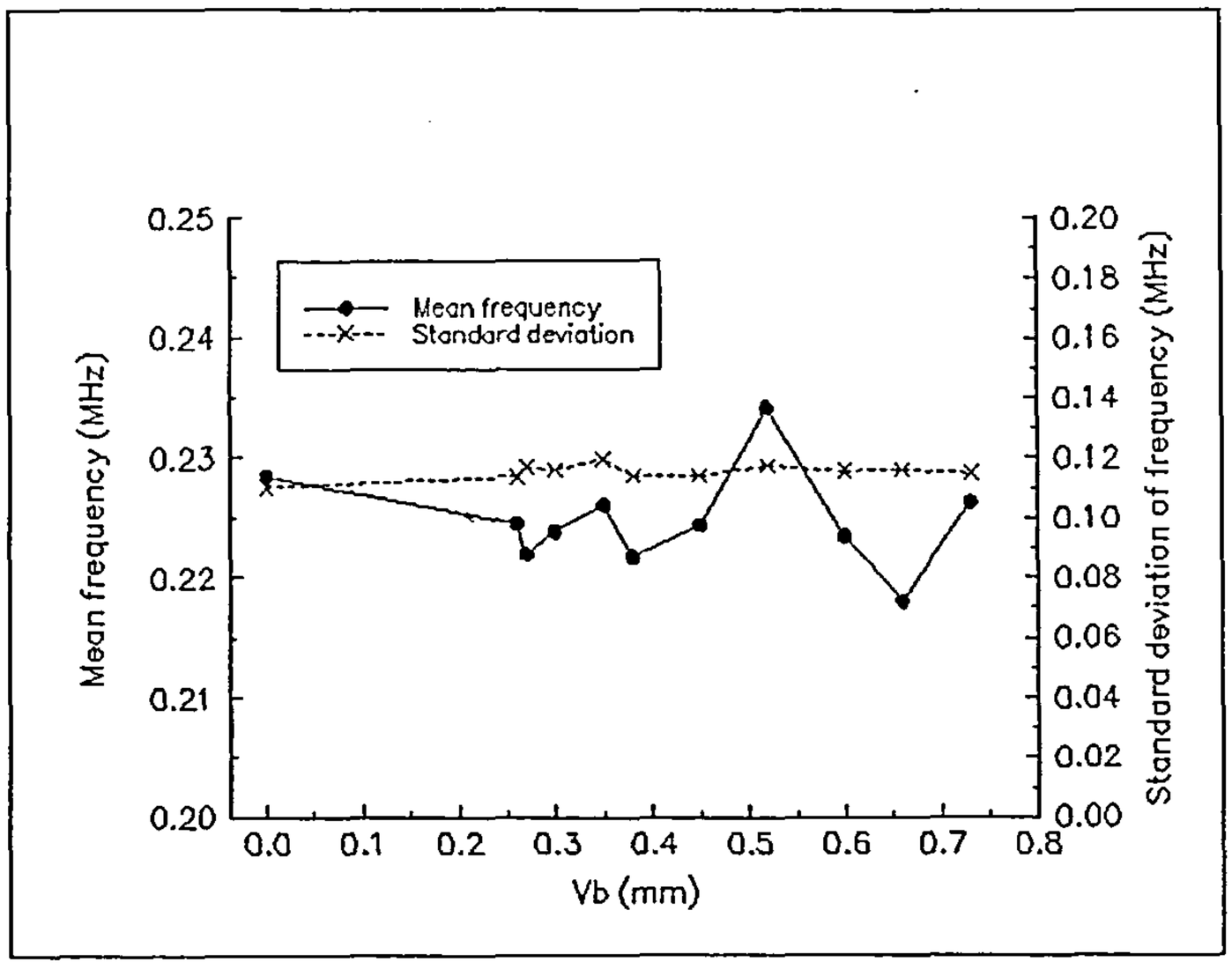

Figure 6.17 Variation of mean frequency and standard deviation of mean frequency with V_b for single point negative rake cutting of annealed En24.

The standard deviation of frequency shows no variation with flank wear land length. This is consistent with observations made in previously described experiments.

Positive rake cutting of quenched and tempered En24

Figure 6.18 shows the results obtained from eight point positive rake cutting of quenched and tempered En24.

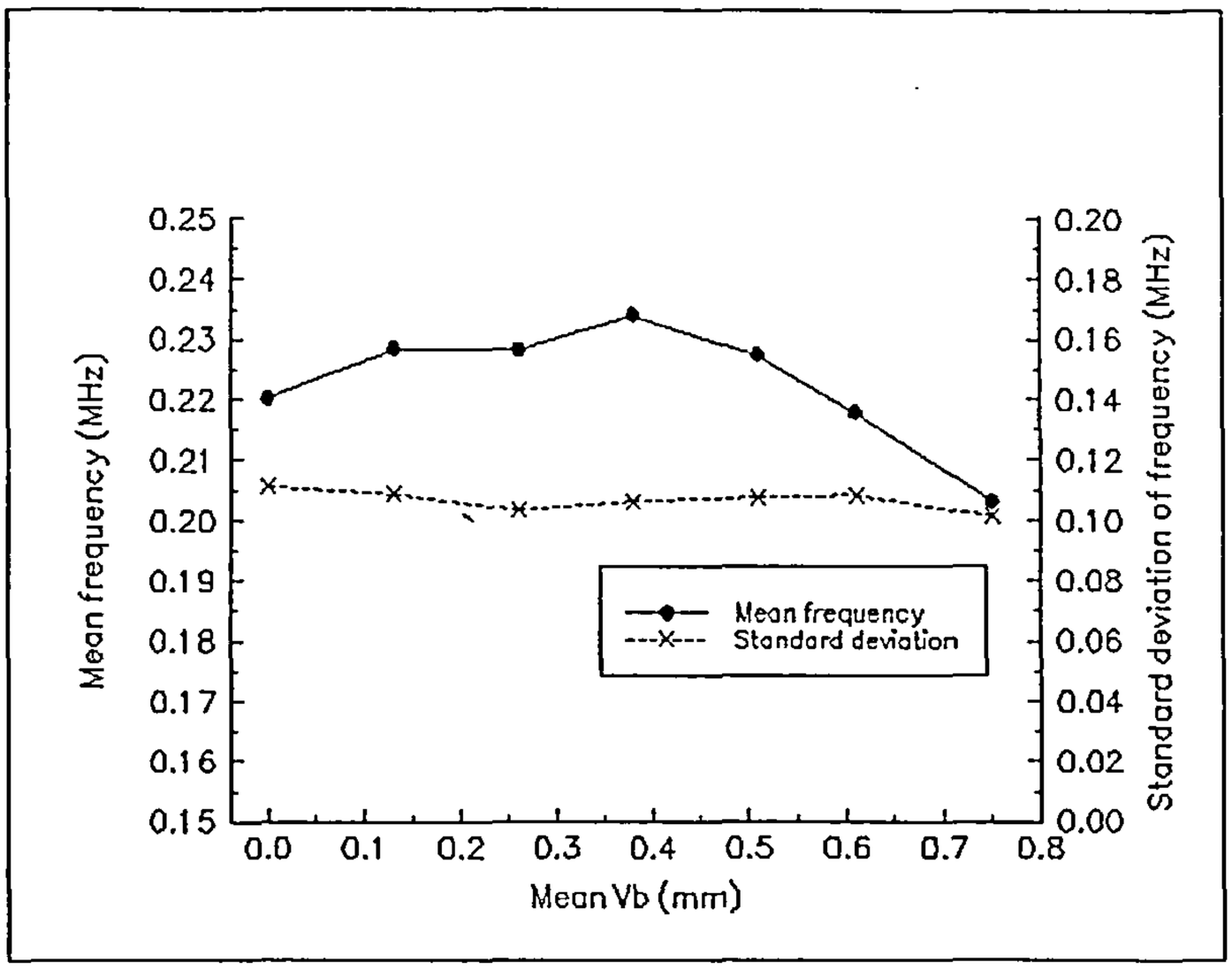

Figure 6.18 Variation of mean frequency and standard deviation of mean frequency with V_b for 8-point positive rake cutting of quenched & tempered En24.

The overall trend of the mean frequency shows a reduction in mean frequency with tool wear as measured by mean flank wear land length. However, unlike results obtained from cutting the softer annealed En24, the mean frequency shows an inclination to increase in the light and medium wear regions of its life until a mean value of V_b of 0.4 mm is reached. The insert chipping which occurred during this test when the mean value of V_b exceeded 0.51 mm (section 6.1.1) is not readily apparent in the graph of mean frequency vs mean V_b.

The standard deviation of frequency again shows little variation with mean flank wear land length.

Negative rake cutting of quenched and tempered En24

Figure 6.19 illustrates the results generated from eight point negative rake cutting of quenched and tempered En24. The mean frequency displays an increase with tool wear which differs from the tendency observed in previously described experiments. Nevertheless there is a similarity between the variation of mean frequency in the early stages of wear when cutting this harder material with a positive rake cutter and the variation observed in figure 6.19. It should be noted that in figure 6.19 the value of mean

V_b does not exceed 0.52 mm whereas the test involving positive rake cutting of this material was terminated when a mean value of V_b of 0.75 mm was achieved.

The standard deviation of frequency shows no variation with tool wear. This is consistent with observations made in other experiments.

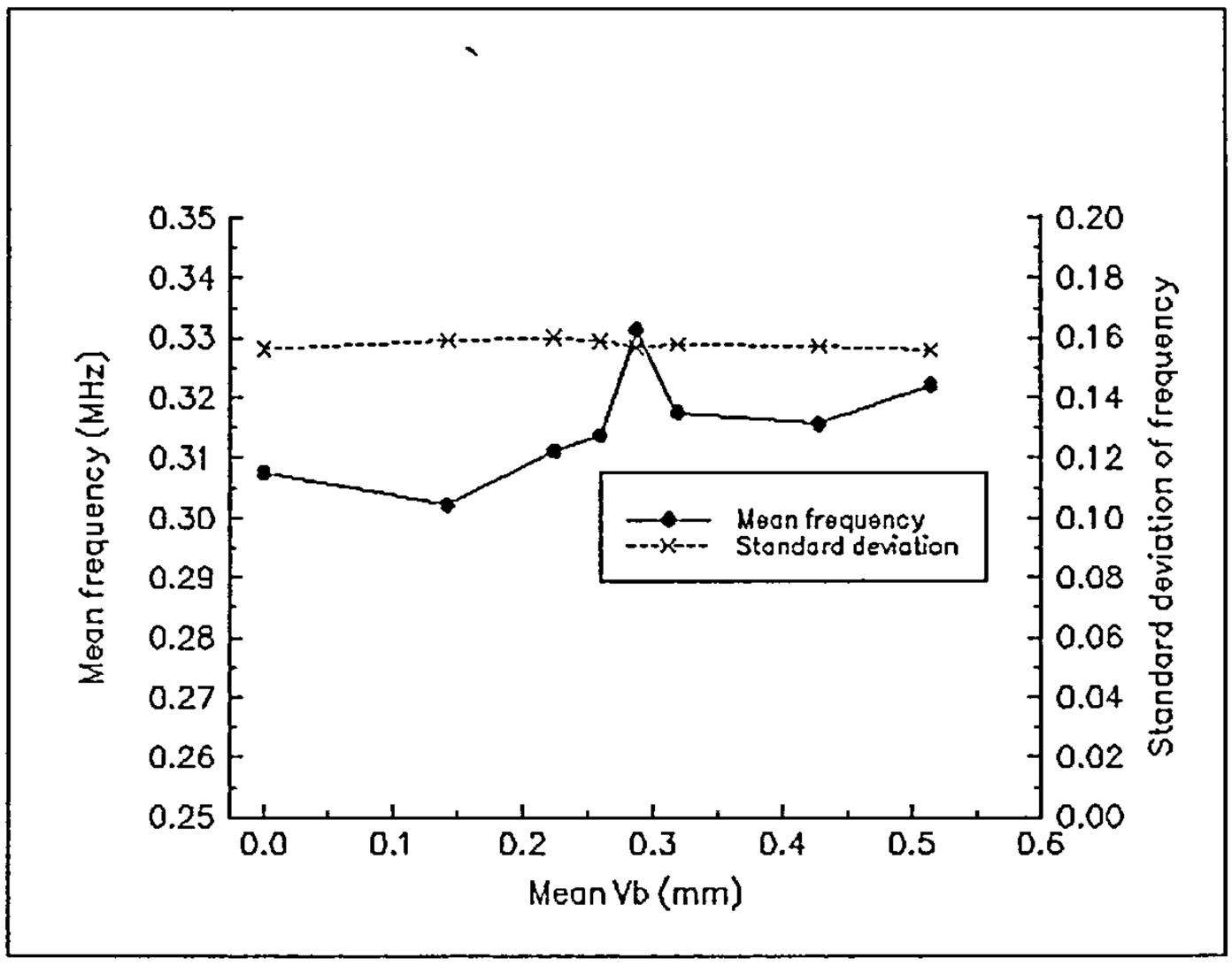

Figure 6.19 Variation of mean frequency and standard deviation of mean frequency with V_b for 8-point negative rake cutting of quenched & tempered En24.

Single point cutting of stainless steel

Figure 6.20 shows the variation in AE mean frequency with flank wear land length for single point positive rake cutting of SS304 stainless steel. In this experiment the mean frequency exhibited a tendency to increase throughout the life of the insert. This was not observed in any of the other experiments although the work involving milling the quenched and tempered En24 demonstrated a tendency for the mean frequency to increase with tool wear in the light and medium stages of wear. This suggests that material properties influence the sense of the change of mean AE frequency and that tool wear affects the magnitude of the changes.

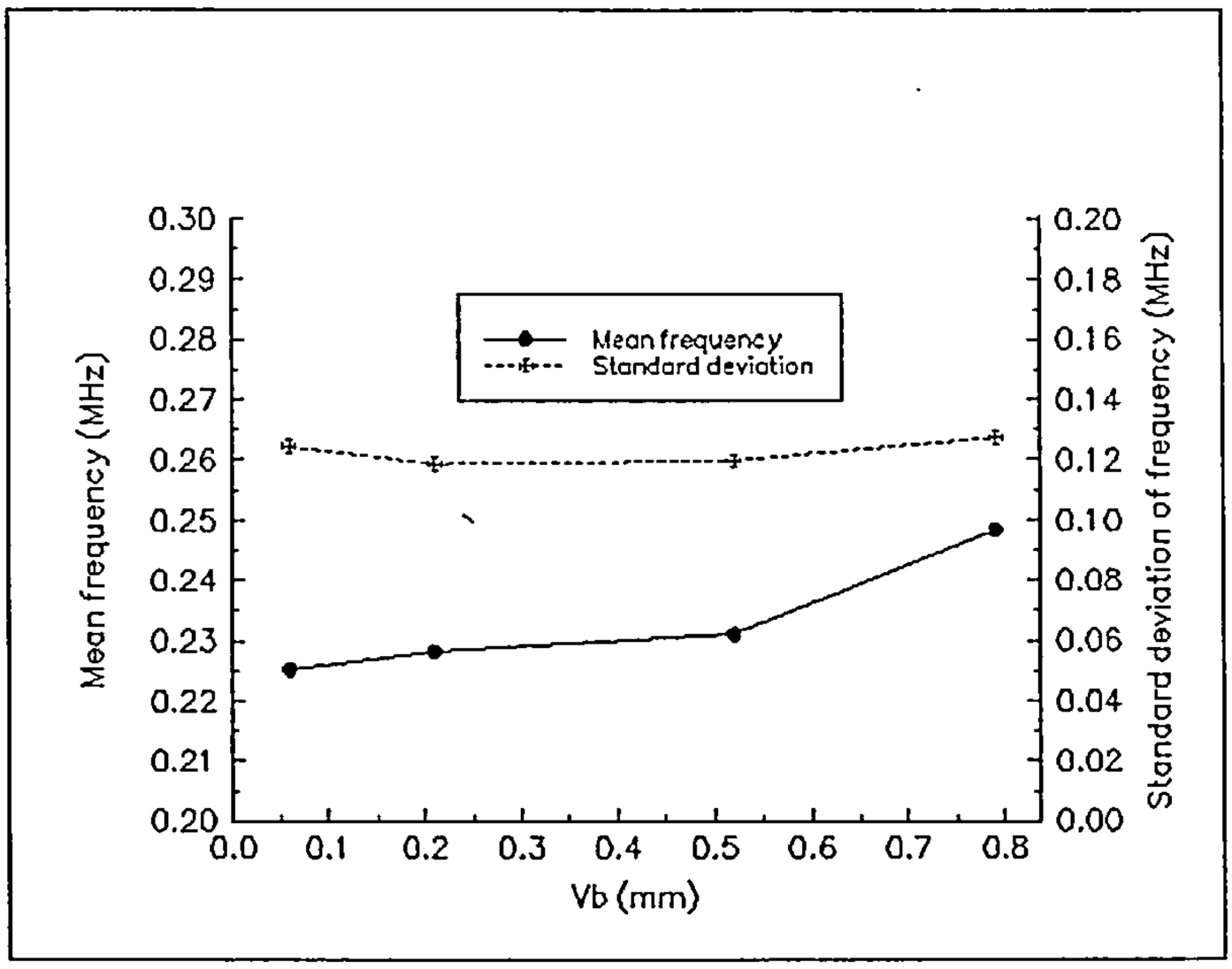

Figure 6.20 Variation of mean frequency and standard deviation of mean frequency with V_b for single point positive rake cutting of stainless steel.

6.3 Frequency-time analysis

Recent work by Jakobsen, Wilkinson et al [6.14] has allowed the acquisition of AE data from individual inserts in a multi-insert cutter. This was achieved through a tool indexer which was attached to the tool holder and which allowed synchronisation of data acquisition to the passage of any selected insert through the workpiece. Figure 6.21 shows the variation of AE mean frequency with data acquisition number for three inserts in the tool holder. This graph shows the results obtained when cutting annealed En24 with an eight point negative rake cutter with a spindle speed of 1200 rev/min corresponding to a cutting speed of 377 m/min. This result is typical of those obtained in this work.

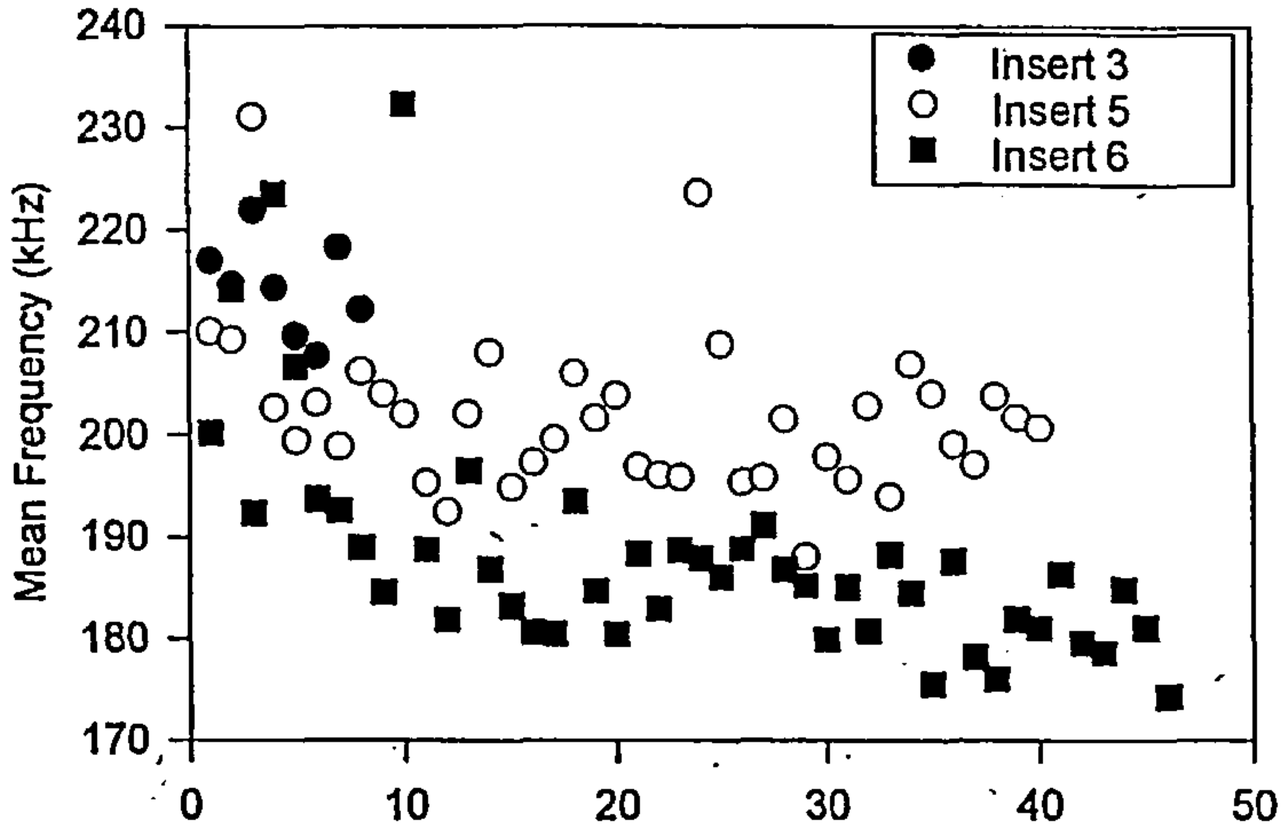

Figure 6.21 Variation of mean frequency with data acquisition number for multi-point milling of annealed En24 with a cutting speed of 377 m/min. Three inserts with different wear land lengths are indicated.

Each of the three inserts denoted in figure 6.21 were characterised by differing wear land lengths. Thus insert 3 started the experiment as a new insert (V_b = 0 mm) and had worn to a V_b value of 0.6 mm at the end of the experiment. The corresponding ranges for inserts 5 and 6 were 0.8 mm to 0.95 mm and 0.98 to 1.14 mm respectively. It is clear from this figure that the trends in the variation of mean frequency with data acquisition for an individual insert mirror those observed for the entire cutter shown in figure 6.16.

We have also carried out a time-frequency analysis of the data obtained from the passage of an individual insert through the workpiece at several stages of wear. This was achieved by moving a rectangular window of width 0.5 ms through the AE data in steps of 0.25 ms and evaluating the frequency spectra at each step. Typical results of this analysis are shown in figures 6.20a and 6.20b for negative rake cutting of annealed En24 at a cutting speed of 192 m/min and depth of cut 0.5 mm. The spectra were divided into six non-overlapping bands of width 50 kHz in the range of significant AE activity of 80 kHz to 380 kHz. The energy in each of these bands was calculated and the four most active bands are shown in figures 6.20a and 6.20b for the period of insert engagement with the workpiece.

Figure 6.22a shows that, when cutting with a relatively new insert (V_b = 0.12 mm), the higher frequency bands (150 kHz to 300 kHz) are significant contributors to the AE signal

during the initial part of the tooth engagement. As the engagement progresses the AE power moves to the lower frequency band (100 kHz to 150 kHz). Figure 6.22b shows that when cutting with a worn insert (V_b = 0.78 mm) significant AE is generated only in the lowest frequency bands (50 kHz to 150 kHz).

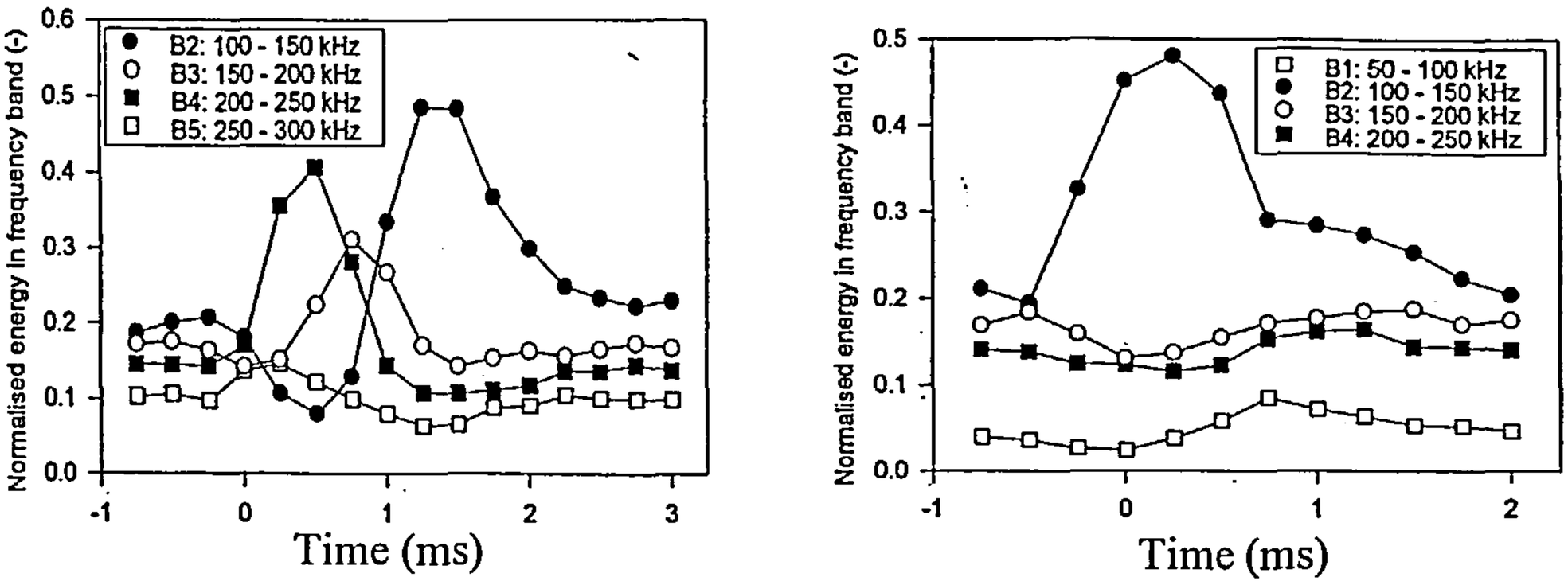

Figure 6.22 Variation of AE frequency content in specified frequency bands during insert engagement (a) New insert with V_b = 0.12 mm (b) Worn insert with V_b = 0.78 mm. Cutting speed = 192 m/min

6.4 Frequency band analysis

It was shown in section 6.3 that the AE content in specific frequency bands would vary with insert wear state. To investigate this further the ratio of the energy content of the AE signal in a low frequency band to that in a high frequency band was considered. Based on the work of Du et al [6.13] and of Jakobsen et al [6.14] the low frequency band was defined as being the range 65 kHz to 155 kHz which is associated with plastic deformation of the workpiece. The high frequency band was defined by the range 155 kHz and 245 kHz which is associated with friction. Figure 6.23a shows the variation of the energy band ratio with mean V_b when cutting annealed En 24 with an eight point positive rake cutter. Figure 6.23b shows the ratio when cutting annealed En24 with an eight point negative rake cutter

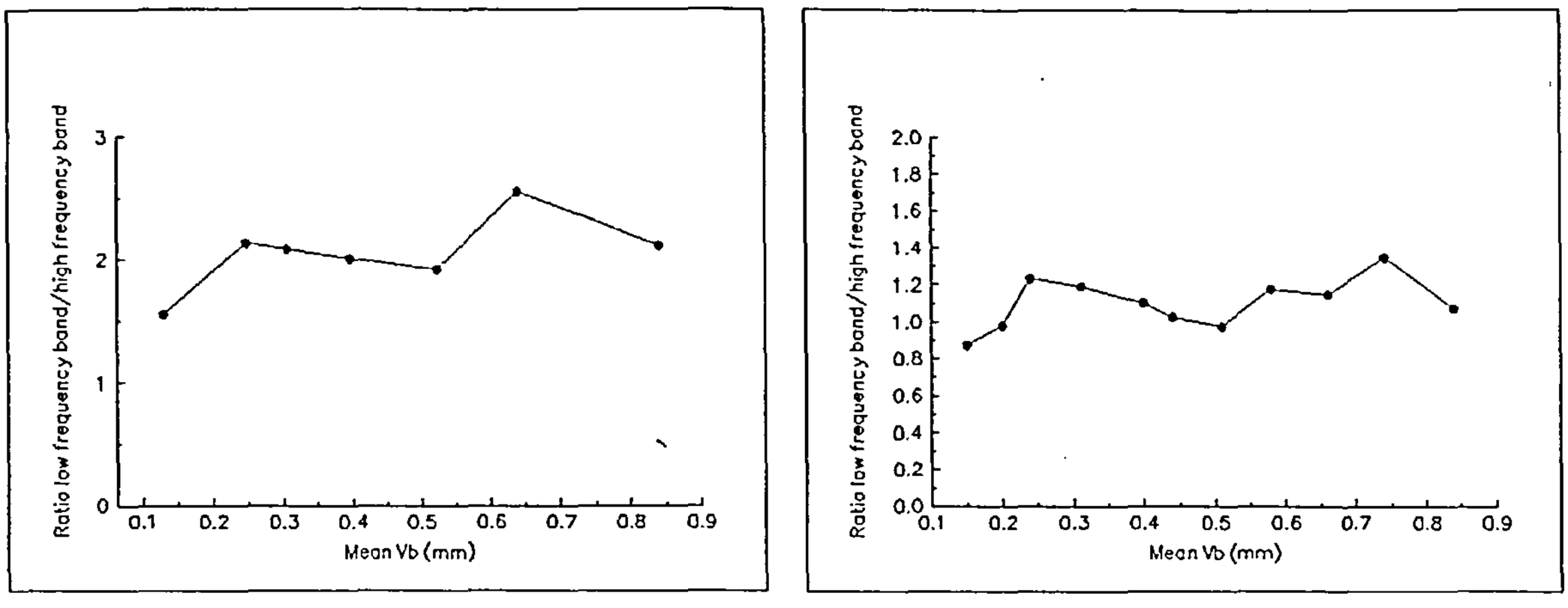

(a) (b)

Figure 6.23 Variation of ratio of low frequency content of AE signal to high frequency content when cutting annealed En24 with a) an 8-point positive rake cutter b) an 8-point negative rake cutter.

It can be seen from these figures that in the case of positive rake cutting a correlation between the frequency band ratio and mean V_b exists although it is weak. A similar although weaker correlation may be discerned when cutting annealed En 24 with a negative rake cutter. This shows that the power in the lower frequency band exhibits a small but progressive increase relative to the higher frequency band as the tool wears. However since these correlations are weak this parameter will not be examined further in this work.

6.5 Conclusions

The results presented in this chapter have shown that, for the range of cutting conditions, materials and insert geometries examined, correlations exist between insert wear and certain properties of the AE signal generated during face milling. These correlations together with those between tool wear and surface profile are illustrated in tabular form in chapter 9.

The long time scale rms AE signal exhibited a relationship to flank wear land length in all the experiments performed although the correlation was rather stronger in the case of negative rake cutting of annealed En24 than in others. In those experiments where insert chipping events took place the rms AE signal was perturbed by those events. In multi-point milling of annealed En24, the rms AE signal proved sensitive to uneven insert wear.

The standard deviation of the rms AE signal indicated the progression of flank wear in the light to medium range of wear ($0<V_b<0.4$ mm) when cutting the softer annealed En24 but not when machining harder materials. The standard deviation was also sensitive to insert chipping although when using quenched and tempered En24 as the workpiece material the sensitivity was weak.

The mean frequency of the AE signal was correlated to flank wear land length although the correlation was weak in the experiments involving fly cutting. Insert chipping events could be related to variations in the mean frequency of the AE signal when positive rake cutting and annealed En24 were used as the cutter/workpiece combination.

The results obtained from the time-frequency analysis show that, when cutting annealed En 24 with a negative rake tool, the mean frequency of the AE signal will progressively move to lower values as insert wear progresses.

It may be deduced from the foregoing that although acoustic emission generated during interrupted cutting may be used to monitor the wear state of the inserts the most useful characteristic of the AE signal to be used varies with workpiece material, cutter geometry and cutting conditions. Therefore it must be concluded that use of only one type of sensor is insufficient to monitor the cutting process.

6.6 References

6.1) J. Roget, P. Souquet and N. Gsib. "Application of acoustic emission to the automatic monitoring of tool condition during machining", Materials Evaluation, 46,(1988), 225-229.

6.2) T. Blum, I. Suzuki and I. Inasaki. "Development of a condition monitoring for cutting tools using an acoustic emission sensor", Bulletin of the Japan Society of Precision Engineers, 22,(1988), 301-308.

6.3) E.N. Diei, D.A. Dornfeld. "Acoustic emission sensing of tool wear in face milling", Transactions of the ASME, Journal of Engineering for Industry, 109,(1987), 234-240.

6.4) E.N. Diei, D.A. Dornfeld. "Acoustic emission from the face milling process - the effects of process variables", Transactions of the ASME, Journal of Engineering for Industry, 109,(1987), 92-99.

6.5) S.S. Cho, K. Komvopoulos. "Correlation between acoustic emission and wear of multi-layer ceramic coated carbide tools", Transactions of the ASME, Journal of Manufacturing Science and Engineering, 119,(1997), 238-246.

6.6) V. Messaritis and W.K.D. Borthwick. "Processing acoustic emission signal data for characterising cutting tool wear and chip management", Proceedings of the International Conference on Computer-Aided Production Engineering, Edinburgh, April 1986, pp 261-268.

6.7) C.R. Heiple, S.H. Carpenter, D.L. Armentrout and A.P. McManigle. "Acoustic emission from single point machining: Source mechanisms and signal changes with tool wear", Materials Evaluation, May 1994, 590-596.

6.8) T.A. Carolan, D.P. Hand, J.S. Barton, J.D.C. Jones, P. Wilkinson, R.L. Reuben. "Assessment of tool wear in milling using acoustic emission detected by a fiber-optic interferometer", Transactions of the ASME, Journal of Manufacturing Science and Engineering, 118,(1996), 428-433.

6.9) T.A. Carolan, S.R. Kidd, D.P. Hand, S.J. Wilcox, P. Wilkinson, J.S. Barton, J.D.C. Jones and R.L. Reuben. "Acoustic emission monitoring of tool wear during the face milling of steels and aluminium alloys using a fibre optic sensor. Part 1: energy analysis", Proceedings of the Institution of Mechanical Engineers, 211,Part B, (1997), 299-309.

6.10) T.A. Carolan, S.R. Kidd, D.P. Hand, S.J. Wilcox, P. Wilkinson, J.S. Barton, J.D.C. Jones and R.L. Reuben. "Acoustic emission monitoring of tool wear during the face milling of steels and aluminium alloys using a fibre optic sensor. Part 2: frequency analysis", Proceedings of the Institution of Mechanical Engineers, 211,Part B, (1997), 311-319.

6.11) T. Blum and I. Inasaki. "Study on acoustic emission from the orthogonal cutting process", Transactions of the ASME, Journal of Engineering for Industry, 112,(1990), 203-211.

6.12) S. Rangwala and D. Dornfeld. "A study of acoustic emission generated during orthogonal metal cutting-2: Spectral Analysis", International Journal of Mechanical Science, 33,(1991), 489-499).

6.13) R. Du, D. Yan, M.A. Elbestawi. "Time-frequency distribution of acoustic emission signals for tool wear detection in turning", 4th World Meeting on Acoustic Emission and 1st International Conference on Acòustic Emission in Manufacturing, The American Society for Nondestructive Testing, Columbus, OH, USA, 1991, pp269-285.

6.14) M.L. Jakobsen, P. Wilkinson, D. Harvey, J.S. Barton, J.D.C. Jones and R.L. Reuben. "The effects of progressive wear on the frequency characteristic of acoustic emission acquired during face milling". In preparation.

Chapter 7

Application of Artificial Neural Networks

The work presented in chapters 5 and 6 has shown that separate correlations exist between cutting tool wear (as measured by the length of the flank wear land) and surface finish characteristics and acoustic emission characteristics. However, there is no universal feature which may be used to identify worn inserts. Indeed much work has been done to investigate the relationship between tool wear and phenomena such as acoustic emission, cutting force, spindle current, insert temperature and machined surface finish as discussed in chapter 2. Although all these techniques demonstrate correlation between the tool wear state and a single measurand none of them used in isolation gives the reliable indication of wear state that is required in a tool wear monitor. Therefore it may be advantageous to consider several of the measured features simultaneously and treat the problem as one of pattern recognition. Such a problem is ideally suited to the application of an artificial neural network which is capable of processing several parameters from multi-sensor inputs.

7.1 Neural networks

An artificial neural network is a set of interconnected computing elements, termed neurons, each of which is designed to mimic the performance of a biological neuron of the type found in the human brain. Therefore it is capable of "learning" to solve simple problems of pattern recognition. Each connection between each neuron has a weighting factor associated with it which represents the degree to which the neural network has learned to solve the problem with which it is presented. Each input to an individual neuron is multiplied by the weighting factor associated with that particular input connection and the weighted inputs are summed by the neuron to produce the *activation level* of the neuron. This weighted sum is further processed by an *activation function* to generate the output of the neuron. The activation function is designed to simulate the operation of a biological neuron in that it is either firing (on) or not firing (off). This device (consisting of inputs, weights, summing unit, activation function and output) is

termed a *perceptron.* As discussed in section 7.1.1 the non-linear activation function may take one of many forms. However it is necessary for the function to be differentiable if the effects of adjusting the network weights is to be calculated. In the training process the weighting factors are systematically adjusted according to a learning rule and thus the neural network can improve its "knowledge" of the problem to which it is applied.

Two types of training rule are available; *supervised* and *unsupervised.* In supervised learning the desired outputs of the neural network are known and are presented to the network along with the training data during the training phase. The neural network weights are adjusted until its actual outputs match the desired outputs. In unsupervised learning the desired outputs are not known and the neural network learns to recognise prominent features in input patterns. This is achieved through a competitive learning strategy which adjusts the network weights in a manner which reinforces the neuron with the largest output. Examples of neural networks which use supervised learning can be seen in *back propagating multi-layer perceptrons*. Examples of unsupervised learning are available as *radial basis function* networks and *self organising Kohonen feature maps*.

The multi-layer perceptron was used in this work and will be discussed in greater detail in section 7.1.1. A radial basis function network adjusts the network weights until they represent the co-ordinates of the centres of the clusters of data within the input patterns. Statistical probability is used to establish to which cluster any particular data point belongs. A Kohonen self organising map adjusts the network weights so that similar input patterns activate the same neuron thus producing a set of output patterns which are related to the clustering characteristics of a set of input patterns.

7.1.1 The multi-layer perceptron

In this work a simple feed-forward, multi-layer perceptron neural network similar to those employed by Wilcox [7.1] and Wilkinson et al [7.2] is trained by means of a back-propagating algorithm. The network has one hidden layer and its architecture is similar to that shown in Figure 7.1. In such a network the flow of information is from the input layer, which simply provides a distribution mechanism to the hidden layer, to the output layer via the hidden layer. There are no means whereby the *signals* may be transmitted backwards through the network and hence this type of network is termed "feed-forward".

The connections between each element (neuron) of the network is associated with a variable weight and it is these weights which are systematically altered in the training process until they converge to steady state values. Thus the input to the i^{th} neuron in the k^{th} layer of the network is given by

$$input(i,k) = \sum_j w_{ij,k}\, output(j,k-1) \qquad (7.1)$$

where $w_{ij,k}$ is the weight between the j^{th} neuron in the $(k\text{-}1)^{th}$ layer and the i^{th} neuron in the k^{th} layer and *output(j,k-1)* is the output of the j^{th} neuron in the $(k\text{-}1)^{th}$ layer.

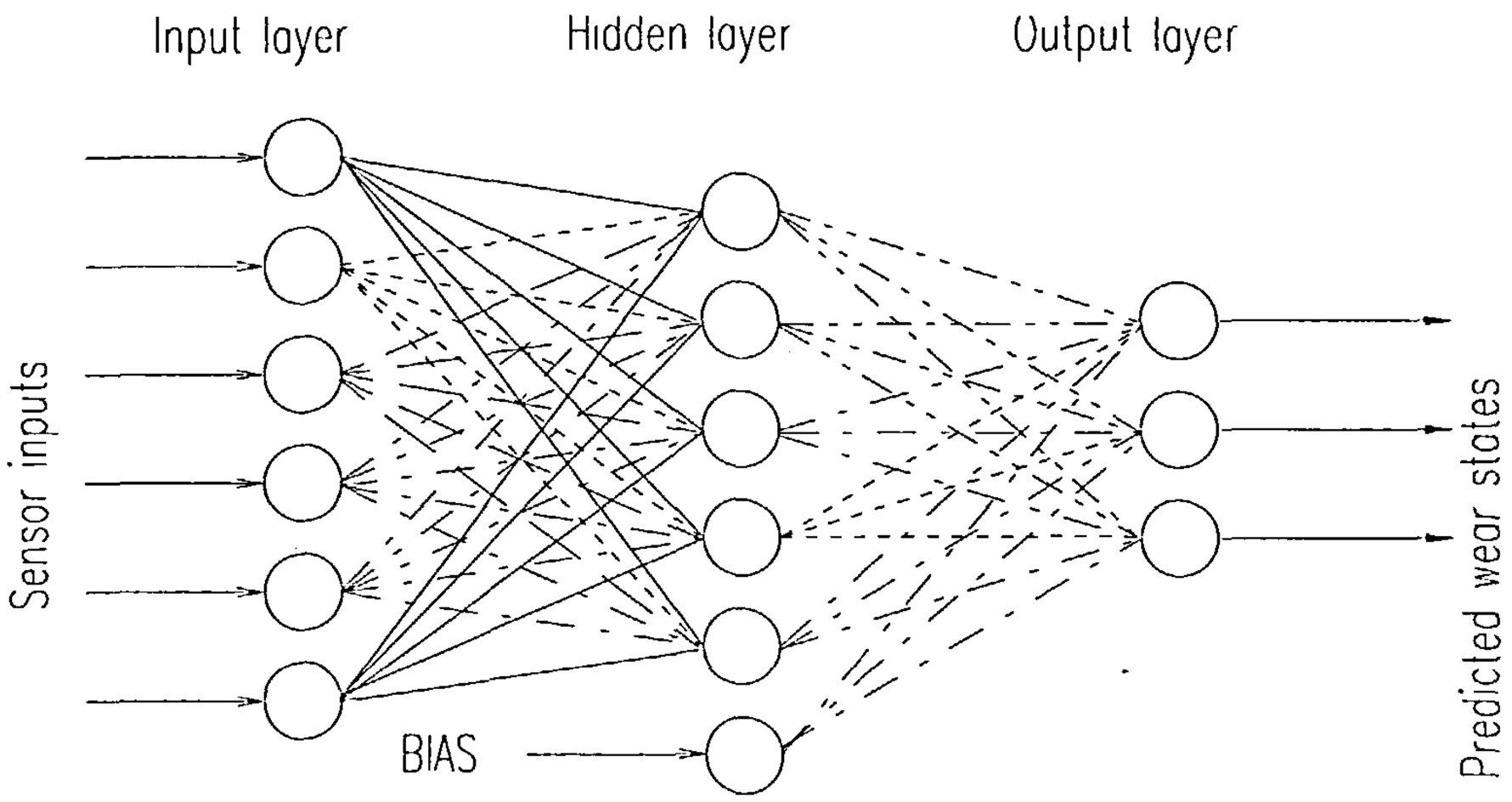

Figure 7.1 Neural network architecture for tool wear monitoring.

The output of an individual neuron may be mechanised in several ways. Threshold (bang-bang) functions, sine functions and hyperbolic tangent functions have all been used [7.3], [7.4]. However the most commonly used activation function is the sigmoid function. Hence the output of the i^{th} neuron in the k^{th} layer is given by

$$output(i,k) = \frac{1}{1+\exp(-input(i,k))} \qquad (7.2)$$

The sigmoid function is shown in Figure 7.2. The reasons for the use of this function are partly historical in that it closely resembles the functioning of neurons in the human brain

[7.3] and considerable confidence and experience in using the function have been accumulated.

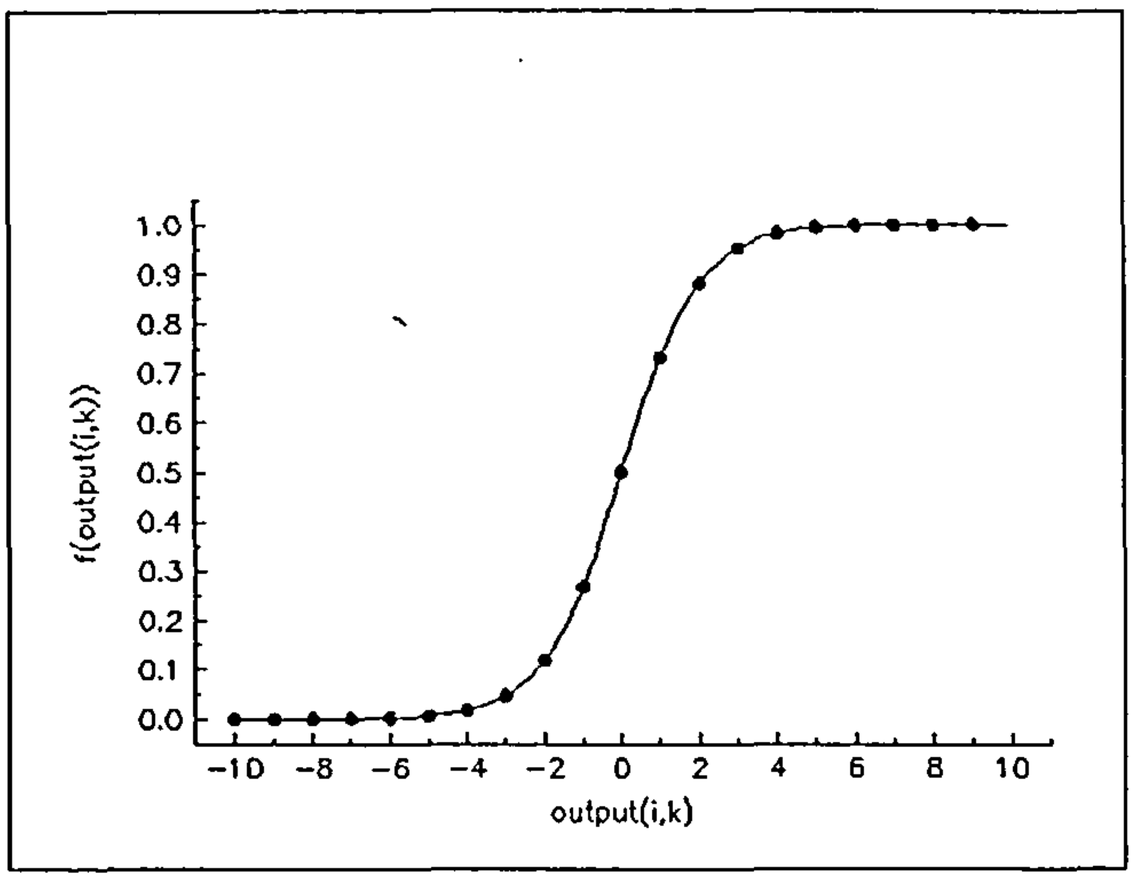

Figure 7.2 Sigmoid function

In order to train the network it is necessary to present it with an input pattern which has been related previously to a known or target output pattern. The signals are propagated through the network according to equations 7.1 and 7.2 and the pattern appearing at the output neurons is compared with the desired or target output pattern. This allows an error, *E*, to be calculated from

$$E = 0.5\sum_{n}\left(t(i)-a(i)\right)^2 \tag{7.3}$$

where n is the total number of neurons in the output layer, *t(i)* is the target value of the i^{th} output layer neuron and *a(i)* is the actual value of the i^{th} output layer neuron. This exercise is repeated for all input/target pattern combinations in the training data set and the individual errors are summed to compute the global error for the network. The objective of the training scheme is to adjust the connection weights of the network so that this error is minimised. This is achieved through a gradient descent on the error.

7.2 Previous applications to tool wear

In general, artificial neural networks have been used in tool wear monitoring to classify sensorial data as being generated by new or worn tools. It may be argued that in a tool

wear monitoring environment it is sufficient to identify a "worn tool" rather than attempt to predict, for example, the precise value of the length of the tool flank wear land. Clearly to try to make this prediction in a multi-point cutting situation would be impractical.

Rangwala and Dornfeld [7.3] used supervised training to enable a back propagating neural network to differentiate a new tool from a worn tool during a turning process. They used cutting force and AE features as inputs to the neural network thus demonstrating that several disparate sensors may be integrated via a neural network to recognise tool wear state over a range of cutting conditions. Also in turning, Lee et al [7.5] have reported some success in predicting flank wear from a ratio of cutting force components, using a back propagating multi-layer perceptron.

Elanayar and Shin [7.6] applied a radial basis function neural network to the problem of predicting flank wear and crater wear in turning from measurements of cutting force. This work examined data from both computer simulations of the cutting process and experimental data taken from cutting tests. The network employed in this work showed a greater ability to predict flank wear than crater wear.

Leem et al [7.7] have shown that a customised neural network which makes use of a self organising Kohonen feature map and an input feature scaling algorithm can successfully classify tool wear data into new, part worn and fully worn states in a turning process. The network in their work was presented with features extracted from force signals and AE signals. The technique allows operation in an unsupervised training mode and on-line monitoring of tool wear which removes the necessity for off-line feature extraction associated with other types of neural network.

As discussed above most of the work involving the application of neural networks to tool wear monitoring has been limited to single point tools. The more complex problem of predicting tool wear in the milling process has not been as widely investigated. Ko and Cho [7.8] have modelled cutting forces using an autoregressive model applied to experimental data. They have shown that a neural network can identify the autoregressive parameters obtained from this model as being due to a fresh tool or a used tool.

Wilcox [7.1] used a multi-layer neural network trained by a back propagating algorithm to predict progressive wear in a milling cutter. He employed features extracted from spindle

current, rms acoustic emission and cutting force as the inputs to the neural network. He also used features associated with the rms AE signal generated from individual inserts to monitor short term events such as tool breakage.

In the majority of examples examined above the features presented to the neural networks have been derived from cutting force and rms acoustic emission measurements. This may be attributed to the availability and reliability of sensors for measuring force and acoustic emission. However in finishing milling where cutting forces are small, variations in cutting force resulting from tool wear may be difficult to measure and features depending on these forces would change only slowly requiring protracted learning times for the neural network. Whilst rms AE measurements may be used in indicating tool wear it has been shown in chapter 6 that they are not sufficiently reliable to monitor the cutting process in its entirety. In order to overcome these limitations Wilkinson et al [7.2] used features extracted from rms AE signals, raw AE signals and surface finish measurements together with a back propagating neural network to improve tool wear monitoring techniques.

7.3 Application to multi-point milling.

In this work a back-propagation algorithm was used to train a feed-forward artificial neural network in a manner identical to that described in section 7.1. The features presented to the neural network were derived from the experimental data discussed in chapters 5 and 6. The features selected were:

1) Surface finish integrated spectral content in the low spatial frequency spectral band (below spindle rotational frequency).

2) Surface finish integrated spectral content in the kinematic spatial frequency spectral band (from spindle rotation frequency to tooth passing frequency).

3) Surface finish integrated spectral content in the high spatial frequency spectral band (above tooth passing frequency).

4) Mean frequency in the raw acoustic emission signal averaged over the range 90-600 kHz.

5) The long time scale rms AE signal.

Although aspects of the variation of fractal dimension of the machined surface with tool wear were discussed in chapter 5 it was shown that neither the divider fractal dimension nor the structure function fractal dimension were sufficiently sensitive to wear state to be included in the features selected. In chapter 6 it was shown that standard deviation of the rms AE signal was sensitive to the mean length of the flank wear land up to lengths of approximately 0.4 mm. However, for advanced wear states with V_b greater than this value, the rms AE signal became almost invariant with flank wear and thus this parameter would make no contribution to prediction of heavy wear states. As the ultimate purpose of a tool wear monitoring scheme is to indicate the end of tool life it was considered that inclusion of this parameter as a feature for the neural network would increase the computational complexity of the scheme with no substantial gain in performance. Therefore it was not included in the features selected.

7.3.1 Network training

The five features selected were normalised to their respective maxima and presented to the neural network as training data. This procedure was performed for each of the cutter/workpiece material combinations described in chapters 5 and 6 separately. In each case the target vector for the neural network was made up of the predefined tool wear states: light wear, medium wear and heavy wear. The definition of these states is shown in table 7.1.

Target 1	Target 2	Target 3	Wear state	V_b range
1	0	0	Light	0 - 0.3 mm
0	1	0	Medium	0.3 - 0.5 mm
0	0	1	Heavy	> 0.5 mm

Table 7.1 Definition of target vector wear states.

This table displays the desired output values of the output neurons of the neural network shown in Figure 7.1. Thus a set of extracted features can be associated with a required target vector through the measured value of V_b.

The training process employed presented the five normalised features and associated targets, at random, to the neural network for a total of 96000 iterations. On each occasion

the weights on each nodal input were adjusted to cause convergence between the predicted and required target vectors. Following each iteration a local error defined as the distance between the required target vector and the predicted vector was calculated and displayed. After 96000 iterations this local error was consistently less than 3×10^{-2}. During the 96000 iterations the weights on each nodal input were recorded every 4000 iterations from which it was confirmed that the weights had converged to their steady state values at the end of the process. At this point it was considered that the neural network was trained and would be able to recognise tools exhibiting any of the three wear states.

The relative contributions of the surface finish features and the acoustic emission features to the complex inter-relationship between tool wear, surface finish and acoustic emission were assessed by separately training the neural network on two sets of reduced features. The network was presented with the surface finish features in isolation and with the acoustic emission data again in isolation. The architecture of the neural network remained unchanged during these training experiments from that used in training on the full feature set. The unused input nodes were presented with zeros. The training period required for the network to be fully functional using these reduced feature sets was prolonged since the information contained in the sets was degraded compared with the full sets. A total of 380 000 iterations was required before convergence of the interconnection weights was achieved.

7.3.2 Network testing

As an elementary precaution the training data were presented to the trained neural network input to verify that the network could recognise these data with errors of less than 3×10^{-2} in each of the three wear states.

The neural network was tested by presenting it with a new set of normalised extracted features associated with known target vectors. The known target vectors were defined by the limits shown in table 7.1. The actual output vector predicted by the neural network was compared with the required target vector. Table 7.2 illustrates the comparison of the target vector with the actual output vector when the neural network was trained and tested on surface finish features and acoustic emission features generated during eight point face

milling of annealed En24 with a negative rake cutter. The training data matrix for this experiment consisted of 27 sets representing a series of feature/target combinations. In each cell of table 7.2 the upper figure represents the required neural network output for the given wear state and the lower figure is the actual output of the neural network for that wear state. Thus row 1 of this table shows that when the value of V_b lies in the range 0 to 0.3 mm (the light wear range according to table 7.1) the required target vector was (1,0,0) but the actual vector was (0.998,0,0.995). The implications of this are discussed below.

Wear State	Light	Medium	Heavy	V_b range
Target	1	0	0	0 mm to 0.3 mm
Actual	0.998	0	0.995	
Target	1	0	0	
Actual	0.157	0.183	0.205	
Target	1	0	0	
Actual	0.980	0.011	0.006	
Target	0	1	0	0.3 mm to 0.5 mm
Actual	0.003	0.766	0.154	
Target	0	1	0	
Actual	0	0.182	0.886	
Target	0	1	0	
Actual	0	0.632	0.543	
Target	0	0	1	greater than 0.5 mm
Actual	0	0	1	
Target	0	0	1	
Actual	0	0	1	
Target	0	0	1	
Actual	0	0	1	

Table 7.2 Comparison of predicted and desired neural network output vectors for negative rake eight point cutting of annealed En24. Note: this information is presented graphically in the form of the performance indicator defined by equation 7.4 in Figure 7.5c

Examination of the data presented in table 7.2 shows that the neural network correctly identified a worn tool state on all occasions in this experiment. This can be seen from the final three rows of the table where the predicted and required output vectors are identical. It can also be observed that where the neural network mis-classifies an input pattern it does so usually in a manner which denotes a heavier state of wear than was actually the case. This occurs, for example, in row 5 of table 7.2 thus suggesting that the neural network would predict tool wear conservatively.

Clearly there are test patterns which are insufficiently differentiated for the neural network to make a valid prediction as to tool wear state shown, for instance, in row 2 of table 7.2. Similarly there are test patterns which show that the is unable to predict precisely the state of wear of the cutter but errs towards a conservative prediction as in row 1 of table 7.2. Whilst this information is available in table 7.2 and others like it for experiments using other cutter/workpiece material combinations, a graphical representation of the neural network performance is desirable to aid in interpretation of its predictions. The graphical display was achieved through the medium of a performance indicator which is defined in the following. The actual output value on an individual output neuron was replaced by its proportion of the total network output summed across all three output neurons. A weight was assigned to each of the output neurons depending on the known wear state of the cutter. A neuron predicting the correct wear state was assigned a weight of +1. A neuron predicting a heavier wear state than the actual wear state was assigned a weight of 0. This may be justified by accepting that although the prediction was incorrect, it would be acceptable in a monitoring system. A neuron predicting a lighter state of wear than the actual wear state was assigned a weight of -1 since such a prediction would not only be incorrect but would be unacceptable in a tool wear monitoring system. For each test of the neural network a *performance indicator* (PI) was defined by

$$PI = \sum_{j=1}^{3} w_j q_j \qquad (7.4)$$

where w_j is the weight associated with output neuron j and q_j is the proportion of total network output on neuron j. The performance indicator could then be used to assess the ability of the neural network to predict the state of tool wear reliably. The criteria upon which the judgement was made were:

$0.5 \leq PI \leq 1.0$	correct prediction
$-0.5 < PI < 0.5$	unable to predict
$-1.0 \leq PI \leq 0.5$	incorrect prediction

A similar series of tests was carried out using the neural network when it had been trained on the reduced data sets. The network was presented with an appropriate set of normalised

extracted features representing either surface finish information or acoustic emission information as required.

7.4 Neural network test results

7.4.1 Eight point positive rake cutting of annealed En24

Figures 7.3a, 7.3b and 7.3c show the change in performance indicator when cutting annealed En 24 with an eight point positive rake cutter. Figure 7.3a shows the change in performance indicator when the network was presented with surface finish features in isolation, Figure 7.3b shows the change when it was presented with acoustic emission features in isolation and Figure 7.3c shows the change in performance when the network was presented with the full set of surface finish and acoustic emission features. From these figures it can be seen that, despite prolonged training, significant errors are generated by the neural network when it is presented with surface finish data alone. From Figure 7.3a the neural network is unable to recognise a medium state of wear from surface finish data alone. Indeed it mis-classifies these patterns into a lighter state of wear than actually existed. However it does generally identify a heavy state of wear from these features. As shown by Figure 7.3b, the use of acoustic emission features alone presents the network with difficulties in recognising a heavy wear state but it has a marginally improved performance in detecting light and medium states of wear. It also mis-classifies one test pattern into a lighter state of wear than that which was known to be correct.

This light/medium wear mis-classification, which is also apparent in Figure 7.3a, coincides with an insert chipping event. The presence of a chipped insert would disturb the smooth evolution of tool wear and would increase the likelihood that a wear state would be mis-classified. In this example the mean length of the flank wear land was 0.26 mm which was very close to the decision boundary for the light/medium wear classification of 0.3 mm shown in table 7.1. Thus a further source of uncertainty could be introduced into the predictions of the network.

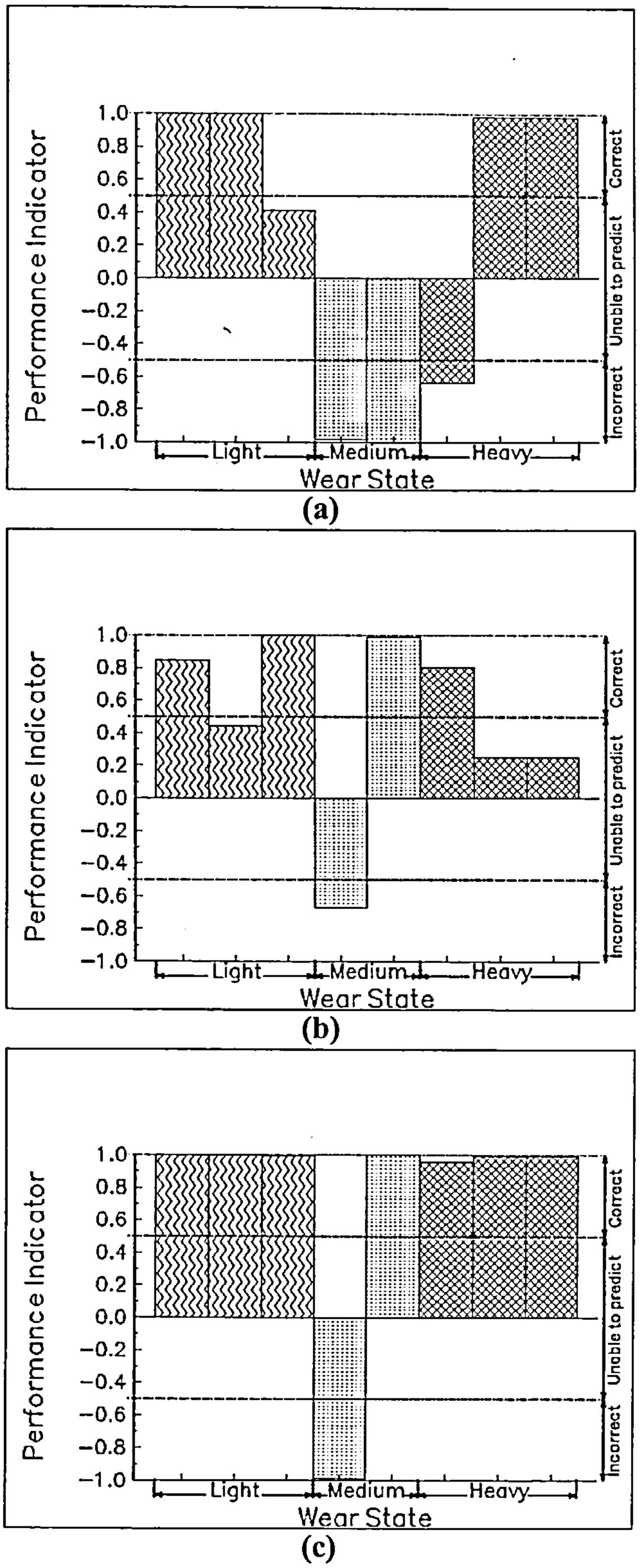

Figure 7.3 Performance indicator vs wear state when cutting annealed En24 with an 8-point positive rake cutter: (a) surface finish only; (b) acoustic emission only; (c) surface finish and acoustic emission.

Figure 7.3c demonstrates the improvement in performance of the neural network when presented with both surface finish and acoustic emission features. The single incorrectly

classified pattern again corresponds to the chipped insert with a flank wear land length close to the light/medium wear decision boundary discussed in the previous paragraph. As stated the boundaries selected for classification into light/medium wear states and medium/heavy wear states are arbitrary and a strong possibility exists that the neural network would classify features corresponding to this particular wear state as light wear. This suggest that in order to recognise a cutter with chipped inserts, the neural network should be specifically trained using features generated by chipped inserts as shown by Wilcox [7.1].

7.4.2 Eight point positive rake cutting of annealed En24 (second data set)

Figures 7.4a, 7.4b and 7.4c show the performance of the neural network when trained on a second set of data corresponding to eight point positive rake cutting of En24. Figure 7.4a shows that the neural network was unable to distinguish light or medium states of wear when presented with surface finish data in isolation but that it could consistently identify worn tools from these features. Figure 7.4b shows the performance of the neural network when presented with acoustic emission features alone. The neural network could detect a medium wear state reliably from these data but both light and heavy wear were not consistently recognised. The performance of the network using the reduced data sets was such that the mis-classified patterns were not placed in a lower wear state than the true wear state. However only the surface finish data gives a reliable indication of a worn tool. The individual flank wear lands were characterised by considerable variations in appearance when the training data for this test were collected making measurement of individual values of V_b complex. This would have affected the determination of the target vectors for any particular test thus leading to confusion in the light/medium stages of wear. Insert chipping occurred during this experiment when the mean value of V_b had reached a value of 0.4 mm, in the centre of the medium wear classification.

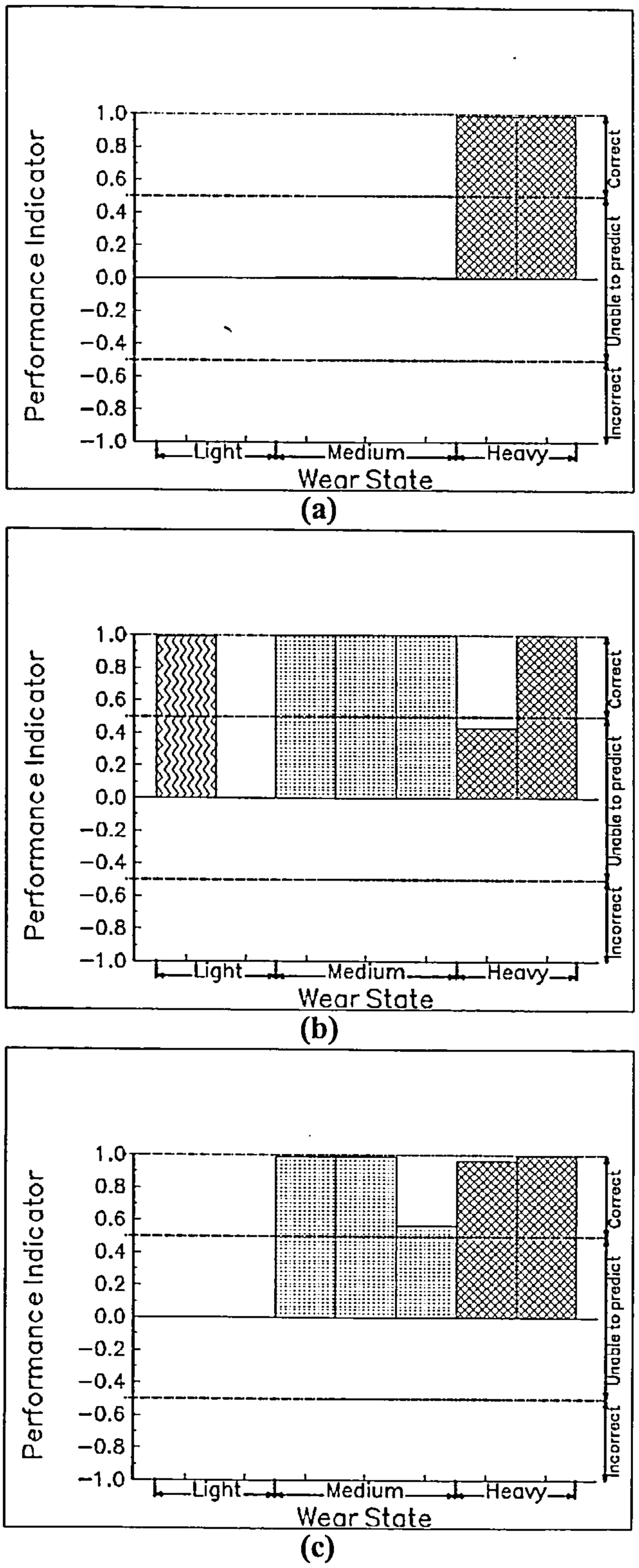

(a)

(b)

(c)

Figure 7.4 Performance indicator vs wear state when cutting annealed En24 with an 8-point positive rake cutter: (a) surface finish only; (b) acoustic emission only; (c) surface finish and acoustic emission. Second experiment.

Although the effects of insert chipping were visible in the evolution of the features presented to the neural network before they were normalised (figures 5.13, 6.4 and 6.13)

they were insufficiently disruptive to affect the prediction of tool wear by the network. Again for the neural network to be truly sensitive to insert chipping it would have to be trained on the appropriate set of features.

Figure 7.4c demonstrates the improvement in performance of the neural network when presented with both surface finish and acoustic emission data. As can be seen from this figure the neural network has difficulty in recognising lightly worn tools however it does identify medium and heavily worn tools accurately.

7.4.3 Eight point negative rake cutting of annealed En24

Figures 7.5a, 7.5b and 7.5c display the performance when the neural network was trained and tested on data generated from multi-point negative rake cutting of annealed En24. Figure 7.5a demonstrates that surface finish features are unaffected by tool wear until the tool is heavily worn, the neural network being unable to recognise tools with a light and intermediate state of wear when presented with surface finish features alone. Similarly Figure 7.5b establishes that acoustic emission features presented in isolation cannot be used reliably to predict heavily worn tools. It can be seen that the network will occasionally mis-classify a heavily worn tool pattern as originating from a lighter state of wear following training on AE features alone.

Considerable improvement in the predictive abilities of the neural network when it is presented with both surface finish and acoustic emission features are apparent from Figure 7.5c. The network generally recognises light and medium wear states assigning heavier wear states to those feature patterns which it mis-classifies. Thus it may be seen to be safe in the wear state identifications which it makes. As in the case of positive rake cutting, the network consistently identifies heavily worn tools correctly.

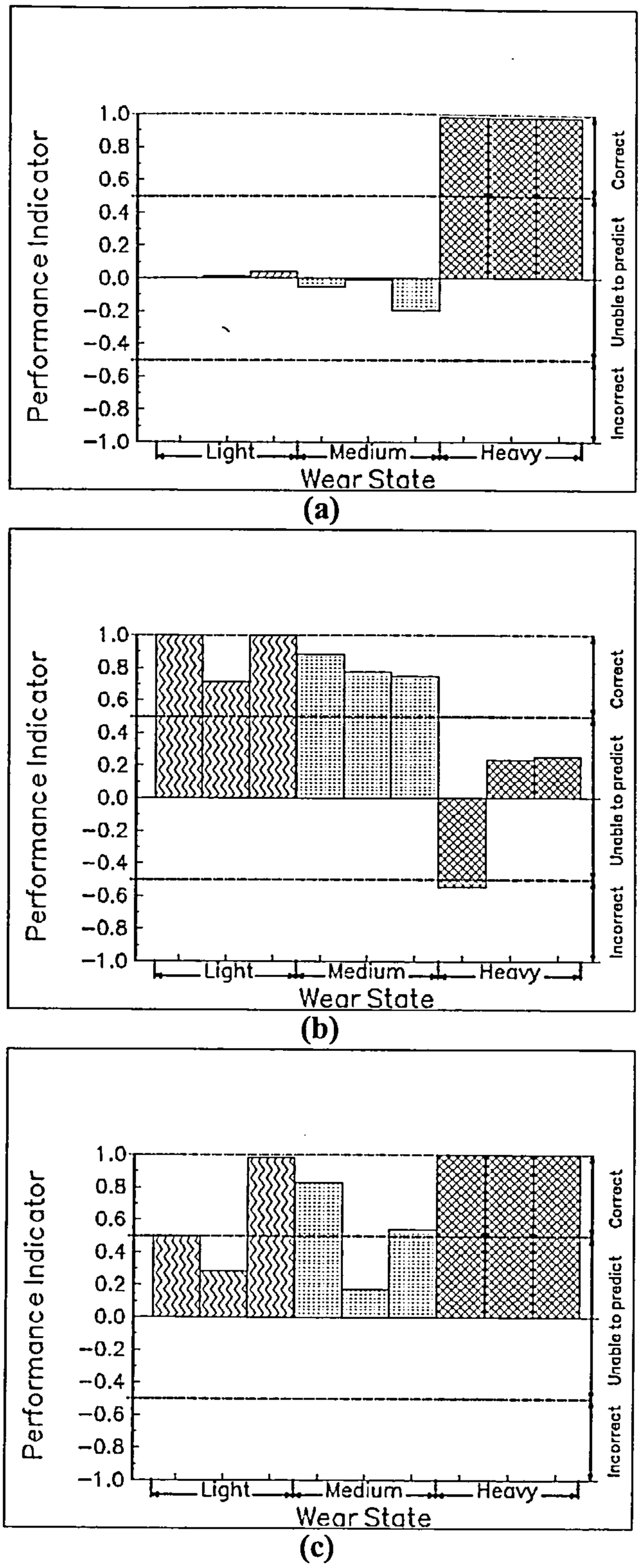

Figure 7.5 Performance indicator vs wear state when cutting annealed En24 with an 8-point negative rake cutter: (a) surface finish only; (b) acoustic emission only; (c) surface finish and acoustic emission.

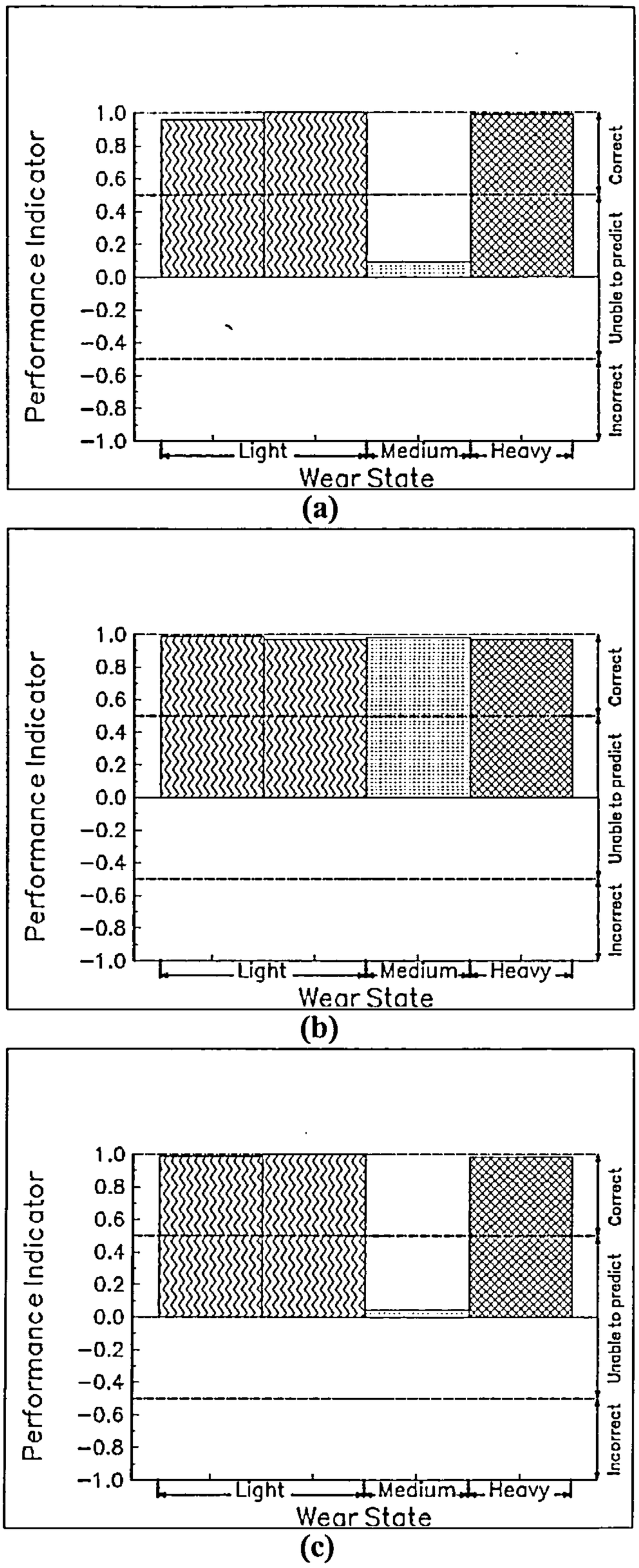

Figure 7.6 Performance indicator vs wear state when cutting annealed En24 with a single point negative rake cutter: (a) surface finish only; (b) acoustic emission only; (c) surface finish and acoustic emission.

7.4.4 Single point negative rake cutting of annealed En24

Figures 7.6a, 7.6b and 7.6c exhibit the variation of the performance indicator with tool wear state when the neural network was presented with features generated in cutting

annealed En24 with a single point negative rake cutter. From figure 8a it may be seen that the neural network has difficulty in recognising the medium wear state from surface finish features alone. However the presentation of acoustic emission features alone results in a consistent recognition of the tool wear state as shown in Figure 7.6b and this would suggest that in this series of experiments AE alone would serve to monitor the wear state. This is confirmed in Figure 7.6c which presents the variation in performance indicator with tool wear state when the network was presented with both AE and surface finish data. It can be seen that the confusion in the features which resulted in mis-classification of the medium wear state when surface finish features alone were used has propagated through to the performance when using a full feature set. The mis-classification of the medium wear state may be explained, in part, by the relatively small training data set which was available for these experiments. This resulted in poor definition of the medium wear state which compromised the ability of the neural network to recognise the medium wear condition.

7.4.5 Eight point positive rake cutting of quenched and tempered En24

Figures 7.7a, 7.7b and 7.7c show the performance indicators obtained when cutting quenched and tempered En24 with an eight point positive rake cutter. Figure 7.7a demonstrates that, in this case, the information contained in the surface finish features alone was insufficiently differentiated to allow the network to recognise either light or intermediate wear in the cutter. As in other cases the heavily worn cutter was recognised consistently. From Figure 7.7b it is clear that the acoustic emission features allowed correct classification of the intermediate and heavy wear states in the cutter but the neural network was not able to distinguish the light wear condition from these features. Combination of AE features and surface finish features did not improve the performance of the neural network as shown in Figure 7.7c. As in the case of single point negative rake cutting this could be partly explained by the small size of the training feature set which resulted in poor definition of the medium wear state. It is also apparent that there is little information in either the surface finish features or the AE features which enabled the neural network to recognise the light wear state.

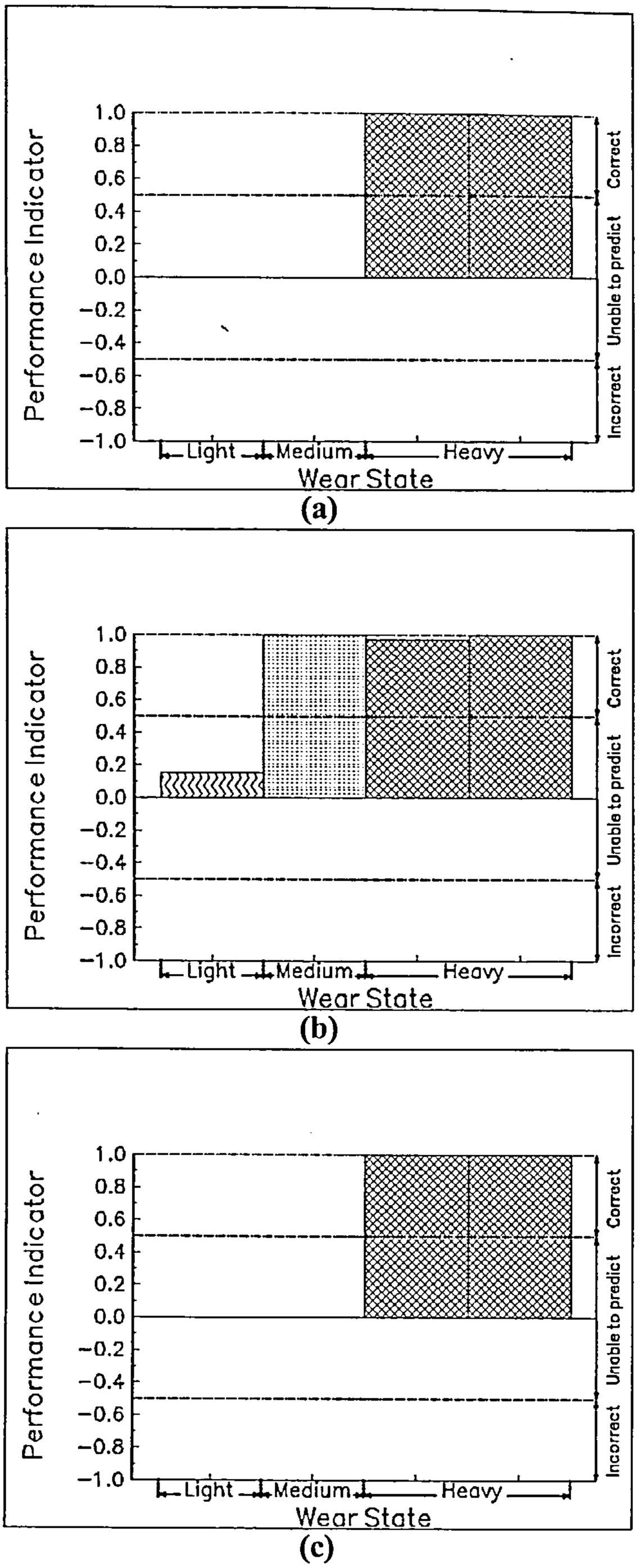

(a)

(b)

(c)

Figure 7.7 Performance indicator vs wear state when cutting quenched and tempered En24 with an eight point positive rake cutter: (a) surface finish only; (b) acoustic emission only; (c) surface finish and acoustic emission.

7.4.6 Eight point negative rake cutting of quenched and tempered En24

Figures 7.8a, 7.8b and 7.8c show the changes in performance indicator with tool wear when the neural network was presented with features derived from cutting quenched and tempered En24 with an eight point negative rake cutter. Figure 7.8a indicates that whilst the neural network was able to recognise a heavily worn tool from surface finish features alone it could not identify light or medium wear states dependably from the same features. Similarly Figure 7.8b suggests that little confidence may be placed in the capacity of the neural network to differentiate any of the wear states reliably when presented with only acoustic emission features from this set of experiments. In particular, the acoustic emission data caused the neural network to underestimate consistently the state of wear of the cutter when it was exhibiting medium wear characteristics. The improvement in performance of the neural network resulting from a combination of acoustic emission features and surface finish features is readily seen from Figure 7.8c. In this case the neural network recognised light and heavy wear states faithfully. The results obtained from the medium wear characteristics were ambiguous in that the network failed to recognise a medium wear state in one set of experiments but did not mis-classify the feature set. It is evident from figures 7.8a and 7.8b that, in this particular experiment, neither the test surface finish features nor the test acoustic emission features contained sufficient information for the neural network to distinguish the true wear state. It may be concluded that this set of features were not representative of the wear state. That the neural network did not classify this data rather than mis-classify it into a less severe state of wear may be taken as indicative of the robustness of the network to faults in the data sets.

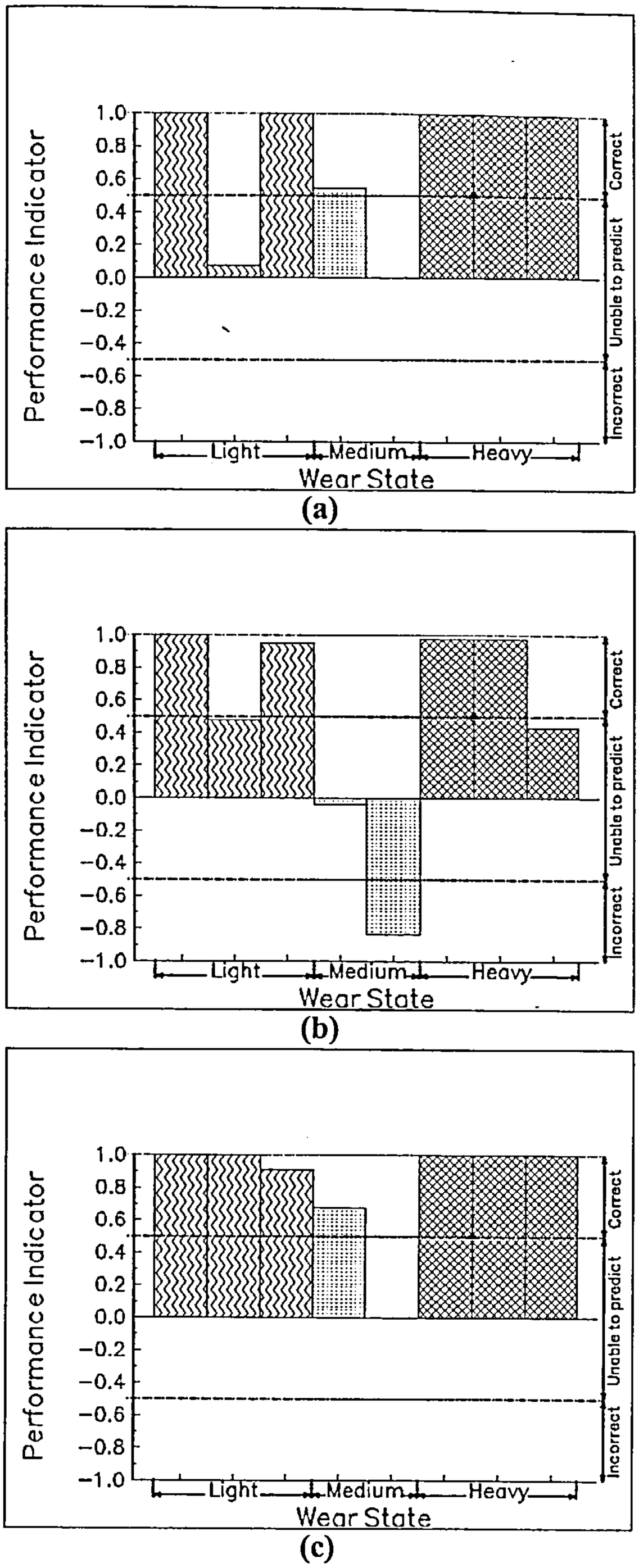

Figure 7.8 Performance indicator vs wear state when cutting quenched and tempered En24 with an eight point negative rake cutter: (a) surface finish only; (b) acoustic emission only; (c) surface finish and acoustic emission.

7.4.7 Single point positive rake cutting of type 304 stainless steel

Figures 7.9a, 7.9b and 7.9c show the performance indicators generated when cutting stainless steel with a single point positive rake cutter. It is evident from Figure 7.9a that

surface finish features alone allow the neural network to classify correctly the insert wear states as either light or heavy but that the medium wear state was incorrectly categorised as light wear. This would be unacceptable in a tool wear monitoring system. The inability of the neural network to predict reliably any of the three wear states in these experiments from AE features alone is demonstrated in Figure 7.9b. Substantial improvement in the performance of the neural network is observable in Figure 7.9c when it is presented with a combination of AE and surface finish features. Although the intermediate wear state has not been recognised it has not been incorrectly classified and the light and heavy wear states have been correctly classified. As in previous examples where a high rate of wear was observed during the experiments, the training data sets in this test was relatively small resulting in poor definition of the medium wear state.

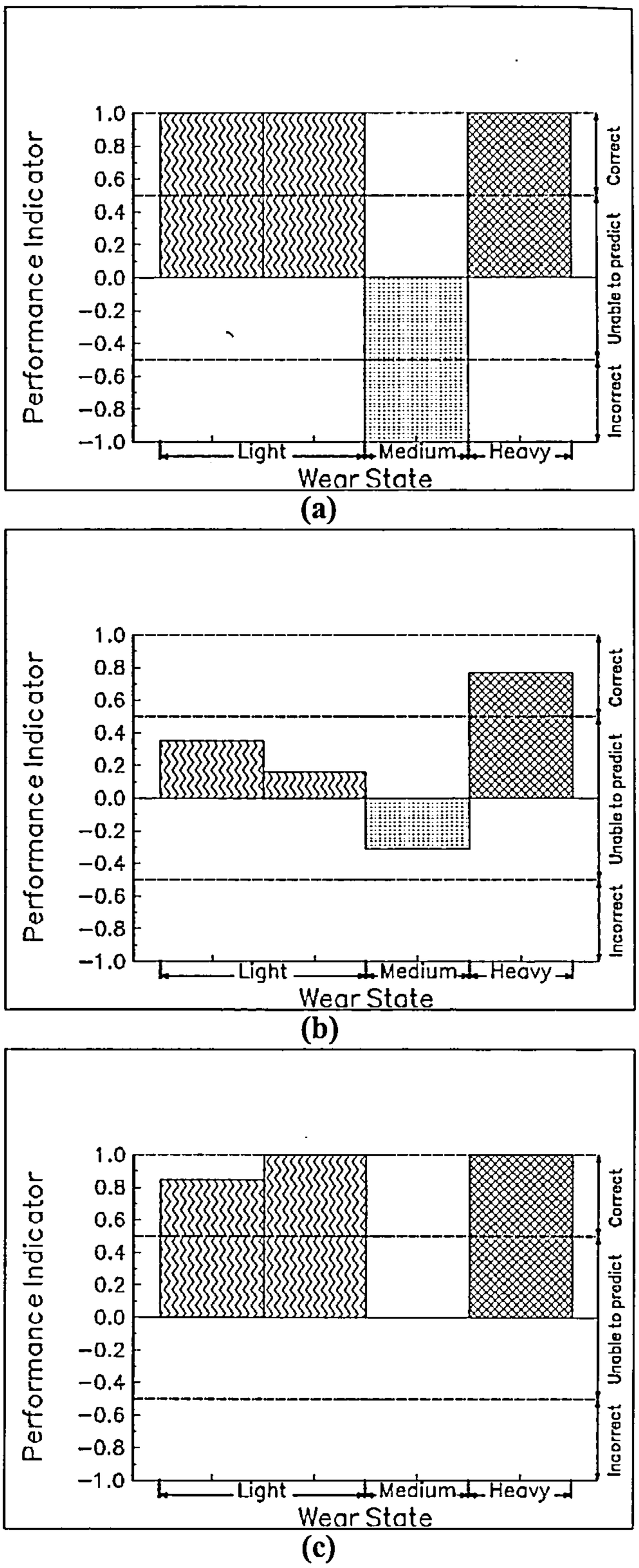

Figure 7.9 Performance indicator vs wear state when cutting stainless steel with a single point positive rake cutter: (a) surface finish only; (b) acoustic emission only; (c) surface finish and acoustic emission.

7.5 Discussion of neural network performance.

It may be seen from figures 7.3a, 7.4a, 7.5a, 7.6a, 7.7a, 7.8a and 7.9a that significant errors are generated by the neural network when operating on surface finish data alone although it is demonstrated that a heavily worn tool can normally be distinguished from other conditions of wear. Similarly, figures 7.3b, 7.4b, 7.5b, 7.6b, 7.7b, 7.8b and 7.9b show that despite extensive training, the neural network does not predict tool wear state reliably when presented with features derived from acoustic emission sources alone. In particular the ability of the network to recognise a heavily worn tool from this reduced data set is limited. Figures 7.3c, 7.4c, 7.5c, 7.6c, 7.7c, 7.8c and 7.9c show the performance of the neural network when presented with surface finish features and acoustic emission features in combination, from which it is apparent that the capacity of the neural network to identify tool wear states has improved. Specifically, the heavily worn wear state was recognised reliably from these feature sets and it may be concluded that the use of surface finish features together with acoustic emission features as inputs to an artificial neural network significantly enhances the potential of such a network to predict tool wear in machining. However there is some variability in the neural network's ability to recognise under all conditions. It may be seen that the light/medium wear states are occasionally mis-classified, but generally these mis-classifications are towards a heavier state of wear than actually existed resulting in pessimistic predictions. The mis-classifications may be explained by the inevitable uneven wear of the inserts during multi-point cutting. The division of wear state into light, medium and heavy was made on the basis of mean flank wear land length and the spread of input feature values would be expected to lead to some mis-classification. This would be particularly apparent when only small or restricted training sets of features were available. In the one case where mis-classification into a lighter state of wear than was known (Figure 7.3c) occurred insert chipping was observed.

In summary, combined surface finish and acoustic emission measurements may be used to predict tool wear successfully in single and multi-point finish face milling. The advantages of using both types of sensor is shown from a comparison of the (a) versions in each of figures 7.3 to 7.9 with the (c) versions where quality control based on surface finish alone would only detect a heavily worn tool. Equally, comparing the (b) versions

with the (c) versions of figures 7.3 to 7.9 shows that use of AE alone is unreliable for tool wear monitoring particularly in heavy states of wear in multi-point cutting.

The reliability of the results is limited by the number of tests which have been performed and a practical system would have to be retrained on the process to which it is to be applied. The most practical way of achieving this would be by using a relatively short learning period supplemented by the tool management system in use by the process operators. It is expected that a system such as that described here could deliver savings in tool changes by allowing cutters to be used closer to the end of life condition. If the use of artificial neural networks were to be extended to other machining processes it is clear that the learning process would have to be performed for each type of cutting or sequence of cutting so that the advantages would only be realised in operations which have a unit of machining which is carried out several times within a tool life or which does not change in nature during tool life.

7.6 References

7.1) S.J. Wilcox. "Cutting tool condition monitoring using multiple sensors and artificial intelligence techniques on a computer numerical controlled milling machine." Ph.D. Thesis, Heriot-Watt University, Edinburgh, 1992.

7.2) P. Wilkinson, R.L. Reuben, J.D.C. Jones, J.S. Barton, D.P. Hand, T.A. Carolan and S.R. Kidd. "Tool wear prediction from acoustic emission and surface characteristics via an artificial neural network", Mechanical Systems and Signal Processing, 13,(1999), 955-966.

7.3) S. Rangwala and D. Dornfeld. "Sensor integration using neural networks for intelligent tool condition monitoring", Transactions of the ASME, Journal of Engineering for Industry, 112,(1990), 219-228.

7.4) R.C. Eberhart, R.W. Dobbins, (editors). "Neural Network PC Tools A Practical Guide", Academic Press, London, 1990.

7.5) J.H. Lee, D.E. Kim and S.J. Lee. "Application of neural networks to flank wear prediction", Mechanical Systems and Signal Processing, 10,(1996), 265-276.

7.6) S. Elanayar and Y.C. Shin. "Robust tool wear estimation with radial basis function neural networks", Transactions of the ASME, Journal of Dynamic Systems, Measurement and Control, 117(1995), 459-467.

7.7) C.S. Leem, D.A. Dornfeld, S.E. Dreyfus. "A customised neural network for sensor fusion in on-line monitoring of cutting tool wear", Transactions of the ASME, Journal of Engineering for Industry, 117(1995), 152-159.

7.8) T.J. Ko and D.W. Cho. "Adaptive modelling of the milling process and application of a neural network for tool wear monitoring", Advanced Manufacturing Technology, (1996), 5-13.

Chapter 8

Discussion

In this chapter the results presented in chapters 5, 6 and 7 will be discussed with reference to the models described in chapter 3. The discussion will be organised into sections which correspond to the chapter headings: surface finish, acoustic emission and the application of artificial neural networks to tool wear monitoring.

8.1 Tool wear effects on the machined surface

8.1.1 The profilometer traces

In chapter 3 it was proposed that the milled surfaces would appear on a profilometer trace as if they had been generated by a statically deflected cutter. As the insert wear increased, the cutting forces and the deflection of the cutter would increase accordingly. This should be reflected as a sawtooth pattern surface which evolves to a steeper profile as wear progresses. Figures 8.1a to 8.1d illustrate the variation in measured profiles obtained from single point negative rake cutting of annealed En24 as insert wear as measured by the length of the flank wear land V_b increased. Each of these graphs shows a portion of the milled surface of length 0.5 mm. The feed employed in this experiment was 0.1 mm per tooth, hence five tooth passes can be seen clearly in each graph. It is interesting to note that as wear progresses and the cutting forces become greater, a low frequency disturbance becomes apparent in the surface profile. It is assumed that this has it source in imperfections in the table slides and the lead screw of the machine tool which become increasingly significant as the cutting forces grow although no direct evidence is presented for this. It can be seen that the profiles approximate to the sawtooth forms postulated in chapter 3 and that they become more severe as wear progresses. Also visible in these figures are the small scale roughness elements resulting from uneven natural wear of the cutting edge.

Figure 8.1 Changes in the milled surface with wear state when cutting annealed En24 with a single point negative rake cutter (a) $V_b = 0.13$ mm, (b) $V_b = 0.27$ mm, (c) $V_b = 0.55$ mm, (d) $V_b = 1.17$ mm,

Figures 8.2a to 8.2d show similar characteristics in the machined surface obtained when cutting type 304 stainless steel with a single point positive rake cutter. The graphs are complicated in this case by the presence of notch wear on the insert which has had a particularly strong effect on Figure 8.2d.

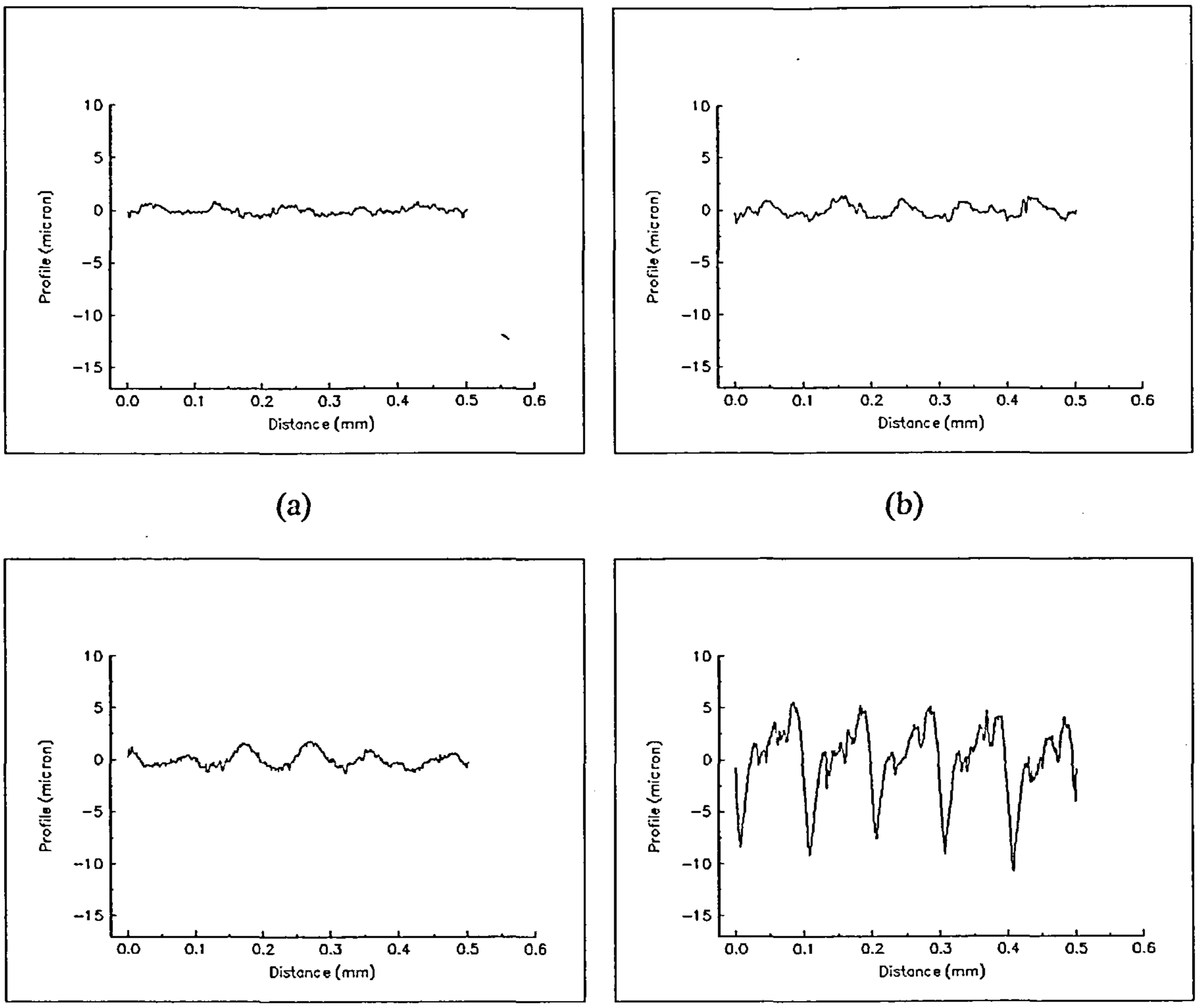

Figure 8.2 Changes in the milled surface with wear state when cutting type 304 stainless steel with a single point positive rake cutter (a) $V_b = 0.05$ mm, (b) $V_b = 0.16$ mm, (c) $V_b = 0.45$ mm, (d) $V_b = 0.75$ mm.

Figures 8.1a to 8.1d and Figures 8.2a to 8.2d illustrate portions of the surface profiles obtained in this work when cutting the workpiece material with single inserts. The effects of multi-point cutting on the generated surface are expected to be broadly similar to those of single point cutting in that an increasingly severe sawtooth profile should be created as flank wear progresses and the cutting forces rise. However the surfaces produced in multi-point cutting will be complicated by the presence of both radial and axial runout. In this work the axial runout of each of the inserts in the cutter was checked by means of a dial gauge and was generally found to be within ± 6.5 μm of the reference insert (designated insert 1 in the cutter). No special adjustment to these settings was made as this work was intended to reflect workshop practice and such adjustment would not normally take place

in a workshop environment. It was not possible to measure the radial runout with any degree of accuracy.

Figure 8.3 shows schematically the effects of axial runout of one of the inserts on the surface produced by multi-point cutting of the workpiece. In the absence of axial runout, of course, the generated surface is expected to resemble the sawtooth already discussed as shown in Figure 8.3a. In the presence of moderate amounts of axial runout, the image of the particular insert involved is predicted to be imprinted on the surface at a rate of once per revolution. This is illustrated in Figure 8.3b. The imprint takes the form of a slightly deeper trough than those produced by the other inserts. If the axial runout present is large, the insert involved again imprints its image on the surface at a rate of once per revolution but additionally in this case some of the machining marks introduced by the other inserts are removed completely by the elevated insert. This is shown in Figure 8.3c.

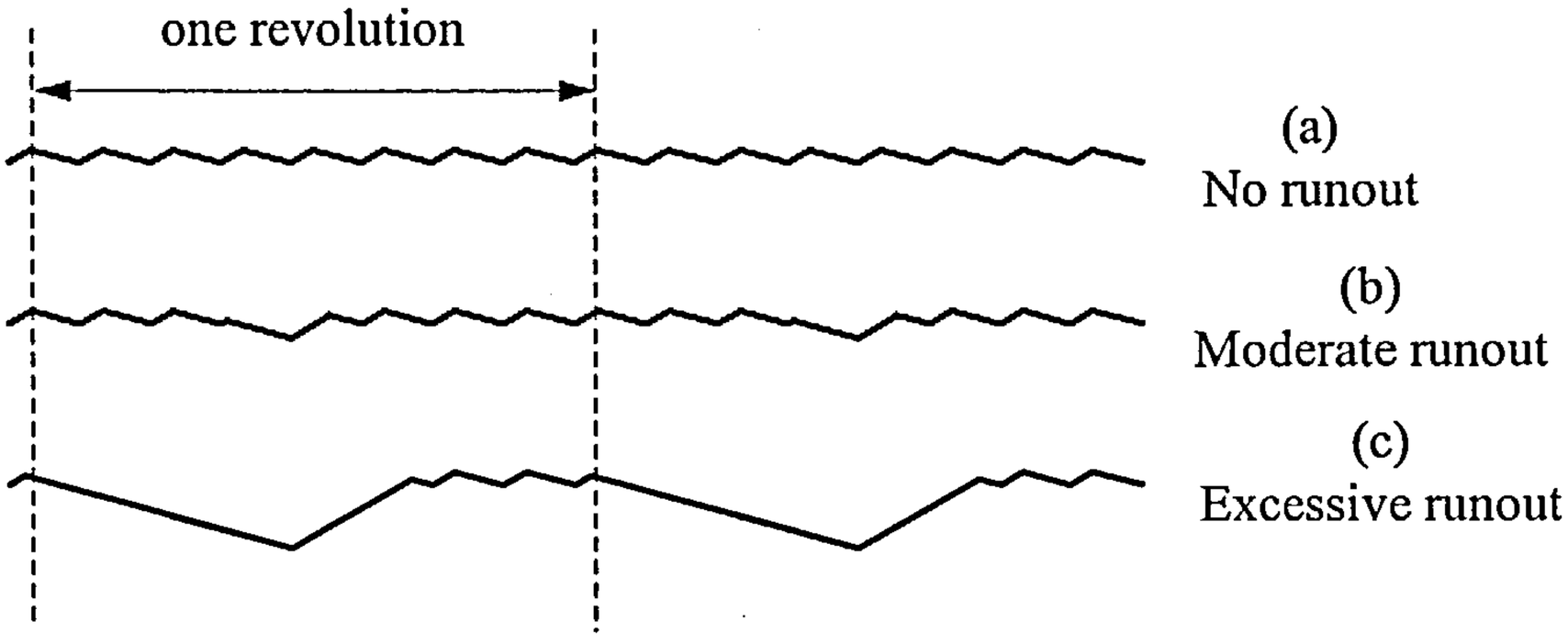

Figure 8.3 The effects of axial runout on the simulated surface profile

The spatial frequency spectrum of the surface generated by a cutter lacking axial runout would be expected to show the insert passing frequency and its harmonics. In the spatial frequency spectrum of the surface generated by a cutter including the effect of axial runout the spindle frequency would manifest itself together with the insert passing frequencies. Larger amounts of axial runout generating a stronger spindle passing frequency and suppressing some of the insert passing frequencies.

Figures 8.4a to 8.4d show 4 mm long portions of the surface profiles generated during eight point milling of annealed En24 with a negative rake cutter for several values of flank wear land length (V_b). The feed employed was again 0.1 mm per insert resulting in a

feed per revolution of 0.8 mm. When comparing these figures with Figures 8.1a to 8.1d and Figures 8.2a to 8.2d the change in the scale of the abscissa should be noted. Figure 8.4a indicates that at least one of the eight inserts suffers from excessive runout since the only clearly visible machining marks are those occurring at the feed per revolution of 0.8 mm and not the feed per insert of 0.1 mm. In the first instance the elevated insert would be expected to wear at a higher rate than the others. This is seen in the reduction in the peak to valley heights of the profile which occurs between the profile of Figure 8.4a and 8.4b and which was discussed in chapter 5 (Figure 5.1a). Thereafter the machining marks of the remaining inserts become visible and as the cutting forces increase with wear of the cutter the deflection experienced by the cutter rises and the profile takes on the appearance of a more severe sawtooth. Towards the end of the cutter life several of the individual inserts had developed wear lands with lengths considerably in excess of 0.7 mm. Under these conditions of wear it would be expected that other mechanisms such as grooving and chipping of the cutting edges were contributing to the surface finish and that the resulting surface profile would be complex. This is demonstrated in Figure 8.4d. The consequences of deterioration of the cutting edges and micro-grooving on the relief faces can be seen in the increasingly prominent surface components at spatial frequencies higher than the insert passing frequency. The significance of this for the changes in integrated spectral content to be expected with tool wear will be discussed in the next section.

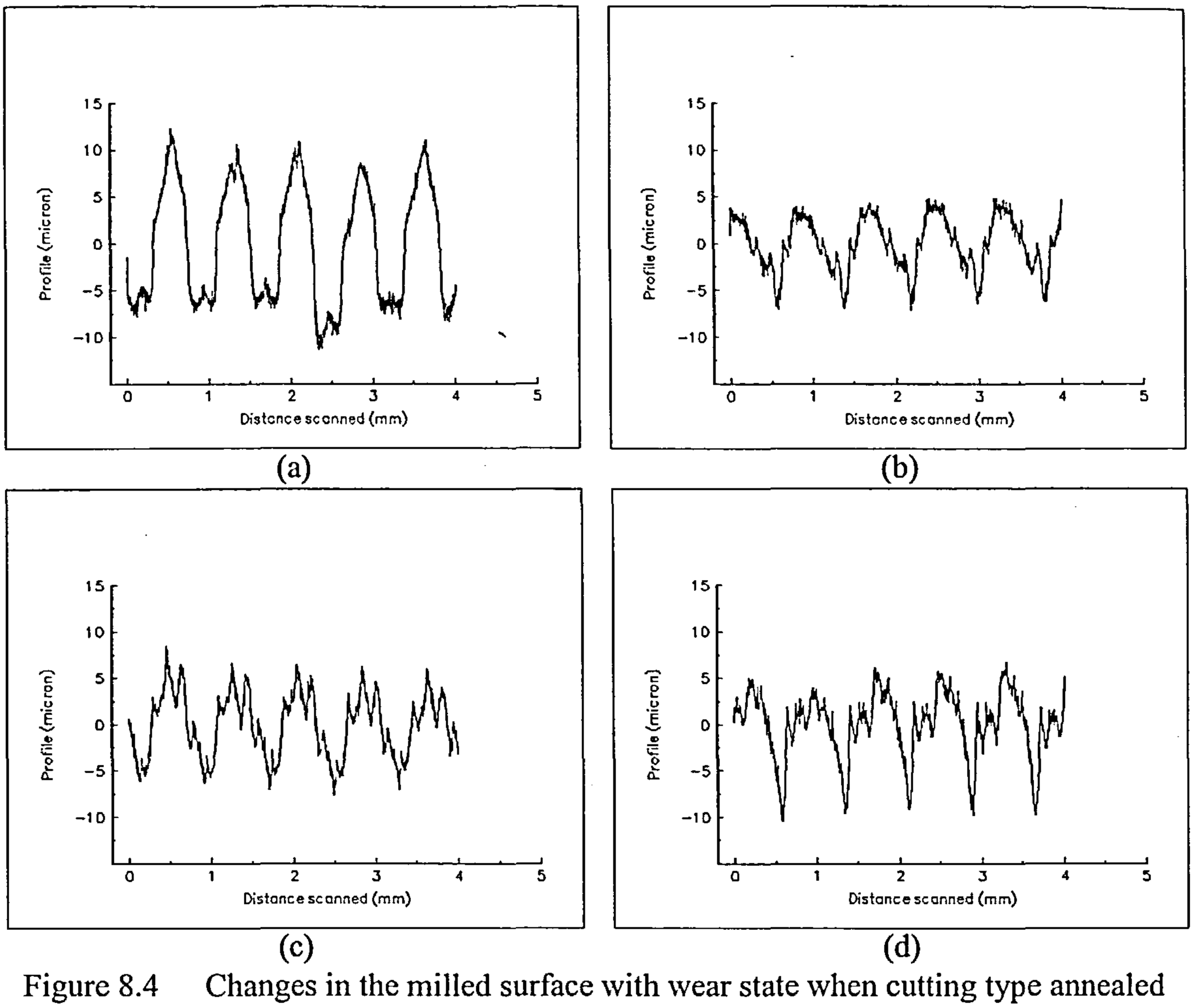

Figure 8.4 Changes in the milled surface with wear state when cutting type annealed En24 with an eight point negative rake cutter (a)new inserts, (b) mean V_b = 0.27 mm, (c) mean V_b = 0.42 mm, (d) mean V_b =0.81 mm.

Figures 8.5a to 8.5d show similar surface characteristics when cutting annealed En24 with an eight point positive rake cutter. The surface profiles illustrated are of length 4 mm and are extracted from a data file corresponding to a total length of 52.4 mm.

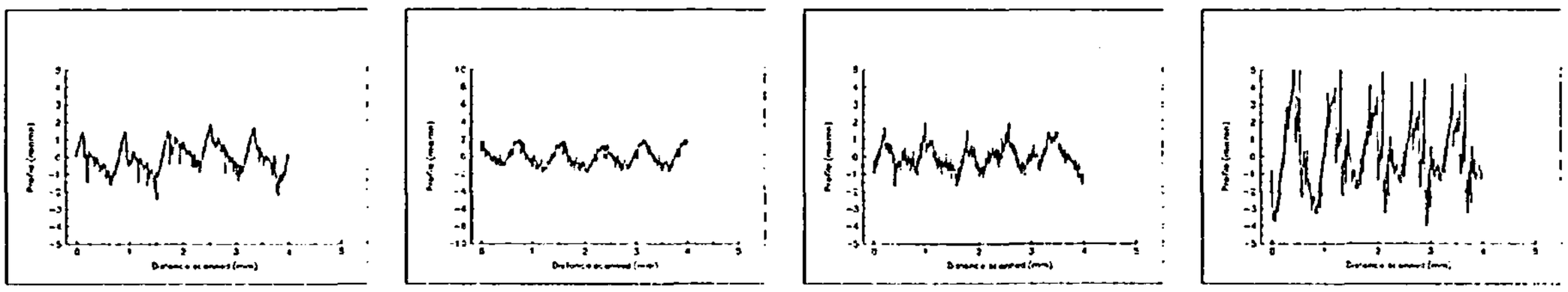

(a) (b) (c) (d)

Figure 8.5 Changes in the milled surface with wear state when cutting annealed En24 with an eight point positive rake cutter (a) mean V_b = 0.13 mm, (b) mean V_b = 0.25 mm, (c) mean V_b = 0.4 mm, (d) mean V_b =0.84 mm.

Figures 8.6a to 8.6d show the machined surfaces obtained when milling the harder quenched and tempered En24 with an eight point positive rake cutter. As in the previous example these profiles represent a 4 mm sample extracted from a total profile length of 52.4 mm.

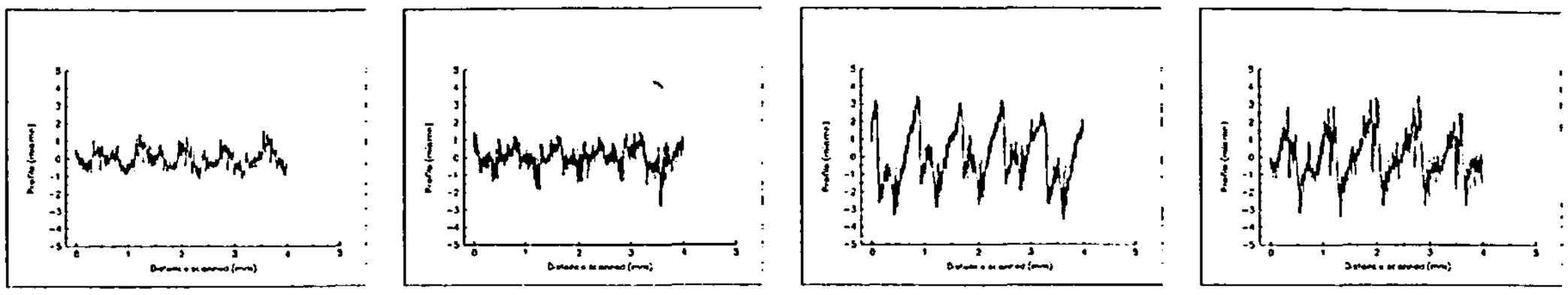

(a) (b) (c) (d)

Figure 8.6 Changes in the milled surface with wear state when cutting quenched & tempered En24 with an eight point positive rake cutter (a) mean $V_b = 0.13$ mm, (b) mean $V_b = 0.38$ mm, (c) mean $V_b = 0.51$ mm, (d) mean $V_b = 0.61$ mm.

Figures 8.7a to 8.7d show the surface profiles obtained by cutting quenched and tempered En24 using an eight point negative rake cutter. The profiles are again 4 mm long and are taken to be representative of the total profile of length 52.4 mm.

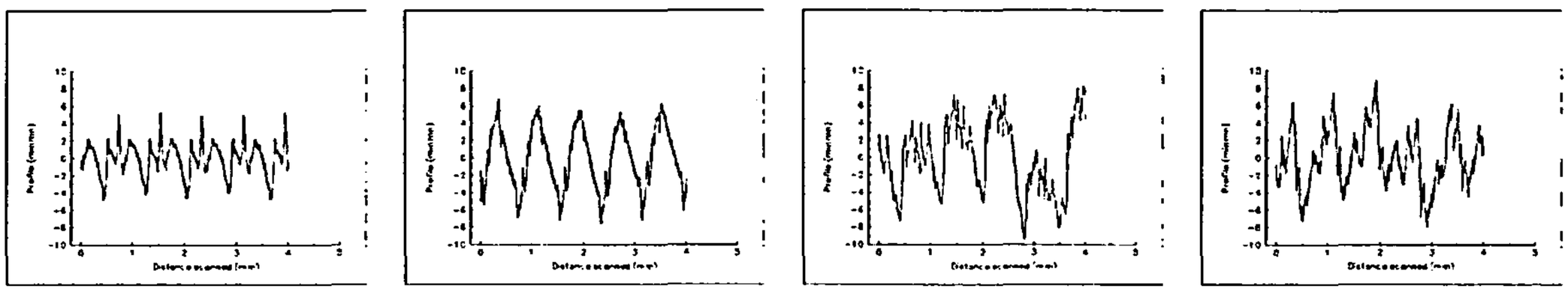

(a) (b) (c) (d)

Figure 8.7 Changes in the milled surface with wear state when cutting annealed En24 with an eight point negative rake cutter (a) new insert, (b) mean $V_b = 0.39$ mm, (c) mean $V_b = 0.49$ mm, (d) mean $V_b = 0.66$ mm.

In all the multi-point cutting examples illustrated above it can be seen that at least one of the inserts suffers from runout. As a result, the dominant feature in the surface profiles, at least until moderate values of V_b are achieved, is an imprint of the affected insert on the profile at a rate of once per revolution of the cutter. Also evident from these figures is the emergence of the high frequency components in the surface finish which were noted

above. This occurs particularly at high values of V_b as evinced by the (c) and (d) versions of Figures 8.1 to 8.7. The most likely source of these high frequencies is to be found in local variations in hardness of the work piece material which will cause uneven wear along the insert cutting edge and the relief face. Although the model discussed in chapter 3 examined the effects of a growing chip on the cutting edge it did not examine the effects of uneven wear of the cutting edge on surface finish and could not be expected to predict these effects. Qualitatively it may be expected that the appearance of micro-grooves on the cutting edge/relief face resulting from uneven wear would be imprinted on the machined surface in such a manner as to increase the high frequency components of the surface spatial frequency spectrum.

8.1.2 The spatial frequency spectra

It was proposed in chapter 3 that, if the effects of insert wear were only to increase the cutting forces, the energy content of the surface profile in a frequency band limited at its lower end by the spindle speed and at its upper end by the insert passing frequency (the kinematic frequency band) would increase linearly with flank wear land length, V_b (Figure 3.29). However examination of the spatial frequency content in this frequency band of the actual surfaces generated in the milling experiments do not show this characteristic in isolation as demonstrated by any of the figures 5.12 to 5.18 of chapter 5 (which will be reproduced below for convenience). It may be concluded from this that other factors in addition to an increase in cutting forces are responsible for the generation of the machined surface profiles. It was also suggested in chapter 3 that, in the absence of mechanisms other than an increased cutting force with wear, the energy content of the surface in a frequency band greater than the insert passing frequency (the high frequency band) would increase initially linearly with wear but eventually attaining a constant value. There is some experimental evidence that this effect does occur as illustrated by figures 5.12 to 5.18. It is particularly noticeable in figure 5.13 which was produced from experimental data derived from cutting annealed En24 with an eight point positive rake cutter. However it is plain from these figures that other mechanisms are also involved in the generation of face milled surfaces.

In attempt to account for other possible mechanisms of surface generation it was further proposed in chapter 3 (figure 3.32) that the presence of an insert cutting edge chip would

disrupt the otherwise smooth evolution of the energy content of the surface with flank wear in both the kinematic and high spatial frequency bands. Figure 3.32 is reproduced below for reference.

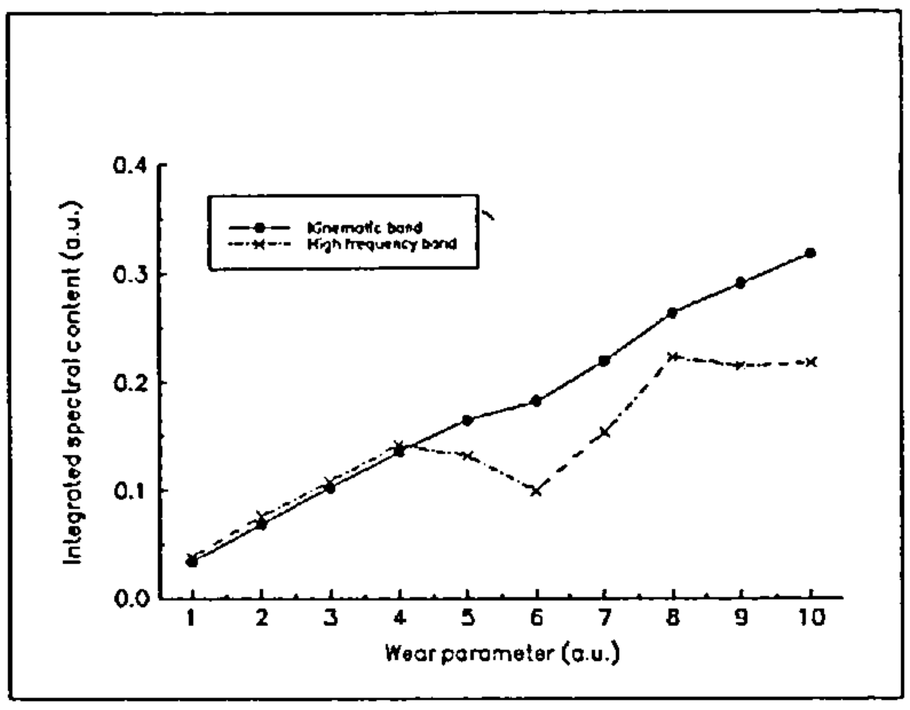

Figure 3.32 Variation in integrated spectral content of the simulated surface profile as flank wear increases combined with a cutting edge chip growth

From this figure it is clear that the high spatial frequency band is expected to show a greater disturbance than kinematic band as a result of the insert chipping in the simulated surface. If the spatial frequency contents of the experimentally generated surfaces are considered individually it can be seen that insert chipping and increased cutting forces account, in large part, for the observed effects. In order to perform this examination figures 5.12 to 5.18 must be reviewed. These figures are reproduced below, without captions, for reference.

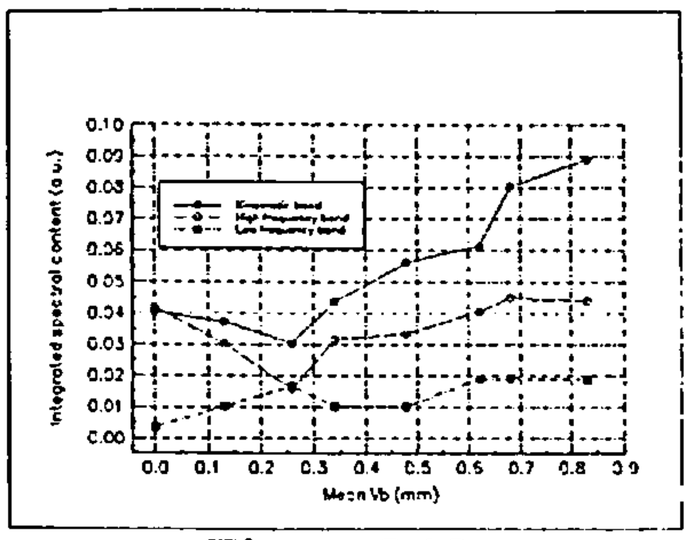

Figure 5.12

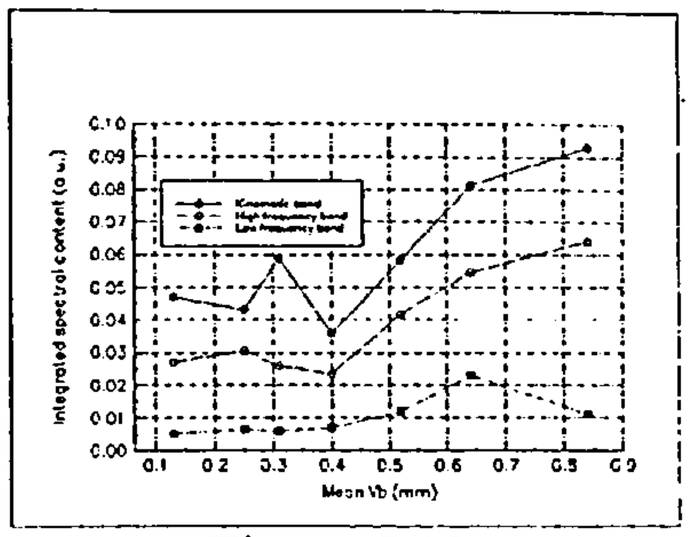

Figure 5.13

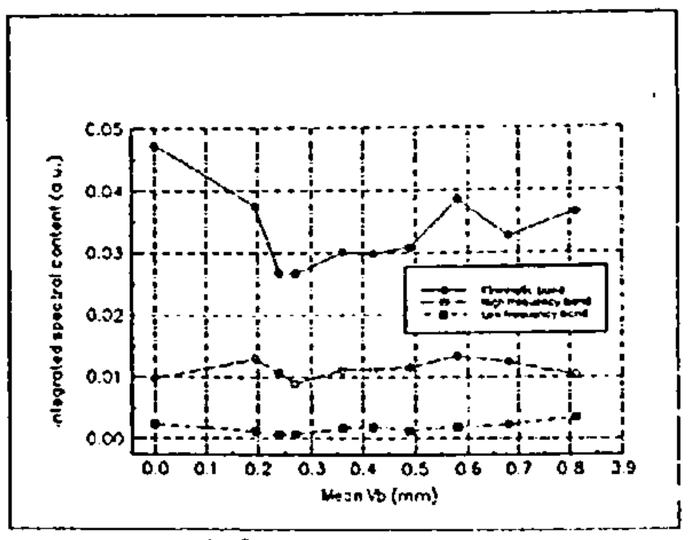

Figure 5.14

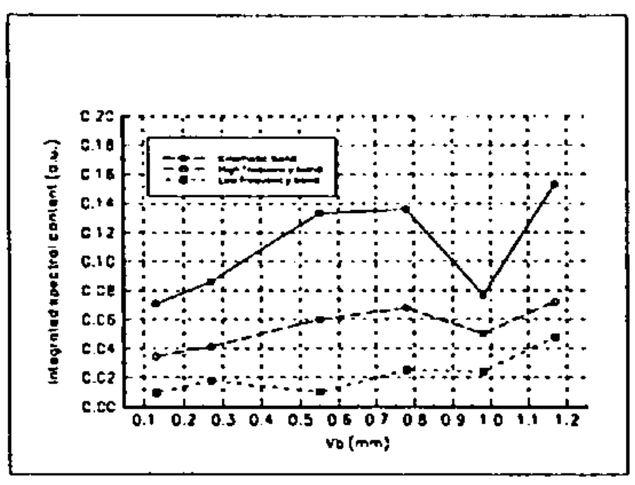

Figure 5.15

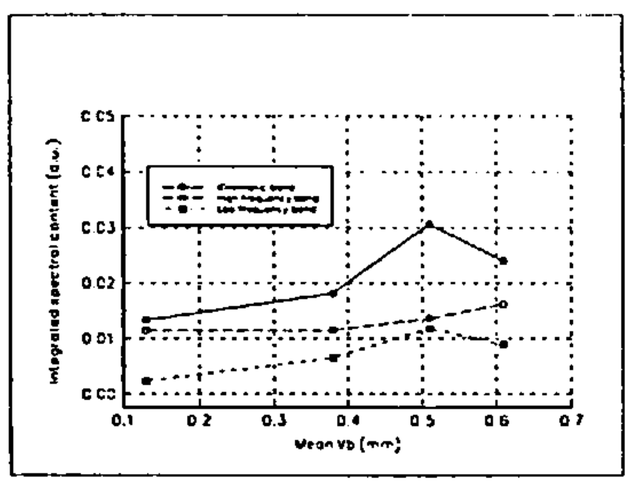

Figure 5.16

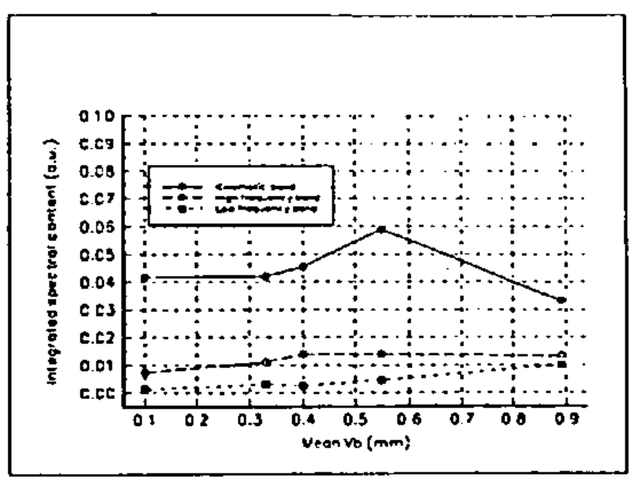

Figure 5.17

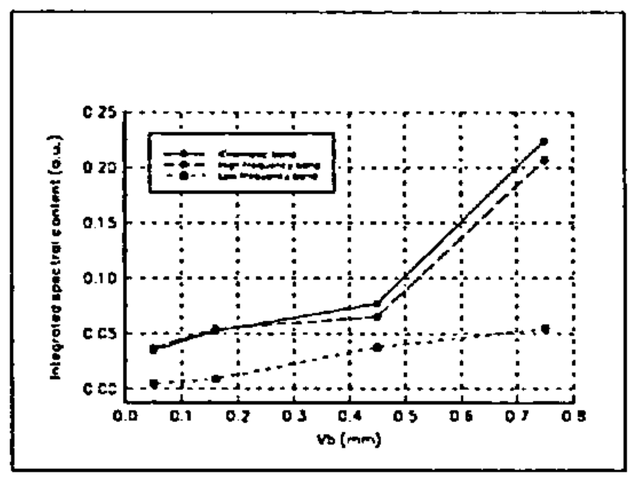

Figure 5.18

Eight point positive rake cutting of annealed En24

Figures 5.12 and 5.13 were produced from experimental data extracted from milled surfaces generated by eight point positive rake cutting of annealed En24. It is plain from the disruption in the evolution of both the kinematic band and high frequency band of spatial frequency content illustrated in figure 5.12 that an insert chipped at an early stage in the cutter life as the mean value of V_b reached 0.26 mm. The further development of the spectral energy with wear followed the trend shown in figure 3.32 until the flank wear land length approached 0.62 mm. At this point the kinematic frequency band indicates that a second insert chipped. This is not reflected in the energy content of the high spatial frequency band and it is suggested that at this stage in the life of the entire cutter the increases in cutting force had started to dominate the high frequency component of the generated surface.

Eight point negative rake cutting of annealed En24

The behaviour of the surface energy content with wear in both the kinematic band and the high frequency band is not as convincing when cutting annealed En24 with an eight point, negative rake tool as it is in the case of positive rake cutting of the same material. This is illustrated in figure 5.14. Although the local minimum in the data from this experiment suggests that one or more of the inserts had chipped in the early stages of wear, no evidence of this was present from examination of the inserts. However uneven wear of the inserts occurred throughout this experiment and it is proposed that this induced fluctuating cutting forces which obscured the more subtle changes in surface profile resulting from progressive wear of the inserts. When the mean value of the flank wear land length had exceeded 0.2 mm the development of surface energy content in both the high frequency band and the kinematic band progressed in the predicted manner. Until this value of mean V_b was attained rapid wear of the tool was observed probably as a result of one or more inserts being subject to excessive runout. This "bedding-in" effect would result in the spatial frequency spectrum being dominated initially by a feature at the tooth passing frequency of 1.25 mm^{-1} (in the case of a single insert being subject to runout). As the remaining inserts started to wear this feature would gradually become less intrusive and the surface integrated spectral content would then be expected to evolve in the predicted manner.

Single point negative rake cutting of annealed En24

The results of this experiment which avoided the complications of uneven wear and runout associated with multi-point cutting are illustrated in figure 5.15. This shows that as annealed En24 is cut with a single point negative rake insert, the variations in kinematic band and high frequency band integrated spectral contents are as described in chapter 3 until the insert was worn out when V_b reached a value of 0.78 mm. The range of the experiment was extended beyond the accepted commercial length of the insert life until the flank wear land length exceeded 1.18 mm to investigate the effects on surface finish of cutting with a blunt insert. The data extracted from this extended range of cutting indicates that the surface appears to have been generated by a chipped insert as demonstrated by the local minimum in integrated spectral content in both kinematic and high frequency bands at a value of V_b of 0.98 mm. Inspection of the insert showed no

indication that insert chipping had taken place but in this extreme wear state the cutting edge of the insert had crumbled, consequently degrading the ability of the insert to cut effectively. The practical effect of this is similar to that of an insert chip. Therefore it is suggested that a discontinuity observed in the smooth evolution of integrated spectral content of the machined surface in both the high frequency and kinematic bands may be taken to indicate a "chip-like" disruption in the cutting edge of the insert rather than merely the occurrence of a chipped insert.

Eight point positive rake cutting of quenched and tempered En24

Cutting of the hardened quenched and tempered En24 induced a higher rate of wear in the inserts than had been observed in the experiments involving the softer annealed material. This resulted in a smaller number of experimental points in this experiment as a consequence of employing natural wear rather than artificial wear. In spite of this it may be seen from figure 5.16 that the evolution of integrated spectral content with mean wear level in both the high frequency and kinematic bands is broadly in agreement with prediction. It was noted that one of the inserts had chipped when the final measurements of flank wear land lengths were made and the mean length was calculated to be 0.61 mm. As can be seen from figure 5.16 this chipping event can be observed in the integrated spectral content of the kinematic band but not in the high frequency band. At this point in the life of the insert considerable variation in the lengths of the individual flank wear lengths was measured with the lower extreme being 0.48 mm and the upper extreme being 0.77 mm. Under these circumstances some of the inserts exhibited grooving of the flank face and it can be appreciated that these would imprint high spatial frequency marks on the surface increasing its high frequency integrated spectral content. Such a process would be expected to conceal the rather more delicate changes in the high frequency band which would result from the chipping of an individual insert.

Eight point negative rake cutting of quenched and tempered En24.

Figure 5.17 demonstrates the variation of integrated spectral content in the high frequency and kinematic frequency bands with tool wear. It can be seen that the evolution of the energy in both of these bands is as predicted until the mean flank wear land exceeded a length of 0.55 mm. Thereafter the high spatial frequency band energy developed as

expected but the kinematic band showed the characteristics of a chipped insert. However inspection of the inserts at the end of this experiment showed no evidence of a chipped insert although one of the inserts showed a considerably heavier (1.04 mm) state of wear than the remaining seven inserts (0.87 mm average). As in the case of eight point and single point negative rake cutting of the softer annealed En24 the kinematic frequency band of integrated spectral content showed the characteristics of insert chipping in the absence of such chipping. Indeed if figure 5.14 is compared with figure 5.17 it can be seen that, following the "bedding-in" period associated with figure 5.14, the high frequency and kinematic bands show remarkably similar characteristics. In all of the cases of negative rake cutting discussed here at least one insert (and only one in the case of single point cutting) was heavily worn at the end of the experiments. It has been suggested above that such heavy wear was accompanied by crumbling of the cutting edge which was not modelled directly in chapter 3. It was further suggested that this crumbling could posses the properties of a "chip-like" event and that this would cause an irregularity to occur in the variation of the kinematic frequency band. The disruption in the kinematic frequency band was not reflected in the high frequency band, a characteristic which was also observed in the eight point positive rake cutting of quenched and tempered En24. This was explained by the appearance of small grooves on the flank wear land which would alter the balance between that portion of surface energy in the high frequency band generated by the increase in cutting force and that portion generated by the imprint at high frequency of grooves on the surface.

Single point positive rake cutting of type 304 stainless steel.

Figure 5.18 shows the behaviour of the integrated spectral content of the machined surface in the kinematic and high spatial frequency bands when cutting type 304 stainless steel. Both of the frequency bands show an increase with tool wear in excess of that predicted by a simple wear process. No evidence of chipping is given by the data although the integrated spectral content variation with wear between a value of V_b of 0.45 mm and the end of the tool life is undefined and none was observed on the insert. The insert did exhibit notch wear and this was accompanied by a crumbling of the cutting edge towards the end of the insert life. It is postulated that this crumbling imprinted marks on the milled surface at higher spatial frequencies than the insert passing frequency and that this was

sufficiently severe to cause a progressive increase in the high frequency band of the integrated spectral content. In addition the increase in cutting force occasioned by the notch wear and edge crumbling was enough to cause an increase in the kinematic band beyond that expected from flank wear alone.

8.1.3 Surface profile fractal dimension and tool wear

The investigation into the effects of tool wear on the fractal geometry of milled surfaces described in chapter 5 was performed as a result of the growing body of evidence that machined surfaces possess fractal characteristics (e.g. [8.1],[8.2], [8.3],[8.4]).

Divider fractal dimension

The first technique, involving the stepping of a pair of dividers at varying separations through the surface profile data, has the advantage that it is conceptually simple and does not impose a heavy computational burden. However, as was noted in chapter 5, it is necessary to exercise caution in interpreting the results from this process when employing it with self affine signals. It was further noted that Brown et al [8.5] had successfully applied the technique to describe turned surfaces. Zhang and Gopalakrishnan [8.6] used a similar method (the box counting algorithm) to relate the fractal dimension of milled surfaces based on area measurements to the surface roughness, R_a, based on profilometer measurements. This work succeeds in establishing fractal dimension as another parameter which gives a measure of surface roughness but it does not give a new technique for tool on-line monitoring of surface roughness as claimed by the authors since the ultimate output of their algorithm is a value of R_a. As was noted in chapter 5, R_a does not correlate well with insert wear land length, V_b, in face milling and therefore it is expected, in the light of the work of Zhang and Gopalakrishnan, that fractal dimension calculated from geometrical data would not correlate with V_b. This was demonstrated to be the case in milling by figures 5.23 to 5.29. It was also observed that the fractal dimension calculated using these divider techniques was insensitive to insert chipping. It is likely that the vagaries of insert runout will mask the subtle changes in divider dimension with tool wear. It was also noted that milled surfaces are not truly self similar in nature but are in fact self affine and therefore care is required in assessing the fractal dimension of such surfaces through geometrical techniques. The changes expected in the characteristics of a

milled surface resulting from progressive tool wear are themselves small. It may be argued that whilst the fractal nature of a milled surface may be revealed by the application of these techniques to a self affine profile, these changes will not be visible in the form of changes in the fractal dimension of the surface.

Structure function dimension

The second technique for calculating fractal dimension was based on statistical methods using the structure function which has been applied to self affine surfaces with some success [8.7]. As with the divider dimension it was observed that although the structure function reveals the fractal nature of the milled surfaces it does not exhibit any consistent changes in fractal dimension of the surface with tool wear. The structure function did demonstrate that the milled surfaces possessed bi-fractal features which is in agreement with the work of Thomas and Thomas [8.2]. He and Zhu also observed bi-fractal behaviour in lapped surfaces and they attributed this to two different processes occurring in the lapping operation. In the present work the bi-fractal characteristics of the milled surfaces may be attributed to different complex mechanisms of surface generation taking place during the cutting process. In particular, shearing of chips from the work piece and rubbing of the inserts on the newly generated surface are expected to influence the appearance of the measured surface profiles. It would be further expected that back-cutting of the work piece would enhance the rubbing aspects of the profile characteristics. As will be seen in the work on acoustic emission and tool wear these mechanisms occurring in the cutting process also effect the generation of AE but in such a manner that tool wear can be recognised.

8.2 Tool wear effects on acoustic emission

8.2.1 Effects on rms AE

It was noted in chapter 6 that a gross geometric relationship was present between the axial rake angle and the variation of rms AE with wear. It was observed that when cutting with a positive rake insert the rms AE tended to increase with wear and when cutting with a negative rake insert the trend was reversed. This general trend was accompanied by some small variations during the cuts. Figure 3.36 of chapter 3 suggests that if the rake angle of

the insert were to change a variation in rms AE would indeed take place. If the local rake angle at the insert cutting edge is examined it may be seen that variation in this angle can take place as the insert wears. Figure 8.8 illustrates this for a positive rake insert. Initially the local rake angle may be considered to be the axial rake angle as shown in Figure 8.8a. As cutting proceeds, if flank wear is accompanied by crater wear the local rake angle becomes more positive as shown in Figure 8.8b. According to figure 3.36 this would result in an initial reduction in the strength of the rms AE signal. As wear becomes more severe and the crater breaks through onto the flank face and/or in the absence of crater wear the edge of the insert begins to deteriorate as demonstrated in Figure 8.8c. This results in the local rake angle becoming less positive with an accompanying rise in the AE signal.

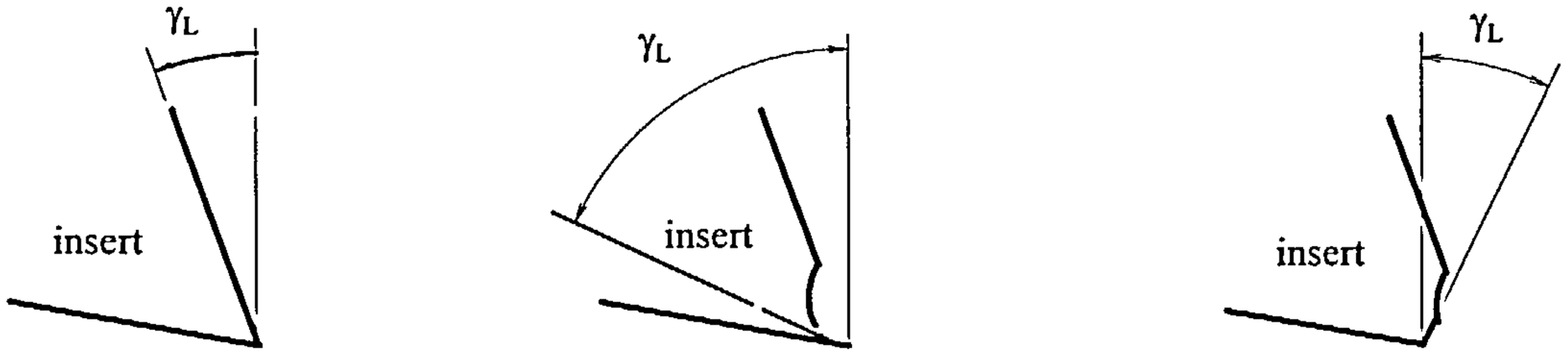

(a) (b) (c)

Figure 8.8 Effect of crater formation on local rake angle γ_L for positive rake insert. (a) new insert. (b) crater forming and γ_L becomes more positive. (c) break-down of cutting edge causing local rake angle to become negative.

Figures 6.4a, 6.4c, 6.9a and 6.10a all show that as the flank wears, the trend of the AE signal is to increase and from the foregoing this is consistent with a reduction in the local angle as illustrated in Figure 8.8c.

In this work crater formation on the rake face of the positive rake inserts was not observed. It may be concluded that the variation in AE with flank wear resulted from a breakdown of the cutting edge which caused the local rake angle to become more negative. It was noted in chapter 6 that the presence of a chipped insert would result in an irregularity in the general trend of the rms AE evolution. The effects of such a chip on the local rake angle are indeterminate as the chipping of an insert is essentially a random

event. Thus prediction of the effects of a chipped insert on direction of change of the rms AE is not possible beyond stating that a disruption in the trend is to be expected. In multi-point cutting the situation is complicated by the presence of several inserts generating AE simultaneously but if it is assumed that all the inserts wear in a similar manner, if not at a similar rate, it can be seen that the trend described here may be established. In the case of single point cutting of stainless steel (figure 6.10a) no complications of multi-point cutting were present and the trend was for the rms AE signal to increase with flank wear.

Similar processes are expected in the case of negative rake inserts. As wear commences the initially negative local rake angle becomes increasingly more positive if crater wear is present until such time as the edge breaks down as a result of the crater breaking through to the flank face or as a result of excessive wear on the flank face. This is illustrated in Figure 8.9.

From figure 3.36, the changes in rms AE following the changes in local rake angle would be an initial reduction in the AE signal as the local rake angle became less negative followed by an increase in rms AE signal as the cutting edge breaks down. In this work crater formation was observed during the experiments with negative rake inserts.

Comparison of figures 6.7a, 6.8a and 6.10a with figure 3.36 shows that the expected trends in rms AE were present in the data. When machining the soft annealed En24 with a multi-point negative rake cutter (figure 6.7a) the dominant geometric mechanism in the generation of the rms AE appears to be a steady increase in local rake angle such as is described in Figure 8.9b. The rms AE signal exhibits a continuous reduction with V_b suggesting either that the cutting edges of the inserts are not degraded in the manner described in Figure 8.9c or if an individual insert does degenerate in this manner its contribution to the rms AE is masked by the other inserts. In the case of fly-cutting the same material (figure 6.8a) it can be seen that as the insert wears there is an initial period where the local rake angle becomes more positive with a consequent reduction in the rms AE followed by a rise in the rms AE as the local rake angle again becomes more negative. However the rise in rms AE is apparently relatively small when compared with the initial reduction and is evidence that in multi-point cutting where several inserts are wearing at different rates, any rise in rms AE generated by an individual insert wearing in the manner of Figure 8.9c would be disguised by the other inserts wearing in the manner described in

Figure 8.9b. Towards the end of the life of a multi-point cutter when it may be expected that all the inserts are wearing at approximately the same rate the overall decline in rms AE would be arrested as most of the inserts would possess an increasingly negative local rake angle. This is illustrated in figure 6.7a as the mean value of V_b exceeds 0.65 mm.

When cutting the hardened quenched and tempered En24 with a multi-point negative rake cutter, craters formed on the rake faces of several inserts much earlier in the wear process compared with cutting annealed En24. Consequent on this is an initial reduction in the rms AE signal as these inserts develop increasingly positive local rake angles. These same inserts would be expected to exhibit earlier edge break down, subsequent reduction in local rake angles and a resultant rise in the overall rms AE signal. This behaviour is illustrated in figure 6.10a.

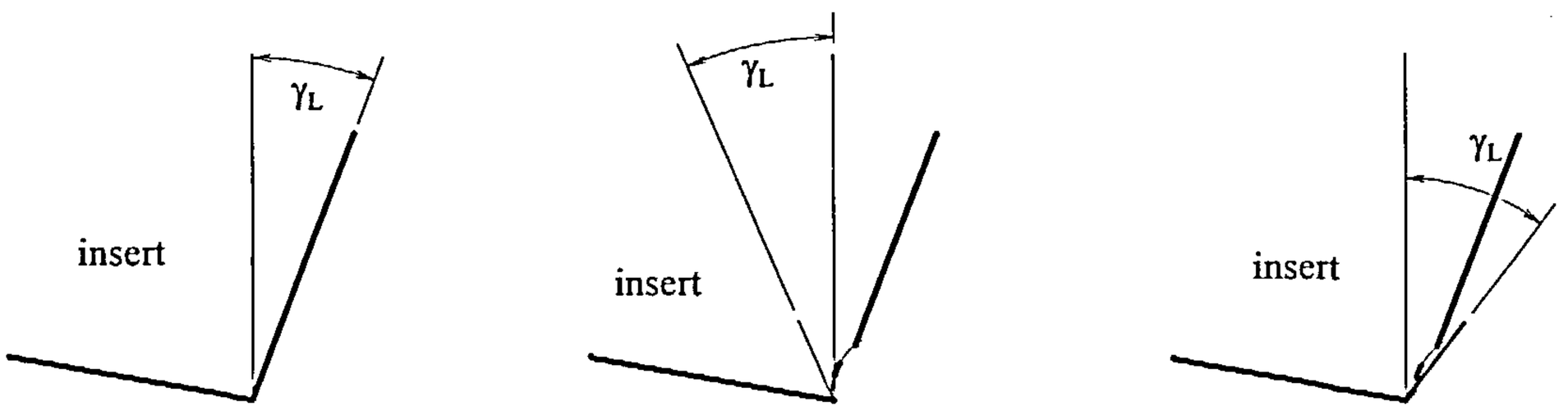

(a) (b) (c)

Figure 8.9 Effect of crater formation on local rake angle γ_L for negative rake insert. (a) new insert. (b) crater forming and γ_L becomes less negative. (c) break-down of cutting edge causing local rake angle to become increasingly negative.

8.2.2 Effects on AE frequency

In chapter 3 it was predicted that changes in local rake angle would cause the frequency function to decrease with an increase in the rake angle as depicted in figure 3.37. This is similar to the variation of rms AE with local rake angle described in section 8.2.1. Thus if changes in local rake angle were the dominant feature effecting changes in the mean AE frequency in the 60 kHz to 1 MHz band it is anticipated that variations in mean AE frequency would reflect the changes in the rms AE signal. However, this is not the case.

In all the experiments conducted in this work the mean frequency was perceived to decrease consistently with flank wear when cutting the soft annealed En24 (figures 6.13a, 6.13b, 6.14, 6.15). This observation holds true regardless of cutter rake angle, local rake angle variations proposed in 8.2.1 and number of cutting inserts. Conversely in all the experiments involving hard materials such as quenched and tempered En24 and type 304 stainless steel the mean frequency was seen to rise with flank wear. The only exception to this was a reduction in mean frequency when cutting quenched and tempered En24 with a multi-point positive rake cutter as the tool approached the end of its life (figure 6.17). It may be concluded that workpiece material properties are dominant in determining the mean frequency of the acoustic emission generated during cutting. It has been noted in chapter 3 that most of the work expended in metal cutting is converted to heat on the shear plane, the rake face/chip interaction zone and the flank/workpiece interaction zone. It was further noted that as the inserts wear the work required to cut the workpiece material will increase thus leading to higher temperatures in these three zones. This temperature rise will not only alter the balance of forces in the cutting zone resulting in the change in shear plane angle upon which figures 3.36 and 3.37 are based but it will also, as a result of thermal softening, bring about changes in the properties of the material from which the AE is generated. If this hypothesis is to be verified it must be demonstrated that there is a correlation between temperature rise in the three zones of deformation and the mean AE frequency. Work in preparation by Jakobsen, Wilkinson et al [8.8] suggests that such a link does exist. In this work we examined the variation of AE energy in discrete frequency bands in the range 100 kHz to 300 kHz during the passage of individual inserts through the workpiece. It was noted that during the first 4 ms of insert engagement the majority of the AE energy was contained in the 100 kHz to 150 kHz band and in the light of the earlier work by Du et al [8.9] it is known that this frequency band is associated with AE generated by shearing and plastic deformation of the workpiece material on the shear plane. This is illustrated by Figure 8.10.

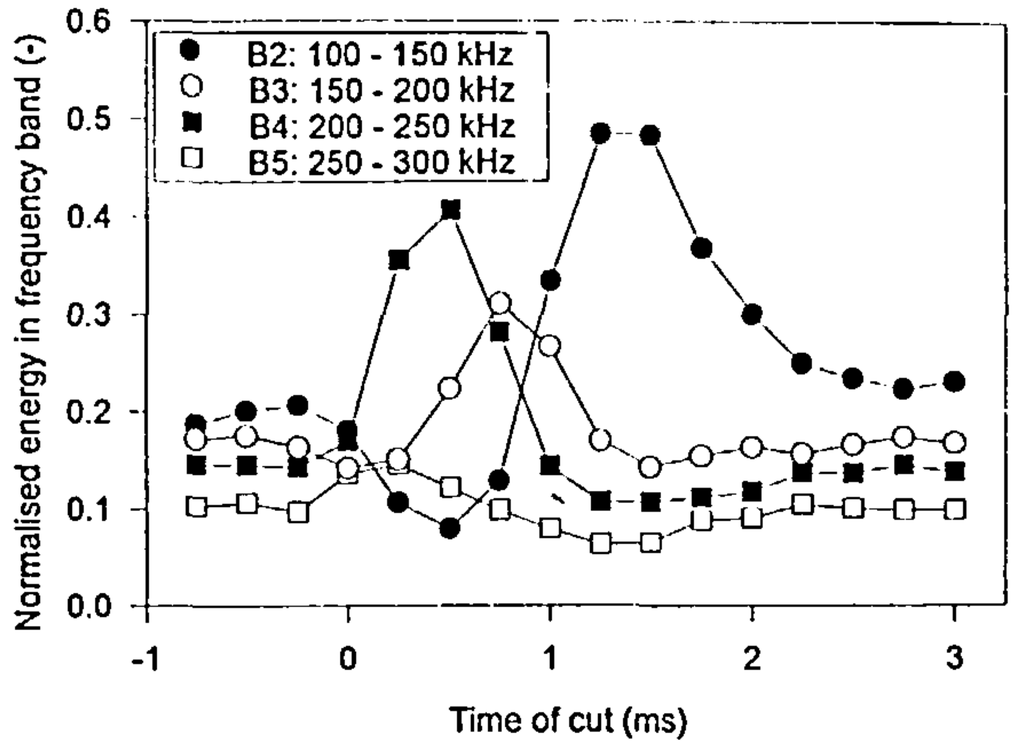

Figure 8.10 Variation of AE energy in several frequency bands during the first 3 ms of a lightly worn (V_b = 0.12 mm) negative rake insert passage through annealed En24

It may be seen that the AE signal in this band decays almost exponentially following engagement of the insert. By fitting an exponential curve to the decay portion of the data it is possible to extract a time constant for the rate of decay of the signal. We observed that this time constant varied with cutting speed and a typical example of this variation is given in table 8.1.

Cutting speed (m/sec)	1.05	1.57	2.36	3.19	6.28
Time constant (msec)	2.8	1.3	0.64	0.46	0.54

Table 8.1 Variation of exponential time constant of AE decay with cutting speed for lightly worn inserts.

Several authors (e.g. Radulescu and Kapoor [8.10], Hou and Komanduri [8.11], Jen and Anagonye [8.12]) have investigated models for temperature prediction during metal cutting. Generally these authors analyse the temperature rise in continuous and interrupted metal cutting using quasi-steady models since it is known that the transient part of the solution to a heat transfer problem in metal cutting is small compared with the cutting timescale. It is however this transient solution which will govern the initial rate of temperature rise in the shear zones and hence the material property changes in these zones.

Radulescu & Kapoor make use of the well known fact that the transient part of the solution to a heat transfer is governed by $e^{-\omega^2 t}$ i.e. ω^2 is the inverse of the time constant. This characterises the rate at which steady state temperature distributions are reached and is given by

$$\omega^2 = \pi^2 \kappa_w \left(\frac{1}{a^2} + \frac{1}{b^2} + \frac{1}{c^2} \right) \qquad (8.1)$$

where κ_w = the workpiece thermal diffusivity

a = b/tan ϕ

b = depth of cut

c = feed per tooth

ϕ = shear angle.

Thermal diffusivity is defined by

$$\kappa_w = \frac{k}{\rho c}$$

where k = thermal conductivity

ρ = density

c = heat capacity

Hou and Komanduri [8.11] show that the time required to establish quasi-steady state temperature distributions is given by

$$t_{quasi-steady} = 5 \times \frac{4\kappa_w}{v^2} \qquad (8.2)$$

where, as before, κ_w is the thermal diffusivity of the work-piece material and v is the cutting speed.

Jen and Anagonye show that the time t_s required to reach steady state temperatures is given by

$$t_s = \frac{\hat{t} d^2}{\kappa_w} \tag{8.3}$$

where $\hat{t}$ is a dimensionless time defined by

$$\hat{t} = 11.7 \exp\left(-0.123\hat{V}\right) \text{ for } \hat{V} \geq 20$$

and

$$\hat{t} = 1.3 \exp\left(-0.0164\hat{V}\right) \text{ for } \hat{V} \langle 20$$

where $\hat{V}$ is a dimensionless velocity given by

$$\hat{V} = \frac{Vd}{\kappa_w}.$$

V is the cutting speed and d is the depth of cut.

Thus these three models establish a relationship between cutting speed and the time for the temperature distributions to reach a quasi-steady state. In this work the following material constants were assumed

k = thermal conductivity ≈ 50 W/m K

ρ = density ≈ 7830 kg/m^3

c = heat capacity ≈ 504 J/kg K

κ_w = thermal diffusivity = 1.267x10^{-5} m^2/sec

The values given for these variables are average values for a plain carbon steel and were used in equations (8.1), (8.2) and (8.3) to predict the required times to achieve quasi-steady state temperature distributions in the cutting zone for a range of cutting speeds as

summarised in table 8.2. The feed rate was kept constant at of 764 mm/min and the depth of cut was maintained at 0.5 mm.

Model	Spindle Speed (rev/min)	Cutting Speed (m/sec)	Time (msec)
Experiment	200	1.047	2.8
Radulescu & Kapoor	200	1.047	0.878
Hou & Komanduri	200	1.047	0.231
Jen & Anagonye	200	1.047	1.43
Experiment	300	1.571	1.3
Radulescu & Kapoor	300	1.571	0.548
Hou & Komanduri	300	1.571	0.103
Jen & Anagonye	300	1.571	0.113
Experiment	450	2.356	0.64
Radulescu & Kapoor	450	2.356	0.297
Hou & Komanduri	450	2.356	0.046
Jen & Anagonye	450	2.356	2.49e-3
Experiment	610	3.194	0.46
Radulescu & Kapoor	610	3.194	0.176
Hou & Komanduri	610	3.194	0.025
Jen & Anagonye	610	3.194	4.27e-5
Experiment	1200	6.283	0.54
Radulescu & Kapoor	1200	6.283	0.049
Hou & Komanduri	1200	6.283	0.0064
Jen & Anagonye	1200	6.283	1.31e-11

Table 8.2 Summary of times required to reach quasi-steady state temperature distributions for varying cutting speeds.

Figure 8.11, which is derived from table 8.2, illustrates the variation of the experimental time constants of decay of the energy in the 100 kHz to 150 kHz band of the AE signal and the theoretical times to achieve quasi-steady state temperature distributions with cutting speed. It can be seen from this figure that the experimental time constants and the theoretical times to quasi-steady state derived from three separate models exhibit such a similarity of variation with cutting speed as to confirm the original assumption that thermal softening effects will alter the frequency content of the AE signal. In order to validate this conclusion further work would be required involving an extensive investigation into AE generated by several workpiece material and insert combinations. This was not within the scope of the current research.

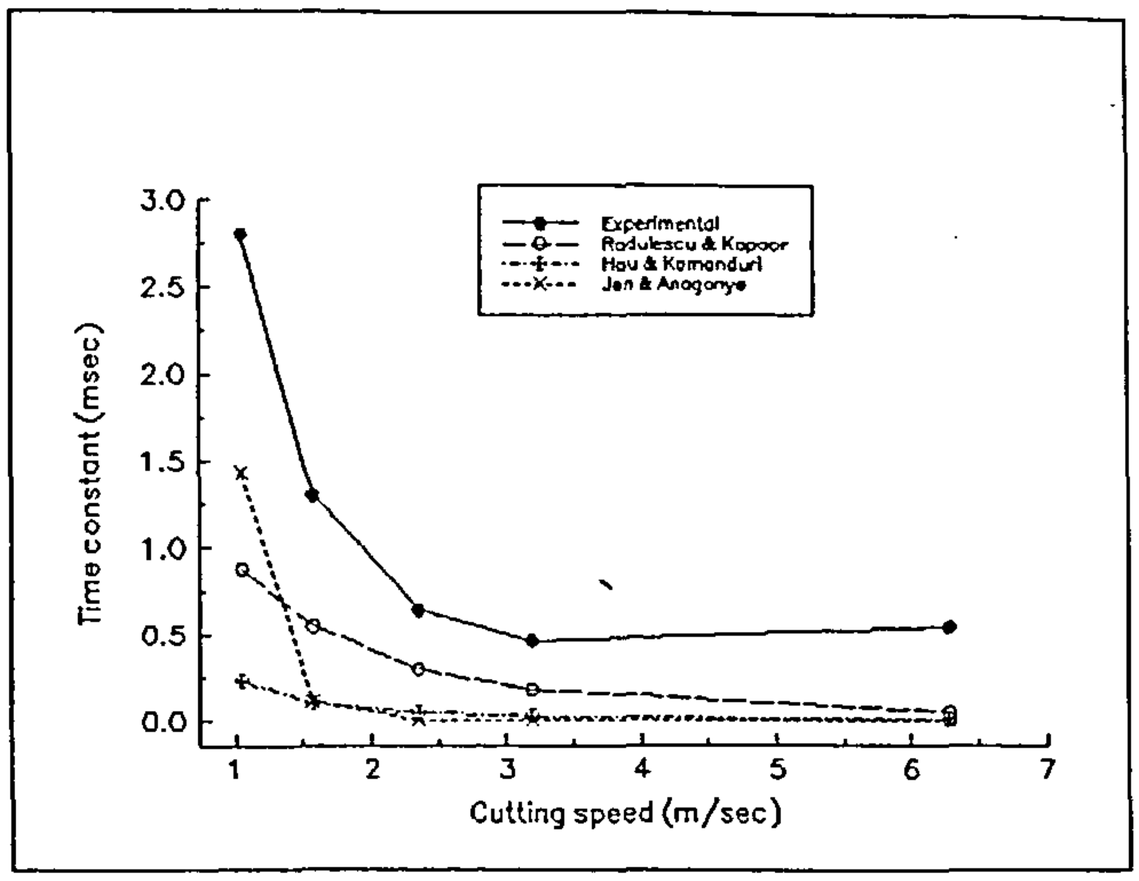

Figure 8.11 Variation in experimental time constant of AE decay in the 100 kHz -150 kHz frequency band and theoretical time to quasi-steady state temperature distributions with cutting speed.

The measurements used to produce the experimental curve in Figure 8.11 were made only in the 100 kHz to 150 kHz frequency band but it may be seen from Figure 8.10 that other frequency bands are similarly affected by temperature changes. Consequently changes in the mean frequency of the overall AE signal with insert wear are to be anticipated. The direction in which these changes in mean frequency take place will be dependant upon the relative changes in the individual frequency bands in the AE signal. As was noted above changes in the AE mean frequency with insert wear do occur; cutting a relatively soft material such as annealed En24 resulting in a reduction in mean frequency and cutting relatively hard materials such as quenched and tempered En24 or type 304 stainless steel resulting in an increase in mean frequency. It is clear from this that both material property effects and insert geometry effects are involved in these changes in mean frequency. As was stated above further research into these phenomena is required to establish the nature of the material effects.

8.3 The use of artificial neural networks in tool wear monitoring

It is clear from the foregoing that several disparate phenomena contribute to the generation of a machined surface and to the production of acoustic emission, although all of these are ultimately related to the forces generated during cutting. In finishing processes, however, the cutting forces are small and changes in these forces with wear

will be correspondingly small. As a result features such as AE and surface finish become practical measurands in assessing tool wear. However, the complex interactions between the cutting inserts and workpiece material make it difficult to state a priori how these measurands will vary with wear. In order to overcome this difficulty a single layer back propagating artificial neural network was trained to recognise variations in features of surface finish and AE and to relate them to the wear state of the cutter. The fusion of sensorial information achieved by this neural network is desirable since, although variation in the measurands with wear was observed, no single measurand would reliably indicate wear state. This was demonstrated particularly when the neural network was presented with a reduced set of features (either surface finish features or AE features alone) and a considerable increase in the time required to train the network was observed. A corollary to this is that it would be expected that additional features presented to the neural network derived from other measurands would reduce the required training time and improve the accuracy of wear state recognition. Although it was recognised that changes in cutting forces were small in finish milling, features derived from these forces could be used to supplement those acquired from AE measurements and surface finish measurements.

The greatest impediment to the successful deployment of a neural network in tool wear monitoring is acknowledged to lie in the size of the required training data sets. It was demonstrated in chapter 7 that a single layer back propagating network presented with AE and surface finish features could be used to improve the identification of tool wear state from a relatively small number of training data sets. However it is likely that the required number of data sets would increase if the simplifications in the milling process employed in this work were relaxed. For example, the cutting speed was maintained at a constant value for any particular combination of workpiece material and cutter. It would be necessary for a practical network to be able to accommodate differing cutting speeds and this would require larger training data sets. Indeed if the neural network were to accommodate any changes in the process variables it would be a prerequisite that the training data sets would be larger. The acquisition of data to supply these training sets is expensive initially and the computing burden required in the training of the network is protracted however ultimately the improvements in identification of tool wear state would compensate for these deficiencies.

The layered perceptron based network used in this work is of course not the only available network for use in neural computing. Radial basis function networks have also been used [8.13] to identify tool wear. They tend to be more complex than the equivalent layered perceptron networks and the number of radial basis functions may be very large [8.14]. Modifications to the single layer network such as the addition of extra hidden layers may enhance the performance of the network but the burden of increased computational complexity rapidly outstrips any benefit in performance which may be achieved.

8.4 Summary

It was predicted in chapter 3 that the integrated spectral content of a milled surface in two frequency bands would contain information about the wear state of the cutting tool which had produced the surface. In particular it was postulated that the energy in the kinematic band would increase linearly with flank wear but that in the event of an insert being chipped this linear increase would be disrupted. Experimental evidence has been presented to support this and it has been seen that the kinematic spatial frequency band is sensitive to progressive wear and discontinuous wear (chipping or chip-like events). It was also suggested that energy variations in the high frequency band would initially increase with tool wear but would eventually reach a plateau at the end of the tool life. Again changes in progressive wear were expected to be reflected in a disruption in the smooth evolution of this energy. This has been demonstrated experimentally although the presence of grooving on the flank face of the inserts, which tends to accompany non-progressive wear, has been seen to produce changes which interact detrimentally with those produced by progressive wear. This has the consequence of making the high spatial frequency band less sensitive to insert wear than the kinematic band.

It has been shown that face milled surfaces exhibit fractal properties. However changes in common measures of those fractal properties such as the divider fractal dimension or the structure fractal dimension with tool wear are insufficiently sensitive to be practical indicators of tool wear state.

Experimental evidence has shown the rms of the AE signal varies with insert wear. The nature of this variation has been shown to depend on a complex interaction between flank wear and the local rake angle of the insert at the cutting edge. It has been shown that the

changes in rms AE with wear can be predicted by the Oxley cutting force model described in chapter 3. Further the disruptions in the smooth evolution of rms AE experienced in the event of short timescale events such as insert chipping can also be explained in terms of the local rake angle through this model.

It was shown that changes in the mean frequency of the AE signal with wear were dependent on the material properties of the workpiece; harder materials resulting in a rise in the mean frequency and softer materials resulting in a decrease in mean frequency. Using annealed En24 as an example it was shown that temperature rises on the shear plane were responsible for the changes in the mean frequency of the AE as a result of thermal softening of the workpiece material. As insert wear progressed the power required to cut the workpiece increased resulting in further changes in cutting temperature on the shear plane. It was accepted that further work into the precise interaction between material properties and acoustic emission during machining is required before this effect may be considered to be of a general nature.

It has been demonstrated that a back propagating artificial neural network presented with surface profile and AE features will enhance the reliability of a tool wear monitoring system. This is accomplished through the capacity of such a network to identify patterns in complex data sets. However the fusion of surface profile data with AE data is a new combination of sensorial information which provides effective discrimination of tool wear state in finish milling.

8.5 References

8.1) L. He, J. Zhu. "The fractal character of processed metal surfaces", Wear,208,(1997), 17-24.

8.2) T.R. Thomas and A.P. Thomas. "Fractals and engineering surface roughness", Surface Topography,1,(1988), 143-152.

8.3) M. Hasegawa, J. Liu, K. Okuda, M. Nunobiki. "Calculation of the fractal dimension of machined surface profiles". Wear,192(1996), 40-45.

8.4) J.C. Russ. "Fractal dimension measurement of engineering surfaces". International Journal of Machine Tools and Manufacture,38(1998) 567-571.

8.5) C.A. Brown, W.A. Johnsen, R.M. Butland. "Scale-sensitive fractal analysis of turned surfaces", Annals of the CIRP, 45,(1996), 515-518.

8.6) G. Zhang and S. Gopalakrishnan. "Fractal geometry applied to on-line monitoring of surface finish". International Journal of Machine Tools and Manufacture,36(1996) 1137-1150.

8.7) R.S. Sayles and T.R. Thomas. "The spatial representation of surface roughness by means of the structure function", Wear, 42,(1977),

8.8) M.L. Jakobsen, P. Wilkinson, D. Harvey, J.S. Barton, J.D.C. Jones and R.L. Reuben. "The effects of progressive wear on the frequency characteristic of acoustic emission acquired during face milling". In preparation.

8.9) R. Du, D. Yan, M.A. Elbestawi. "Time-frequency distribution of acoustic emission signals for tool wear detection in turning", 4th World Meeting on Acoustic Emission and 1st International Conference on Acoustic Emission in Manufacturing, The American Society for Nondestructive Testing, Columbus, OH, USA, 1991, pp269-285.

8.10) R. Radulescu, S.G. Kapoor. "An analytical model for prediction of tool temperature fields during continuous and interrupted cutting". Trans. ASME, Journal of Engineering for Industry, 116(1994), 135-143.

8.11) Z.B. Hou, R. Komanduri. "General solutions for stationary/moving plane heat source problems in manufacturing and tribology". International Journal of Heat and Mass Transfer, 43(2000), 1679-1698.

8.12) T-C. Jen, A.U. Anagonye. "An improved transient model of tool temperatures in metal cutting". Proceedings of the ASME Heat Transfer Division, 4(1998), 87-95.

8.13) S. Elanayar and Y.C. Shin. "Robust tool wear estimation with radial basis function neural networks", Transactions of the ASME, Journal of Dynamic Systems, Measurement and Control, 117(1995), 459-467.

8.14) Simon Haykin. "Neural Networks A Comprehensive Foundation". Macmillan College Publishing Company, Inc. New York, 1994.

Chapter 9

Conclusions

The conclusions which are drawn from this work will be considered in this chapter and they will be presented in subdivisions which correspond to the manner in which the experiments were discussed in the earlier chapters.

9.1 Tool wear monitoring and surface finish

9.1.1 Measurement of surface profile

Conventional measures of surface profile such as centre line average, R_a, have been shown to present insufficient reliability to be used in a tool wear monitoring system when monitoring the face milling process. This is apparent from the fact that R_a has been shown to vary from location to location on the milled surface. If it is not possible to obtain consistency in the measurements of this parameter on a single workpiece it is unlikely that a wear sensitive trend will be observable across a range of workpieces. However, as shown in figures 9.1a, 9.1b and 9.1c, the spectral content in the low frequency band, the kinematic frequency band and the high frequency band of the machined surface profile show reasonable agreement at different locations on the surface. Thus it may be concluded that the frequency descriptors of surface profile discussed in chapter 5 are a valid alternative to conventional surface profile measures. Further, as was shown in chapter 5 and briefly shown in figures 9.1a, 9.1b and 9.1c, these descriptors are sensitive to insert flank wear as measured by the flank wear land length.

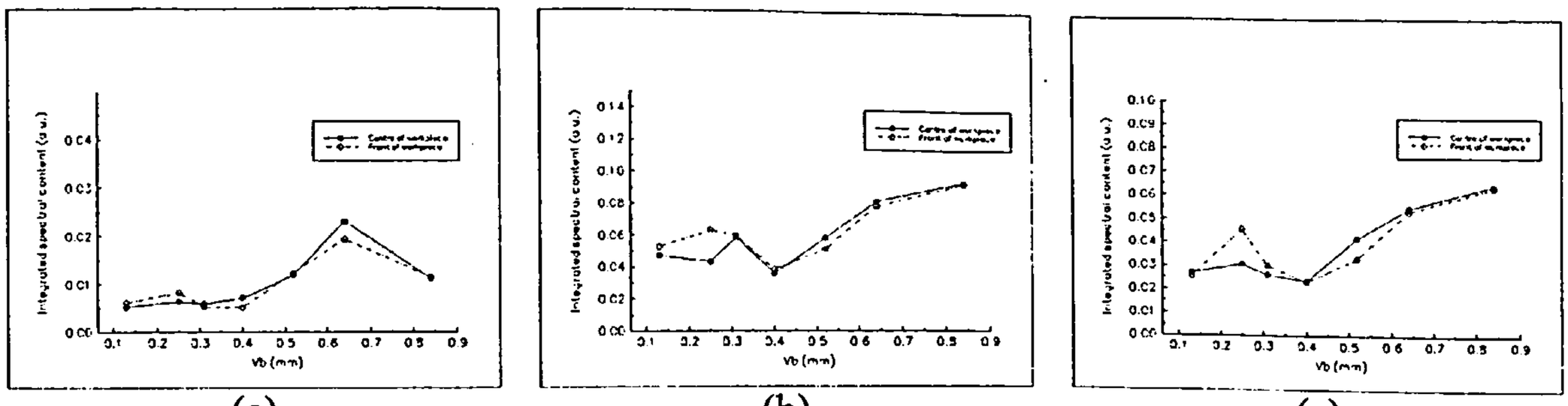

(a) (b) (c)

Figure 9.1 Variation of integrated spectral content with V_b from two locations on a typical milled surface. a) low frequency band, b) kinematic band, c) high frequency band

9.1.2 Spatial frequency content of the surface profile

In all the experiments conducted in this work the spectral content in both the high spatial frequency band and the kinematic spatial frequency band increased with insert wear but the spectral content in the low spatial frequency band is less conclusive. It is possible that the low frequency band data was contaminated by effects not directly involved with tool wear such as minor defects in the machine tool table drive train which would obscure the subtle changes in surface profile resulting from tool wear alone. Thus the low spatial frequency band may be considered to contain information regarding the general condition of the machine tool in addition to the wear state of the inserts and therefore the use of this parameter alone would find limited application in the monitoring of insert wear.

There is no evidence that insert geometry in the form of the cutter axial rake angle affected the trend in the variation of spectral content with insert wear in the kinematic and high frequency bands. However insert geometry does have an effect on the sensitivity of the spectral content to flank wear. This was shown in the experiments involving positive rake cutters which generated data which was more sensitive to flank wear than the negative rake cutters. Uneven wear of the inserts in the early portion of tool life in those experiments involving multi-point cutting caused a reversal in the general tendency of the spectral content in these two spatial frequency bands to increase. However as the mean flank wear length of the cutter approached a value of approximately 0.3 mm the increasing trend in the spectral content of the two frequency bands became established in all of the experiments. If this is examined from the perspective of a tool wear monitoring system the recognition of the medium and heavy wear stages of tool life are important. It

may be concluded that the spectral content of the surface profile in the kinematic and high spatial frequency bands will be reliable indicators of progressive tool wear when the middle and end stages of tool life are approached.

It was shown in chapter 5 that spectral content of the surface profile in the three spatial frequency bands could be used to detect short time scale events such as insert chipping. The surface profile data required to recognise tool chipping will be obtained either inter-operationally by using the fibre-optic instrument described in chapter 4 or by using a conventional profilometer off line also as described in chapter 4. In either case the data will be acquired some time after the occurrence of the chipping incident which will reduce the applicability of this technique to the monitoring of short time scale events. This limitation would be overcome by the availability of an instrument which would be capable of measuring surface characteristics during the cutting operation. However considerable difficulties would arise in trying to deploy such an instrument in the hostile environment of a machining process.

9.1.3 Fractal dimension of the surface profile

The machined surfaces produced during this work all possessed profiles which exhibited fractal properties which could therefore be described in terms of the fractal dimension of the profile. Two techniques were employed to calculate the fractal dimensions of the profiles, a direct geometrical technique and a statistical technique. In neither case was the fractal dimension sensitive to progressive changes in insert wear land length. This statement is qualified by noting that when using positive rake cutters a change in the geometrically derived fractal dimension of approximately 7% across the life of the tool was observed. Clearly fractal dimension obtained from either of these techniques cannot be used to monitor progressive tool wear. However it is to be expected that fractal dimension derived from spectral techniques would demonstrate sensitivity to flank wear in a similar manner to that obtained from the integrated spectral content of the surface profile. This method was not investigated as it was considered to be an extension of the spectral technique used to obtain the variation in spectral content of the surface profile with flank wear.

Results obtained from the structure function based fractal dimension illuminated the bi-fractal nature of milled surface profiles. Although no systematic variation in fractal dimension in either of the two fractal zones considered was observed, large discrepancies in the fractal dimensions of the profiles in the two zones were related to insert chipping events. The use of this information in the detection of insert chipping is, however, not practical since it would not be available to a tool condition monitoring system until some time after the event had occurred. As was discussed above this limitation also applies to the use of surface spectral information in detecting insert chipping.

9.1.4 Summary of surface profile characteristics

As can be seen from the above the spatial spectral content of a milled surface profile contains information regarding the wear state of the generating inserts. It has been shown that the spatial spectral content is sensitive to progressive insert wear and therefore it should be considered as a candidate measurand for inclusion in a tool wear monitoring system with the proviso that measurements should be made either inter-operationally or during the cutting process. Fractal dimension as derived from either the direct divider method or the structure function method exhibits insufficient sensitivity to progressive insert wear for it to be considered as a useful indicator of insert wear. It is unlikely that the fractal dimension derived from spectral techniques will give more information on insert wear state than is available from the spectral content of the surface profile.

9.2 Tool wear monitoring and acoustic emission

9.2.1 RMS acoustic emission signals

The results obtained in this work demonstrate that the 0.55 ms rms value of the AE signal is sensitive to insert flank wear. The trend of the rms signal revealed a dependency on the gross insert geometry, generally decreasing with flank wear land length when using negative rake cutters and generally increasing with flank wear land length when using positive rake cutters. These general trends were moderated in some cases by the formation of crater wear on the insert rake face and by the breakdown of the cutting edge in the earlier stages of insert wear. Therefore it may be concluded that the rms AE signal is determined not only by flank wear land length but also by local changes in the insert

geometry at the cutting edge. As the insert approaches the end of its useful life, changes at the cutting edge become relatively insignificant and variations in the rms AE signal become dependant on the flank wear land length, V_b. Workpiece material properties appeared to have no effect on the variation of rms AE with flank wear in the experiments performed in this work. However for this to become a uniformly applicable conclusion tests using workpiece materials with a differing range of machinability indices would have to be carried out.

The normalised standard deviation or relative dispersion of the rms AE signal was also seen to be correlated to insert flank wear land length in the initial stages of insert wear when cutting relatively soft materials. Therefore this parameter may be used as an indicator of the onset of moderate insert wear in such processes but it is not sufficiently responsive to advanced insert wear to be useable in a tool wear monitoring environment.

Insert chipping is detectable in both the rms AE signal and the relative dispersion of the rms AE signal although the latter parameter demonstrates reduced sensitivity to these short term events when cutting harder materials.

It may be concluded that for the range of materials tested in this work the rms AE signal provides a measurand which is sensitive to insert flank wear throughout the life of the insert. However knowledge of the insert geometry is required if efficient use of this parameter is to be made in insert wear monitoring. The relative dispersion of the rms signal provides information on the wear state of the inserts until a flank wear land length of approximately 0.5 mm is attained but beyond this length relative dispersion of the rms AE signal gives no further insight into the problem. Similarly although both the rms AE signal and the relative dispersion of the rms AE signal can be used to detect insert chipping the relative dispersion does not generate reliable data across the entire range of material hardness.

The foregoing leads to the conclusion that rms AE is a useful indicator of insert wear but it is by no means a universally applicable indicator of wear. Uneven wear and individual insert chipping in multi-point cutting may lead to ambiguous identification of insert wear state, the first of these usually occurring at the beginning of tool life and the second towards the end of tool life. It could also be noted that although the workpiece material properties had no effect on the general trend of the rms AE signal, the sensitivity of the

rms AE signal to changes in flank wear land length were affected by these properties. Therefore it may be inferred that other measurands besides rms AE are required to assess insert wear reliably.

9.2.2 Mean frequency of AE signals

The mean frequency of the AE signal was shown to be correlated with insert wear. The trends in the variation of mean frequency with flank wear land length demonstrated a dependence on material workpiece properties rather than on insert geometry. When cutting the softer annealed En24 the mean frequency of the AE signal reduced with insert wear and when cutting the harder quenched and tempered En24 and stainless steel it increased except in the case of eight point positive rake cutting of quenched and tempered En24. In the latter case the mean frequency showed a tendency to increase with flank wear in the early stages of insert wear conforming to the trend exhibited in other experiments on harder materials. However as wear progressed into later stages of insert life the mean frequency reduced with insert wear manifesting the characteristics seen in machining a softer material. The tendency for mean frequency of the AE signal to reduce as wear progresses is consistent with the observations of Jakobsen, Wilkinson et al [9.1] when cutting annealed En24. Thermal softening of the workpiece material was shown by these authors to effect a displacement of the AE power into lower frequency bands thereby lowering the mean frequency observed in the AE signal. These authors did not report work on single point cutting or on machining different materials. However it may argued that in single point cutting significant thermal softening does not occur as a result of the relatively long time interval over which the insert is not cutting and the system is cooling. This would account for the comparatively weak correlation between insert wear and AE mean frequency when using a single point negative rake cutter with annealed En24. When machining quenched and tempered En24 and stainless steel it is likely that competition exists between the strain hardening characteristics of the material and the thermal softening of the material. This could account for the observed differences in the trend of the mean frequency of the AE signal with wear when compared with that seen when cutting annealed En24. In particular when cutting type 304 stainless steel with a single point cutter the thermal softening effects have limited scope to develop for the reasons described above and this particular material is known to possess strong strain

hardening characteristics. However further work extending that of Jakobsen, Wilkinson et al into machining a range of harder materials with varying work hardening characteristics is required. It should be noted that in the experiment which produced this contrary trend, insert chipping occurred in the late stages of insert life and this phenomenon has been shown to disrupt the evolution of AE mean frequency with insert wear in other experiments.

9.3 Sensor fusion through an artificial neural network.

The rms of the AE signal, the mean frequency of the AE signal and the surface profile spectral content in the kinematic band and the high frequency band were all correlated with insert wear in finish milling of a range of engineering materials. Table 9.1 illustrates graphically the manner in which these measurands varied as insert wear progressed. In some instances the measurand was only weakly correlated and these are indicated in the table by shading. It can be seen from this table that insert geometry has an influence on the trend of rms AE in that rms AE increases with insert wear when cutting with positive rake inserts, the converse being true when cutting with negative rake inserts. Further it can be seen that when cutting relatively soft materials the mean frequency falls with increasing wear whereas it rises with wear when cutting harder materials. The surface profile spatial frequency content is seen to increase in both the high frequency band and the kinematic band with increasing wear in general. However the table also demonstrates that in isolated cases the measurands are either weakly correlated with insert wear or the measurand varies in a manner which is contrary to that expected. These exceptions may be taken as evidence that no single sensor can provide data which is a universal solution to the problem of identifying tool wear state. In this work it has been shown that an artificial neural network using five features extracted from an AE signal and surface profile measurements can achieve a considerable improvement in the reliability of an insert wear assessment scheme when compared with the performance of a single sensor. This has been shown to be true over a broad range of workpiece materials, cutting conditions and insert types and is of particular importance in finish milling where other sensors may not deliver sufficient sensitivity to insert wear.

9.4 Future work

In order to exploit the continuing improvement in computer technology a combination of artificial neural networks of the type discussed above with an expert system is recommended. This could mitigate some of the expense involved in acquiring training data for a neural network. It is recognised that this work considered finish milling only and that in other milling activities additional sensorial information, for example indicators of tool wear such as those discussed in chapter 2, would be available to aid in the assessment of wear state. As a result it would be beneficial to investigate the fusion of features extracted from these additional sensors with the AE and surface profile features to generate a tool wear monitoring scheme potentially applicable throughout the entire milling process envelope.

Sensor performance is critical in tool wear monitoring. In this work a novel non-contacting AE transducer was used which allowed not only the measurement of the rms value of the AE signal but also its frequency content. This device requires an optically clean reflective surface located either on the workpiece as in this work or on the tool holder as described by Jakobsen, Wilkinson et al as a target. The requirement for an optically clean surface impedes operation of this sensor in the presence of coolant. However Jakobsen et al [9.2] have reported some success in using a perspex shield to protect the transducer and target surface when performing a slot milling operation whilst applying coolant. Further development of this sensor to enhance its performance in the presence of coolant would be useful. Similarly the optical transducer used to measure surface profile inter-operationally would not operate efficiently in the presence of coolant and development of this transducer is also required.

The machining processes examined in the experimental trials were performed in the absence of coolant. It is desirable to understand AE generation processes in the presence of coolant to help establish the credibility of AE detection as a practical technique in tool wear monitoring. For example it may be anticipated that contact between coolant and hot inserts will be a source of AE and the lubricant effects of coolant would be expected to modify the AE generated by friction in the cutting process. Therefore experiments involving coolant are recommended for future investigation in conjunction with further

development of the non-contacting transducer to allow it to operate in this environment. This would allow the necessary measurement of the frequency content of the AE signal.

9.5 Machine shop usage

The work of this thesis has been carried out at essentially constant cutting conditions and it has been demonstrated that both surface finish parameters and AE features may be used to detect progressive wear. However, in practical industrial usage cutting conditions vary from operation to operation such as in changing from roughing cuts to finishing cuts. These changes will result in alterations to the cutting forces which will, for example, affect the shear plane angle resulting in modifications to the generated AE. Similarly surface profiles are expected to be influenced. Such non-wear related changes in AE and surface profile parameters will be detected by the tool wear monitoring system and mis-classification of the wear state could result.

Ideally a tool wear monitoring system should be impervious to changes in cutting conditions but as presently constituted the system described in this thesis would not meet this requirement. Silva et al [9.3] demonstrated that a small "zone of influence" exists in which the performance of a tool wear monitoring system used in turning is not materially affected by cutting conditions. These authors employed a self organising Kohonen neural network to show that acceptable (better than 80% correct prediction) performance could be achieved in a zone of small variations in cutting conditions around the network training cutting conditions. When attempting to classify wear state at cutting conditions under different cutting conditions the performance of the network was severely reduced. It is anticipated that a similar zone of influence will exist around the cutting conditions used in this thesis. If radically different cutting conditions were to be employed it would be necessary to provide the monitoring system with a degree of adaptability. This could be achieved by allowing an expert system to alter the feature values presented to the neural network to account for variations in cutting conditions. Such a system would require a knowledge of the effects of cutting conditions on transducer output. This could be acquired either empirically from a series of tests encompassing all possible cutting conditions or mathematically from a model relating cutting conditions to AE and surface profile generation. The former approach is envisaged as being expensive and hence the latter technique is recommended as being most likely to produce a practicable result. It

will be necessary to develop functional relationships between the AE features discussed in this work and the cutting variables and between surface profile features and the cutting variables. These relationships will then form the basis of an adaptive controller which will be capable of eliminating the effects of various cutting conditions on wear state classification. It is recognised that considerable work is required to achieve this aim although Emel and Kannatey-Asibu [9.4] have reported some progress in removing the effects of cutting conditions from AE signals in turning.

			Acoustic emission trends with wear		Surface profile trends with wear	
Insert geometry	**Number of inserts**	**Workpiece material**	**rms**	**Mean frequency**	**Kinematic band**	**High frequency band**
positive rake	8	Annealed En24	↗	↘	↗	↗
positive rake	8	Annealed En24	↗	↘	↗	↗
negative rake	8	Annealed En24	↘	↘	↘	→
negative rake	1	Annealed En24	↘	↘	↗	↗
positive rake	8	Hardened En24	↗	↘	↗	↗
negative rake	8	Hardened En24	↘	↗	↗	↗
positive rake	1	Stainless steel	↗	↗	↗	↗

Table 9.1 Summary of feature trends as insert wear progresses in single point and eight point milling of a range of engineering materials. Shading indicates that the measurand correlation with wear was weak.

9.5 References

9.1) M.L. Jakobsen, P. Wilkinson, D. Harvey, J.S. Barton, J.D.C. Jones and R.L. Reuben. "The effects of progressive wear on the frequency characteristic of acoustic emission acquired during face milling". In preparation.

9.2) M.L. Jakobsen, D. Harvey, T.A. Carolan, J.S. Barton, J.D.C. Jones and R.L. Reuben. "Optical probing of acoustic emission from a rotating tool holder with a Sagnac interferometer". Proceedings of the Institution of Mechanical Engineers, 213,Part B, (1999), 171-181.

9.3) R.G. Silva, K.J. Baker, S.J. Wilcox, R.L. Reuben. "The adaptability of a tool wear monitoring system under changing cutting conditions". Mechanical Systems and Signal Processing, 14, 2,(2000), 287-298

9.4) E. Emel and E. Kannatey-Asibu. "Acoustic emission monitoring of the cutting process - Negating the influence of varying cutting conditions". Transactions of the ASME, Journal of Engineering Materials and Technology, 113(1991), 456 - 464.